The Cyaphide-Azide 1,3-Dipolar Cycloaddition Reaction for the Synthesis of Mechanically Interlocked Molecules

Alex J. Mapp

University College

University of Oxford

Michaelmas 2025

A thesis submitted for the degree of

Doctor of Philosophy

Abstract

The Cyaphide-Azide 1,3-Dipolar Cycloaddition Reaction for the Synthesis of Mechanically Interlocked Molecules

Alex J. Mapp University College

DPhil Inorganic Chemistry Michaelmas 2025

This thesis describes the chemistry of the cyaphide-azide 1,3-dipolar cycloaddition reaction, and its use in the synthesis of mechanically interlocked molecules.

Chapter 1. The high-yielding synthesis of mechanically interlocked molecules requires both a templating strategy in which the molecular components are organised into an interlocked manner and an efficient covalent bond forming reaction to trap the final product. The copper-catalysed azide-alkyne click reaction is popular in an active-metal templating approach, where the copper(I) ion fulfils both criteria. Whilst metal ions have been used as catalysts and/or templates for the synthesis of mechanically interlocked molecules, they are rarely incorporated into the final product due to the lack of general covalent bond forming strategies involving inorganic species. The isolobal analogy can be used to relate the copper-catalysed azide-alkyne click reaction with the phosphaalkyne-azide and cyaphide-azide 1,3-dipolar cycloaddition reactions. The former has been used to prepare a new class of triazaphosphole ligands; however, the latter is limited to a single literature example. The cyaphide transfer reagent, (^{Dipp}NacNac)Mg(CP)(dioxane), can be used to prepare a series of metal-cyaphide complexes, presenting an opportunity to explore the cycloaddition chemistry of these organometallic reagents with azides for the synthesis of inorganic mechanically interlocked molecules.

Chapter 2. The cyaphide-azide 1,3-dipolar cycloaddition reaction proceeds rapidly and regioselectively under mild conditions and in the absence of a catalyst to yield the corresponding metal-triazaphosphole complexes in excellent yields. This reaction has been demonstrated with gold(I), magnesium(II), and germanium(II) cyaphide complexes, and the resulting metal-triazaphosphole complexes display enhanced stability. This reaction is reminiscent of the CuAAC reaction and has been extended to bis-azides, providing insight into its potential applicability for the synthesis of mechanically interlocked molecules. The resulting gold(I) triazaphosphole complexes were subject to further functionalisation through Lewis acid coordination, methylation, and halogenation reactions.

Chapter 3. The cyaphide-azide 1,3-dipolar cycloaddition reaction can be used as a capping technique to yield a new class of organometallic [2]rotaxanes. A perethylated pillar[5]arene threads electron-deficient bis-azides, and the generated pseudo[2]rotaxanes were found to readily undergo rapid 1,3-dipolar cycloaddition reactions with two equivalents of (IDipp)Au(CP) to afford [2]rotaxanes in good yields (up to 65%). The resulting interlocked products have enhanced air- and moisture-stability over their non-interlocked counterparts, and can therefore be purified using column chromatography.

Chapter 4. The synthesis of a bis-cyaphide reagent for use in the synthesis of [*n*]catenanes was targeted. We first aimed to prepare dinuclear gold(I) bis-cyaphide complexes through the use of bis-N-heterocyclic carbene (bis-NHC) ligands. Bis-cyaphide complexes of *Janus*-type (facially opposed) bis-NHCs rapidly decompose under an inert atmosphere. Although not isolable, bis-cyaphide complexes of alkyl-bridged bis-NHCs demonstrated improved stability, and could be trapped with an azide to yield the cycloaddition products as adducts of the cyaphide transfer by-product, (^{Dipp}NacNac)MgCl.

Chapter 5. A bis-imidazolium [2]rotaxane can be used to coordinate two gold(I) halide moieties, which can undergo cyaphide transfer. The resulting dinuclear gold(I) bis-cyaphide [2]rotaxane is indefinitely stable under an inert atmosphere in contrast to the related non-interlocked species discussed in Chapter 4. The bis-cyaphide [2]rotaxane can undergo straightforward post-synthetic modification *via* the cyaphide-azide 1 ,3-dipolar cycloaddition reaction, which has been used to generate a new efficient gold(I)-BODIPY photosensitizer for singlet oxygen generation. The conversion of the bis-cyaphide [2]rotaxane into a [2]catenane through its reaction with bis-azides proved challenging due to the rapid nature of the reaction, resulting in the formation of a multitude of cycloaddition products.

Acknowledgements

To my supervisors, Prof. Jose Goicoechea and Prof. Paul Beer: I feel incredibly grateful to have had two excellent supervisors. It was a privilege to be your final Oxford student. Your enthusiasm for my project and constant support has driven me on in the toughest periods. Jose, I will miss our regular teams calls, and always felt your encouragement from across the Atlantic. Paul, I will miss our chats in Oxford and your "crazy ideas". I'm sorry I didn't explore them all.

To my colleagues in the Goicoechea group: Thank you for the constant laughs and support during my time in Oxford. I joined the group at an exciting time, when it was very sociable and full of excellent chemists. I will always cherish the memories of our conference trips to San Sebastián and Vancouver. A special mention to Eric Yang, who taught me pretty much everything I know about cyaphide and synthetic chemistry. I would also like to thank Aaron King and Matt Reveley, who made a difficult period incredibly fun. I will always be grateful for our friendship.

I would also like to thank Prof. Meera Mehta and all the members of her group for making the lab transition seamless. The lab has continued to be a fun and enjoyable work environment during the final months of my DPhil project. I would also like to thank the members of the Beer group, particularly those I have collaborated with, Jamie Wilmore and Andrew Taylor.

To my family and friends: thank you for supporting me in pursuing my DPhil. Although you had no idea what I was doing, I am grateful for your support nonetheless.

Perhaps most importantly, thank you to my partner, Dani, for your endless love and encouragement during my time at Oxford. Meeting you has been the biggest reward from my time in Oxford. Thank you for showing an enormous amount of love and listening to me during the most difficult times – it must have been incredibly frustrating and frankly, quite boring.

List of Abbreviations

Ad	1-adamantyl
AMT	active metal template
anal.	analysis
Anth	anthracene
approx.	approximately
Ar	aryl
Bn	benzyl
BODIPY	boron-dipyrromethene
Bu	butyl
calcd.	calculated
Cp*	1,2,3,4,5-pentamethylcyclopentadienyl
CuAAC	copper(I)-catalysed azide-alkyne click reaction
CuAAC-AMT	copper(I)-catalysed azide-alkyne click active metal template
Cy	cyclohexyl
d	doublet
DBU	1,8-Diazabicyclo[5.4.0]undec-7-ene
DCE	1,2-dichloroethane
DCM	dichloromethane
dcype	1,2-bis(dicyclohexylphosphino)ethane
dd	doublet of doublets
depe	1,2-bis-(diethylphosphino)ethane
1,2-DFB	1,2-difluorobenzene
DFT	density functional theory

diox	dioxane
Dipp	2,6-diisopropylphenyl
^{Dipp}NacNac	Dipp substituted β-diketiminate
	N,*N*-bis(2,6-diisopropylphenyl)-pentane-2,4-diimine
^{Dipp}PDI	Dipp substituted PDI
	1,1′(pyridine-2,6-diyl)bis(*N*-(2,6-diisopropylphenyl)ethan-1-imine)(*N*-(2,6-diisopropylphenyl)vinylamine)
DMAP	4-dimethylaminopyridine
DMF	dimethylformamide
DMSO	dimethylsulfoxide
DOSY	diffusion-ordered spectroscopy
DPBF	diphenylisobenzofuran
dppe	1,2-bis(diphenylphosphino)ethane
en	ethylene diamine
equiv.	equivalents
Et	ethyl
hex	hexane
IDipp	Dipp substituted unsaturated NHC 1,3-bis(2,6-diisopropylphenyl)imidazole-2-ylidene
^{i}Pr	isopropyl
IR	infrared
ISC	intersystem crossing
J	coupling constant
K_a	association constant
KHMDS	potassium bis(trimethyl)silylamide

m	multiplet
Me	methyl
Mes	mesityl
MIM	mechanically interlocked molecule
$NaBAr^F$	sodium tetrakis[3,5-bis(trifluoromethyl)phenyl]borate
NacNac	β-diketiminate
NHC	N-heterocyclic carbene
NMR	nuclear magnetic resonance
P[*n*]A	pillar[*n*]arene
P5A	pillar[5]arene
PDI	pyridine-2,6-diimine
pent	pentane
Ph	phenyl
ppm	parts per million
PS	photosensitizer
p-tol	*para*-tolyl
q	quartet
RCM	ring closing metathesis
RT	room temperature
s	singlet
$^1O_2$	singlet oxygen
sept	septet
SOC	spin-orbit coupling
t	triplet
TBA	*tetra*-n-butylammonium

^{t}Bu	*tert*-butyl
THF	tetrahydrofuran
Tf	triflate
TLC	thin layer chromatography
TMS	trimethylsilane
tol	toluene
UV	ultraviolet
vis	visible

List of Compounds

1a	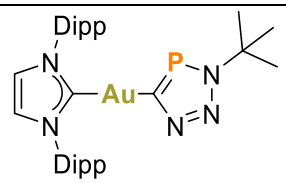
1b	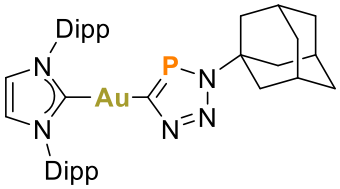
1c	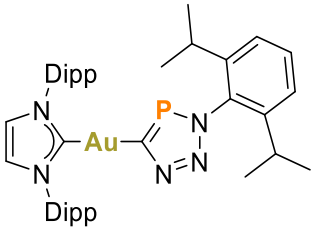
2	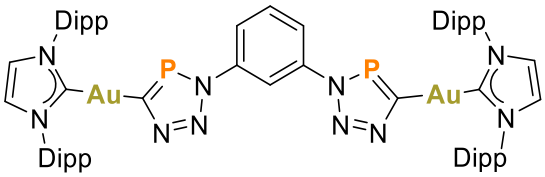
3a	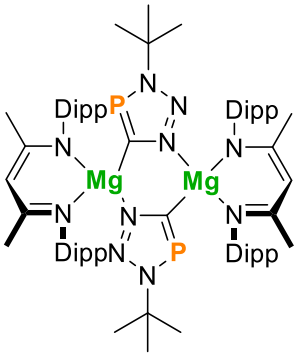

3b	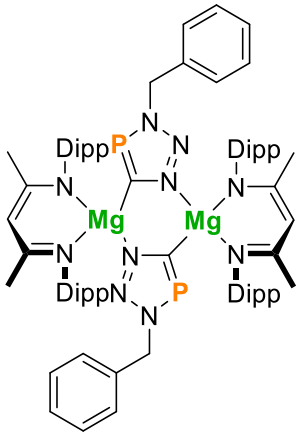
3c	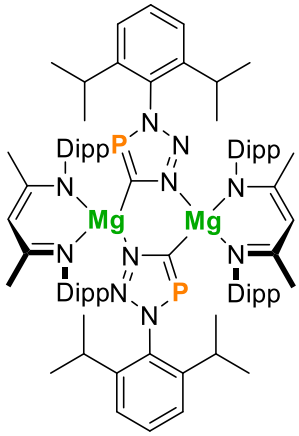
4	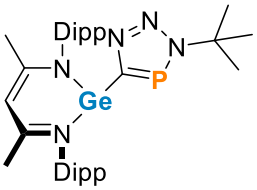
5a	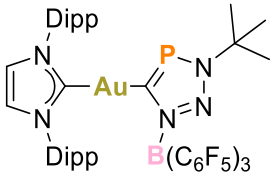
5c	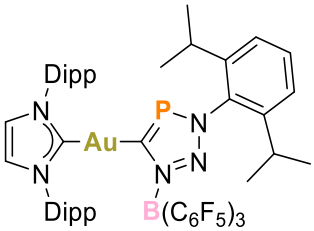

6	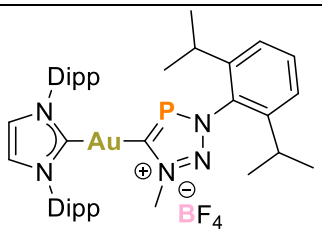
7a	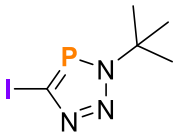
7b	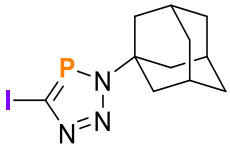
7c	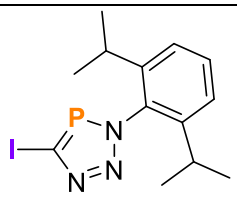
8a	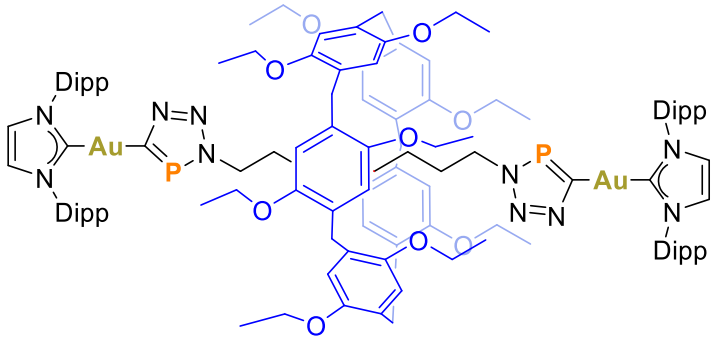
8b	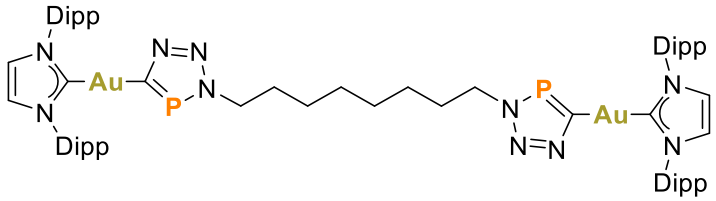
9	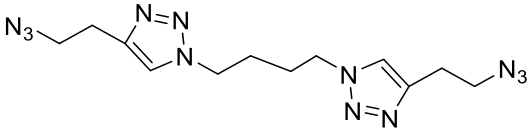

10a	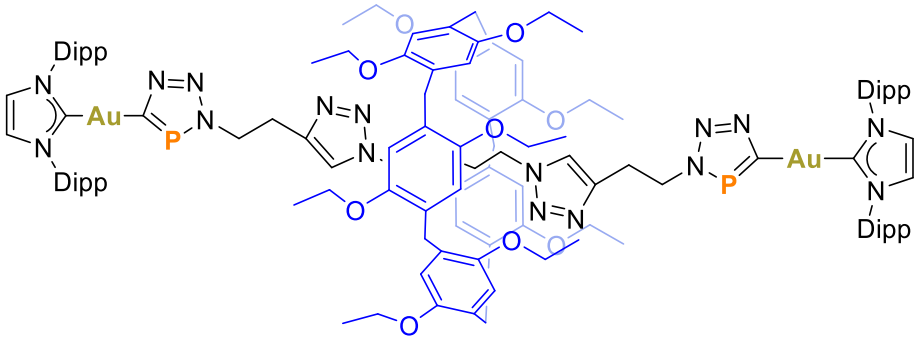
10b	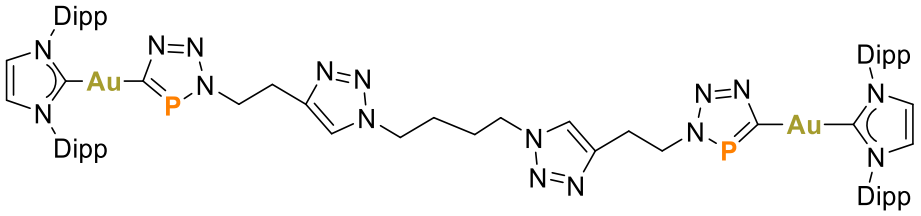
[11]	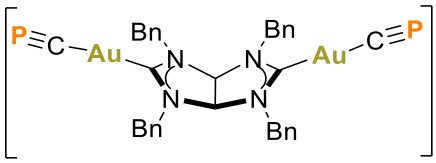
12	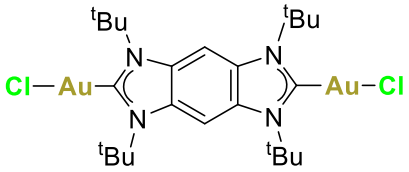
[13]	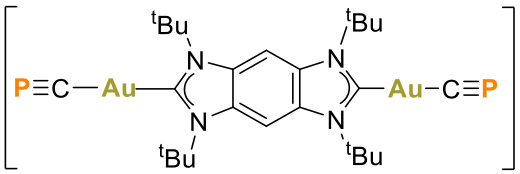
[14]	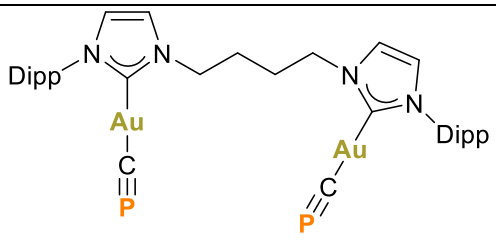

15	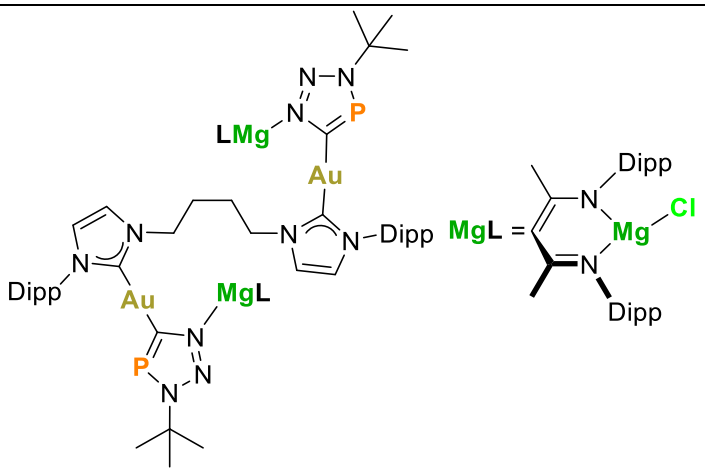
16	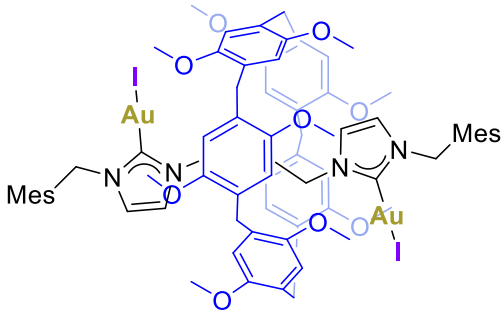
17	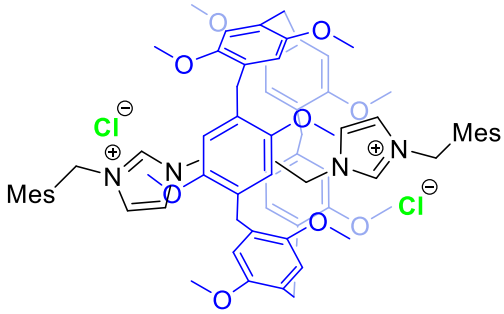
18	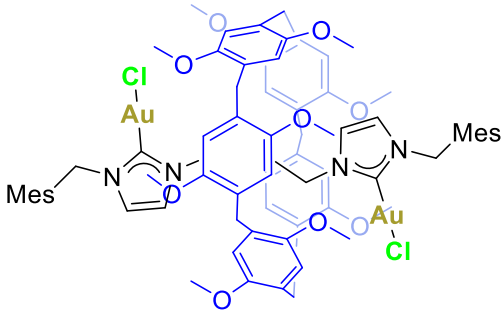

19	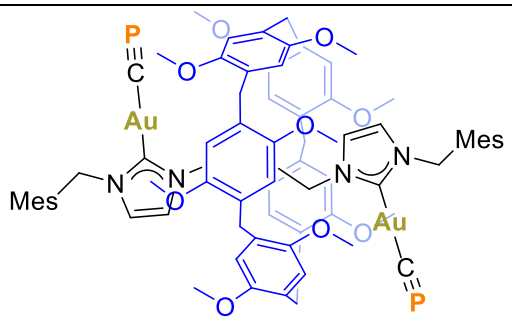
20a	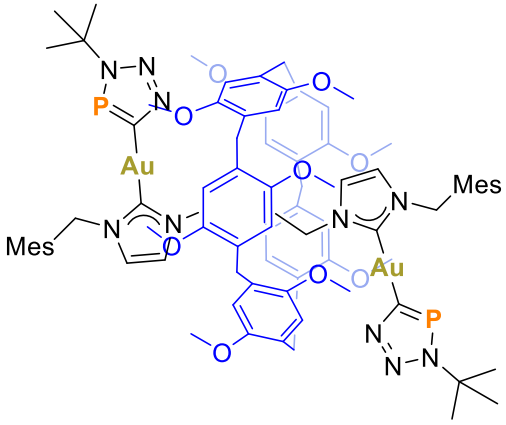
20b	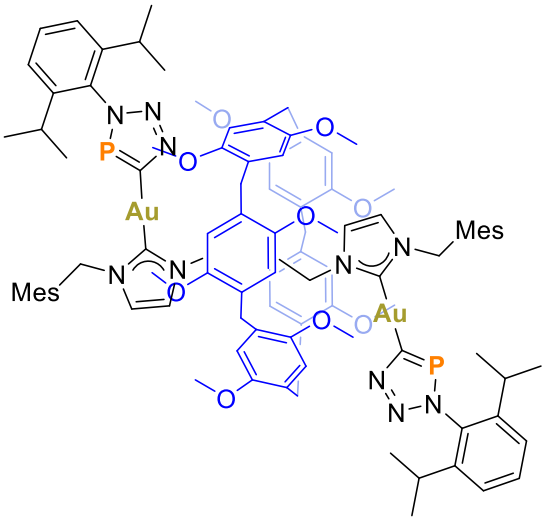

21	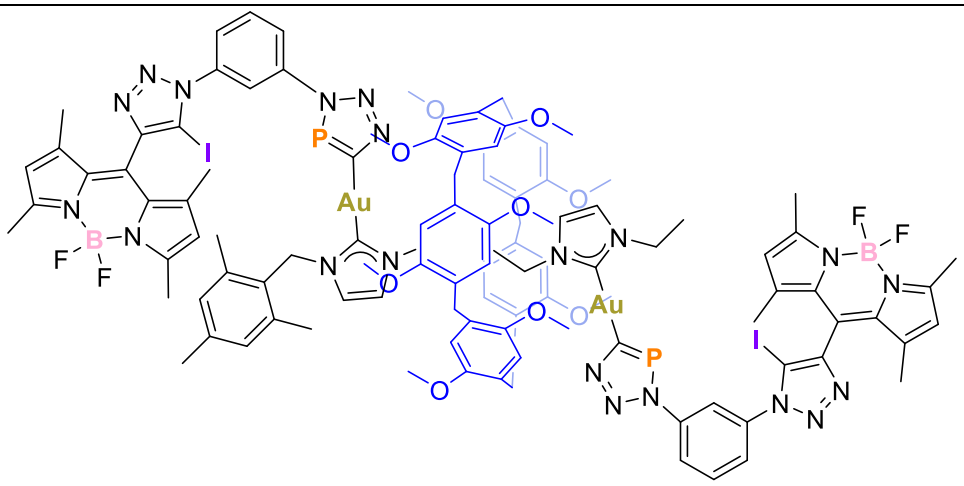

Table of contents

Cyaphide-azide 1,3-Dipolar Cycloaddition Reactions

Synthesis and Reactivity of a Dinuclear Gold(I) Bis-cyaphide [2]Rotaxane

Chapter 1

Introduction

Abstract

The high-yielding synthesis of mechanically interlocked molecules requires both a templating strategy in which the molecular components are organised into an interlocked manner and an efficient covalent bond forming reaction to trap the final product. The copper-catalysed azide-alkyne click reaction is popular in an active-metal templating approach, where the copper(I) ion fulfils both criteria. Whilst metal ions have been used as catalysts and/or templates for the synthesis of mechanically interlocked molecules, they are rarely incorporated into the final product due to the lack of general covalent bond forming strategies involving inorganic species. The isolobal analogy can be used to relate the copper-catalysed azide-alkyne click reaction with the phosphaalkyne-azide and cyaphide-azide 1,3-dipolar cycloaddition reactions. The former has been used to prepare a new class of triazaphosphole ligands; however, the latter is limited to a single literature example. The cyaphide transfer reagent, (^{Dipp}NacNac)Mg(CP)(dioxane), can be used to prepare a series of metal-cyaphide complexes, presenting an opportunity to explore the cycloaddition chemistry of these organometallic reagents with azides for the synthesis of inorganic mechanically interlocked molecules.

1.1 Mechanically interlocked molecules

Mechanically interlocked molecules (MIMs) are a type of supramolecular architecture that possess a mechanical bond. This unique bond has been defined by Bruns and Stoddart as "*an entanglement in space between two or more molecular entities (component parts) such that*

they cannot be separated without breaking or distorting chemical bonds between atoms".[1] The archetypal examples of MIMs are [*n*]rotaxanes and [*n*]catenanes (**Figure 1.1**), where *n* denotes the number of molecular components that are mechanically interlocked. The most common form of a MIM, a [2]rotaxane, consists of a macrocycle encapsulating a dumbbell-shaped axle featuring bulky stoppers at each end, which prevent the axle from escaping the macrocyclic cavity ("dethreading"). Higher order [*n*]rotaxanes usually contain more than one macrocycle locked onto an axle. An [*n*]catenane consists of *n* macrocycles that are linked together like rings in a chain.

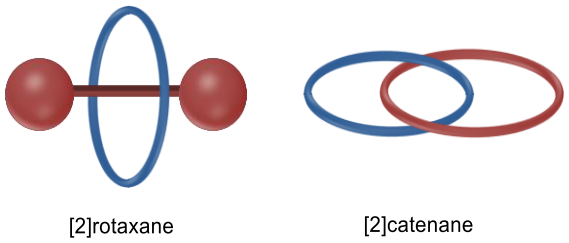

Figure 1.1. Cartoon representation of a [2]rotaxane and [2]catenane.

The identification of high-yielding and facile synthetic routes to form MIMs has been challenging due to the inherent difficulty of spatially arranging two or more molecular components prior to the formation of a mechanical bond. Due to their unique topology, MIMs have found applications as molecular machines,[2] catalysts,[3] dyes,[4] and molecular sensors.[5]

1.1.1 Synthesis of organic mechanically interlocked molecules

Wasserman reported the first synthesis of a MIM in the 1960s,[6] *via* a statistical approach, essentially relying on the fact that a small portion of the starting materials would be in an interlocked conformation prior to the execution of a ring-closing reaction. An acyloin condensation reaction afforded a [2]catenane in 0.0001% yield, determined by detection of deuterium in the product by infrared (IR) spectroscopy (**Scheme 1.1**). The authenticity of the

reported [2]catenane formation was heavily debated at the time due to the extraordinarily low yield and lack of experimental evidence.[7] Its formation was confirmed by Leigh in 2023.[8]

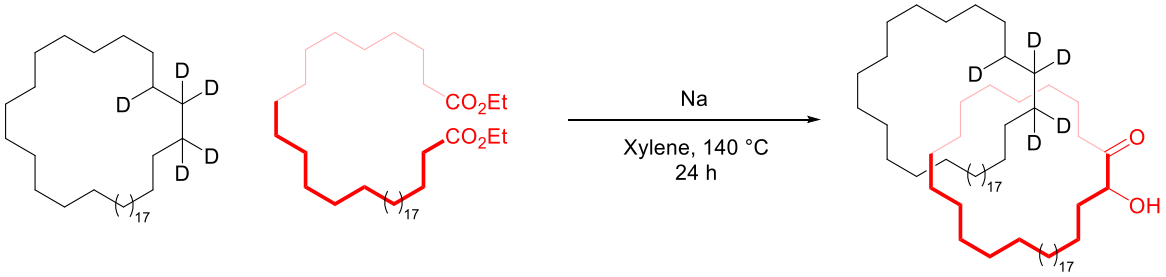

Scheme 1.1. Wasserman's statistical [2]catenane synthesis.[6] Et = ethyl.

In 1983, Sauvage and co-workers described the passive copper(I) ion templated synthesis of a [2]catenane, demonstrating for the first time the use of non-covalent interactions to overcome the difficulty of pre-arranging the molecular components (**Scheme 1.2**).[9] A homoleptic bis-phenanthroline complex is formed about the copper(I) ion, arranging the molecular components in an orthogonal manner such that they can form a [2]catenane following double ring-closure by Williamson ether synthesis in 27% yield (**Scheme 1.2a**). Utilising a preformed macrocycle as one of the molecular components and threading the other through its cavity to form a pseudo[2]rotaxane before ring-closing afforded higher yields (42%) for [2]catenane formation due to a higher degree of pre-organisation (**Scheme 1.2b**).[9]

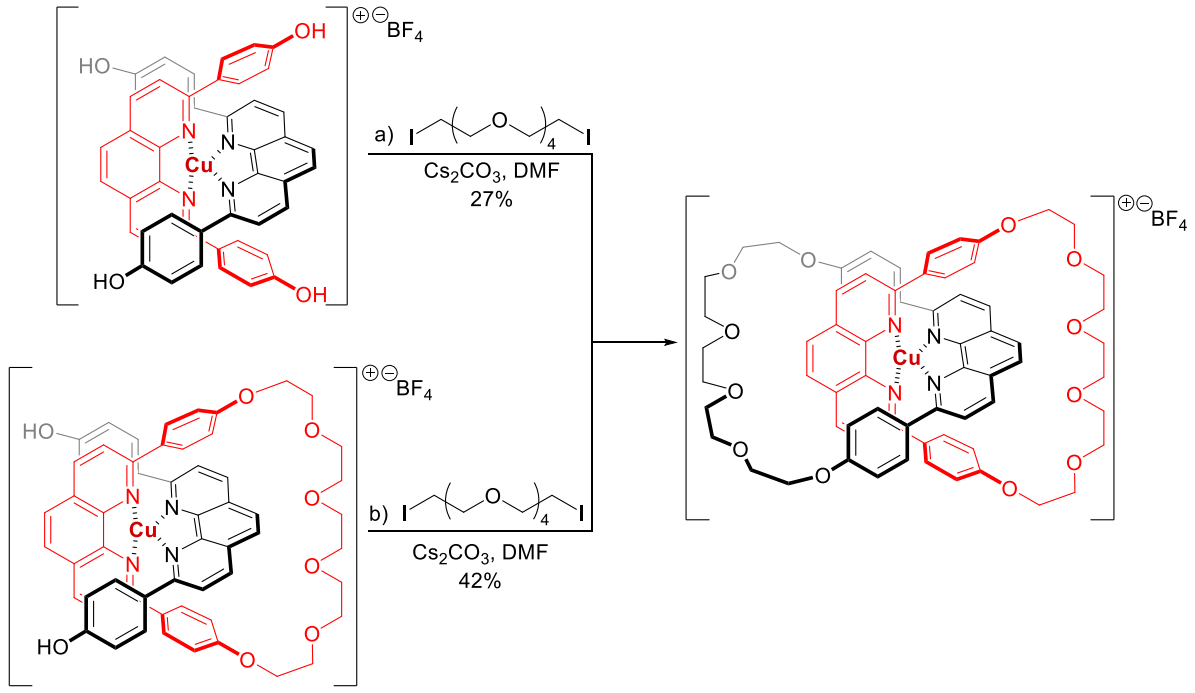

Scheme 1.2. Sauvage's Cu(I) templated synthesis of a [2]catenane.[9] Metal-ligand interactions are depicted as dashed bonds. DMF = dimethylformamide.

This led to further developments in passive templating approaches through the use of various transition metal templates with different coordination geometries (**Figure 1.2**).[10] Examples include linear gold(I),[11] square planar palladium(II),[12] trigonal bipyramidal zinc(II),[13] and various octahedral transition metals.[14,15] This has also been extended to lanthanides[16] and main group metals (e.g. sodium crown ether templation).[17–20] Other non-covalent interactions that do not involve metals have been used to arrange the molecular components, such as π-π stacking,[21] hydrogen bonding,[22] anion templation,[23] ion-dipole interactions,[24] and ion-ion interactions.[25]

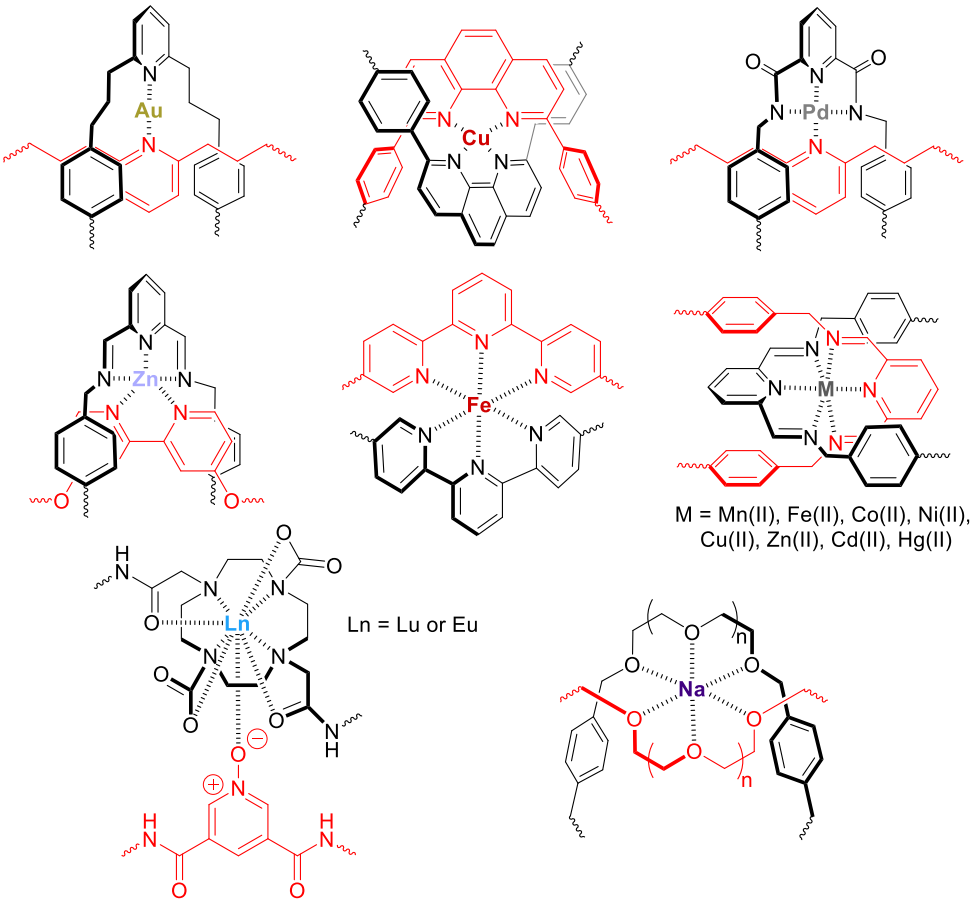

Figure 1.2. Various metal ion templates for the synthesis of mechanically interlocked molecules.

In 2006, Leigh and co-workers took full advantage of the versatile chemistry of copper(I), by using it both as a template to organise the molecular components, as well as catalysing the bond forming reaction to form a MIM.[26,27] In this active metal template approach (AMT), a copper(I) ion coordinated within the cavity of the macrocycle was used to catalyse an azide-alkyne "click" reaction between two half axles to form the [2]rotaxane. The AMT approach can proceed both stoichiometrically and catalytically (**Figure 2**). Since this development, a series of transition metal-catalysed AMT reactions have been used to access MIMs.[28]

The three general templating approaches for the synthesis of MIMs can be summarised as follows (**Figure 1.3**):[29]

i) Capping at each end of a templated pseudorotaxane assembly *via* the attachment of bulky groups to form a [2]rotaxane;

ii) Clipping of an acyclic ligand around the template site of a stoppered thread (rotaxane) or macrocycle (catenane);

iii) The active metal template approach, in which the templating species also plays a role in the covalent bond formation to form the interlocked structure.

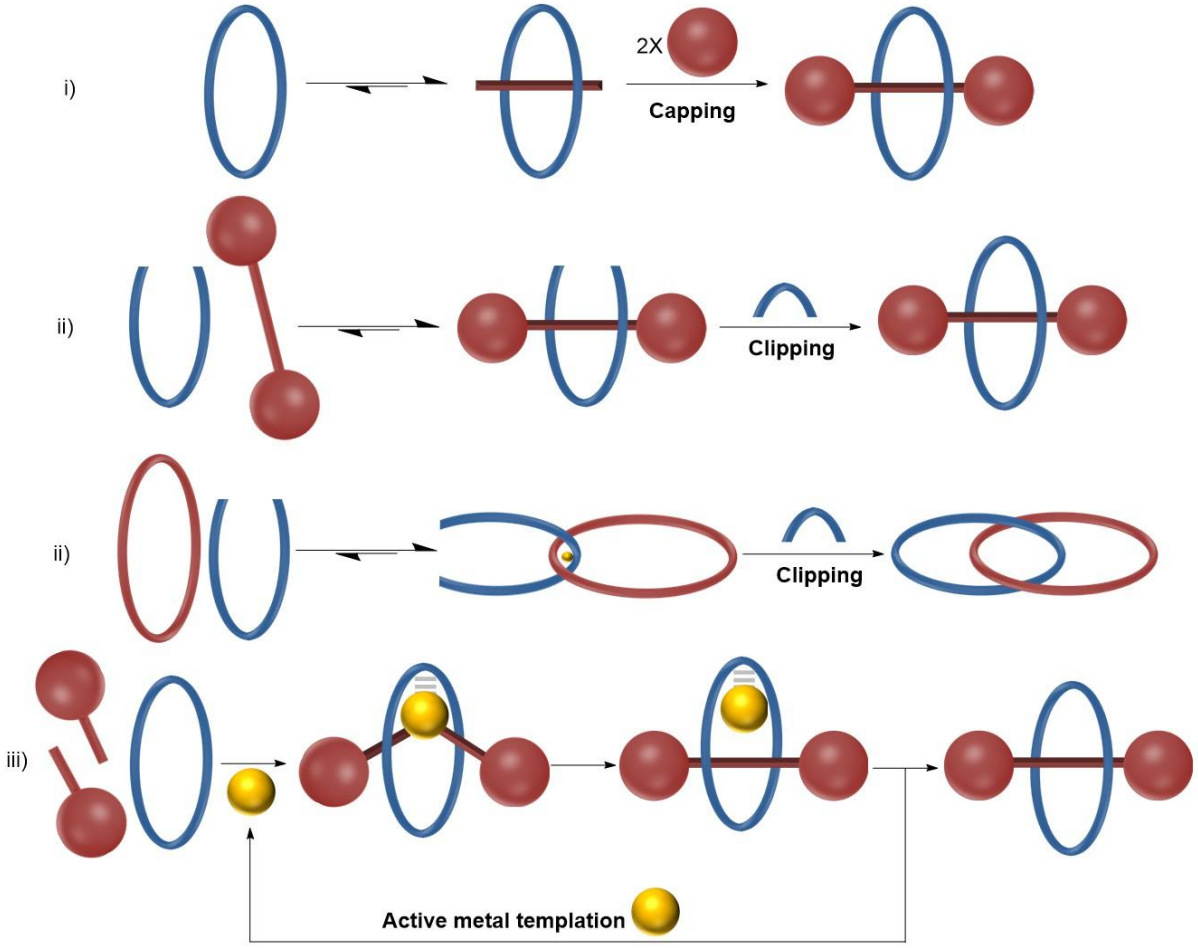

Figure 1.3. Cartoon schematic of three general templating approaches for the synthesis of [2]catenanes and [2]rotaxanes. Reproduced from reference 29.

The copper(I)-catalysed azide-alkyne "click" (CuAAC) reaction has become a widely used reaction for the synthesis of mechanically interlocked molecules.[30] The broad applicability of the CuAAC reaction is owed to its many advantages, namely, its functional group tolerance,

facile execution, mild reaction conditions, and excellent selectivity.[31] It can also be carried out in non-polar solvents, which maximise the non-covalent interactions in the templating strategy. It is a catalytic variant of the Huisgen 1,3-dipolar cycloaddition reaction between azides and alkynes, which produces a mixture of the 1,4- and 1,5- regioisomers of the 1,2,3-triazole (**Scheme 1.3**).[32] However, the CuAAC reaction, independently reported by Meldal and Sharpless, produces the 1,4-regioisomer selectively, owing to a different mechanism.[33,34] The regioselective synthesis of the 1,5-disubstituted 1,2,3-triazole has been achieved by ruthenium(II) catalysis.[35]

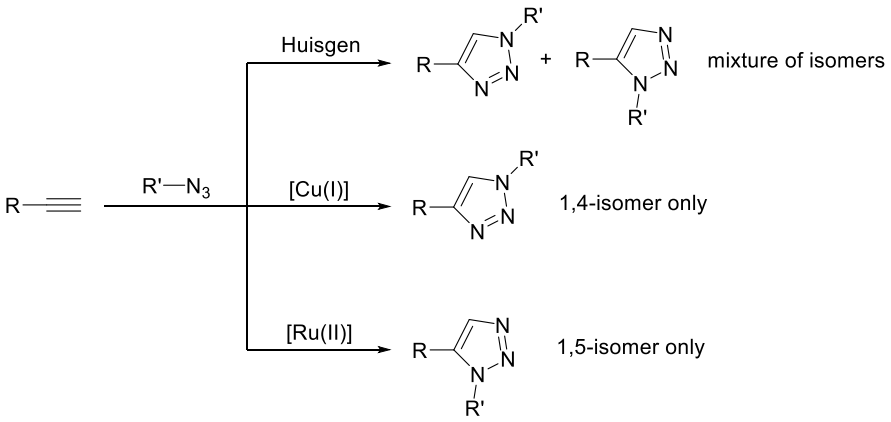

Scheme 1.3. Huisgen 1,3-dipolar cycloaddition reaction between an azide and an alkyne to produce a mixture of regioisomers. The copper(I) and ruthenium(II) catalysed variants produce only the 1,4- and 1,5-regioisomers, respectively.

Leigh and co-workers optimised the CuAAC-AMT strategy by stirring a mixture of a macrocycle, $[Cu(MeCN)_4]PF_6$, an alkyne (5 equiv.), and an azide (5 equiv.) in dichloromethane (DCM) for 24 hours, followed by demetallation with KCN, to synthesise [2]rotaxane in an impressive 94% yield (**Scheme 1.4**).[26] Addition of pyridine as a competing ligand allowed the copper(I) species to turn over catalytically, producing the [2]rotaxane in 82% yield (**Scheme 1.4)**. The versatility of this strategy has since been demonstrated for the synthesis of a wide range of copper(I) coordinating macrocycles.[27]

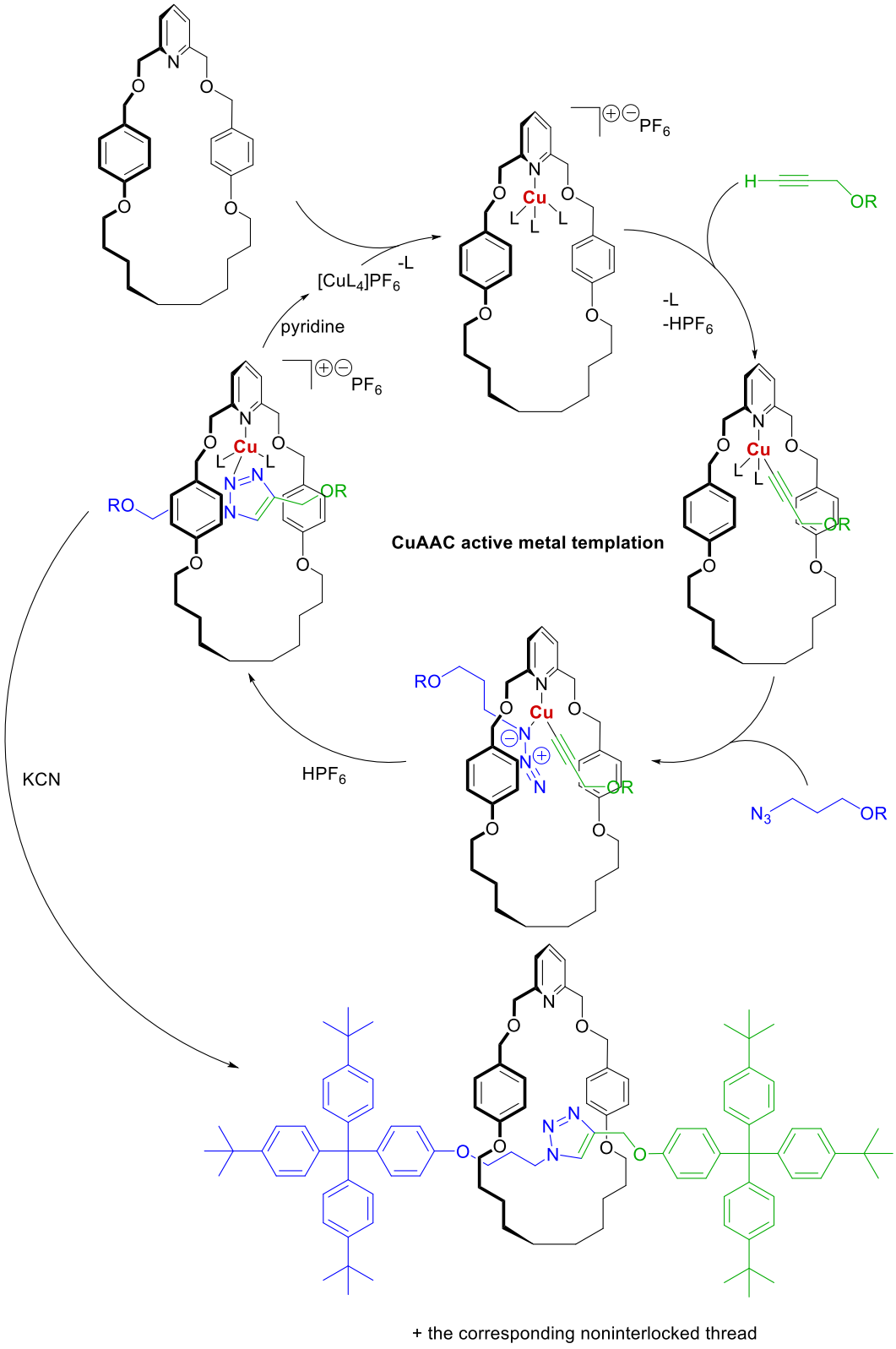

Scheme 1.4. Catalytic cycle for the CuAAC-AMT synthesis of a [2]rotaxane. Reproduced from reference 27.

Grubbs' catalysed ring-closing metathesis (RCM) of alkenes is also a popular reaction for the synthesis of MIMs in high yields, as it possesses similar advantages to the CuAAC reaction.[36,37] Prior to the discovery of these two reactions, the synthesis of MIMs was met with great difficulty due to ineffectiveness of the covalent bond forming reactions used (Williamson ether synthesis, amide/ester bond formation, Glaser and Eglinton couplings, imine-bond formation, metal-ligand coordination, and the Menschutkin alkylation of pyridines with alkyl halides), resulting in poor yields.

1.1.2 Synthesis of inorganic MIMs

As outlined in the previous sections, the synthesis of MIMs is inherently difficult without effective templating methods and covalent bond forming reactions to capture the MIM. The popularity of the CuAAC reaction in the active metal template approach is because it meets both criteria.

Although a variety of transition metals have played a prominent role in the templated synthesis of MIMs, they are rarely incorporated into the final product in a permanent fashion due to the lack of suitable covalent bond forming reactions involving inorganic species. Metal-ligand coordination as a capping technique was pioneered by Ogino, who showed that dative bond formation between a cobalt(III) complex and the amine end-groups on the axle of a pseudo[2]rotaxane produced the resulting [2]rotaxanes, albeit in very low yields (ca. 7%) (**Scheme 1.5**).[38] Ogino then went on to show that yields could be improved to 19% by tuning the size of the macrocycle and axle.[39] Since then, MIMs have been used as ligand linkers for the preparation of metal organic rotaxane frameworks through dative bond formation.[40–42]

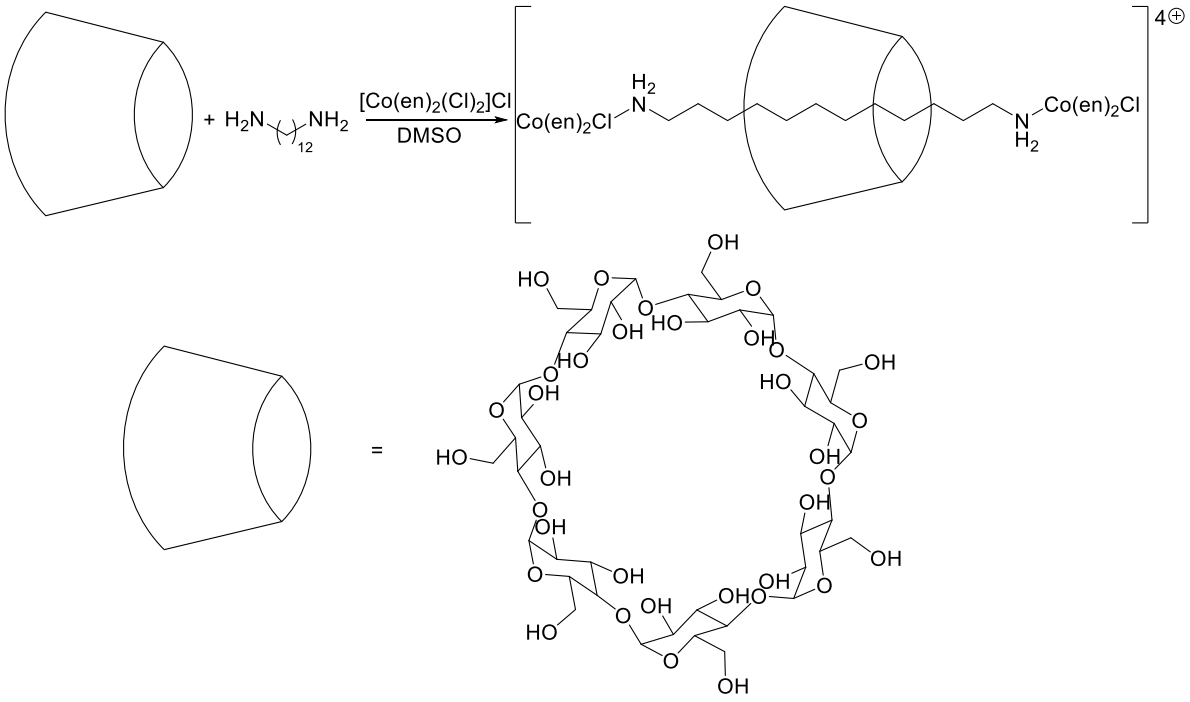

Scheme 1.5. Ogino's synthesis of a [2]rotaxane via dative bond formation with Co(III) complexes.[38]

en = ethylene diamine.

A benefit of metal-ligand dative bond formation in the synthesis of MIMs can be its reversibility, allowing them to be prepared under thermodynamic control. Under equilibrium conditions, the self-assembly of the MIM is driven by secondary non-covalent interactions, often leading to much higher yields. This was first demonstrated by Fujita, who prepared a palladium(II) [2]catenane in high yields (>90% as determined by ^{1}H NMR in D_2O) by dissolving the corresponding metallocycle at high concentrations (>50 mM) (**Scheme 1.6**).[43] At low concentrations (1 mM), the palladium(II) macrocycle is only species present in solution.

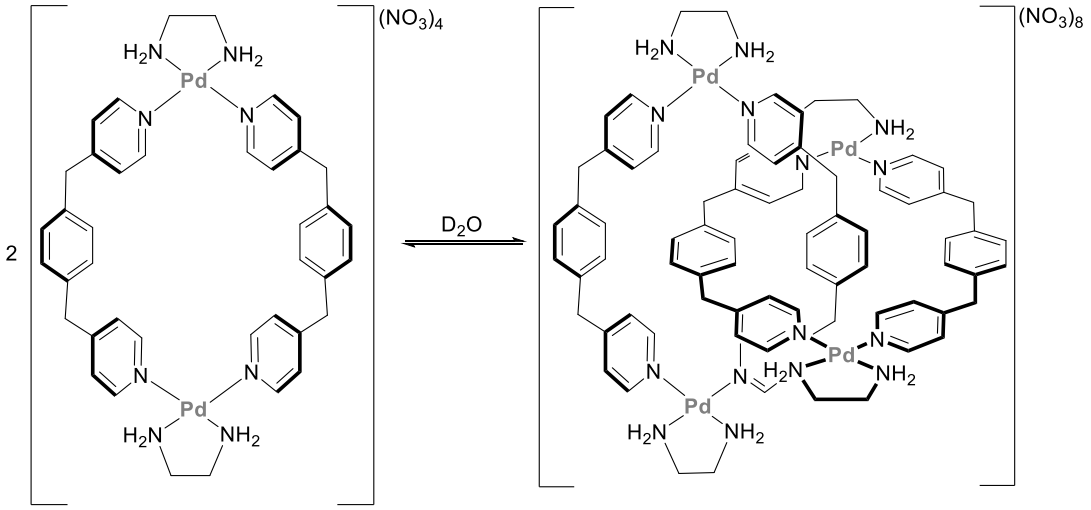

Scheme 1.6. Fujita's synthesis of a palladium(II) [2]catenane under thermodynamic control.[43]

The lability of the palladium(II)-pyridine dative bonds allows them to be broken so that the interlocked structure can be formed through π-π interactions and the hydrophobic effect, before reforming again to yield the resulting [2]catenane. Employing a more polar solvent medium (1 M $NaNO_3$ in D_2O) resulted in the quantitative formation of the palladium(II) [2]catenane, even at low concentration (10 mM), due to an enhanced hydrophobic effect.

The reversibility of [2]catenane formation was confirmed by control experiments with the analogous platinum(II) complex at high concentration (70 mM). In contrast to the aforementioned palladium(II) complex, the platinum(II) species forms dative bonds with pyridine irreversibly.[44] In this case, the corresponding catenane was formed in significantly lower yields (ca. 12% by ^{1}H NMR in D_2O) as the kinetic products (the metallacycle and oligomeric species) are preferentially formed. Furthermore, dilution did not influence the product ratios. Heating the platinum(II) metallacycle in highly polar media (5 M $NaNO_3$) labilises the platinum(II)–pyridine dative bonds and allows the [2]catenane to be formed quantitatively (by ^{1}H NMR spectroscopy).[45] Once formed, the platinum(II) [2]catenane does not dissociate into two macrocycles, even after heating in D_2O. This provides unequivocal

evidence that the reversibility of [2]catenane formation for the palladium(II) complex is a result of breaking and reforming the palladium(II)–pyridine bonds.

The use of metal-ligand coordination to prepare [2]rotaxanes *via* self-assembly has been demonstrated by Wisner and co-workers.[46] In this case, the lability of palladium(II)–pyridine dative bonds in the non-interlocked axle was exploited in combination with a macrocycle to yield a rotaxane in good yield (76%) after five days (**Scheme 1.7**). This self-assembly is driven by hydrogen bond templation between N–H bonds on the macrocycle and the additional thiocyanate ligands on the palladium(II).

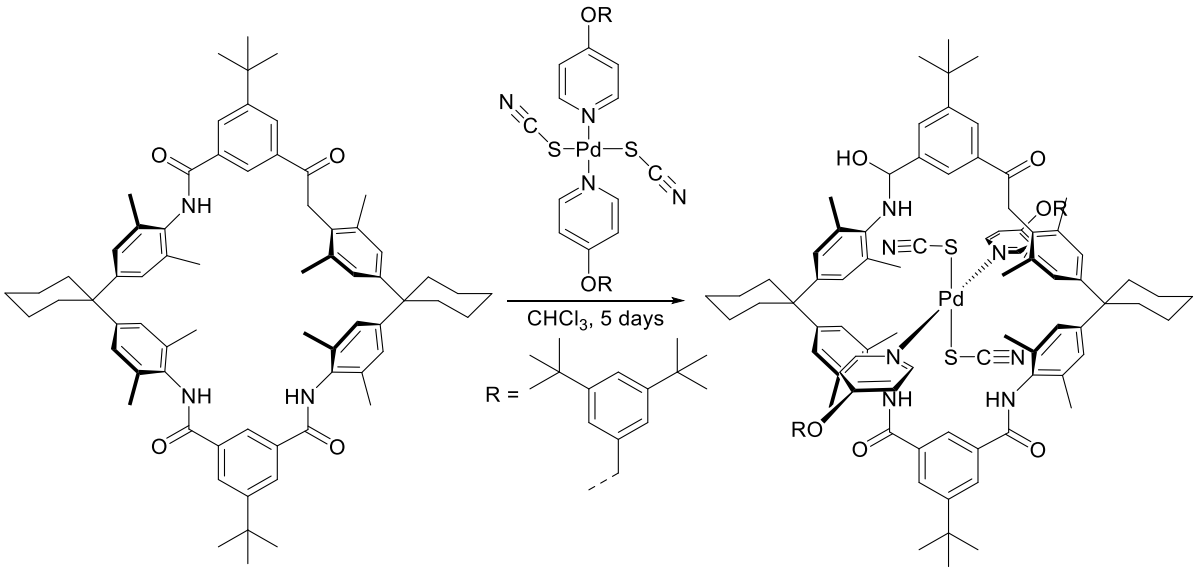

Scheme 1.7. Wisner's synthesis of a [2]rotaxane *via* the metal-ligand self-assembly of an inorganic axle into a macrocycle.[46]

Leigh and Winpenny demonstrated the preparation of hybrid organic-inorganic rotaxanes in 23% yield from the self-assembly of heterometallic rings around an ammonium cation axle (**Scheme 1.8**).[47] The formation of the interlocked molecules is driven by hydrogen bonds between the bridging fluoride ligands in the ring and the N–H bonds of the axle.

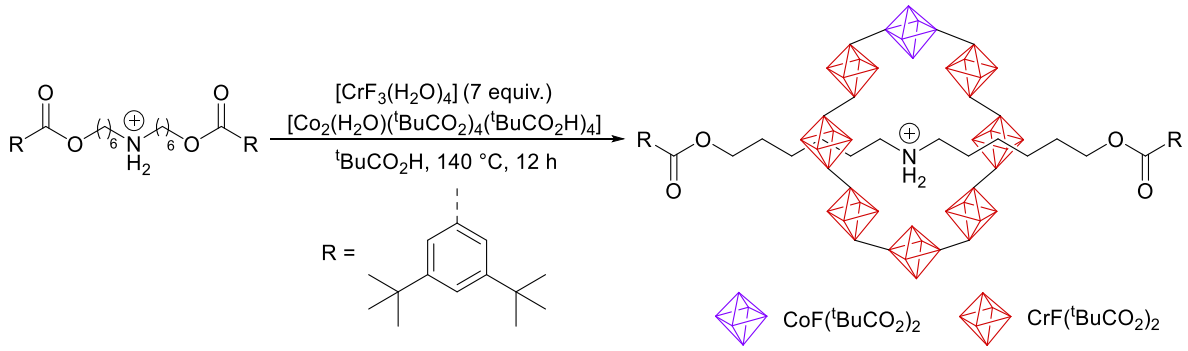

Scheme 1.8. Leigh and Winpenny's synthesis of a hybrid inorganic-organic [2]rotaxane *via* the metal-ligand self-assembly of an inorganic macrocycle around an ammonium axle.[47] ^{t}Bu = tert-butyl.

Another method to introduce inorganic species into MIMs is through their post-synthetic modification. This route presents its own challenges, as it can be difficult to prepare MIMs with reactive functionalities whilst also maintaining the mechanical bond during a post-synthetic modification step.[48] A notable report of this route from Goldup discloses a stimuli-responsive [2]rotaxane–gold catalyst.[49] The [2]rotaxane was synthesised *via* the CuAAC-AMT strategy, with the axle containing a phosphine oxide moiety that was subsequently reduced and coordinated to a gold(I) chloride (**Scheme 1.9**). It is worth noting that this approach uses a small-macrocycle modification of the CuAAC-AMT strategy,[50] where the phenyl groups of the phosphine are sufficiently bulky to act as a stopper.

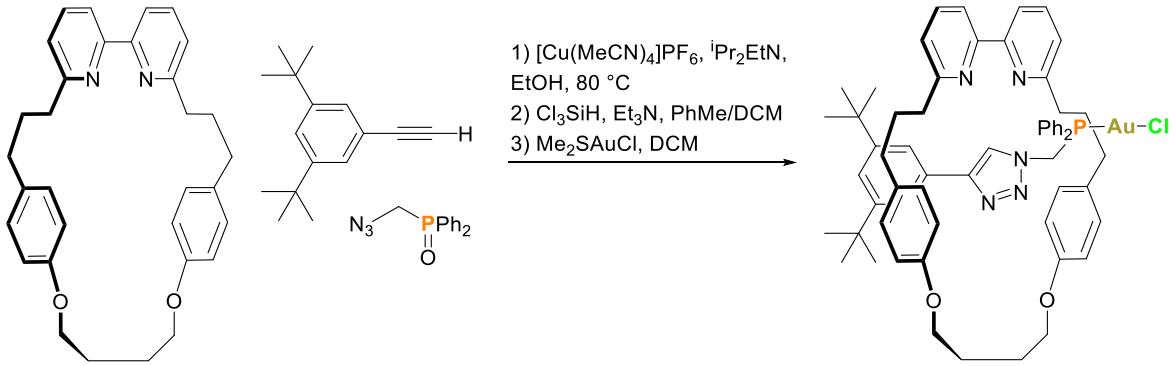

Scheme 1.9. Goldup's post modification of a [2]rotaxane to coordinate gold(I) chloride.[49] Me = methyl and Ph = phenyl.

The mechanical bond in the [2]rotaxane stabilised the electron-rich phosphine moiety against oxidation, as it required no special handling, whilst the corresponding non-interlocked structure was air-sensitive and reverted back to the phosphine oxide upon standing in $CDCl_3$. This highlights the additional difficulties of introducing reactive main group centres into MIMs such as phosphorus(III). In the presence of copper(I) or zinc(II) guest ions, the gold(I) [2]rotaxane was found to be a highly active and selective catalyst for Toste's gold(I) modification of the Ohe-Uemura cyclopropanation reaction between an alkyne and alkene.[51,52]

The incorporation of organometallic metal complexes into MIMs through the formation of non-dative covalent bonds, which are intrinsically less labile, is comparatively rare due to the lack of useful protocols. This is where covalent bond formation occurs at the ligand rather than the metal, and has predominantly relied on the use of molecular subcomponents containing alkynyl groups. Gladysz has prepared rotaxanes by the homocoupling of two platinum(II) butadiynyl half-axles within the cavity of a macrocycle, where the optimum yield (41%) depends on the length of the axle (**Scheme 1.10**).[53,54]

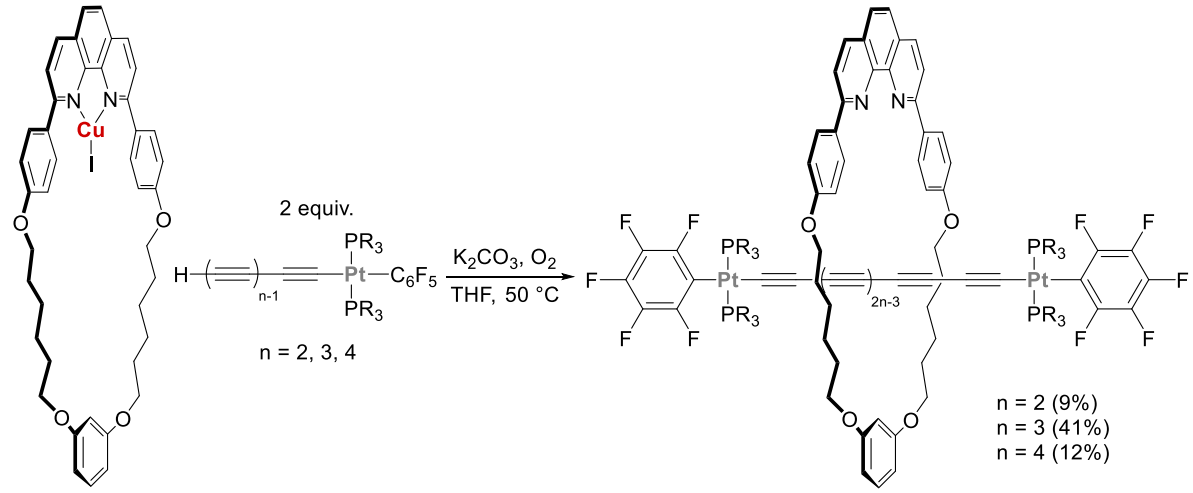

Scheme 1.10. Gladysz's alkynyl homocoupling of two organometallic platinum(II) half axles to yield a [2]rotaxane.[53,54] R = *para*-tolyl.

Wang used a similar protocol by capping the alkynyl end group of a pseudo[2]rotaxane with a platinum (II) complex, *trans*-$Pt(PEt_3)_2I_2$, to yield the corresponding [2]rotaxane in excellent yields (86%).[55] This was then used as a building block to construct more complex organometallic rotaxane-based dendrimers.

There is also the possibility of incorporating metals into one of the interlocked components before forming the MIM. Pöthig has shown that the unique silver(I) organometallic pillarplex macrocycles display excellent host-guest properties with long-chain aliphatic bis-amines and subsequently reported that they can be used to prepare [2]rotaxanes in near quantitative yields (98%) through condensation capping reactions (**Scheme 1.11**).[56,57]

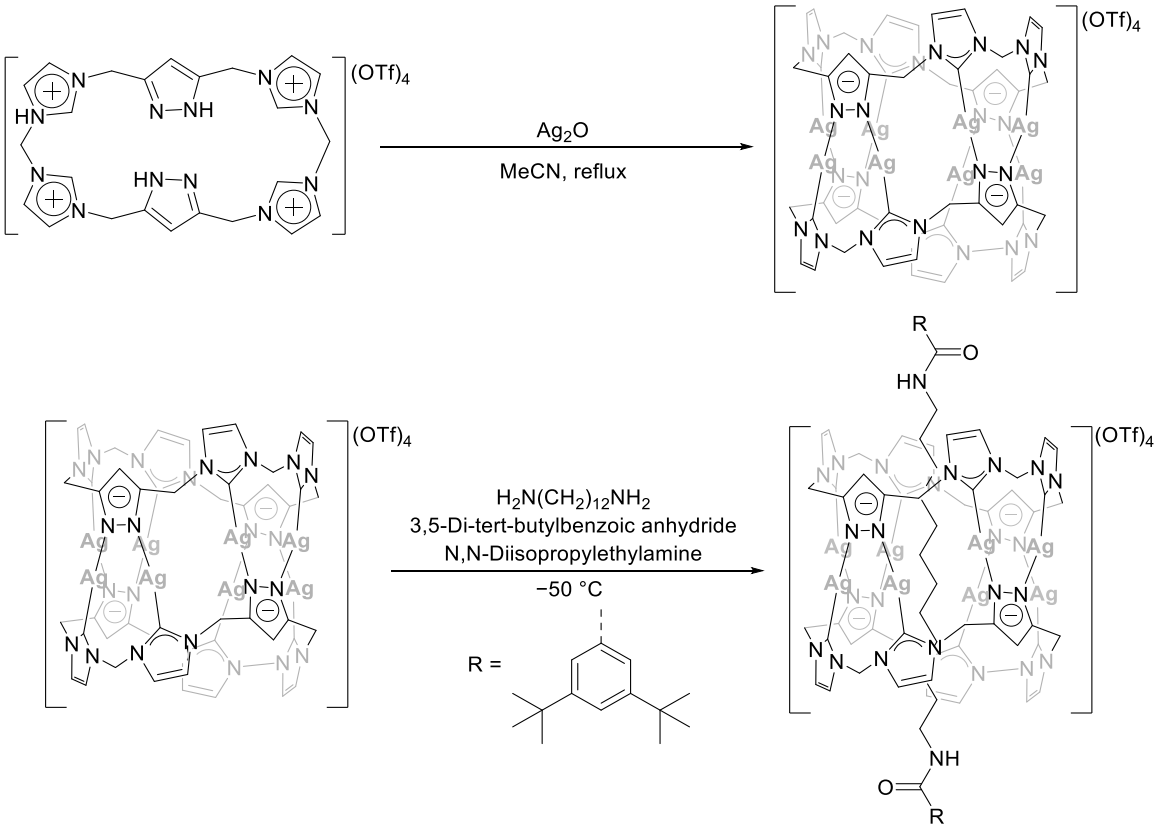

Scheme 1.11. Pöthig's synthesis of a silver(I) pillarplex macrocycle (top) and the subsequent synthesis of a silver(I) pillarplex [2]rotaxane.[56,57] OTf = triflate.

The resulting silver(I) [2]rotaxane can undergo a transmetallation reaction to produce the corresponding gold(I) [2]rotaxane in excellent yields (88%) (**Scheme 1.12, top**). Remarkably, the silver(I) atoms can be reversibly removed by an acid-base reaction to produce the entirely organic [3]rotaxane (**Scheme 1.12, bottom**).

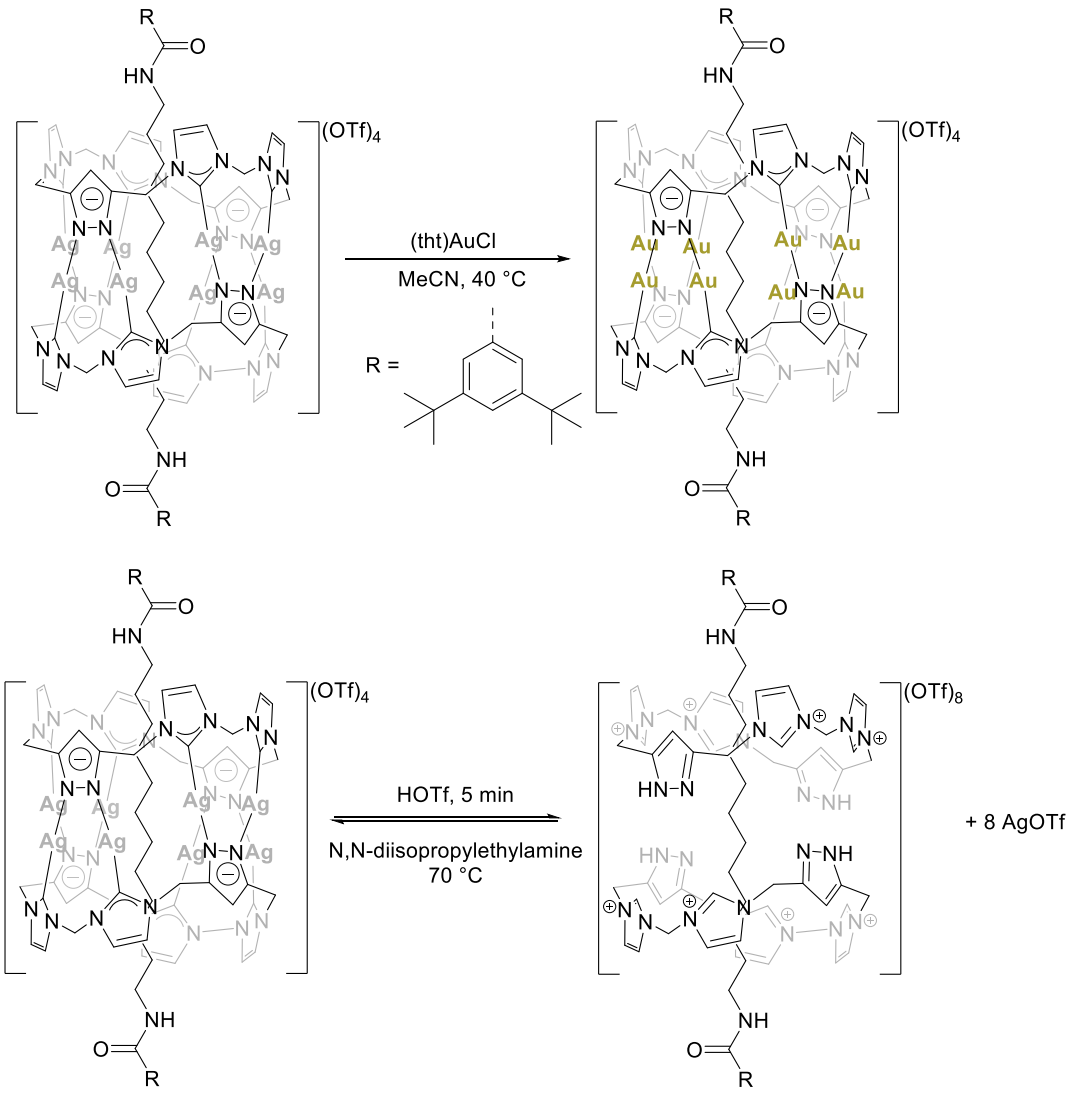

Scheme 1.12. Transmetallation of a [2]rotaxane and pH-dependent interconversion between a [2]- and [3]rotaxane *via* demetallation of the silver(I) pillarplex macrocycle.[57] tht = tetrahydrothiophene.

1.2 Synthesis of 3H-1,2,3,4-triazaphosphole derivatives

According to the isolobal analogy, the sp^2 C−H fragment in aromatic species can be replaced by a trivalent phosphorus atom, which has allowed chemists to envisage and successfully

prepare novel phosphorus-containing heterocycles.[58] 1,4-Disubstituted 1,2,3-triazoles are common motifs in MIMs due to the popularity of CuAAC reactions, and are isolobal to the 3,5-disubstituted 3H-1,2,3,4-triazaphosphole (**Figure 1.4**). Retrosynthetic analysis of these aromatic heterocycles can be used to identify appropriate reactants for their synthesis, which are also isolobal. In this case, phosphaalkynes (R−C≡P) are the phosphorous-containing heavy analogues of alkynes, whilst the cyaphide ion (C≡P$^-$) is the heavy analogue of the acetylide ion, an intermediate in the CuAAC reaction.

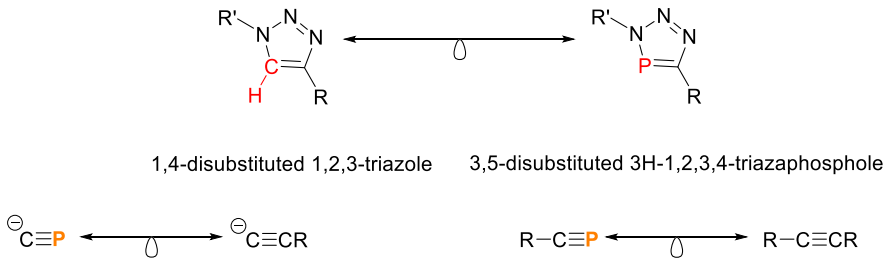

Figure 1.4. Phosphorus-containing species that are isolobal to species in the CuAAC reaction.

The phosphorus analogues are in violation of the classical "double bond rule",[59,60] in that their π-bonds are the result of relatively inefficient 2p–3p orbital overlap and are therefore weaker. Compounds containing carbon-phosphorus multiple bonds are often very reactive, making their preparation a significant challenge.[61]

1.2.1 Phosphaalkyne-azide 1,3-dipolar cycloaddition reaction

Based upon the isolobal analogy, the 3,5-disubstituted 3H-1,2,3,4-triazaphospholes can be prepared by replacing the alkyne with a phosphaalkyne in the Huisgen 1,3-dipolar cycloaddition reaction. This was first reported independently by Regitz and Carrie in 1984 (**Scheme 1.13**),[62,63] and relied on the use of *tert*-butyl phosphaalkyne (^{t}Bu−C≡P), a kinetically stable phosphaalkyne that can be readily prepared at room temperature.[64] Subsequent examples of this reaction featured phosphaalkynes with other large alkyl groups (1-adamantyl (Ad),[65]

isopropyl (^{i}Pr),[66] neopentyl ($CH_2{}^{t}Bu$),[66] 1-methyl-1-cyclohexyl,[66] 1-methyl-1-cyclopentyl,[66] and mesityl (Mes)).[67] A 1,5-shift was observed where (R′ = trimethylsilane (TMS) or H).[68]

It is interesting to note that, in contrast to the Huisgen 1,3-dipolar cycloaddition reactions, the reaction between phosphaalkynes and organic azides proceeds in the absence of a catalyst to produce a single regioisomer of the 3H-1,2,3,4-triazaphosphole derivative, even when sterically demanding R groups are omitted (with the exception of H and TMS). Therefore, the regioselectivity is attributed to electronic effects, despite the small difference in Pauling electronegativities between phosphorus (2.19) and carbon (2.55).[68]

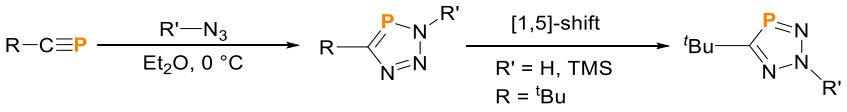

Scheme 1.13. A 1,3-dipolar cycloaddition reaction between organic azides and kinetically stabilised phosphaalkynes produces a 3H-1,2,3,4-triazaphosphole derivative. In certain cases (R′ = H or TMS and R = ^{t}Bu) a [1,5]-shift of the R′ group was observed.[62–68] R = ^{t}Bu, Ad, ^{i}Pr, $^{t}BuCH_2$, 1-methyl-1-cyclohexyl, 1-methyl-1-cyclopentyl, Mes. R' = H, Me, ^{t}Bu, Ph, CO_2Me, 1-napthyl, TMS.

In all the examples mentioned herein, the phosphaalkyne-azide “click” reaction has relied on the isolation of kinetically stabilised phosphaalkynes. In the absence of sterically demanding R groups, phosphaalkynes are prone to oligomerisation owing to the inherent weakness of the C≡P π-bonds. This has precluded their use in room temperature 1,3-dipolar cycloaddition reactions with azides. Fuchs *et al*. were able to generate phosphaethyne (HC≡P) under flash pyrolytic conditions and subsequently react it with methylazide to generate the 3H-1,2,3,4-triazaphosphole derivative (**Scheme 1.14**).[69]

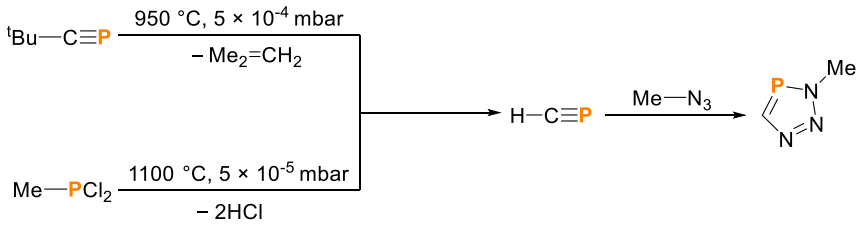

Scheme 1.14. Synthesis of HCP under flash pyrolytic conditions and its 1,3-dipolar cycloaddition reaction with methyl azide.[69]

In 2001, Guillemin and Denis developed a simplified synthetic strategy to access kinetically unstabilized phosphaalkynes (**Scheme 1.15**).[70] Despite this advance, the synthesis of such phosphaalkynes remains challenging and time-consuming, and has inspired chemists to search for alternative routes to stabilise the C≡P bond.

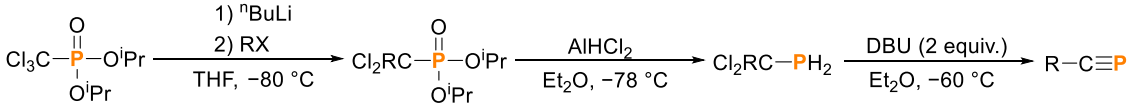

Scheme 1.15. Guillemin and Denis' synthetic route to kinetically unstabilised phosphaalkynes.[70] R = H, Me, Et, n-butyl (^{n}Bu), $PhCH_2CH_2$, cyclohexyl (Cy), 1-propylene, 1-butylene. DBU = 1,8-Diazabicyclo[5.4.0]undec-7-ene.

1.2.2 Phosphaalkene-azide 1,3-dipolar cycloaddition reaction

The use of phosphaalkenes (e.g. R(TMS)C=PCl) in cycloaddition reactions with azides provides a greater scope of 3H-1,2,3,4-triazaphospholes. Carrié (R = TMS), and subsequently Märkl (R = Ph) demonstrated the reactivity of phosphaalkenes with organic azides to access the 3H-1,2,3,4-triazaphosphole derivatives (**Scheme 1.16**).[71,72] The 4,5-dihydro-3H-1,2,3,4-triazaphosphole intermediate undergoes spontaneous aromatization *via* α-elimination of Me_3SiCl to form the 3H-1,2,3,4-triazaphosphole. This is therefore limited to the phosphaalkynes containing groups that can spontaneously eliminate trimethylsilane.

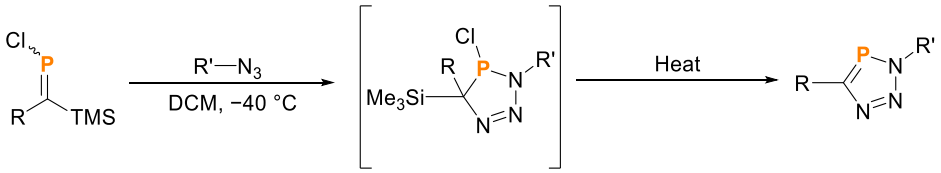

Scheme 1.16. A 1,3-dipolar cycloaddition between organic azides and phosphaalkenes.[71,72] Where R = TMS or Ph, and R′ = Benzyl (Bn), Ph, Me, CH_2CN, CH_2COOEt.

1.2.3 Masked precursor to the phosphaethyne-azide 1,3-dipolar cycloaddition reaction

More recently, Transue *et al.* reported the use of dibenzo-7-phosphanorbornadiene as a masked precursor to phosphaethyne.[73] The authors successfully "sandwiched" phosphaethyne between anthracene and triphenylphosphine *via* a substitution reaction between ClP(Anth) (Anth = anthracene) and methylenetriphenylphosphorane (**Scheme 1.17**). The resulting species was reacted with 7 equivalents of tetra-n-butylammonium azide ($TBAN_3$) at 80 °C in a high-pressure vessel to yield the 1,2,3,4-phosphatriazolate anion. The product identity was confirmed by comparison of ^{1}H, ^{13}C, and ^{31}P NMR spectra with those of $HCPN_3Me$ and [K(2.2.2-crypt)][$AdCPN_3$].

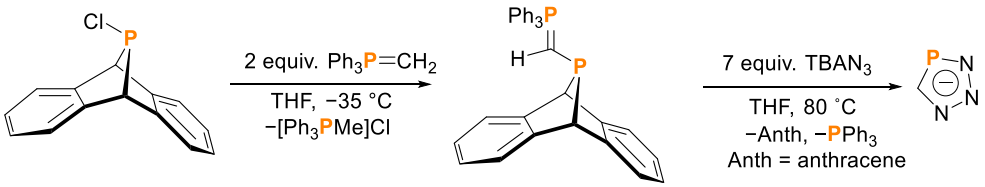

Scheme 1.17. Synthesis of dibenzo-7-phosphanorbornadiene and its use as a molecular precursor to phosphaethyne, demonstrated by its 1,3-dipolar cycloaddition reaction with $TBAN_3$ to yield the 1,2,3,4-phosphatriazolate anion.[73]

1.3 Metal-cyaphide complexes

1.3.1 Cyaphide-azide 1,3-dipolar cycloaddition reaction

Recently, novel metal complexes featuring the cyaphide ligand have been shown to undergo "click" reactivity with organic azides within the coordination sphere of the metal. Müller and W. Jones reported the synthesis of a (dcype)Pt(Mes)(C≡P) complex (dcype = 1,2-Bis(dicyclohexylphosphino)ethane), *via* a photochemical C(sp)–C(sp^2) activation of the Pt(0)-η^2-Mes-phosphaalkyne complex (**Scheme 1.18**).[74] The cyaphide ligand in the resulting complex underwent a regioselective 1,3-dipolar cycloaddition with Dipp−N_3 (Dipp = 2,6-di(isopropyl)phenyl) to yield the first metal complex featuring an anionic 1,2,3,4-phosphatriazolate ligand. This complex was fully characterised by NMR spectroscopy and single crystal X-ray diffraction (SC-XRD).

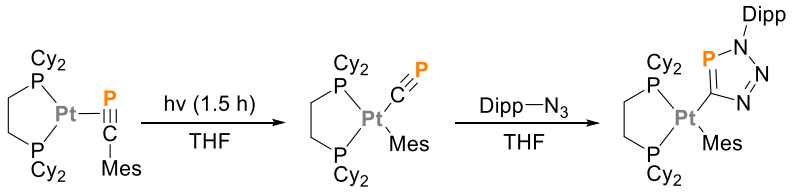

Scheme 1.18. Synthesis of a (dcype)Pt(Mes)(C≡P) type complex *via* photochemical C(sp)–C(sp^2) activation of a η^2-Mes-phosphaalkyne ligand, followed by a 1,3-dipolar cycloaddition with an organic azide within the coordination sphere of platinum(II).[74]

1.3.2 A cyaphide transfer reagent

The reactivity of metal-cyaphide complexes in 1,3-dipolar cycloaddition reactions presents an interesting avenue to explore; however, these complexes remain scarce due to a dearth of synthetic protocols. A magnesium cyaphide complex has been reported by the Goicoechea group as a cyaphide transfer reagent, which reacts analogously to a Grignard reagent, owing to the ionic nature of the Mg–CP bond.[75] Salt metathesis between [Na(diox)$_n$][PCO] (diox = dioxane) and ^{i}Pr$_3$SiOTf in toluene yields the silyl-phosphaethynolate compound,

$^{i}Pr_3SiOCP$,[76] which can be reduced using C. Jones' magnesium(I) reagent, $\{(^{Dipp}NacNac)Mg\}_2$,[77] cleaving the C−O bond to yield an equimolar mixture of (^{Dipp}NacNac)Mg(CP)(diox) and (^{Dipp}NacNac)Mg(OSi^{i}Pr$_3$)(diox) (where ^{Dipp}NacNac = *N*,*N*-bis(2,6-diisopropylphenyl)-pentane-2,4diimine) (**Scheme 1.19**).

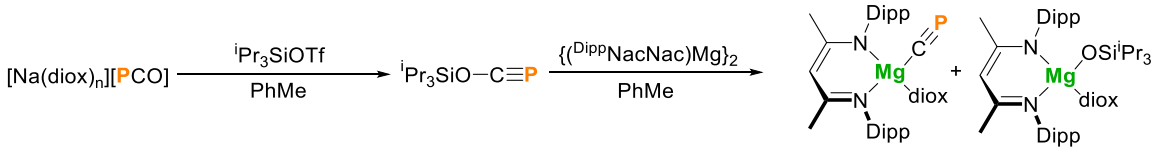

Scheme 1.19. Two-step synthesis of the magnesium-cyaphide transfer reagent.[75] diox = dioxane.

Due to their similar solubilities, isolation of pure (^{Dipp}NacNac)Mg(CP)(diox) is challenging. It can be separated from (^{Dipp}NacNac)Mg(OSi^{i}Pr$_3$)(diox) in low yields (~20%) by fractional crystallisation from hexane, but this is tedious and impractical on larger scales. It should also be noted that (^{Dipp}NacNac)Mg(CP)(diox) is unstable to vacuum, making it challenging to isolate as a solid reagent. Despite this, (^{Dipp}NacNac)Mg(OSi^{i}Pr$_3$)(diox) is relatively unreactive due to the strong oxophilicity of magnesium, so the mixture can be used *in situ* as a cyaphide transfer reagent. Indeed, independent addition of (^{Dipp}NacNac)ECl (E = Ge or Sn), (IDipp)AuCl (IDipp = bis(1,3-bis(2,6-diisopropylphenyl)imidazol-2-ylidene), or (^{Dipp}PDI)CoCl (^{Dipp}PDI = (pyridine-2,6-diyl)bis(N-(2,6-diisopropylphenyl)ethan-1-imine) to the mixture resulted in salt metathesis to produce the corresponding metal-cyaphide complexes (**Scheme 1.20**). It should be noted that (^{Dipp}NacNac)Ge(CP) is unstable and therefore cannot be isolated. The remaining metal-cyaphide complexes were isolated by crystallisation and fully characterised by SC-XRD, NMR and IR spectroscopy, and elemental analysis.

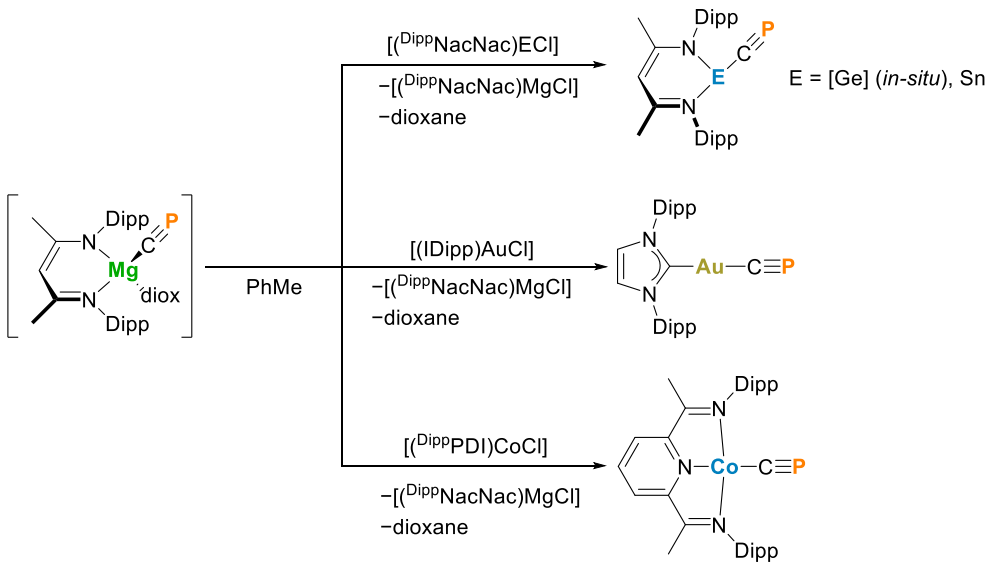

Scheme 1.20. Use of (^{Dipp}NacNac)Mg(CP)(diox) as a cyaphide transfer reagent to prepare various metal-cyaphide complexes.[75]

Whilst the *in-situ* method has been successful in generating metal-cyaphide complexes, it is somewhat impractical. Despite being unreactive, (^{Dipp}NacNac)Mg(OSi^{i}Pr$_3$)(diox) is difficult to remove from reaction mixtures, which severely impacts the yields of new metal-cyaphide complex. The requirement to generate ^{i}Pr$_3$SiOCP in benzene or toluene limits the solvent choice for using (^{Dipp}NacNac)Mg(CP)(diox), which is relevant in later sections (Chapters 4 and 5).

Recently, a more practical magnesium cyaphide transfer agent was reported. Dioxane can be removed from the reaction mixture by treating an *in-situ* generated solution of ^{i}Pr$_3$SiOCP with anhydrous MgCl$_2$, resulting in the formation of an insoluble polymer [Mg(diox)$_x$Cl$_2$]$_n$. This can be removed by filtration to produce a dioxane-free benzene solution of ^{i}Pr$_3$SiOCP, which can subsequently be reduced by {(^{Dipp}NacNac)Mg}$_2$ at 80 °C to yield the solvent-free dimeric complex {(^{Dipp}NacNac)Mg(CP)}$_2$ ([Mg(CP)]$_2$) (**Scheme 1.21**).[78] Gratifying, upon cooling, [Mg(CP)]$_2$ crystallises from the reaction mixture. Although unstable to vacuum, it can be

isolated in excellent yields (70%) on a gram scale by filtration, followed by washing generously with pentane, then allowing to dry under an inert atmosphere in the glovebox.

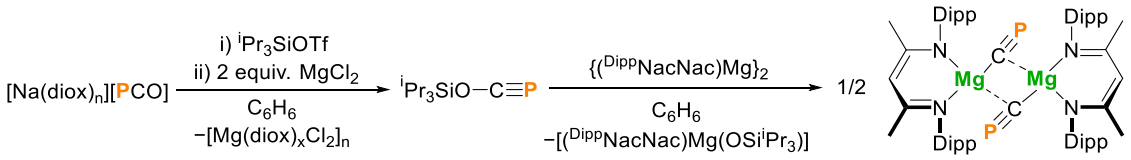

Scheme 1.21. Synthesis of solvent-free dimeric $[Mg(CP)]_2$.[78]

Given the access to a greater variety of metal-cyaphide complexes, this prompted us to investigate the scope and applicability of the cyaphide-azide 1,3-dipolar cycloaddition reaction, which is the subject of the research discussed in Chapter 2.

1.4 3H-1,2,3,4-triazaphosphole ligands

The pioneering work by Regitz and Carrie has offered a novel, facile, and high-yielding synthetic route to access new ligands with unique electronic properties. The 3H-1,2,3,4-triazaphosphole derivatives have several potential donor sites through the phosphorus and nitrogen lone pairs, although the lone pair of N–R′ is delocalised into the aromatic system and not available for ligation (**Figure 1.5**).[79]

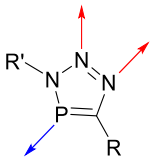

Figure 1.5. Possible coordination modes of 3H-1,2,3,4-triazaphosphole derivatives.

The C. Jones group have used this “click” chemistry to synthesise tripodal ligand systems featuring 3H-1,2,3,4-triazaphosphole moieties (**Figure 1.6**).[80] The three ligands were obtained in excellent yields within three hours *via* the reaction of the appropriate phosphaalkyne, R−C≡P (R = ^{t}Bu or Me), with the triazide at room temperature. These ligands were essentially

isostructural to the previously reported tris(N-heterocyclic carbene) species,[81,82] but offered different electronic properties. The phosphaalkene moieties, $RP{=}CR_2$, within the 3H-1,2,3,4-triazaphosphole heterocycle are weaker σ-donors but stronger π-acceptors in comparison to the N-heterocyclic carbenes. This offers an opportunity to explore new catalysts featuring these tripodal ligand systems.

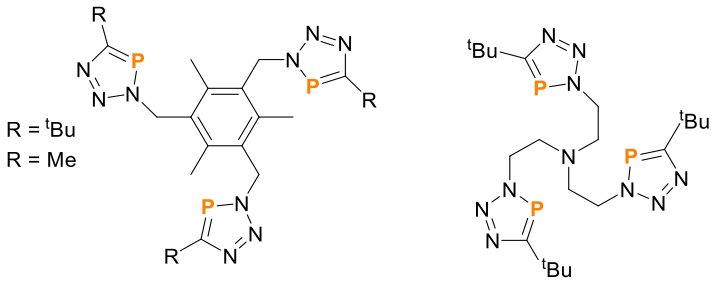

Figure 1.6. Examples of tripodal ligands featuring 3H-1,2,3,4-triazaphosphole moieties synthesised by the C. Jones group.[80]

The ligating properties of this new class of ligands were demonstrated through the coordination of platinum(0) to one of the tripodal triazaphosphole ligands (**Scheme 1.22**).[80] Addition of one equivalent of $Pt(nb)_3$ (nb = norbornene) to the ligand resulted in an unstable species that could not be isolated, thought to be the tridentate platinum(0) complex as determined by $^{31}P\{^1H\}$ NMR spectroscopy at 0 °C. This is presumably due to the large coordination cavity, resulting in weakly bound platinum(0). However, addition of a further equivalent of $Pt(nb)_3$ resulted in the coordination of a second platinum(0) centre to afford a bimetallic complex. –°

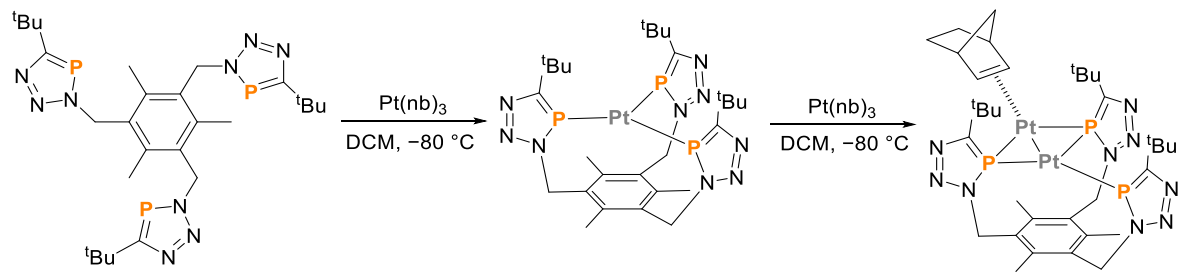

Scheme 1.22. Coordination of platinum(0) to a tripodal triazaphosphole ligand.[80]

Although the nature of this bridging interaction was not explored further, phosphabenzene ligands are known to bridge Pd(0)–Pd(0) bonds through σ- and low-lying π-orbitals at phosphorus.[83] The second platinum(0) centre has a further interaction with a molecule of norbornene and a short Pt–Pt bond. Similar unsupported Pt(0)–Pt(0) bonds have been attributed to the mixing of filled 5d orbitals with low-lying empty p-orbitals.[84,85]

This work was further extended by investigating the reactions of the phosphaalkynes with 1,1′-diazidoferrocene, *cis*-1,3,5-triazidocyclohexane, or poly(allylazide) to give the corresponding triazaphosphole compounds (**Figure 1.7**).[86] The compounds were obtained in quantitative or near-quantitative yields at ambient temperature, mostly within a few hours (the polymer compounds were stirred for 3 days), proving the generality of this synthetic route.

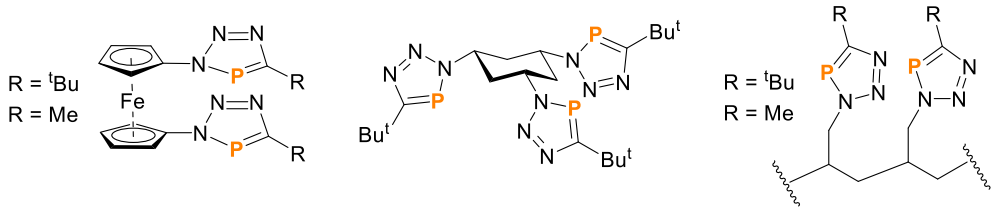

Figure 1.7. Further examples of ligands featuring 3H-1,2,3,4-triazaphosphole moieties synthesised by the C. Jones group.[86]

In an attempt to chemically oxidise the bistriazaphosphole-ferrocene species, reaction with $Ag[Al\{OC(CF_3)_3\}_4]$ resulted in the formation of the dimeric species as a result of two silver(I) centres bridging the bistriazaphosphole-ferrocene ligand *via* the nitrogen atoms adjacent to the triazaphosphole carbon (**Scheme 1.23**).[86] It was postulated that this coordination imparts a barrier to its oxidation. This result demonstrated the versatility in the coordination modes of the triazaphophole.

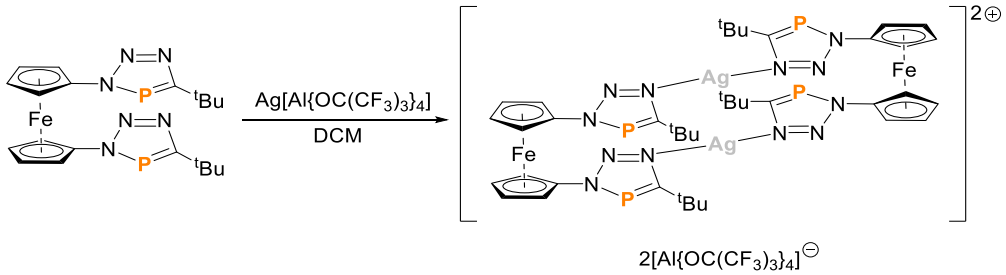

Scheme 1.23. Coordination of silver(I) to the bistriazaphosphole-ferrocene.[86]

The Müller group have synthesised pyridyl- and benzyl-functionalised triazaphospholes *via* phosphaalkyne-azide "click" chemistry (**Figure 1.8**).[87,88] The synthesis of the TMS-substituted compounds demonstrated the "click" reaction between an azide and trimethylsilylphosphaethyne (TMS−C≡P) for the first time. The reactions were performed under ambient conditions, and the desired products were obtained in excellent yields (81–94%).

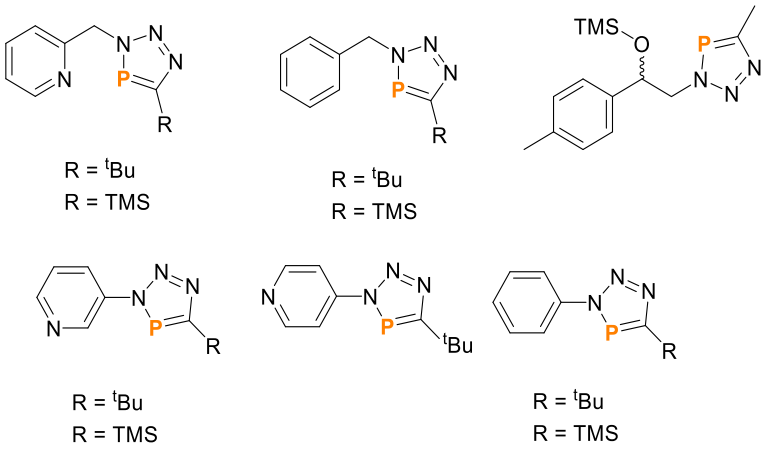

Figure 1.8. Pyridyl- and benzyl-functionalised ligands featuring 3H-1,2,3,4-triazaphosphole derivatives synthesised by the Müller group.[87–90]

The authors were also successful in the synthesis of a novel functionalised 3H-1,2,3,4-triazaphosphole derivative containing a phosphorus-oxygen donor combination, giving access to chiral chelating ligands based upon triazaphospholes (**Figure 1.8, top right**).[89]

Müller and co-workers then targeted ligands with the pyridyl and triazaphosphole moieties in direct conjugation by omitting the methylene linker (**Figure 1.8, bottom**).[88] However, an obstacle arises with the use of 2-azidopyridine, as it exists in an open-closed equilibrium with the pyridotetrazole (**Scheme 1.24**).[90] This equilibrium is shifted towards the closed pyridotetrazole at room temperature, and therefore precludes its use in phosphaalkyne-azide "click" chemistry under ambient conditions. The use of 2-azidopyridine is required due to the unavailability of pyridine-based phosphaalkynes. Therefore, the "click" reactions with phosphaalkynes were carried out at elevated temperatures (T = 65–85 ˚C) to shift the equilibrium towards the open 2-azidopyridine. In contrast, the reactions of 3- and 4-azidopyridine with the phosphaalkynes to obtain the 3H-1,2,3,4-triazaphosphole compounds proceeded at room temperature (**Figure 1.8, bottom left and centre**).

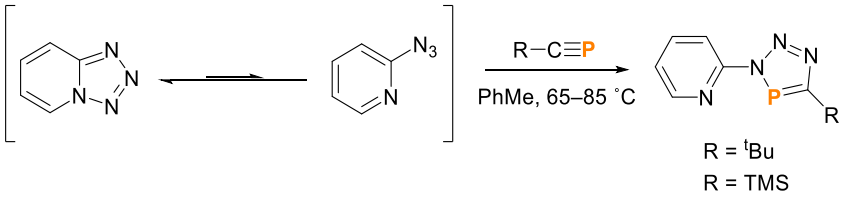

Scheme 1.24. Open-closed equilibrium of 2-azidopyridine with pyridotetrazole and its 1,3-dipolar cycloaddition reactivity with phosphaalkynes at elevated temperatures.[88]

The coordination chemistry of the pyridyl-functionalised triazaphosphole ligands was demonstrated by their reaction with a rhenium(I) carbonyl complex, resulting in an *N*,*N*-chelating coordination mode where the least nucleophilic nitrogen atom of the triazaphosphole is bound to the rhenium(I) centre (S**cheme 1.25**).[87,88]

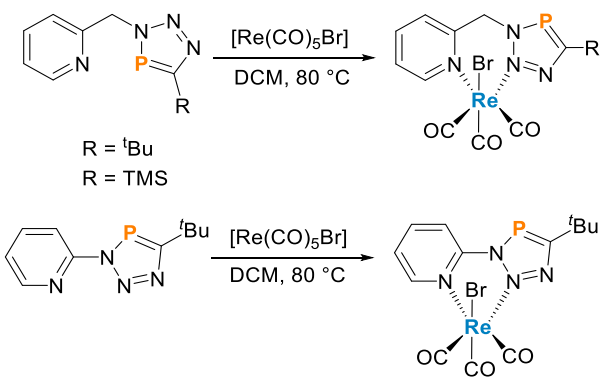

Scheme 1.25. *N,N*-chelation of rhenium(I) to pyridyl-functionalised triazaphosphole ligands.[87,88]

The CO stretching frequencies of these complexes were slightly lower than those of the triazole analogues due to the electron-rich triazaphosphole.

1.5 Triazaphospholenium salts and their coordination chemistry

Müller and co-workers have reported the alkylation of a 3H-1,2,3,4-triazaphosphole to yield the corresponding triazaphospholenium salt, a phosphorus analogue of 1,2,3-triazolylidenes, a class of mesoionic carbenes.[91] Alkylation of the most nucleophilic nitrogen atom was achieved by refluxing a DCM solution of the triazaphosphole with trimethyloxonium tetrafluoroborate, a variant of Meerwein's salt, a strong alkylating reagent (**Scheme 1.26**).[92,93]

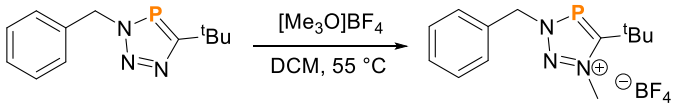

Scheme 1.26. Methylation of a triazaphosphole to yield a triazaphospholenium salt.[91]

A stoichiometric reaction between the triazaphospholenium salt and $CuBr{\cdot}SMe_2$ results in the quantitative formation of a Cu(I) dimer, bridged by two bromide ligands, where each Cu(I) centre is coordinated to a triazaphospholenium ligand and a further bromide ligand (**Scheme 1.27**). Two equivalents of $CuBF_4$ are formed as a by-product as a result of an anion exchange reaction to form the dinuclear $[Cu_2Br_4]^{2-}$ core.

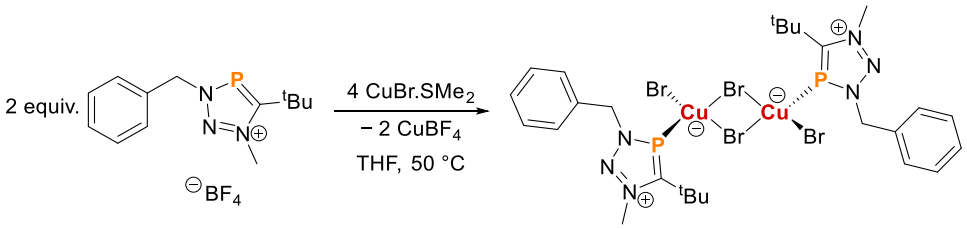

Scheme 1.27. Formation of a Cu(I) dimer with coordination of a triazaphospholenium ligand.[91]

In a subsequent report from the Müller group, alkylation of the pyridyl-functionalised triazaphospholes was achieved using a similar strategy, and their coordination chemistry to Cu(I) was explored.[94] In this case, using one equivalent of Meerwein's salt results in the alkylation of the more nucleophilic pyridyl nitrogen. Reacting with a further equivalent of Meerwein's salt results in alkylation of the triazaphosphole, as per the previous report. The coordination compounds are summarised in **Figure 1.9**, displaying different coordination modes of the Cu(I) to the phosphorus of the triazaphospholenium ligands. In these cases, the cationic triazaphosphole ligand enforces coordination at the π-acidic phosphorus with an electron-rich copper(I) centre.

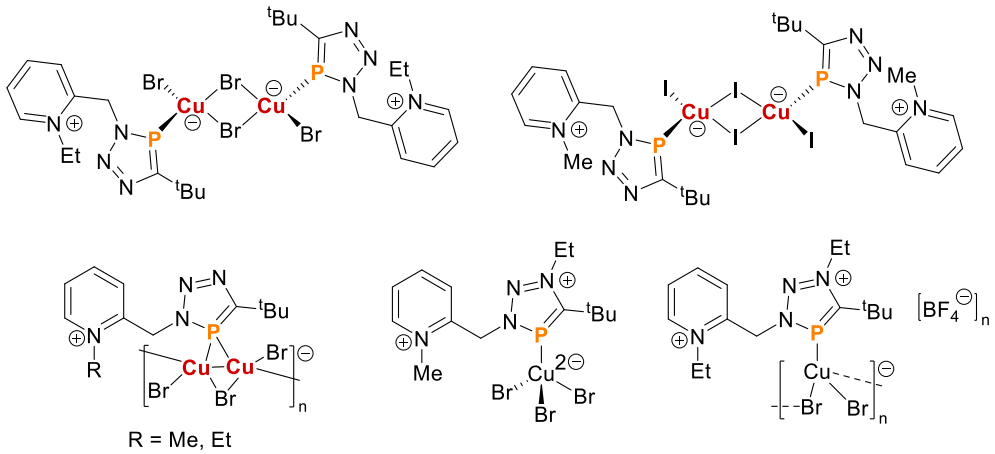

Figure 1.9. Cu(I) coordination modes to pyridinium-triazaphospholenium ligands.[94]

1.6 Aims

The overall aim of this project was to develop the chemistry of the cyaphide-azide 1,3-dipolar cycloaddition reaction and explore its use for the synthesis of inorganic MIMs.

The first aim of the project was therefore to determine the scope and limitations of the cyaphide-azide 1,3-dipolar cycloaddition reaction, which is discussed in Chapter 2. To this end, the reactivity of aliphatic, aromatic, and bis-azides with select examples of metal-cyaphide complexes from the s-, p-, and d-block was investigated. The reactivity of the resulting metal-triazaphospholes was also explored.

The next aim was to determine if the cyaphide-azide 1,3-dipolar cycloaddition reaction could offer a general route for the synthesis of inorganic MIMs. As a proof of concept study, we aimed to prepare inorganic [2]rotaxanes *via* a capping approach using the 1,3-dipolar cycloaddition reaction of the gold-cyaphide complex, (IDipp)Au(CP). This work is detailed in Chapter 3.

We then turned our attention to preparing a more challenging inorganic MIM, a [2]catenane, by the same reaction, which is the subject of Chapter 4. The aim of this work was to prepare a stable bis-cyaphide species capable of undergoing simultaneous 1,3-dipolar cycloaddition reactions with a bis-azide in a macrocyclization reaction, such that a [2]catenane could be prepared by a clipping approach.

After the challenges faced in Chapter 4, we aimed to explore whether the mechanical bond in a [2]rotaxane could be used to stabilise a bis-cyaphide complex, whilst maintaining its 1,3-dipolar cycloaddition reactivity with azides. This work is detailed in Chapter 5.

Following this, we also aimed to prepare a highly efficient photosensitizer for singlet oxygen generation by functionalisation of the bis-cyaphide [2]rotaxane with BODIPY-azides *via* the 1,3-dipolar cycloaddition reaction. The motivation for this work is that the presence of heavy

gold(I) atoms is known to improve the efficiency of singlet oxygen generation. Furthermore, the mechanical bond offers distinct advantages by enhancing the stability and solubility of the inorganic MIM. This work is also detailed in Chapter 5.

1.7 References

1. C. J. Bruns and F. Stoddart, *The nature of the mechanical bond: from molecules to machines*, Wiley, Hoboken, New Jersey, 2017.
2. S. Erbas-Cakmak, D. A. Leigh, C. T. McTernan and A. L. Nussbaumer, *Chem. Rev.* **2015**, *115*, 10081–10206.
3. D. A. Leigh, V. Marcos and M. R. Wilson, *ACS Catal.* **2014**, *4*, 4490–4497.
4. E. Arunkumar, N. Fu and B. D. Smith, *Chem. Eur. J.* **2006**, *12*, 4684–4690.
5. A. Caballero, F. Zapata and P. D. Beer, *Coord. Chem. Rev.* **2013**, *257*, 2434–2455.
6. E. Wasserman, *J. Am. Chem. Soc.* **1960**, *82*, 4433–4434.
7. R. Brückner, *Eur. J. Org. Chem.* **2019**, *2019*, 3289–3319.
8. A. S. Baluna, A. Galan, D. A. Leigh, G. D. Smith, J. T. J. Spence, D. J. Tetlow, I. J. Vitorica-Yrezabal and M. Zhang, *J. Am. Chem. Soc.* **2023**, *145*, 9825–9833.
9. C. O. Dietrich-Buchecker, J. P. Sauvage and J. P. Kintzinger, *Tetrahedron Lett.* **1983**, *24*, 5095–5098.
10. J. E. M. Lewis, P. D. Beer, S. J. Loeb and S. M. Goldup, *Chem. Soc. Rev.* **2017**, *46*, 2577–2591.
11. S. M. Goldup, D. A. Leigh, P. J. Lusby, R. T. McBurney and A. M. Z. Slawin, *Angew. Chem. Int. Ed.* **2008**, *47*, 6999–7003.
12. A. Fuller, D. A. Leigh, P. J. Lusby, I. D. H. Oswald, S. Parsons and D. B. Walker, *Angew. Chem. Int. Ed.* **2004**, *43*, 3914–3918.
13. K. S. Chichak, S. J. Cantrill, A. R. Pease, S.-H. Chiu, G. W. V. Cave, J. L. Atwood and J. F. Stoddart, *Science* **2004**, *304*, 1308–1312.
14. D. A. Leigh, P. J. Lusby, S. J. Teat, A. J. Wilson and J. K. Y. Wong, *Angew. Chem. Int. Ed.* **2001**, *40*, 1538–1543.
15. D. A. Leigh, R. G. Pritchard and A. J. Stephens, *Nat. Chem.* **2014**, *6*, 978–982.

16. F. Zapata, O. A. Blackburn, M. J. Langton, S. Faulkner and P. D. Beer, *Chem. Commun.* **2013**, *49*, 8157.

17. S. Tung, C. Lai, Y. Liu, S. Peng and S. Chiu, *Angew. Chem. Int. Ed.* **2013**, *52*, 13269–13272.

18. A. Inthasot, S.-T. Tung and S.-H. Chiu, *Acc. Chem. Res.* **2018**, *51*, 1324–1337.

19. H. M. Tay, T. C. Tse, A. Docker, C. Gateley, A. L. Thompson, H. Kuhn, Z. Zhang and P. D. Beer, *Angew. Chem. Int. Ed.* **2023**, *62*, e202214785.

20. H. M. Tay, A. Docker, C. Hua and P. D. Beer, *Chem. Sci.* **2024**, *15*, 13074–13081.

21. G. Barin, A. Coskun, M. M. G. Fouda and J. F. Stoddart, *ChemPlusChem* **2012**, *77*, 159–185.

22. N. H. Evans, *Eur. J. Org. Chem.* **2019**, *2019*, 3320–3343.

23. M. S. Vickers and P. D. Beer, *Chem. Soc. Rev.* **2007**, *36*, 211–225.

24. F. Diederich, L. Echegoyen, M. Gómez-López, R. Kessinger and J. F. Stoddart, *J. Chem. Soc. Perkin Trans. 2* **1999**, 1577–1586.

25. D. J. Hoffart, J. Tiburcio, A. de la Torre, L. K. Knight and S. J. Loeb, *Angew. Chem. Int. Ed.* **2008**, *47*, 97–101.

26. V. Aucagne, K. D. Hänni, D. A. Leigh, P. J. Lusby and D. B. Walker, *J. Am. Chem. Soc.* **2006**, *128*, 2186–2187.

27. V. Aucagne, J. Berná, J. D. Crowley, S. M. Goldup, K. D. Hänni, D. A. Leigh, P. J. Lusby, V. E. Ronaldson, A. M. Z. Slawin, A. Viterisi and D. B. Walker, *J. Am. Chem. Soc.* **2007**, *129*, 11950–11963.

28. J. D. Crowley, S. M. Goldup, A.-L. Lee, D. A. Leigh and R. T. McBurney, *Chem. Soc. Rev.* **2009**, *38*, 1530.

29. K. D. Hänni and D. A. Leigh, *Chem. Soc. Rev.* **2010**, *39*, 1240–1251.

30. R. Jamagne, M. J. Power, Z.-H. Zhang, G. Zango, B. Gibber and D. A. Leigh, *Chem. Soc. Rev.* **2024**, *53*, 10216–10252.

31. O. Š. Miljanić, W. R. Dichtel, I. Aprahamian, R. D. Rohde, H. D. Agnew, J. R. Heath and J. Fraser Stoddart, *QSAR Comb. Sci.* **2007**, *26*, 1165–1174.

32. R. Huisgen, *Proc. Chem. Soc.* **1961**, 357.

33. V. V. Rostovtsev, L. G. Green, V. V. Fokin and K. B. Sharpless, *Angew. Chem.* **2002**, *114*, 2708–2711.

34. C. W. Tornøe, C. Christensen and M. Meldal, *J. Org. Chem.* **2002**, *67*, 3057–3064.

35. B. C. Boren, S. Narayan, L. K. Rasmussen, L. Zhang, H. Zhao, Z. Lin, G. Jia and V. V. Fokin, *J. Am. Chem. Soc.* **2008**, *130*, 8923–8930.

36. B. Mohr, J. Sauvage, R. H. Grubbs and M. Weck, *Angew. Chem. Int. Ed. Engl.* **1997**, *36*, 1308–1310.

37. B. Taghavi Shahraki, S. Maghsoudi, Y. Fatahi, N. Rabiee, S. Bahadorikhalili, R. Dinarvand, M. Bagherzadeh and F. Verpoort, *Coord. Chem. Rev.* **2020**, *423*, 213484.

38. H. Ogino, *J. Am. Chem. Soc.* **1981**, *103*, 1303–1304.

39. H. Ogino and K. Ohata, *Inorg. Chem.* **1984**, *23*, 3312–3316.

40. D. J. Hoffart and S. J. Loeb, *Angew. Chem.* **2005**, *117*, 923–926.

41. S. J. Loeb, *Chem. Commun*. **2005**, 1511–1518.

42. V. N. Vukotic, K. J. Harris, K. Zhu, R. W. Schurko and S. J. Loeb, *Nat. Chem.* **2012**, *4*, 456–460.

43. M. Fujita, F. Ibukuro, H. Hagihara and K. Ogura, *Nature* **1994**, *367*, 720–723.

44. M. Fujita, J. Yazaki and K. Ogura, *Chem. Lett.* **1991**, *20*, 1031–1032.

45. M. Fujita, F. Ibukuro, K. Yamaguchi and K. Ogura, *J. Am. Chem. Soc.* **1995**, *117*, 4175–4176.

46. B. A. Blight, J. A. Wisner and M. C. Jennings, *Chem. Commun.* **2006**, 4593.

47. C.-F. Lee, D. A. Leigh, R. G. Pritchard, D. Schultz, S. J. Teat, G. A. Timco and R. E. P. Winpenny, *Nature* **2009**, *458*, 314–318.

48. P. Waelès, M. Gauthier and F. Coutrot, *Angew. Chem. Int. Ed.* **2021**, *60*, 16778–16799.

49. M. Galli, J. E. M. Lewis and S. M. Goldup, *Angew. Chem. Int. Ed.* **2015**, *54*, 13545–13549.

50. H. Lahlali, K. Jobe, M. Watkinson and S. M. Goldup, *Angew. Chem. Int. Ed.* **2011**, *50*, 4151–4155.

51. K. Miki, K. Ohe and S. Uemura, *J. Org. Chem.* **2003**, *68*, 8505–8513.

52. M. J. Johansson, D. J. Gorin, S. T. Staben and F. D. Toste, *J. Am. Chem. Soc.* **2005**, *127*, 18002–18003.

53. N. Weisbach, Z. Baranová, S. Gauthier, J. H. Reibenspies and J. A. Gladysz, *Chem. Commun.* **2012**, *48*, 7562.

54. H. Amini, Z. Baranová, N. Weisbach, S. Gauthier, N. Bhuvanesh, J. H. Reibenspies and J. A. Gladysz, *Chem. Eur. J.* **2019**, *25*, 15896–15914.

55. W. Wang, L.-J. Chen, X.-Q. Wang, B. Sun, X. Li, Y. Zhang, J. Shi, Y. Yu, L. Zhang, M. Liu and H.-B. Yang, *Proc. Natl. Acad. Sci.* **2015**, *112*, 5597–5601.

56. P. J. Altmann and A. Pöthig, *J. Am. Chem. Soc.* **2016**, *138*, 13171–13174.

57. P. J. Altmann and A. Pöthig, *Angew. Chem. Int. Ed.* **2017**, *56*, 15733–15736.

58. J. A. W. Sklorz and C. Müller, *Eur. J. Inorg. Chem.* **2016**, *2016*, 595–606.

59. K. S. Pitzer, *J. Am. Chem. Soc.* **1948**, *70*, 2140–2145.

60. R. S. Mulliken, *J. Am. Chem. Soc.* **1950**, *72*, 4493–4503.

61. M. Regitz, *Chem. Rev.* **1990**, *90*, 191–213.

62. W. Rösch and M. Regitz, *Angew. Chem. Int. Ed.* **1984**, *23*, 900–901.

63. Y. Y. C. Y. L. Ko, R. Carrié, A. Muench and G. Becker, *J. Chem. Soc. Chem. Commun.* **1984**, 1634–1635.

64. G. Becker, G. Gresser and W. Uhl, *Z. Für Naturforsch. B.* **1981**, *36*, 16–19.

65. T. Allspach, M. Regitz, G. Becker and W. Becker, *Synthesis* **1986**, *1986*, 31–36.

66. W. Rösch, U. Vogelbacher, T. Allspach and M. Regitz, *J. Organomet. Chem.* **1986**, *306*, 39–53.

67. A. Mack, E. Pierron, T. Allspach, U. Bergsträßer and M. Regitz, *Synthesis* **1998**, *1998*, 1305–1313.

68. W. Rösch, T. Facklam and M. Regitz, *Tetrahedron* **1987**, *43*, 3247–3256.

69. E. P. O. Fuchs, M. Hermesdorf, W. Schnurr, W. Rösch, H. Heydt, M. Regitz and P. Binger, *J. Organomet. Chem.* **1988**, *338*, 329–340.

70. J.-C. Guillemin, T. Janati and J.-M. Denis, *J. Org. Chem.* **2001**, *66*, 7864–7868.

71. Y. Y. C. Y. L. Ko and R. Carrié, *J. Chem. Soc. Chem. Commun*. **1984**, 1640–1641.

72. G. Märkl, I. Troetsch-Schaller and W. Hölzl, *Tetrahedron Lett.* **1988**, *29*, 785–788.

73. W. J. Transue, A. Velian, M. Nava, M.-A. Martin-Drumel, C. C. Womack, J. Jiang, G.-L. Hou, X.-B. Wang, M. C. McCarthy, R. W. Field and C. C. Cummins, *J. Am. Chem. Soc.* **2016**, *138*, 6731–6734.

74. T. Görlich, D. S. Frost, N. Boback, N. T. Coles, B. Dittrich, P. Müller, W. D. Jones and C. Müller, *J. Am. Chem. Soc.* **2021**, *143*, 19365–19373.

75. D. W. N. Wilson, S. J. Urwin, E. S. Yang and J. M. Goicoechea, *J. Am. Chem. Soc.* **2021**, *143*, 10367–10373.

76. D. Heift, Z. Benkő and H. Grützmacher, *Dalton Trans.* **2014**, *43*, 5920.

77. C. Jones, *Nat. Rev. Chem.* **2017**, *1*, 0059.

78. D. C. Wannipurage, E. S. Yang, A. D. Chivington, J. Fletcher, D. Ray, N. Yamamoto, M. Pink, J. M. Goicoechea and J. M. Smith, *J. Am. Chem. Soc.* **2024**, *146*, 27173–27178.

79. L. Nyulaszi, T. Veszpremi, J. Reffy, B. Burkhardt and M. Regitz, *J. Am. Chem. Soc.* **1992**, *114*, 9080–9084.

80. S. L. Choong, C. Jones and A. Stasch, *Dalton Trans.* **2010**, *39*, 5774.

81. K. Meyer and S. C. Bart, in *Advances in Inorganic Chemistry*, Elsevier, **2008**, vol. 60, pp. 1–30.

82. C. Vogel, F. W. Heinemann, J. Sutter, C. Anthon and K. Meyer, *Angew. Chem. Int. Ed.* **2008**, *47*, 2681–2684.

83. M. T. Reetz, E. Bohres, R. Goddard, M. C. Holthausen and W. Thiel, *Chem. Eur. J.* **1999**, *5*, 2101–2108.

84. A. Dedieu and R. Hoffmann, *J. Am. Chem. Soc.* **1978**, *100*, 2074–2079.

85. P. Pyykkö, *Chem. Rev.* **1997**, *97*, 597–636.

86. S. L. Choong, A. Nafady, A. Stasch, A. M. Bond and C. Jones, *Dalton Trans.* **2013**, *42*, 7775.

87. J. A. W. Sklorz, S. Hoof, M. G. Sommer, F. Weißer, M. Weber, J. Wiecko, B. Sarkar and C. Müller, *Organometallics* **2014**, *33*, 511–516.

88. J. A. W. Sklorz, S. Hoof, N. Rades, N. De Rycke, L. Könczöl, D. Szieberth, M. Weber, J. Wiecko, L. Nyulászi, M. Hissler and C. Müller, *Chem. Eur. J.* **2015**, *21*, 11096–11109.

89. J. A. W. Sklorz, M. Schnucklake, M. Kirste, M. Weber, J. Wiecko and C. Müller, *Phosphorus Sulfur Silicon Relat. Elem.* **2016**, *191*, 558–562.

90. C. K. Lowe-Ma, R. A. Nissan and W. S. Wilson, *J. Org. Chem.* **1990**, *55*, 3755–3761.

91. M. Papke, L. Dettling, J. A. W. Sklorz, D. Szieberth, L. Nyulászi and C. Müller, *Angew. Chem. Int. Ed.* **2017**, *56*, 16484–16489.

92. H. Meerwein, G. Hinz, P. Hofmann, E. Kroning and E. Pfeil, *J. Für Prakt. Chem.* **1937**, *147*, 257–285.

93. H. Meerwein, E. Battenberg and H. Gold, *J. Für Prakt. Chem.* **1939**, *154*, 83–156.

94. L. Dettling, M. Papke, M. J. Ernst, M. Weber and C. Müller, *Chem. Eur. J.* **2024**, *30*, e202400592.

Chapter 2

Cyaphide-azide 1,3-Dipolar Cycloaddition Reactions

The work detailed in this chapter was completed in collaboration with Dr. Eric Yang.

Abstract

The cyaphide-azide 1,3-dipolar cycloaddition reaction proceeds rapidly and regioselectively under mild conditions and in the absence of a catalyst to yield the corresponding metal-triazaphosphole complexes in excellent yields. This reaction has been demonstrated with gold(I), magnesium(II), and germanium(II) cyaphide complexes, and the resulting metal-triazaphosphole complexes display enhanced stability. This reaction is reminiscent of the CuAAC reaction and has been extended to bis-azides, providing insight into its potential applicability for the synthesis of mechanically interlocked molecules. The resulting gold(I) triazaphosphole complexes were subject to further functionalisation through Lewis acid coordination, methylation, and halogenation reactions.

2.1 Azides in 1,3-dipolar cycloaddition reactions

As discussed in Section 1.2.1, the well-established phosphaalkyne-azide 1,3-dipolar cycloaddition reaction (**Scheme 2.1a**), first reported by Regitz and Carrié,[1,2] is limited by the dearth of accessible kinetically stable phosphaalkynes.[3] To broaden the scope of this reaction, we have turned our attention to the metal-cyaphide complexes recently isolated by our group.[4] The principal aim of this project is to use the 1,3-dipolar cycloaddition reaction of metal-cyaphide complexes with organic azides for the preparation of mechanically interlocked molecules (MIMs). Until now, there was only one example of a metal-cyaphide complex being

used in this reaction, which was reported by Müller and W. Jones, and the subsequent reactivity of the platinum(II) triazaphosphole complex was not explored (**Scheme 2.1b**).[5]

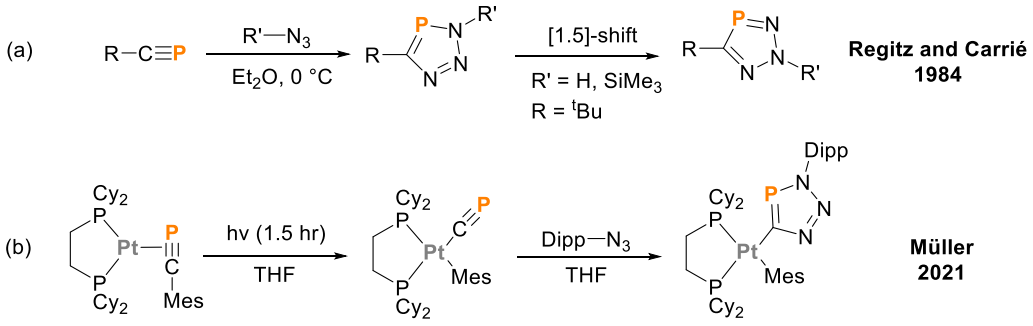

Scheme 2.1 (a) The 1,3-dipolar cycloaddition reactions of azides with phosphaalkynes, and (b) the 1,3-dipolar cycloaddition of Dipp–N_3 with a platinum(II)-cyaphide complex.

With a range of metal-cyaphide complexes at our disposal, we sought to expand the scope of the cyaphide-azide 1,3-dipolar cycloaddition reaction and explore the chemistry of the resulting metal-triazaphosphole complexes.

2.2 Cyaphide-azide 1,3-dipolar cycloaddition reactions

2.2.1 Synthesis of (IDipp)Au(CPN$_3$R) (R = ^{t}Bu, Ad, Dipp)

The cyaphide ligand in the (IDipp)Au(CP) complex displays phosphaalkyne-type reactivity towards transition metals by acting as a bridging ligand in an η^1:η^2 coordination mode, thereby maximising the π-interaction with the metal (**Scheme 2.2**).[6]

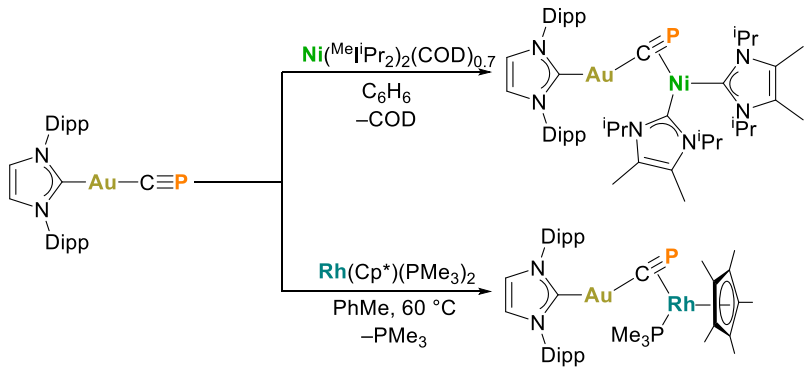

Scheme 2.2. Phosphaalkyne-type reactivity of the cyaphide ligand in (IDipp)Au(CP), acting as a bridging ligand towards electron-rich transition metal complexes.[6]

Encouraged by this reactivity, we reasoned that the phosphaalkyne analogy could be extended to its reactivity with azides. Indeed, the addition of *tert*-butyl azide (^{t}Bu–N_3), 1-adamantyl azide (Ad–N_3), or 2,6-diisopropylphenyl azide (Dipp–N_3) to a toluene solution of (IDipp)Au(CP) resulted in the rapid and quantitative formation of the respective gold(I) triazaphosphole complexes, (IDipp)Au(CPN_3R) [R = ^{t}Bu (**1a**), Ad (**1b**), Dipp (**1c**); **Scheme 2.3**] as evidenced by $^{31}P\{^{1}H\}$ NMR spectroscopy. The complexes display a single peak in their $^{31}P\{^{1}H\}$ NMR spectra at 191.2 ppm (**1a**), 189.3 ppm (**1b**), and 209.3 ppm (**1c**), in the typical range of organic 3H-1,2,3,4-triazaphospholes (161–212 ppm).[7]

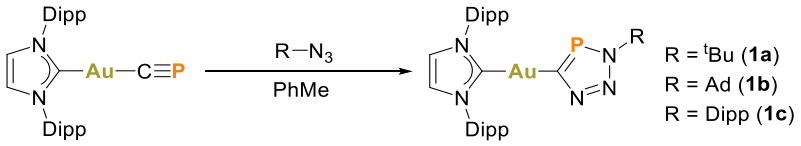

Scheme 2.3 Synthesis of gold(I) triazaphosphole complexes **1a-c.**

The complexes were isolated by crystallisation in very good yields (86–90%) by concentrating the reaction mixtures under vacuum and storing them at −30 °C for 3 days. The triazaphosphole carbon nuclei in **1a–c** can be identified as doublets in their $^{13}C\{^{1}H\}$ spectra at 205.2 ppm ($^{1}J_{C–P}$ = 82.0 Hz), 204.5 ppm ($^{1}J_{C–P}$ = 81.9 Hz), and 208.0 ppm ($^{1}J_{C–P}$ = 83.3 Hz), for **1a**, **1b** and

1c, respectively. The strong σ-donating ability of the triazaphospholide anion results in slightly higher IDipp carbene $^{13}C\{^{1}H\}$ NMR chemical shift for the triazaphosphole complexes at 196.5 ppm (**1a**), 196.5 ppm (**1b**), and 195.8 ppm (**1c**), in comparison to the cyaphide complex at 193.0 ppm. This can be explained by the trans influence, where a strong σ-donating ligand increases electron density at the metal, weakening the metal–carbene bond trans to it and deshielding the carbene carbon.[8,9]

The identity of the triazaphosphole (**1a**–**c**) complexes as the 3H-1,2,3,4-regioisomers was confirmed by SC-XRD (**Figure 2.1**), revealing linear gold(I) centres κ-C bonded to the triazaphospholes with C2–Au1–C1 angles of 179.5(3)°, 177.81(8)°, and 177.25(16)°, for **1a**, **1b** and **1c**, respectively. The Au1–C1 bond lengths are approximately the same at 2.022(8) Å (**1a**), 2.024(2) Å (**1b**), and 2.015(4) Å (**1c**). The C2– Au1 bond lengths are also very similar at 2.029(8) Å (**1a**), 2.027(2) Å (**1b**), and 2.019(4) Å (**1c**). In **1a**–**c**, the triazaphospholes possess similar C1–P1 bond lengths of 1.685(8) Å, 1.715(2) Å , and 1.719(4) Å, for **1a**, **1b** and **1c**, respectively, and almost identical C1–P1–N3 bond angles of 88.4(4)°, 88.42(9)°, 87.7(2)°, respectively.

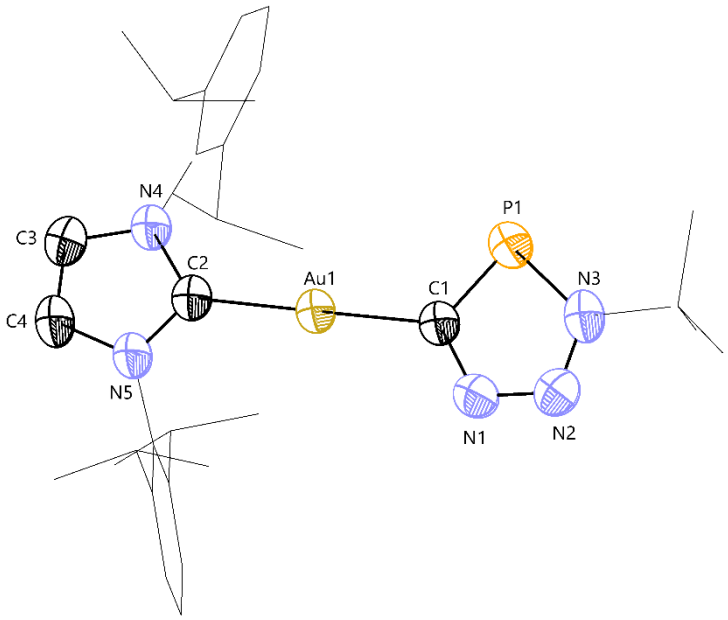

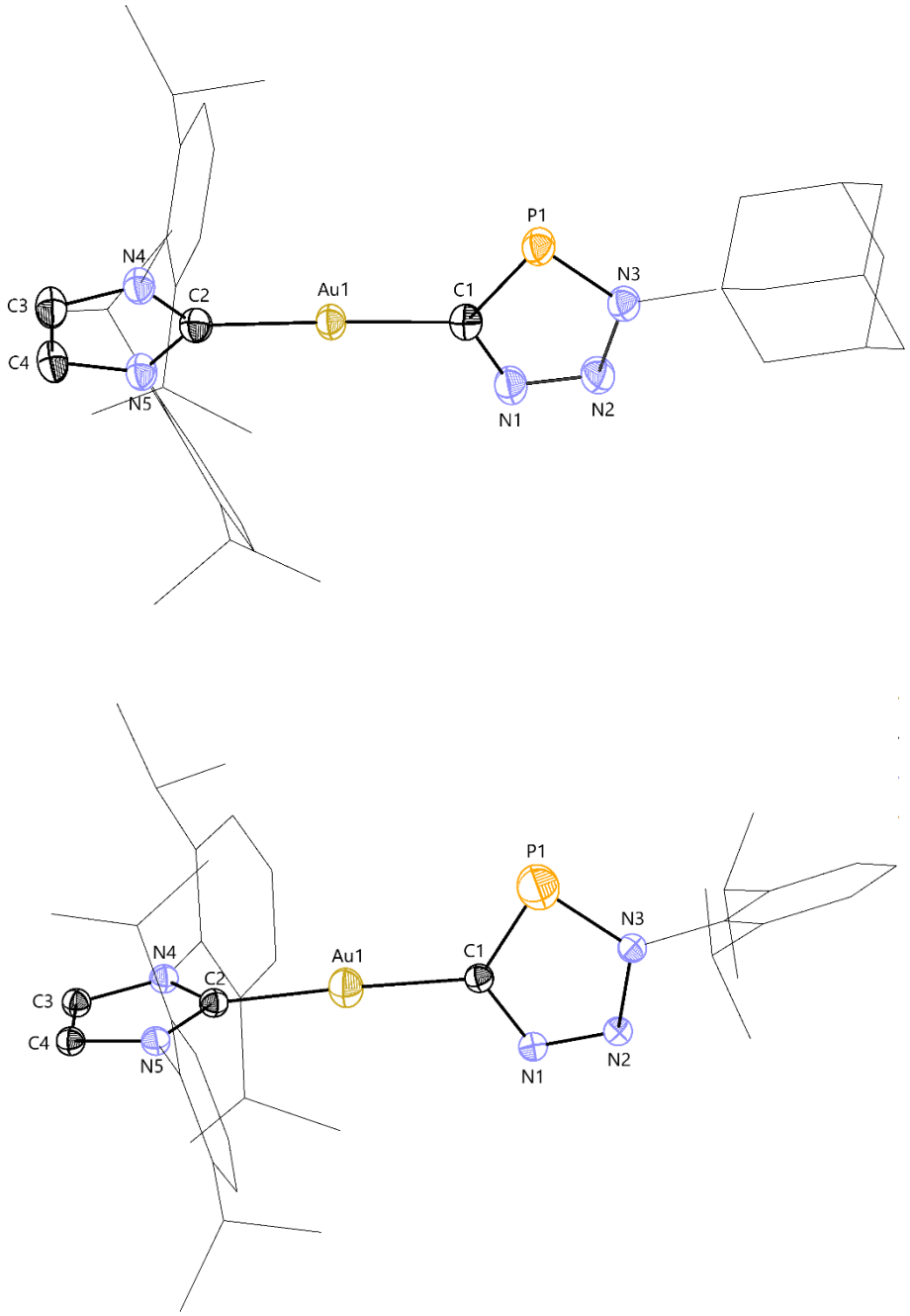

Figure 2.1. SC-XRD structure of the gold(I) triazaphosphole complexes, **1a** (top), **1b** (middle), and **1c** (bottom). Anisotropic displacement ellipsoids depicted at 50% probability. Hydrogen atoms, disorder components, and co-crystallised solvent molecules are omitted for clarity. Alkyl and aryl substituents are depicted as wireframes for clarity.

2.2.2 Synthesis of [(IDipp)Au(CPN$_3$)]$_2$(C$_6$H$_4$)

To assess whether this reaction would be suitable for building larger supramolecular architectures such as MIMs, we wanted to explore the reactivity of (IDipp)Au(CP) with molecules containing two azide functionalities. Molecules containing 1,3-disubstituted aromatic rings with (iodo)triazoles are very common as scaffolds for anion recognition due to their optimal binding pocket configuration as a result of the 1,3-substitution on the planar aromatic ring.[10] We therefore investigated the reactivity of 1,3-diazidobenzene with two equivalents of complex (IDipp)Au(CP) (**Scheme 2.4**).

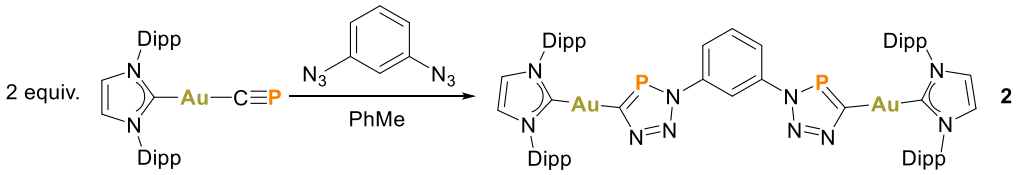

Scheme 2.4. Synthesis of a bimetallic gold(I) 1,3-bis(triazaphosphole)benzene complex **2**.

The reaction proceeded rapidly and quantitatively at room temperature, as evidenced by the resulting $^{31}P\{^1H\}$ NMR spectrum, which displays a single peak at 200.8 ppm after three hours. The product was isolated in moderate yields (63%) by crystallisation from the reaction mixture and was identified as the bimetallic gold(I) 1,3-bis(triazaphosphole)benzene complex **2** — the result of two simultaneous cyaphide-azide 1,3-dipolar cycloaddition reactions. The triazaphosphole carbon and IDipp carbene atoms appear as doublets at 208.2 ppm ($^1J_{C–P}$ = 84.1 Hz) and 194.2 ppm ($^3J_{C–P}$ = 10.0 Hz), respectively, in the $^{13}C\{^1H\}$ NMR spectrum. The ^1H NMR spectrum is consistent with a fully symmetric structure.

SC-XRD confirmed the proposed structure (**Figure 2.2**). The asymmetric unit contains two crystallographically unique molecules of **2** of similar bond metrics. The C2–Au1–C1 angles are 173.2(4)° and 172.6(4)°, and the C6–Au2–C5 angles are 173.4(4)° and 174.5(4)°, distorting slightly from linearity due to the bulkiness of the Dipp substituents. The remaining bond

metrics are similar to those observed for **1a–c**, with Au–C bond lengths to the carbene and triazaphosphole of approximately 2.02 Å.

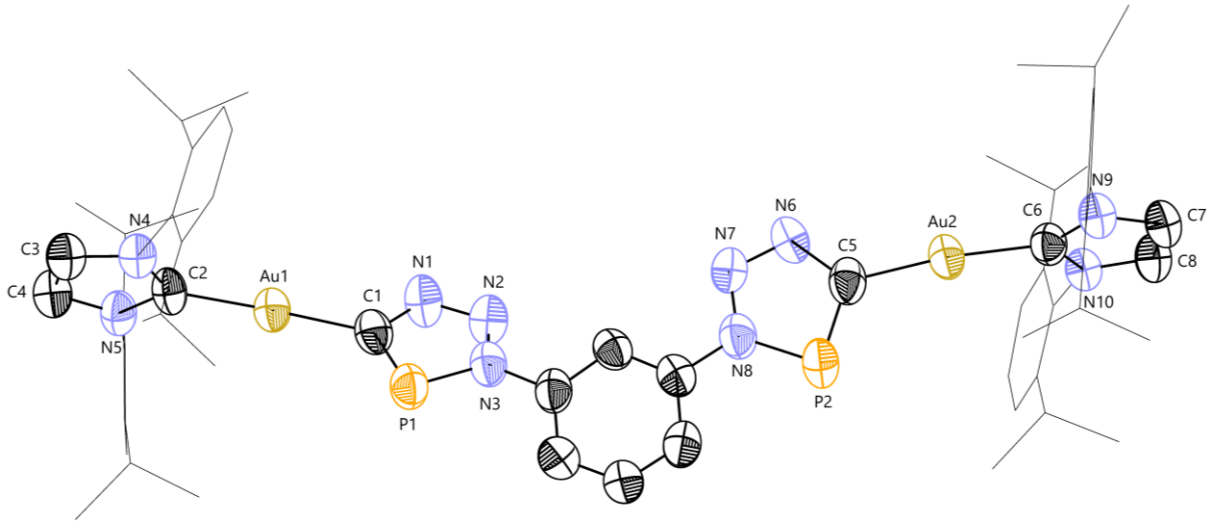

Figure 2.2. SC-XRD structure of the bimetallic gold(I) 1,3-bis(triazaphosphole)benzene complex **2**. Anisotropic displacement ellipsoids depicted at 50% probability. Hydrogen atoms, disorder components, and co-crystallised solvent molecules are omitted for clarity. Dipp substituents are depicted as wireframes for clarity.

2.2.3 Synthesis of {(^{Dipp}NacNac)Mg(CPN$_3$R)}$_2$ (R = ^{t}Bu, Bn, Dipp)

The reaction of organic azides with an *in-situ* generated solution of highly-ionic complex (^{Dipp}NacNac)Mg(CP)(diox) was explored in order to expand the scope of the 1,3-dipolar cycloaddition reaction. For aliphatic azides (R = ^{t}Bu or Bn), this proceeds cleanly to afford the dimeric magnesium(II) triazaphosphole complexes {(^{Dipp}NacNac)Mg(CPN$_3$R)}$_2$, **3a** (R = ^{t}Bu) and **3b** (R = Bn) (**Scheme 2.5**).

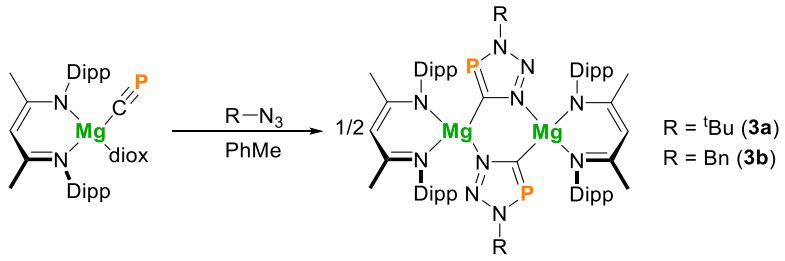

Scheme 2.5. Synthesis of magnesium(II) triazaphosphole dimers **3a** and **3b**.

The compounds crystallise rapidly upon standing, allowing their facile isolation from the reaction mixture. **3a** was isolated in excellent yields (91%), displaying a single peak at 224.3 ppm in the $^{31}P\{^{1}H\}$ NMR spectrum, higher than a typical organic triazaphosphole or gold(I) triazaphosphole (191.2 ppm in **1a**). The triazaphosphole carbon appears as a doublet at 207.2 ppm ($^{1}J_{C–P}$ = 93.3 Hz), similar to the gold(I) complexes. The ^{1}H NMR spectrum of **3a** features a significantly upfield-shifted resonance at −0.64 ppm for the methyl groups of the isopropyl ^{Dipp}NacNac substituents that are in close proximity to the aryl diatropic ring current. This provides evidence that the dimeric structure is retained in solution, which was further supported by ^{1}H DOSY (diffusion-ordered spectroscopy) measurements giving an estimated molecular weight of 1073 g mol^{-1} (actual: 1168 g mol^{-1}).[11] The dimeric structure is retained even in the presence of donor solvents (e.g. THF, MeCN, pyridine), strong Lewis acids (e.g. $B(C_6F_5)_3$), or strong Lewis bases (e.g. 4-dimethylaminopyridine (DMAP)). **3b** was isolated in modest yields (43%) and was found to be insoluble in common laboratory solvents, precluding its characterisation by NMR spectroscopy.

Reaction with the electron-poor aromatic azide, Dipp–N_3, ultimately resulted in an intractable mixture of products, as shown by $^{31}P\{^{1}H\}$ NMR spectroscopy. The combination of a highly reactive electron-rich cyaphide with an electron-poor azide results in inverse electron cycloaddition pathways, producing alternative regiochemical outcomes and a complex reaction mixture. Despite this, crystals suitable for SC-XRD were obtained, allowing the structural

characterisation of {(^{Dipp}NacNac)Mg(CPN$_3$Dipp)}$_2$ (**3c**) (**Figure 2.3, bottom**). As **3c** exhibits the same dimeric structure as **3a** and **3b**, we do not attribute the multitude of products formed in the reaction mixture to the steric demands of the Dipp substituent, but rather to the electronic effects of the aryl substituent.

SC-XRD reveals dimeric structures of the 3H-1,2,3,4 regioisomer for all three of the complexes (**Figure 2.3**). The magnesium(II) centres are bridged by the carbon and adjacent nitrogen atoms of the triazaphospholes, in a manner reminiscent of previously reported magnesium β-diketiminate complexes of nitrogen-heterocycles.[12] The dimeric structure results in weaker σ-donor ability of the triazaphospholes and increased steric bulk around the magnesium(II) centres corresponding to slightly longer Mg–C bond lengths in comparison to monomeric (^{Dipp}NacNac)Mg(CP)(diox) (2.118(2) Å) for **3a** (2.162(2) Å), **3b** (2.164(3) Å) and **3c** (2.191(1) Å).

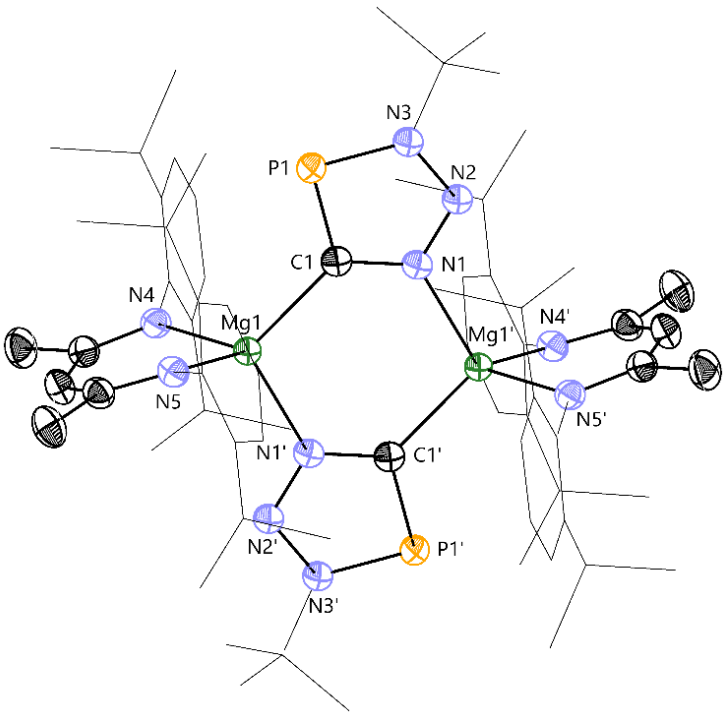

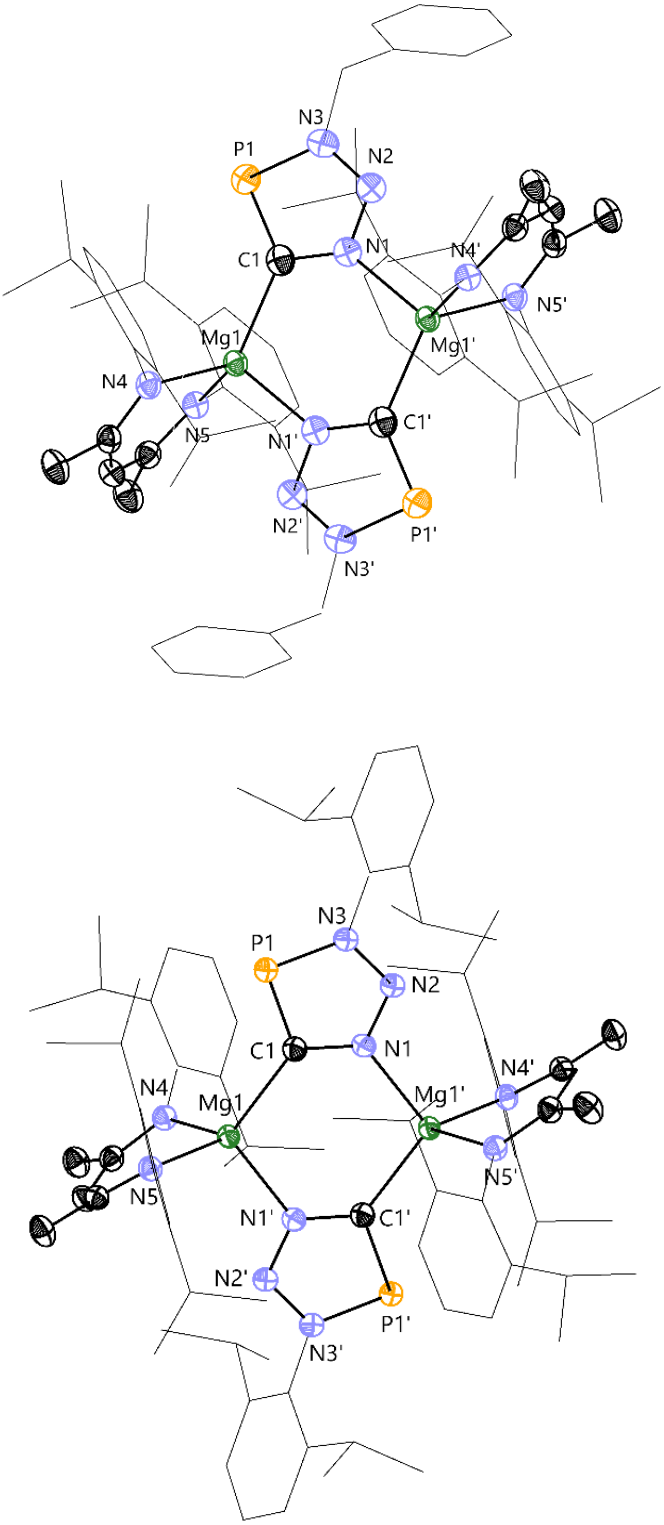

Figure 2.3. SC-XRD structure of the magnesium(II) triazaphosphole dimeric complexes, **3a** (top), **3b** (middle), and **3c** (bottom). Anisotropic displacement ellipsoids depicted at 50% probability. Hydrogen atoms, disorder components, and co-crystallised solvent molecules are omitted for clarity. Alkyl and aryl substituents are depicted as wireframes for clarity.

2.2.4 Synthesis of (^{Dipp}NacNac)Ge(CPN$_3$^{t}Bu)

The germanium(II) cyaphide complex, (^{Dipp}NacNac)Ge(CP), is kinetically unstable and therefore cannot be isolated. The species can however, be generated *in situ*, by the addition of (^{Dipp}NacNac)GeCl to a benzene solution of (^{Dipp}NacNac)Mg(CP)(diox), evidenced by the emergence of a new signal at 106.4 ppm in the $^{31}P\{^1H\}$ NMR spectrum and a new signal for the ^{Dipp}NacNac γ-H in the ^{1}H NMR at 5.08 ppm.[4] We wanted to explore whether the 1,3-dipolar cycloaddition reaction with azides was fast enough to kinetically trap this species. Indeed, addition of ^{t}Bu–N$_3$ to an *in situ* generated solution of (^{Dipp}NacNac)Ge(CP) results in the rapid formation of the germanium(II) triazaphosphole complex, (^{Dipp}NacNac)Ge(CPN$_3$^{t}Bu) (**4**) (**Scheme 2.6**).

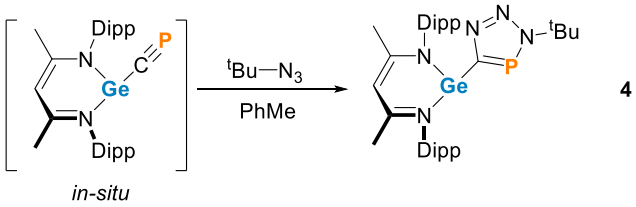

Scheme 2.6. Synthesis of the germanium(II) triazaphosphole complex **4**.

4 is stable indefinitely under an inert atmosphere, and even in ambient atmosphere for several days. Similar to the other metal-triazaphospholes, it can be isolated straightforwardly by crystallisation from the reaction mixture. The $^{31}P\{^1H\}$ NMR spectrum contains a single peak at 196.9 ppm, and the $^{13}C\{^1H\}$ NMR spectrum reveals a doublet at 199.4 ppm ($^1J_{C–P}$ = 105.1 Hz) for the triazaphosphole phosphorus and carbon, respectively.

The solid-state structure of **4** was determined by SC-XRD (**Figure 2.4**), featuring a three-coordinate germanium(II) centre with a Ge–C bond length of 2.038(2) Å.

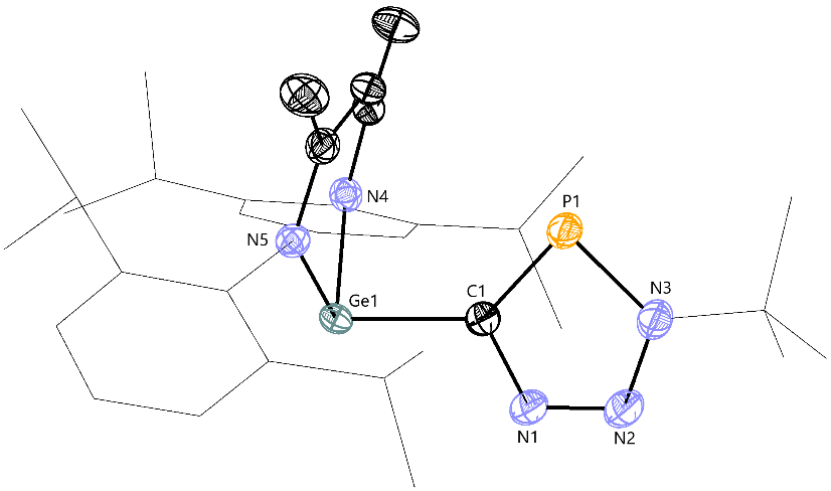

Figure 2.4. SC-XRD structure of the germanium(II) triazaphosphole complex **4**. Anisotropic displacement ellipsoids depicted at 50% probability. Hydrogen atoms, disorder components, and co-crystallised solvent molecules are omitted for clarity. Dipp substituents are depicted as wireframes for clarity.

2.3 Reactivity of metal-triazaphospholes

2.3.1 Synthesis of (IDipp)Au(CPN$_3$R){B(C$_6$F$_5$)} (R = ^{t}Bu, Dipp)

The four lone pairs of the triazaphosphole ligand open it up to further coordination with Lewis acids, as evidenced by the formation of dimers in the case of the magnesium(II) complexes (Section 2.2.3). We wanted to explore whether the disubstituted triazaphospholes present in the gold(I) complexes could form adducts with Lewis acids. Gratifyingly, the addition of one equivalent of B(C$_6$F$_5$)$_3$ to complexes **1a** or **1c** in toluene solution results in the formation of the trisubstituted triazaphosphole complexes **5a** or **5c**, respectively (**Scheme 2.7**).

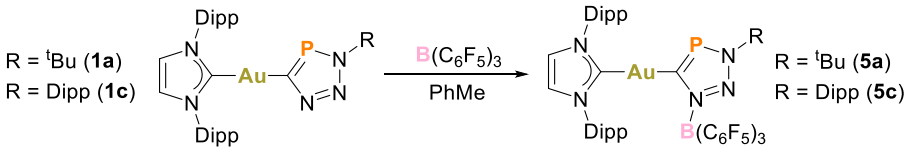

Scheme 2.7. Synthesis of the gold(I) triazaphosphole B(C$_6$F$_5$)$_3$ adducts **5a** and **5c**.

In comparison to the disubstituted precursors, the triazaphosphole $^{31}P\{^{1}H\}$ NMR resonances are downfield shifted to 203.5 ppm (**5a**) and 220.4 ppm (**5c**). Similarly, this is the case for the triazaphosphole carbon $^{13}C\{^{1}H\}$ NMR resonances, which also reveal slightly smaller $^{1}J_{C–P}$ coupling constants. These resonances were observed at 207.3 ppm ($^{1}J_{C–P}$ = 77.0 Hz) and 210.4 ppm ($^{1}J_{C–P}$ = 80.3 Hz) for **5a** and **5c**, respectively. These changes are a result of electron donation to the $B(C_6F_5)_3$, deshielding the phosphorus and carbon nuclei. This also influences the σ-donating ability of the triazaphosphole, evident by the upfield shift of the $^{13}C\{^{1}H\}$ NMR resonance for the IDipp carbene carbon atoms in comparison to the disubstituted precursors, at 190.9 ppm (**5a**) and 190.4 ppm (**5c**). The $^{11}B\{^{1}H\}$ NMR spectra feature a single broad resonance at −5.52 ppm (**5a**) and −5.02 ppm (**5a**), typical of $B(C_6F_5)_3$ adducts. Restricted rotation about the B–N bond, due to the steric hindrance imposed by the Dipp substituents of the IDipp ligand, results in spectroscopically inequivalent C_6F_5 groups, evidenced by complex $^{19}F\{^{1}H\}$ NMR spectra.

The solid-state structures determined by SC-XRD (**Figure 2.5**) reveal $B(C_6F_5)_3$ coordination to the triazaphosphole at the nitrogen adjacent to the carbon (N1), which itself is bonded to the (IDipp)Au unit. This is analogous to the coordination pattern exhibited by the dimeric magnesium(II) species, suggesting this nitrogen atom (N1) is the most Lewis basic.

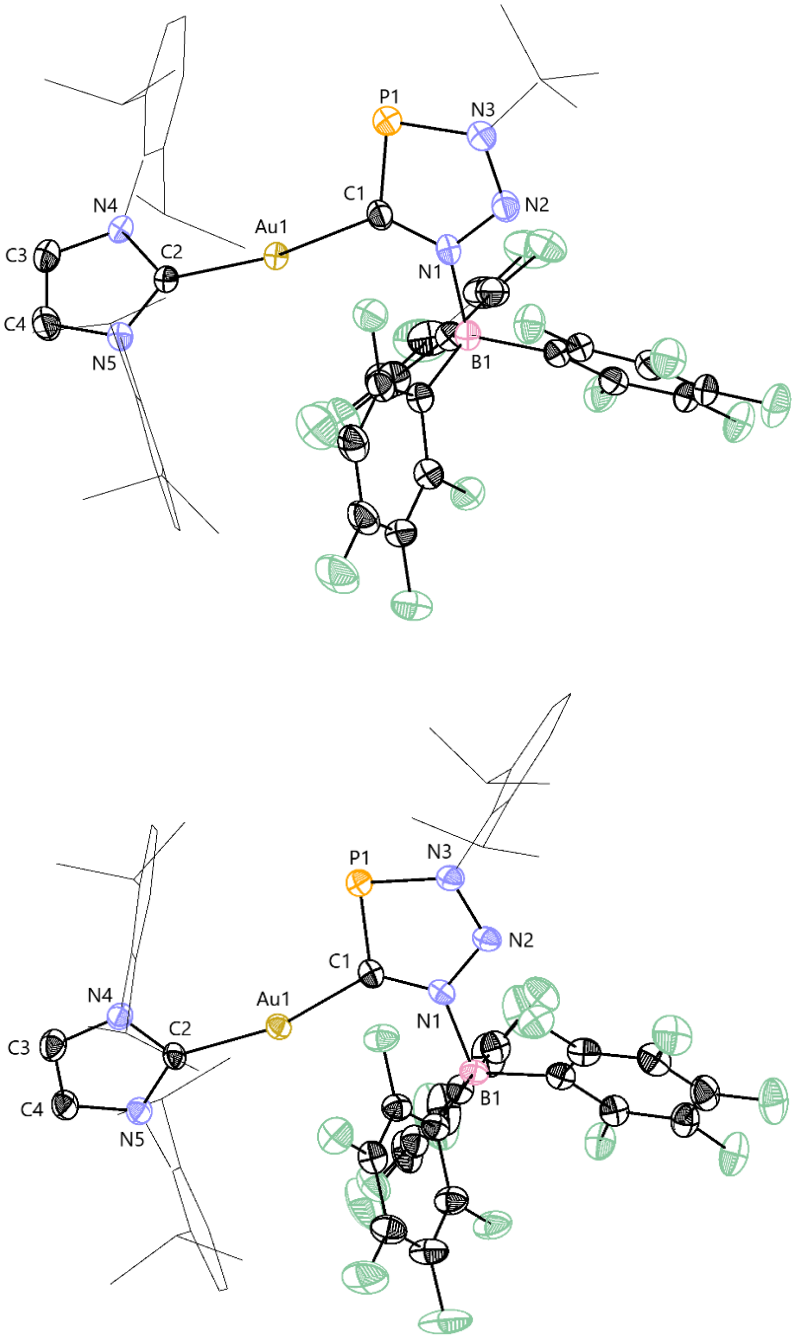

Figure 2.5. SC-XRD structure of the gold(I) triazaphosphole $B(C_6F_5)_3$ adducts **5a** (top) and **5c** (bottom). Anisotropic displacement ellipsoids depicted at 50% probability. Hydrogen atoms, disorder components, and co-crystallised solvent molecules are omitted for clarity. Alkyl and Dipp substituents are depicted as wireframes for clarity.

The bond metric parameters are almost identical to the disubstituted precursors. The C2–Au1–C2 bond angles bend slightly to 170.35(19)° (**5a**) and 165.09(14)° (**5c**) in order to

accommodate the large $B(C_6F_5)_3$ group. The B–N bond lengths are 1.606(6) Å (**5a**) and 1.604(5) Å (**5c**). These species are isolobal to the mesoionic phosphorus-containing carbenes reported by Müller.[13,14]

2.3.2 Synthesis of [(IDipp)Au(CPN$_3$DippMe)][BF$_4$]

As a more direct analogue of the mesoionic carbene reported by Müller (Section 1.5),[13,14] we attempted the methylation of **1a** with trimethyloxonium tetrafluoroborate, $[Me_3O][BF_4]$; a variant of the strong alkylating agent Meerwein's salt.[15] Alkylation of triazoles and iodotriazoles to produce the corresponding positively charged (iodo)triazolium analogues has been previously used to improve the potency and selectivity of anion binding, particularly in aqueous media, through chelated charge-assisted halogen bonding interactions.[10]

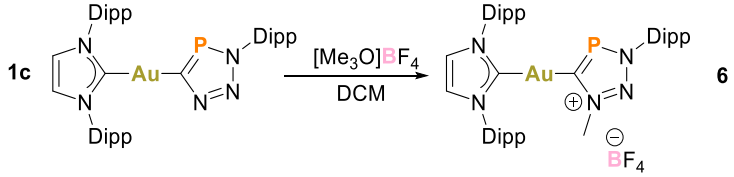

Scheme 2.8. Synthesis of the methylated gold(I) triazaphosphole **6**.

The methylation reaction proceeds at room temperature in DCM to afford the methylated gold(I) triazaphospholenium salt **6** as the single product (**Scheme 2.8**). This was determined by the observation of a single resonance in the $^{31}P\{^1H\}$ NMR spectrum at 236.9 ppm. The chemical shift is significantly downfield shifted in comparison to that of the precursor complex. This is suspected to be due to the positive charge present on the triazaphospholenium heterocycle, which was also observed by Müller.[13] The $^{13}C\{^1H\}$ NMR resonance of the triazaphospholenium carbon atom at 206.8 ppm is at a similar chemical shift to that of the precursor (**1c**: 208.0 ppm), whilst the IDipp carbene carbon atom is upfield shifted to 187.4 ppm (**1c**: 195.8 ppm) as a result of the stronger σ-donating ability of the triazaphospholenium mesoionic carbene. The ^1H NMR spectrum is almost identical to the

precursor, featuring one further resonance at 3.95 ppm for the methyl group of the triazaphospholenium. The $^{11}B\{^{1}H\}$ NMR and $^{19}F\{^{1}H\}$ NMR spectra feature signals at −1.14 ppm and −153.06 ppm, respectively, confirming the presence of a BF_4^- counteranion.

SC-XRD confirms methylation at the most nucleophilic nitrogen atom (N1) of the triazaphosphole, as expected (**Figure 2.6**). It is worth noting that this is the same nitrogen atom engaged in bonding to a Lewis base in **5a** and **5c**. The bond metrics are almost identical to the precursor **1c**, with a new N1−C5 bond length of 1.464(4) Å, analogous to Müller's compound 1.471(3) Å.

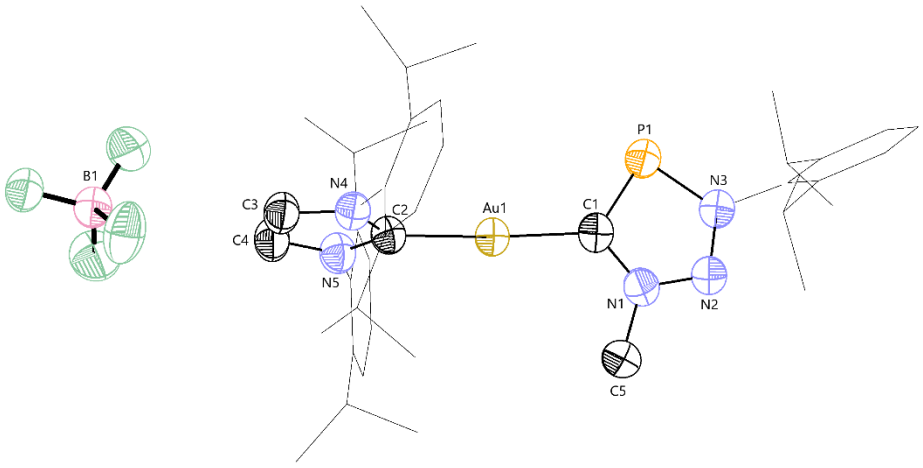

Figure 2.6. SC-XRD structure of the gold(I) methylated triazaphospholenium BF_4^- salt **6**. Anisotropic displacement ellipsoids depicted at 50% probability. Hydrogen atoms, disorder components, and co-crystallised solvent molecules are omitted for clarity. Dipp substituents are depicted as wireframes for clarity.

2.3.3 Synthesis of ICPN$_3$R (R = ^{t}Bu, Ad, Dipp)

The gold(I) triazaphosphole species **1a–c** react with iodine at room temperature to produce the first examples of halogenated triazaphospholes (**Scheme 2.9**). Cleavage of the Au–$C_{triazaphosphole}$ bond affords the corresponding iodotriazaphospholes **7a–c**, with the concomitant formation of (IDipp)AuI.

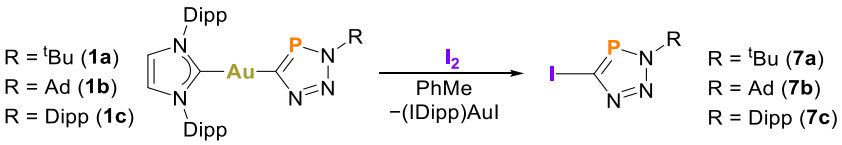

Scheme 2.9. Synthesis of iodotriazaphospholes **7a–c**.

The iodotriazaphosphole $^{13}C\{^{1}H\}$ NMR resonance is shifted significantly upfield to 120.8 ppm ($^{1}J_{C–P}$ = 80.6 Hz) (**7a**), 120.5 ppm ($^{1}J_{C–P}$ = 80.8 Hz) (**7b**), and 123.4 ppm ($^{1}J_{C–P}$ = 83.5 Hz) (**7c**) in comparison the gold-triazaphosphole precursors [205.2 ppm (**1a**), 204.5 ppm (**1b**), and 208.0 ppm (**1c**)]. This is presumably due to a lack of metal-ligand backbonding and a greater electron density at the triazaphosphole carbon.

The $^{31}P\{^{1}H\}$ NMR spectra of **7a** and **7b** feature pseudo-triplet multiplets at 179.9 ppm and 180.1 ppm, respectively, whereas the $^{31}P\{^{1}H\}$ NMR spectrum of **7c** features a singlet at 194.7 ppm. A singlet would be expected for the phosphorus atom in the iodotriazaphospholes; therefore we propose that the pseudo-triplets in **7a** and **7c** are a result of aggregation of these compounds in solution. The bulkier Dipp substituent in **7c** prevents this aggregation, therefore producing a singlet in the $^{31}P\{^{1}H\}$ NMR spectrum.

To probe this further, the $^{31}P\{^{1}H\}$ NMR spectra of **7b** was explored in different solvents (**Figure 2.7**). In hexane, a non-π-stacking solvent, this signal appears as a pseudo-triplet as the iodotriazaphospholes aggregate. Whereas, in benzene and 1,2-difluorobenzene (1,2-DFB), the resonance broadens as the solvent molecules break up the aggregates as a result of solvent involvement in the π-stacking interactions.

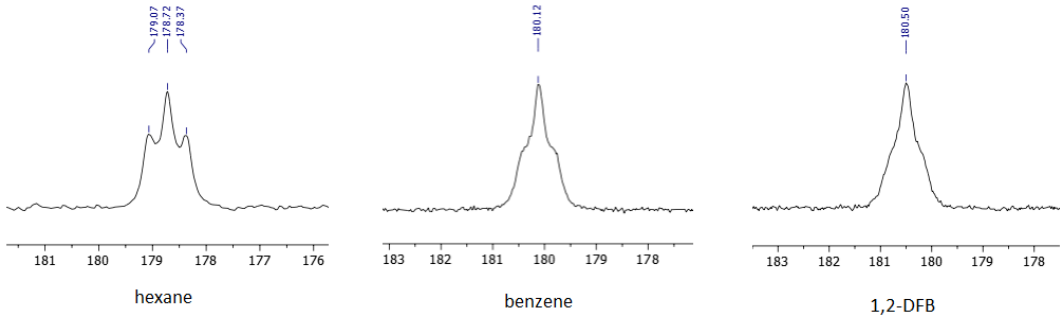

Figure 2.7. $^{31}P\{^{1}H\}$ NMR spectra of **7b** in different solvents.

This hypothesis was further supported by DFT calculations performed by Dr. Eric Yang, which suggest aggregation of **7a** in the gas-phase is highly thermodynamically favoured with a π–π stacking energy of −11.1 kcal mol^{-1}.

Further support for the presence of aggregation in solution was obtained by SC-XRD (**Figure 2.8**). The solid-state structure of **7a** displays close I···I (5.63 Å), I···π (4.78 Å), and π···π (4.23 Å) interactions between neighbouring molecules. Halogen bonding has been exploited for anion binding,[16] where iodotriazoles produce an electron-deficient σ-hole capable of non-covalent interactions with electron-rich species. The C1–I1 bond lengths are 2.083(6) Å (**7a**) and 2.080(3) Å (**7b**), with the remaining bond metrics being similar to the respective precursors. **7c** could only be obtained as an oil and therefore crystals suitable for SC-XRD were unattainable, presumably as a result of the bulky Dipp subsituent preventing the crystal-packing of the iodotriazoles.

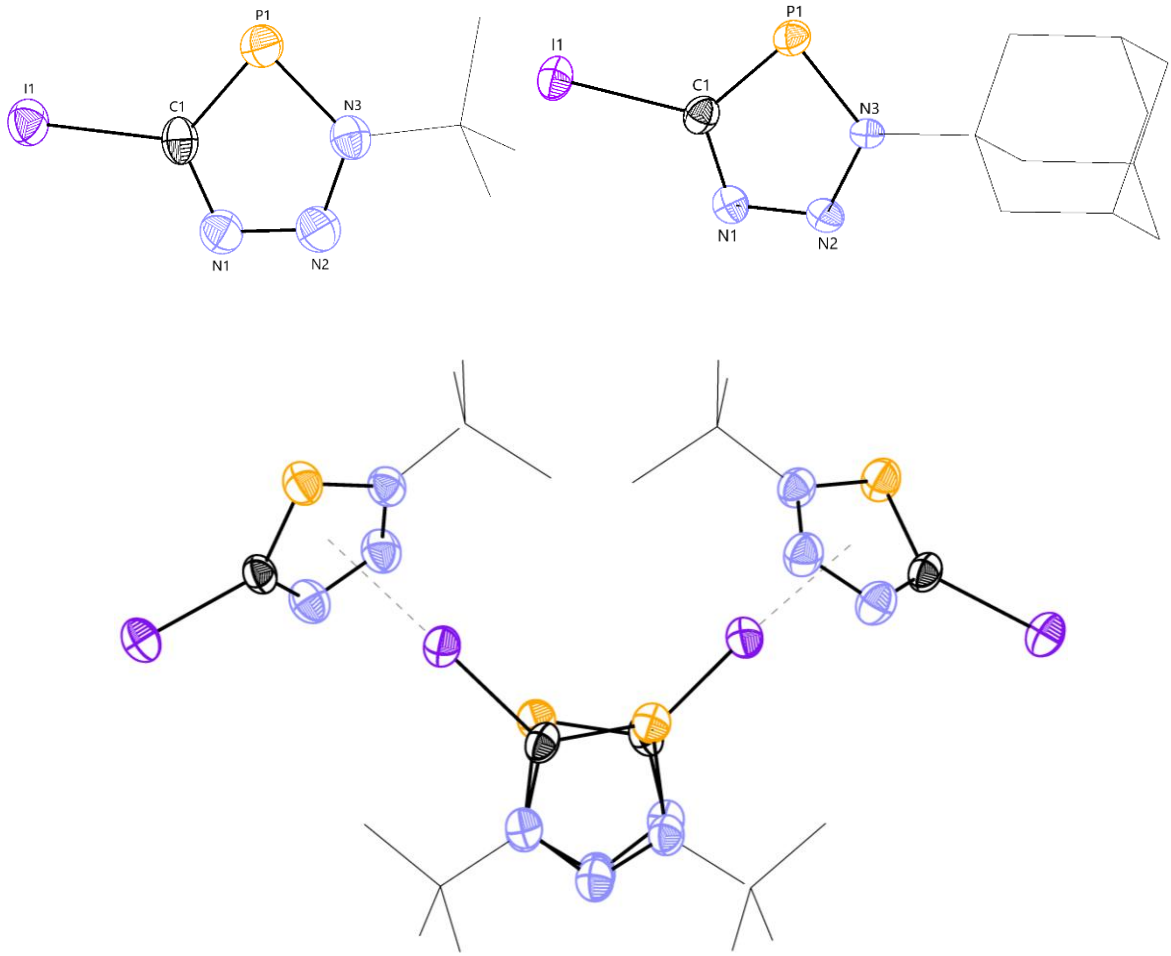

Figure 2.8. SC-XRD structure of the aliphatic iodotriazaphohles **7a** (top left) and **7b** (top right). Tetrameric aggregation of **7a** in the solid-state with I···π interactions shown as dashed lines (bottom). Anisotropic displacement ellipsoids depicted at 50% probability. Hydrogen atoms, disorder components, and co-crystallised solvent molecules are omitted for clarity. Aliphatic substituents are depicted as wireframes for clarity.

2.4 Conclusions

Organic azides react with metal-cyaphide complexes in a 1,3-dipolar cycloaddition reaction to yield the corresponding metal-triazaphospholes. The reaction proceeds rapidly at room temperature and in the absence of a catalyst, to yield a single regioisomer of the triazaphospholes, which demonstrate enhanced stability over the starting materials.

The reaction has broad applicability with examples across the s-, p-, and d-block. For the highly ionic magnesium(II) cyaphide complex, the reaction is only compatible for electron-rich aliphatic azides. The Lewis acidic magnesium(II) coordinates to the nitrogen adjacent to the carbon on the triazaphosphole of a second molecule, yielding dimeric species.

The reactivity of metal-triazaphospholes was explored further, with Lewis acid coordination and methylation at the most nucleophilic nitrogen atom adjacent to the triazaphosphole carbon. Reaction with iodine resulted in the first examples of halogenated triazaphospholes, which give insight into their halogen bond forming capabilities.

The cyaphide-azide 1,3-dipolar cycloaddition reaction displays many of the advantages of the CuAAC reaction, and was further extended to molecules containing two azide functionalities, giving insight to its potential as a covalent bond forming reaction for the preparation of MIMs, which will be the subject of the next chapter.

The work in this chapter has been published in *Chemistry – A European Journal:*

E. S. Yang, A. Mapp, A. Taylor, P. D. Beer, J. M. Goicoechea, *Chem. Eur. J.* **2023**, *29*, e202301648.

Dr. Eric Yang contributed to the DFT experiments in section 2.3.3 and the synthesis and characterisation of:

Complexes **1a** and **1b** in section 2.2.1

Complexes **3a** and **3b** in section 2.2.3

Complex **4** in section 2.2.4

Complex **5a** in section 2.3.1

Iodotriazaphospholes **7a** and **7b** in section 2.3.3

2.5 Experimental

2.5.1 Synthesis of (IDipp)Au(CP) from solvent-free [Mg(CP)]$_2$

[Mg(CP)]$_2$ (250 mg, 0.258 mmol) was dissolved in toluene (5 mL) with 5 drops of dioxane. (IDipp)AuCl (272 mg, 0.438 mmol, 1.7 equiv.) was added, and the reaction mixture was stirred for 1 h. The reaction mixture was filtered *via* cannula filtration to remove (^{Dipp}NacNac)MgCl(diox), and the filtrate was collected directly into a flask containing pentane (30 mL). The reaction mixture was stored at −35 ºC overnight to yield the product as a yellow solid. Yield: 190 mg, 0.30 mmol, 69% yield.

2.5.2 Synthesis of 1a

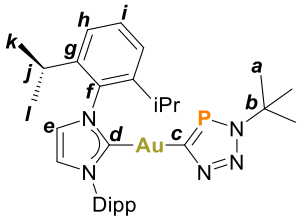

Tert-butyl azide (8 mg, 0.08 mmol) was added to a solution of (IDipp)Au(CP) (50 mg, 0.08 mmol) in toluene (1 mL) and stirred at room temperature for 2 h. The solution was concentrated by slow evaporation, yielding colorless crystals suitable for SC-XRD. The mixture was then stored at −35 ºC for 3 days to yield colorless crystals, which were isolated by filtration. Yield: 50 mg, 0.07 mmol, 86%.

^{1}H NMR (600 MHz, C_6D_6): δ(ppm) 7.18 (t, $^3J_{H–H}$ = 7.8 Hz, 2H, H_i), 7.06 (d, $^3J_{H–H}$ = 7.8 Hz, 4H, H_h), 6.35 (s, 2H, H_e), 2.69 (sept, $^3J_{H–H}$ = 6.9 Hz, 4H, Dipp H_j), 1.53 (d, $^3J_{H–H}$ = 6.9 Hz, 12H, $H_{k/l}$), 1.42 (s, 9H, H_a), 1.10 (d, $^3J_{H–H}$ = 6.9 Hz, 12H, $H_{k/l}$).

$^{13}C\{^{1}H\}$ NMR (151 MHz, C_6D_6): δ(ppm) 205.2 (d, $^{1}J_{C–P}$ = 82.0 Hz, C_c), 196.5 (d, $^{3}J_{C–P}$ = 11.1 Hz, C_d), 145.9 (C_g), 134.8 (C_f), 130.7 (C_i), 124.3 (C_h), 122.7 (C_e), 59.7 (d, $^{2}J_{C–P}$ = 5.1 Hz, C_b), 32.0 (d, $^{3}J_{C–P}$ = 5.0 Hz, C_a), 29.1 (C_j), 24.9 ($C_{k/l}$), 24.0 ($C_{k/l}$).

$^{31}P\{^{1}H\}$ NMR (162 MHz, C_6D_6): δ(ppm) 191.2 (s).

Elemental Anal. Calcd. (%) for $C_{32}H_{45}AuN_5P$: C, 52.82; H, 6.23; N, 9.62. Found: C, 52.49; H, 6.31; N, 9.00.

2.5.3 Synthesis of 1b

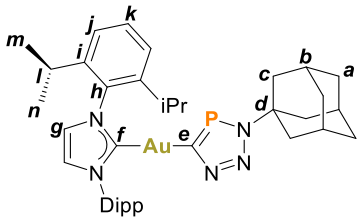

1-Adamantyl azide (20 mg, 0.11 mmol) was added to a solution of (IDipp)Au(CP) (71 mg, 0.11 mmol) in toluene (1 mL) and stirred at room temperature for 16 h. The solution was concentrated under vacuum, then stored at −35 ºC for 3 days to yield colorless crystals, which were isolated by filtration. Yield: 82 mg, 0.10 mmol, 90%.

^{1}H NMR (600 MHz, C_6D_6): δ(ppm) 7.20 (t, $^{3}J_{H–H}$ = 7.8 Hz, 2H, H_k), 7.07 (d, $^{3}J_{H–H}$ = 7.8 Hz, 4H, H_j), 6.39 (s, 2H, H_g), 2.70 (sept, $^{3}J_{H–H}$ = 6.9 Hz, 4H, H_l), 2.17 (d, $^{3}J_{H–H}$ = 2.8 Hz, 6H, H_c), 1.85–1.77 (m, 3H, H_b), 1.54 (d, $^{3}J_{H–H}$ = 6.9 Hz, 12H, $H_{m/n}$), 1.45–1.37 (m, 6H, H_a), 1.11 (d, $^{3}J_{H–H}$ = 6.9 Hz, 12H, $H_{m/n}$).

$^{13}C\{^{1}H\}$ NMR (151 MHz, C_6D_6): δ(ppm) 204.5 (d, $^{1}J_{C–P}$ = 81.9 Hz, C_e), 196.5 (d, $^{3}J_{C–P}$ = 11.0 Hz, C_f), 145.9 (C_i), 134.8 (C_h), 130.7 (C_k), 124.3 (C_j), 122.8 (C_g), 60.2 (d, $^{2}J_{C–P}$ = 4.4 Hz, C_d), 45.8 (d, $^{3}J_{C–P}$ = 5.1 Hz, C_c), 36.5 (C_a), 30.3 (C_b), 29.2 (C_l), 24.9 ($C_{m/n}$), 24.0 ($C_{m/n}$).

$^{31}P\{^{1}H\}$ NMR (162 MHz, C_6D_6): δ(ppm) 189.3 (s).

Elemental Anal. Calcd. (%) for $C_{38}H_{51}AuN_5P$: C, 56.64; H, 6.38; N, 8.69. Found: C, 57.05; H, 6.17; N, 8.43.

2.5.4 Synthesis of 1c

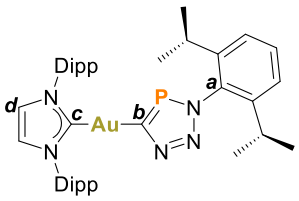

2,6-Diisopropylphenyl azide (17 mg, 0.08 mmol) was added to a solution of (IDipp)Au(CP) (50 mg, 0.08 mmol) in toluene (1 mL) and stirred at room temperature for 16 h. Crystals suitable for SC-XRD were obtained by concentrating the toluene solution *in vacuo,* followed by layering with hexane (5 mL). The supernatant solution was removed, and the crystals were washed with pentane (2 × 2 mL), then dried under vacuum. Yield: 54 mg, 0.06 mmol, 81%.

^{1}H NMR (600 MHz, C_6D_6): δ(ppm) 7.12–7.09 (m, 2H, Dipp Ar-H), 7.02–7.00 (m, 7H, Dipp Ar-H), 6.32 (s, 2H, H_d), 2.68 (sept, $^{3}J_{H–H}$ = 6.9 Hz, 4H, Dipp ^{i}Pr CH), 2.15 (sept, $^{3}J_{H–H}$ = 6.8 Hz, 2H, Dipp ^{i}Pr CH), 1.54 (d, $^{3}J_{H–H}$ = 6.9 Hz, 12H, Dipp Me), 1.08 (d, $^{3}J_{H–H}$ = 6.9 Hz, 12H, Dipp Me) 0.83 (d, $^{3}J_{H–H}$ = 6.8 Hz, 6H, Dipp Me),* 0.82 (d, $^{3}J_{H–H}$ = 6.8 Hz, 6H, Dipp Me).* *overlapping doublets

$^{13}C\{^{1}H\}$ NMR (151 MHz, C_6D_6): δ(ppm) 208.0 (d, $^{1}J_{C–P}$ = 83.3 Hz, C_b), 195.8 (d, $^{3}J_{C–P}$ = 10.9 Hz, C_c), 146.6 (Dipp Ar-C), 145.7 (Dipp Ar-C), 138.1 (d, $^{2}J_{C–P}$ = 6.3 Hz, C_a), 134.7 (Dipp Ar-C), 130.8 (Dipp Ar-C), 128.9 (Dipp Ar-C), 124.3 (Dipp Ar-C), 123.5 (Dipp Ar-C), 122.8 (C_d), 29.1 (Dipp ^{i}Pr CH), 28.3 (Dipp ^{i}Pr CH), 24.0 (Dipp Me), 24.4 (Dipp Me), 24.2 (Dipp Me), 24.0 (Dipp Me).

The Dipp resonances could not be distinguished between the IDipp and triazaphosphole and are therefore assigned generally.

$^{31}P\{^{1}H\}$ NMR (162 MHz, C_6D_6): δ(ppm) 209.3 (s).

Elemental Anal. Calcd. (%) for $C_{40}H_{54}N_5AuP \cdot 0.5(C_7H_8)$: C, 61.03; H, 6.76; N, 7.57. Found: C, 60.90; H, 6.49; N, 7.24.

2.5.5 Synthesis of 2

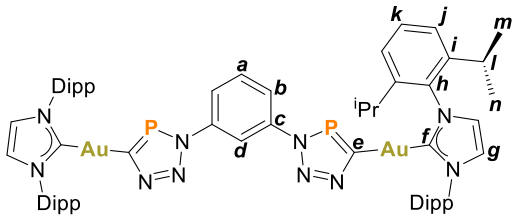

1,3-Diazidobenzene (3.82 mg, 0.024 mmol) was added to a solution of (IDipp)Au(CP) (30 mg, 0.048 mmol) in toluene (1 mL) and stirred at room temperature for 16 h. The resulting precipitate was isolated by filtration. The filtrate was concentrated under vacuum, then stored at −35 ºC for 3 days to yield orange crystals, which were isolated by filtration. Yield: 22 mg, 0.016 mmol, 63%.

^{1}H NMR (600 MHz, CD_2Cl_2): δ(ppm) = 8.03 (s, 1H; H_d), 7.64 (dd, $^{3}J_{H–H}$ = 8.1 Hz, $^{4}J_{H–H}$ = 2.1 Hz, 2H; H_b), 7.55 (t, $^{3}J_{H–H}$ = 7.8 Hz, 4H; H_k), 7.39 (t, $^{3}J_{H–H}$ = 8.1 Hz, 1H; H_a), 7.36 (d, $^{3}J_{H–H}$ = 7.8 Hz 8H; H_j), 7.25 (s, 4H; H_g), 2.69 (sept, $^{3}J_{H–H}$ = 6.9 Hz, 8H; H_l), 1.41 (d, $^{3}J_{H–H}$ = 6.9 Hz, 24H; $H_{m/n}$), 1.26 (d, $^{3}J_{H–H}$ = 6.9 Hz, 24H; $H_{m/n}$).

$^{13}C\{^{1}H\}$ NMR (151 MHz, CD_2Cl_2): δ(ppm) = 208.2 (d, $^{1}J_{C–P}$ = 84.1 Hz; C_e), 194.2 (d, $^{3}J_{C–P}$ = 10.0 Hz; C_f), 146.3 (C_i), 143.2 (d, $^{2}J_{C–P}$ = 7.6 Hz; C_c) 134.8 (C_h), 130.9 (C_k), 130.4 (C_a), 124.5 (C_j), 123.8 (C_g), 120.7 (d, $^{3}J_{C–P}$ = 5.4 Hz; C_b), 115.8 (t, $^{3}J_{C–P}$ = 6.5 Hz; C_d), 29.3 (C_l), 24.7 ($C_{m/n}$), 24.2 ($C_{m/n}$).

$^{31}P\{^{1}H\}$ NMR (162 MHz, CD_2Cl_2): δ(ppm) 200.8 (s).

Elemental Anal. Calcd. (%) for $C_{62}H_{78}Au_2N_{10}P_2 \cdot 0.5(C_7H_8)$: C, 52.47; H, 5.54; N, 9.87. Found: 52.74; H, 5.40; N, 9.16.

2.5.6 Synthesis of 3a

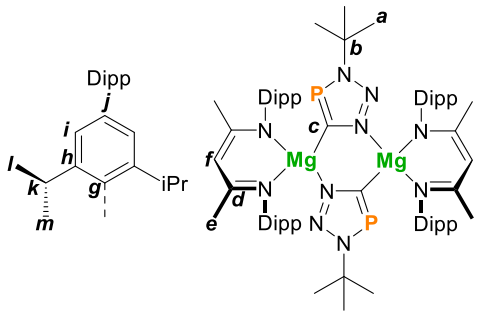

(^{Dipp}NacNac)Mg(CP)(diox.) (approx. 130 mg, 0.23 mmol) was generated *in situ* in toluene (1 mL). Tert-butyl azide (23 mg, 0.23 mmol) was added, and the solution was swirled to ensure complete mixing. The reaction solution was allowed to stand for 16 h, resulting in the formation of colorless crystals suitable for SC-XRD. The supernatant was decanted, and the crystals were washed with hexane (3 × 1 mL), then dried under vacuum. Yield: 120 mg, 0.10 mmol, 91%.

^{1}H NMR (400 MHz, C_6D_6): δ(ppm) 7.12–6.95 (m, 8H, H_i), 6.94–6.87 (m, 4H, H_j), 4.97 (s, 2H, H_f), 3.88 (sept, $^{3}J_{H–H}$ = 6.8 Hz, 4H, H_k), 2.57 (sept, $^{3}J_{H–H}$ = 6.8 Hz, 4H, H_k), 1.67 (d, $^{3}J_{H–H}$ = 6.8 Hz, 12H, $H_{l/m}$), 1.66 (s, 12H, H_e), 1.54 (s, 18H, H_a), 1.30 (d, $^{3}J_{H–H}$ = 6.8 Hz, 12H, $H_{l/m}$), 0.99 (d, $^{3}J_{H–H}$ = 6.8 Hz, 12H, $H_{l/m}$), −0.64 (d, $^{3}J_{H–H}$ = 6.8 Hz, 12H, $H_{l/m}$).

$^{13}C\{^{1}H\}$ NMR (126 MHz, C_6D_6): δ(ppm) 207.2 (d, $^{1}J_{C–P}$ = 93.3 Hz, C_c), 168.2 (C_d), 146.6 (C_g), 143.2 (C_h), 141.7 (C_h), 124.7 (C_i), 124.2 (C_j), 122.9 (C_i), 95.0 (C_f), 61.0 (d, $^{2}J_{C–P}$ = 2.9 Hz, C_b), 31.8 (d, $^{3}J_{C–P}$ = 4.6 Hz, C_a), 30.0 (C_k), 27.6 (C_k), 25.0 ($C_{l/m}$), 24.7 ($C_{l/m}$), 24.4 ($C_{l/m}$), 24.2 (C_e), 24.0 ($C_{l/m}$).

Restricted rotation about the N–C_{Dipp} bond due to steric clash results in inequivalence of the Dipp resonances.

$^{31}P\{^{1}H\}$ NMR (162 MHz, C_6D_6): δ(ppm) 224.3 (s).

Elemental Anal. Calcd. (%) for $C_{68}H_{100}Mg_2N_{10}P_2\cdot(C_6H_{14})$: C, 70.86; H, 9.16; N, 11.17. Found: C, 70.68; H, 8.56; N, 10.84.

2.5.1 Synthesis of 3b

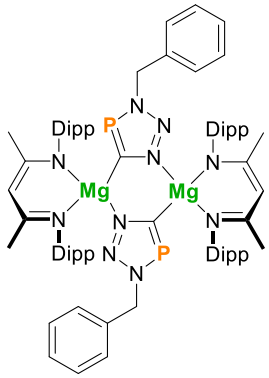

(^{Dipp}NacNac)Mg(CP)(diox.) (approx. 65 mg, 0.11 mmol) was generated *in situ* in toluene (1 mL). Benzyl azide (14 mg, 0.11 mmol) was added, and the solution was swirled to ensure complete mixing. The reaction solution was allowed to stand for 3 h, resulting in the formation of colorless crystals. The supernatant was decanted, and the crystals were washed with hexane (3 × 1 mL), then dried under vacuum. Yield: 30 mg, 0.05 mmol, 43%.

Elemental Anal. Calcd. (%) for $C_{80}H_{112}Mg_2N_{10}P_2\cdot(C_6H_{14})$: C, 72.66; H, 8.38; N, 10.59. Found: C, 72.26; H, 7.89; N, 9.94.

The low solubility of {(^{Dipp}NacNac)Mg(CPN_3Bn)}$_2$ in polar organic solvents eg. THF, DMSO, and DCM, precluded characterization by NMR spectroscopy.

2.5.2 Synthesis of 4

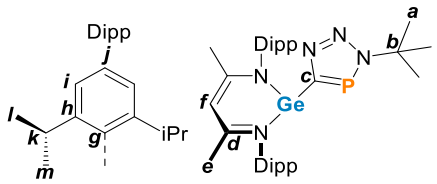

(^{Dipp}NacNac)Mg(CP)(diox.) (approx. 42 mg, 0.07 mmol) was generated *in situ* in toluene (1 mL). (^{Dipp}NacNac)GeCl (38 mg, 0.07 mmol) was added, and the reaction mixture was stirred for 3 h. The reaction mixture was filtered, then tert-butyl azide (7 mg, 0.07 mmol) was added to the filtrate. The reaction solution was stirred for 16 h, then the solvent was removed under vacuum. The residue was washed with hexane (3 × 1 mL), then recrystallized from toluene at −35 ºC over 3 days. Yield: 32 mg, 0.06 mmol, 70%.

^{1}H NMR (500 MHz, C_6D_6): δ(ppm) 7.16–7.09 (m, 4H, H_i), 6.98 (dd, $^{3}J_{H–H}$ = 6.3, 2.9 Hz, 2H, H_j), 5.22 (s, 1H, H_f), 3.66 (sept, $^{3}J_{H–H}$ = 6.8 Hz, 2H, H_k), 2.92 (sept, $^{3}J_{H–H}$ = 6.8 Hz, 2H, H_k), 1.63 (s, 9H, H_a), 1.60 (s, 6H, H_e), 1.38 (d, $^{3}J_{H–H}$ = 6.8 Hz, 6H, $H_{l/m}$), 1.18 (d, $^{3}J_{H–H}$ = 6.8 Hz, 6H, $H_{l/m}$), 0.98 (d, $^{3}J_{H–H}$ = 6.8 Hz, 6H, $H_{l/m}$), 0.62 (d, $^{3}J_{H–H}$ = 6.8 Hz, 6H, $H_{l/m}$).

^{13}C{^{1}H} NMR (126 MHz, C_6D_6): δ(ppm) 199.4 (d, $^{1}J_{C–P}$ = 105.1 Hz, C_c), 166.7 (C_d), 146.3 (C_g), 143.6 (C_h), 141.6 (C_h), 127.5 (C_i), 124.9 (C_j), 124.4 (C_i), 100.1 (d, $^{5}J_{C–P}$ = 6.7 Hz, C_f), 60.5 (d, $^{2}J_{C–P}$ = 4.5 Hz, C_b), 32.4 (d, $^{2}J_{C–P}$ = 5.7 Hz, C_a), 29.4 (C_k), 28.7 (d, $^{6}J_{C–P}$ = 3.9 Hz, C_k), 26.0 ($C_{l/m}$), 24.9 ($C_{l/m}$)), 24.7 ($C_{l/m}$), 23.7 (C_e/$C_{l/m}$), 23.6 (C_e/$C_{l/m}$).

Restricted rotation about the N–C_{Dipp} bond due to steric clash results in inequivalence of the Dipp resonances.

^{31}P{^{1}H} NMR (162 MHz, C_6D_6): δ(ppm) 196.9 (s).

Elemental Anal. Calcd. (%) for $C_{30}H_{41}GeN_2P$: C, 64.57; H, 7.97; N, 11.07. Found: C, 65.11; H, 8.28; N, 10.68.

2.5.3 Synthesis of 5a

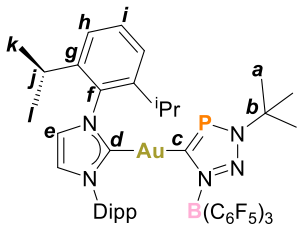

1a (20 mg, 0.03 mmol) and $B(C_6F_5)_3$ (14 mg, 0.03 mmol) were dissolved in toluene (0.5 mL). The reaction mixture was stirred for 1 h, then concentrated by slow evaporation. Storage at −35 ºC over 7 days yielded colorless crystals, which were isolated by filtration, washed with pentane (3 × 0.5 mL), then dried under vacuum. Yield: 19 mg, 0.02 mmol, 56%.

^{1}H NMR (600 MHz, C_6D_6): δ(ppm) 7.34 (t, $^3J_{H–H}$ = 7.8 Hz, 2H, H_i), 7.06 (d, $^3J_{H–H}$ = 7.8 Hz, 4H, H_h), 6.28 (s, 2H, H_e), 2.55 (b, 4H, H_j), 1.35 (b, 12H, $H_{k/l}$), 1.00 (s, 9H, H_a), 0.95 (d, $^3J_{H–H}$ = 6.9 Hz, 12H, $H_{k/l}$).

^{13}C{^{1}H} NMR (151 MHz, C_6D_6): δ(ppm) 207.3 (d, $^1J_{C–P}$ = 77.0 Hz, C_c), 190.9 (d, $^3J_{C–P}$ = 3.5 Hz, C_d), 149.9 (b, $B(C_6F_5)$), 148.3 (b, $B(C_6F_5)$), 145.7 (C_g), 140.7 (b, $B(C_6F_5)$), 139.1 (b, $B(C_6F_5)$), 137.9 (b, $B(C_6F_5)$), 136.3 (b, $B(C_6F_5)$), 134.5 (C_f), 130.9 (C_i), 124.3 (C_h), 123.9 (C_e), 63.7 (C_b), 30.3 (d, $^3J_{C–P}$ = 5.1 Hz, C_a), 29.0 (C_j), 24.8 ($C_{k/l}$), 23.7 ($C_{k/l}$).

^{31}P{^{1}H} NMR (162 MHz, C_6D_6): δ(ppm) 203.5 (s).

^{19}F{^{1}H} NMR (377 MHz, C_6D_6): δ(ppm) −124.46–−135.30 (m, $B(C_6F_5)_3$ *ortho* C**F**), −156.82–−161.17 (m, $B(C_6F_5)_3$ *para* C**F**), −161.18–−168.19 (m, $B(C_6F_5)_3$ *meta* C**F**).

^{11}B{^{1}H} NMR (128 MHz, C_6D_6): δ(ppm) −5.52 (b, **B**$(C_6F_5)_3$).

Elemental Anal. Calcd. (%) for $C_{50}H_{45}AuBF_{15}N_5P \cdot 2(C_7H_8)$: C, 54.02; H, 4.25; N, 4.92. Found: C, 53.95 H, 3.82; N, 5.25.

2.5.4 Synthesis of 5c

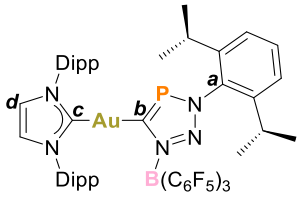

1c (20 mg, 0.03 mmol) and $B(C_6F_5)_3$ (14 mg, 0.03 mmol) were dissolved in toluene (0.5 mL) and stirred for 1 h. The solvent was removed *in vacuo*, and the residue extracted into DCM (1 mL) and filtered. Storage at −35 ºC over 7 days yielded colorless crystals, which were isolated by filtration, washed with pentane (3 × 0.5 mL), then dried under vacuum. Yield: 13 mg, 0.0097 mmol, 41%.

^{1}H NMR (600 MHz, C_6D_6): δ(ppm) 7.27 (t, $^3J_{H–H}$ = 7.8 Hz, 2H, Dipp Ar-H), 7.04 (m, $^3J_{H–H}$ = 7.8 Hz, 5H, Dipp Ar-H), 6.92 (d, $^3J_{H–H}$ = 7.8 Hz, 2H, Dipp Ar-H), 6.27 (s, 2H, H_d), 2.51 (b, 4H, Dipp ^{i}Pr CH), 2.27 (b, 2H, Dipp ^{i}Pr CH), 1.30 (b, 12H, Dipp Me), 1.10 (b, 6H, Dipp Me), 0.95 (d, $^3J_{H–H}$ = 6.9 Hz, 12H, Dipp Me), 0.91 (b, 6H, Dipp Me)

^{13}C{^{1}H} NMR (151 MHz, C_6D_6): δ(ppm) 210.4 (d, $^1J_{C–P}$ = 80.3 Hz, C_b), 190.4 (d, $^3J_{C–P}$ = 2.2 Hz, C_c), 149.6 (b, $B(C_6F_5)$), 148.0 (b, $B(C_6F_5)$), 145.9 (Dipp Ar-C), 145.6 (Dipp Ar-C), 140.8 (b, $B(C_6F_5)$), 139.1 (b, $B(C_6F_5)$), 138.0 (b, $B(C_6F_5)$), 136.4 (b, $B(C_6F_5)$), 134.9 (d, $^3J_{C–P}$ = 3.8 Hz, C_a) 134.40 (Dipp Ar-C), 131.0 (Dipp Ar-C), 124.3 (Dipp Ar-C), 124.2 (Dipp Ar-C), 123.9 (C_d), 29.0 (Dipp ^{i}Pr), 28.4 (Dipp ^{i}Pr), 24.7 (Dipp Me), 24.6 (Dipp Me), 23.8 (Dipp Me), 23.7 (Dipp Me).

One of the Dipp Ar-C peaks could not be located.

The Dipp resonances could not be distinguished between the IDipp and triazaphosphole and are therefore assigned generally.

$^{31}P\{^{1}H\}$ NMR (162 MHz, C_6D_6): δ(ppm) 220.4 (s).

$^{19}F\{^{1}H\}$ NMR (565 MHz, C_6D_6): δ(ppm) −124.41–−167.21 (m, $B(C_6F_5)_3$ C**F**).

$^{11}B\{^{1}H\}$ NMR (128 MHz, C_6D_6): δ(ppm) −5.02 (b, **B**$(C_6F_5)_3$).

Elemental Anal. Calcd. (%) for $C_{58}H_{54}AuBF_{15}N_5P$: C, 51.80; H, 4.05; N, 5.21. Found: C, 50.88; H, 3.91; N, 5.90.

2.5.10 Synthesis of 6

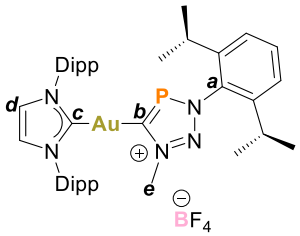

1b (20 mg, 0.024 mmol) and $[Me_3O][BF_4]$ (3.91 mg, 0.026 mmol) were dissolved in DCM (1 mL) and stirred for 16 h. The solvent was removed *in vacuo*, and the solids were washed with Et_2O (3 × 1 mL), then dried under vacuum to afford a yellow solid. Crystals suitable for SC-XRD were grown by layering a DCM solution of **6** with hexane. Yield: 14 mg, 0.015 mmol, 62%.

^{1}H NMR (600 MHz, CD_2Cl_2): δ (ppm) = 7.60 (t, $^{3}J_{H–H}$ = 7.8 Hz, 2H; Dipp *para*-H), 7.55 (t, $^{3}J_{H–H}$ = 7.8 Hz, 1H; Dipp *para*-H), 7.41 (s, 2H; H_d)*, 7.40 (d, $^{3}J_{H–H}$ = 7.8 Hz, 4H; Dipp *meta*-H)*, 7.32 (d, $^{3}J_{H–H}$ = 7.8 Hz, 2H; Dipp *meta*-H), 3.95 (s, 3H; C_e), 2.64 (sept, $^{3}J_{H–H}$ = 6.9 Hz, 4H; Dipp iPr CH), 1.98 (sept, $^{3}J_{H–H}$ = 6.8 Hz, 2H; Dipp ^{i}Pr CH), 1.37 (d, $^{3}J_{H–H}$ = 6.9 Hz, 12H; Dipp Me), 1.29 (d, $^{3}J_{H–H}$ = 6.9 Hz, 12H; Dipp Me), 1.10 (6H, $^{3}J_{H–H}$ = 6.9 Hz, 12H; Dipp Me), 1.06 (6H, $^{3}J_{H–H}$ = 6.9 Hz, 6H; Dipp Me).

*overlapping peaks

The Dipp resonances could not be distinguished between the IDipp and triazaphosphole and are therefore assigned generally.

$^{13}C\{^1H\}$ NMR (151 MHz, C_6D_6): δ (ppm) = 206.8 (d, $^1J_{C–P}$ = 84.8 Hz; C_b), 187.4 (d, $^3J_{C–P}$ = 6.4 Hz; carbene C_c), 146.4 (Dipp *ipso*-C), 145.3 (Dipp *meta*-C), 134.2 (Dipp *meta*-C), 133.7 (d, $^2J_{C–P}$ = 3.6 Hz; C_a), 132.2 (Dipp *para*-C), 131.4 (Dipp *para*-C), 124.9 (C_d), 124.9 (Dipp *meta*-C), 124.8 (Dipp *meta*-C), 46.4 (d, $^3J_{C–P}$ = 3.1 Hz; C_e), 29.3 (Dipp iPr CH), 28.9 (Dipp iPr Me), 24.9 (Dipp Me), 24.4 (Dipp Me), 24.3 (Dipp Me), 24.1 (Dipp Me).

$^{31}P\{^1H\}$ NMR (162 MHz, C_6D_6): δ (ppm) = 236.9 (s).

$^{19}F\{^1H\}$ NMR (565 MHz, CD_2Cl_2): δ(ppm) −153.06.

$^{11}B\{^1H\}$ NMR (193 MHz, CD_2Cl_2): δ(ppm) −1.14 (br).

2.5.5 Synthesis of 7a

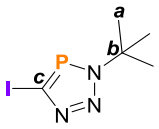

A solution of iodine in hexane (4 mL, 0.016 M, 0.06 mmol) was added dropwise to a stirred solution of **1a** (47 mg, 0.06 mmol) in toluene (5 mL). After stirring for 4 h, all volatiles were removed under vacuum. The residue was extracted with hexane (2 × 3 mL), which was then evaporated to dryness under vacuum to afford the product as an off-white powder. Crystals suitable for SC-XRD were obtained from hexane at −35 °C. Yield: 10 mg, 0.04 mmol, 58%.

^1H NMR (600 MHz, C_6D_6): δ(ppm) 1.18 (d, $^4J_{H–P}$ = 0.9 Hz, 9H, H_a).

$^{13}C\{^1H\}$ NMR (151 MHz, C_6D_6): δ(ppm) 120.8 (d, $^1J_{C–P}$ = 80.6 Hz, C_c), 62.3 (d, $^2J_{C–P}$ = 6.0 Hz, C_b), 31.3 (d, $^3J_{C–P}$ = 6.4 Hz, C_a).

$^{31}P\{^{1}H\}$ NMR (162 MHz, C_6D_6): δ(ppm) 179.9 (m).

Elemental Anal. Calcd. (%) for $C_5H_9N_3IP$: C, 22.32; H, 3.37; N, 15.62. Found: C, 20.97; H, 2.67; N, 14.89.

2.5.6 Synthesis of 7b

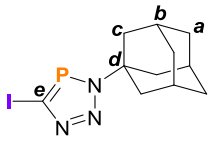

A solution of iodine in hexane (0.8 mL, 0.1 M, 0.08 mmol) was added to a solution of **1b** (64 mg, 0.08 mmol) in toluene (1 mL), which was then stirred for 16 h. All volatiles were removed under vacuum, and the resulting residue was extracted with hexane (2 × 3 mL). The hexane solution was evaporated to dryness, yielding the product as a colorless solid. Yield: 16 mg, 0.05 mmol, 58%.

^{1}H NMR (400 MHz, C_6D_6): δ(ppm) 1.96–1.91 (m, 6H, H_c), 1.81–1.75 (m, 3H, H_b), 1.41–1.31 (m, 6H, CH_a).

$^{13}C\{^{1}H\}$ NMR (151 MHz, C_6D_6): δ(ppm) 120.5 (d, $^{1}J_{C-P}$ = 80.8 Hz, C_e), 62.9 (d, $^{2}J_{C-P}$ = 5.3 Hz, Ad C_d), 45.2 (d, $^{3}J_{C-P}$ = 6.5 Hz, C_c), 35.9 (C_a), 30.0 (d, $^{4}J_{C-P}$ = 0.7 Hz, C_b).

$^{31}P\{^{1}H\}$ NMR (162 MHz, C_6D_6): δ(ppm) 180.1 (m).

Elemental Anal. Calcd. (%) for $C_{11}H_{15}N_3IP \cdot 0.5(C_6H_6)$: C, 43.53; H, 4.70; N, 10.88. Found: C, 42.96; H, 4.73; N, 10.77.

2.5.7 Synthesis of 7c

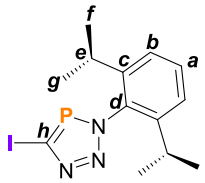

A solution of iodine in hexane (0.8 mL, 0.1 M, 0.08 mmol) was added *via* syringe to a solution of **1c** (67 mg, 0.08 mmol) in toluene (5 mL). The solution was stirred at room temperature for 16 h. All volatiles were removed under vacuum, and the resulting residue was extracted with hexane (2 × 3 mL). The hexane solution was evaporated to dryness, yielding the product as a dark red oil. Yield: 22 mg, mmol, 76%.

^{1}H NMR (400 MHz, C_6D_6): δ(ppm) 6.98 (d, 2H, $^{3}J_{H–H}$ = 7.8 Hz, H_b), 2.10 (sept, $^{3}J_{H–H}$ = 6.8 Hz, 2H, H_e), 0.91 (d, $^{3}J_{H–H}$ = 6.8 Hz, 6H, $H_{f/g}$), 0.86 (d, $^{3}J_{H–H}$ = 6.9 Hz, 6H, $H_{f/g}$).

H_a resonance overlaps with the solvent peak.

^{13}C{^{1}H} NMR (151 MHz, C_6D_6): δ(ppm) 146.3 (d, $^{3}J_{C–P}$ = 1.6 Hz, C_c), 134.8 (d, $^{2}J_{C–P}$ = 6.3 Hz, C_d), 130.9 (C_a), 124.1 (C_b), 123.4 (d, $^{1}J_{C–P}$ = 83.5 Hz, C_h), 28.7 (C_e), 24.3 ($C_{f/g}$), 24.1 ($C_{f/g}$).

^{31}P{^{1}H} NMR (162 MHz, C_6D_6): δ(ppm) 194.7 (s).

Elemental Anal. Calcd. (%) for $C_{13}H_{17}N_3IP$: C, 41.84; H, 4.59; N, 11.26. Found: C, 46.36; H, 5.25; N, 10.56.

2.6 References

1. W. Rösch and M. Regitz, *Angew. Chem. Int. Ed.* **1984**, *23*, 900–901.
2. Y. Y. C. Y. L. Ko, R. Carrié, A. Muench and G. Becker, *J. Chem. Soc. Chem. Commun.* **1984**, 1634–1635.
3. J.-C. Guillemin, T. Janati and J.-M. Denis, *J. Org. Chem.* **2001**, *66*, 7864–7868.
4. D. W. N. Wilson, S. J. Urwin, E. S. Yang and J. M. Goicoechea, *J. Am. Chem. Soc.* **2021**, *143*, 10367–10373.
5. T. Görlich, D. S. Frost, N. Boback, N. T. Coles, B. Dittrich, P. Müller, W. D. Jones and C. Müller, *J. Am. Chem. Soc.* **2021**, *143*, 19365–19373.
6. E. S. Yang and J. M. Goicoechea, *Angew. Chem. Int. Ed.* **2022**, *61*, e202206783.
7. R. C. Storr and T. L. Gilchrist, *Sci. Synth.* **2004**, *13*, 1
8. H. V. Huynh, Y. Han, R. Jothibasu and J. A. Yang, *Organometallics* **2009**, *28*, 5395–5404.
9. S. Dery, C. Ehinger, J. Roudin, Y. Kakiuchi, D. Gioffrè and C. Copéret, *J. Am. Chem. Soc.* **2025**, *147*, 18054–18063.
10. A. Brown and P. D. Beer, *Chem. Commun.* **2016**, *52*, 8645–8658.
11. R. Evans, Z. Deng, A. K. Rogerson, A. S. McLachlan, J. J. Richards, M. Nilsson and G. A. Morris, *Angew. Chem. Int. Ed.* **2013**, *52*, 3199–3202.
12. L. Davin, R. McLellan, A. Hernán-Gómez, W. Clegg, A. R. Kennedy, M. Mertens, I. A. Stepek and E. Hevia, *Chem. Commun.* **2017**, *53*, 3653–3656.
13. M. Papke, L. Dettling, J. A. W. Sklorz, D. Szieberth, L. Nyulászi and C. Müller, *Angew. Chem. Int. Ed.* **2017**, *56*, 16484–16489.
14. L. Dettling, N. Limberg, R. Küppers, D. Frost, M. Weber, N. T. Coles, D. M. Andrada and C. Müller, *Chem. Commun.* **2023**, *59*, 10243–10246.
15. H. Meerwein, G. Hinz, P. Hofmann, E. Kroning and E. Pfeil, *J. Für Prakt. Chem.* **1937**, *147*, 257–285.

16. J. Pancholi and P. D. Beer, *Coord. Chem. Rev.* **2020**, *416*, 213281.

Chapter 3

An Inorganic Click Reaction for the Synthesis of [2]Rotaxanes

Abstract

The cyaphide-azide 1,3-dipolar cycloaddition reaction can be used in a capping technique to yield a new class of inorganic [2]rotaxanes. A perethylated pillar[5]arene threads electron-deficient bis-azides, and the generated pseudo[2]rotaxanes were found to readily undergo rapid 1,3-dipolar cycloaddition reactions with two equivalents of (IDipp)Au(CP) to afford the [2]rotaxanes in good yields (up to 65%). The resulting interlocked products have enhanced air- and moisture-stability over their non-interlocked counterparts, and can therefore be purified using column chromatography.

3.1 Pillar[5]arene-based rotaxanes

The pillar[*n*]arenes are a class of compounds containing *n* benzene-1,4-diether units joined at the 2,5-positions by methylene linkers in a cyclic manner, giving a pillar-like structure. They are a relatively new class of macrocycles, first reported by Ogoshi in 2008,[1] and have since been used extensively in the field of supramolecular chemistry due to their ease of synthesis, good solubility, and excellent host-guest properties.[2] They are prepared by solvent-templated condensation reactions of benzene-1,4-diether units with paraformaldehyde, in the presence of a Lewis acid catalyst such as $BF_3{\cdot}OEt_2$. The size of the pillar[*n*]arenes is dependent on the nature of the solvent template. Reactions in 1,2-dichloroethane (1,2-DCE) result in the formation of pillar[5]arene, **P5A^{R}** (**Scheme 3.1**).

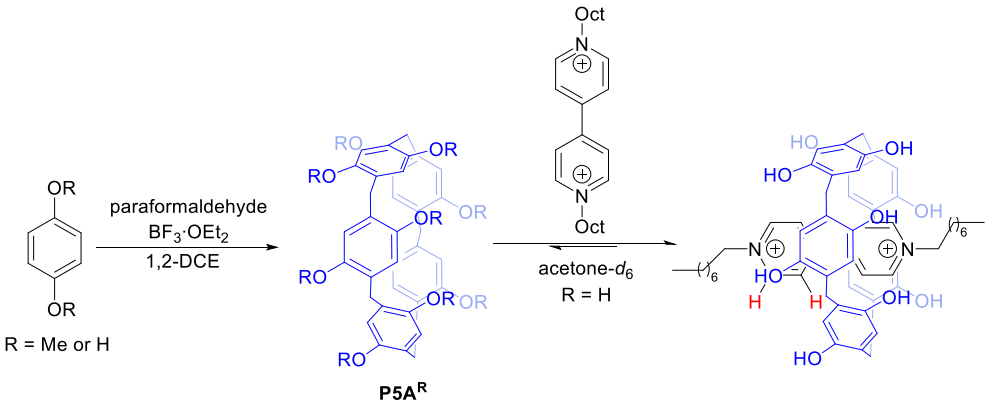

Scheme 3.1. Synthesis of pillar[5]arene, **P5A^{R}**.[1]

In Ogoshi's seminal report, the host-guest properties of **P5A^{H}** were demonstrated by its threading of a dioctyl viologen salt (featuring charged bipyridinium groups). This was evidenced by the diagnostic upfield shift of the 4,4'-bipyridinium resonances (**highlighted in red in Scheme 3.1**) in the ^{1}H NMR spectrum in acetone-d_6 (**Scheme 3.1**). This is attributed to non-covalent interactions between the π-electron-rich cavity of **P5A^{H}** and the electron-deficient dicationic viologen salt.

Bunchuay carried out a series of ^{1}H NMR studies in $CDCl_3$ of **P5A^{Et}** with simple, uncharged diisocyanides of various lengths, revealing exceptionally strong binding affinities ($K > 10^5\ M^{-1}$) (**Scheme 3.2**).[3] For aryl isocyanide guests, the stronger electron-withdrawing ability of the para-substituted groups resulted in stronger binding affinities (NO_2 > NC > I > Me).

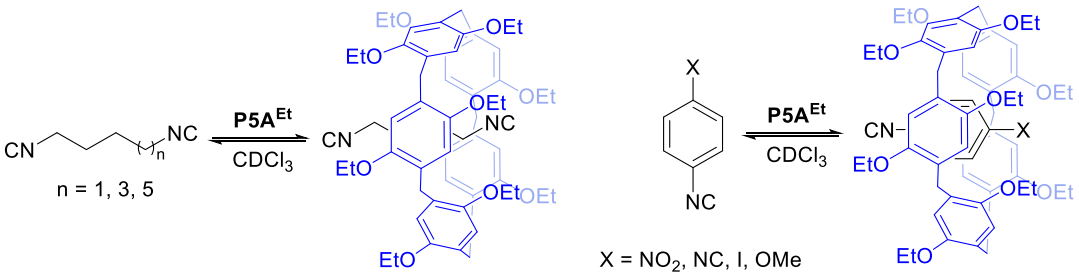

Scheme 3.2. Binding equilibrium of diisocyanides with **P5A^{Et}** in $CDCl_3$ to form [2]pseudorotaxanes.[3]

For 1,10-diisocyanodecane, the addition of more than one equivalent of **P5A^{Et}** yielded the pseudo[3]rotaxane, as a result of two **P5A^{Et}** macrocycles threading (**Scheme 3.3**).

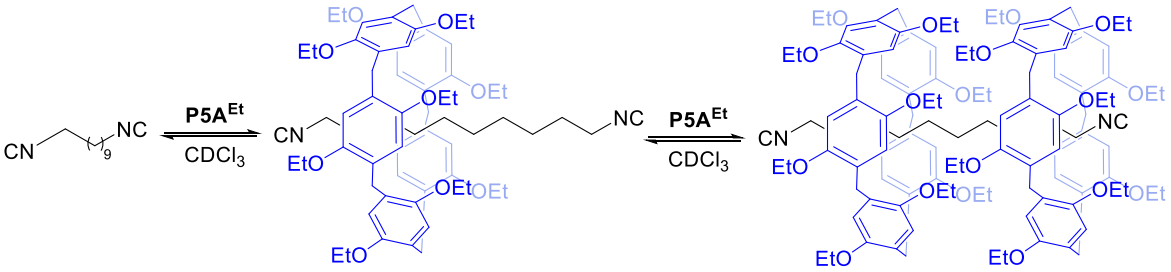

Scheme 3.3. Binding equilibrium of 1,10-diisocyanodecane with **P5A^{Et}** in $CDCl_3$ to form [2]- and [3]pseudorotaxanes.[3]

The pseudorotaxanes were characterised by SC-XRD, demonstrating their exceptional stability and providing insight into the non-covalent interactions responsible for the strong binding affinities. In addition to the C–H···π interactions between the electron-deficient alkyl chain and aromatics of the **P5A^{Et}** cavity, unconventional C–H···C hydrogen bonds between the **P5A^{Et}** ethoxy groups and carbon termini of the isocyanide end-groups provided additional stabilisation to the pseudorotaxanes.

Ogoshi demonstrated that **P5A^{Me}** forms pseudo[2]rotaxanes with simple long-chain axles prepared by the CuAAC reaction, containing two 1,4-substituted triazoles joined by electron-deficient alkyl linkers (**Scheme 3.4**).[4] The formation of pseudo[2]rotaxanes was facilitated by multiple C–H···π, C–H···O, and C–H···N non-covalent interactions between the two components. NMR titration studies in $CDCl_3$ revealed that **P5A^{Me}** has stronger binding affinities with *N*-substituted butylene linkers ($K = 1.9 \times 10^4\ M^{-1}$) than *C*-substituted butylene linkers ($K = 4.4 \times 10^2\ M^{-1}$) due to stronger non-covalent interactions in the more electron-deficient linkers.

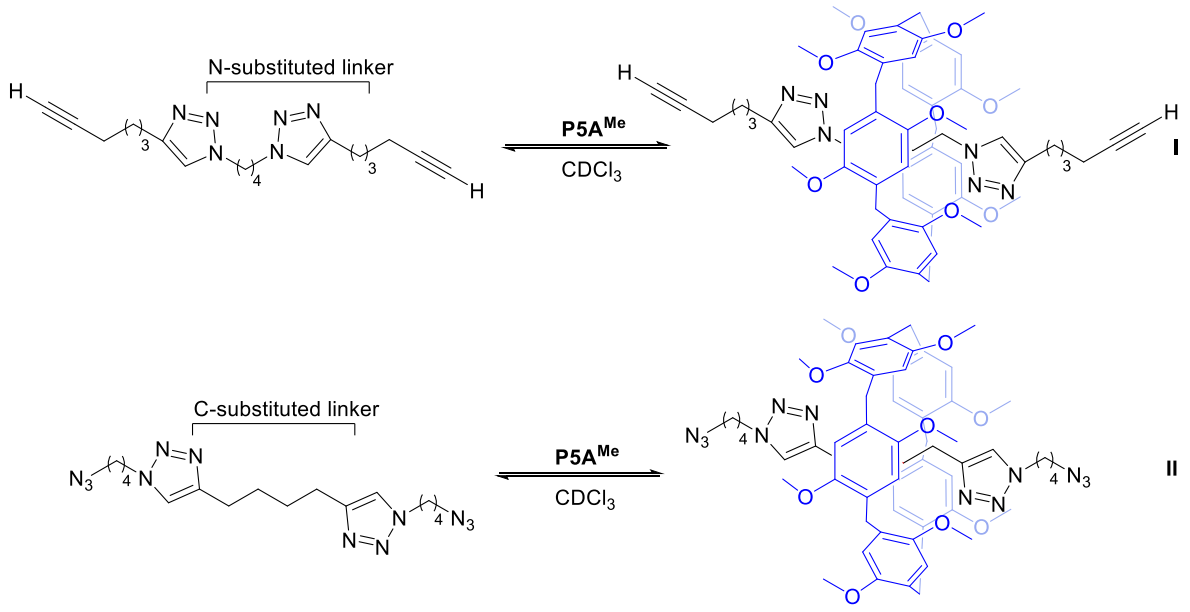

Scheme 3.4. Binding equilibrium of 1,4-disubstituted triazole axles with **P5A^{Me}** in $CDCl_3$ to form pseudo[2]rotaxanes.[4]

The pseudo[2]rotaxanes were capped with stoppers containing bulky Dipp groups by the CuAAC reaction (**Scheme 3.5**). In the [2]rotaxanes, the **P5A^{Me}** macrocycle resides on the *N*-substituted linkers on the axle, consistent with the stronger binding constant.

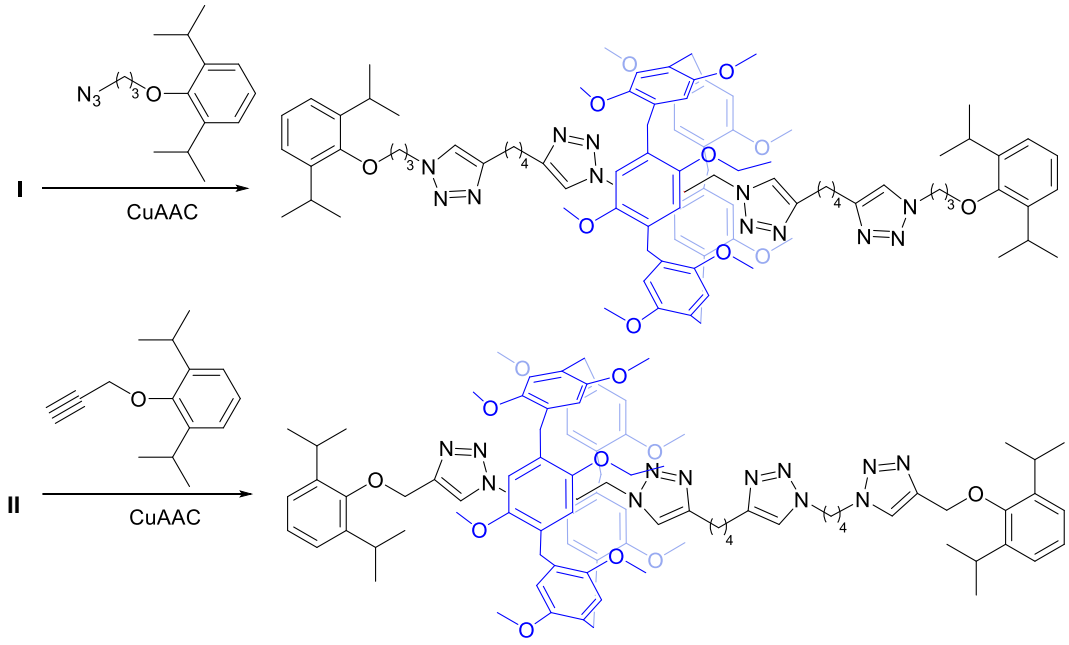

Scheme 3.5. Ogoshi's synthesis of **P5A^{Me}**-based rotaxanes *via* the CuAAC reaction.[4]

We were inspired by the simplicity of this work, as all the molecular components of the mechanically interlocked molecules (MIMs) are straightforward to prepare and display strong binding affinities in common solvents. We reasoned that the cyaphide-azide 1,3-dipolar cycloaddition reaction between the azide end-groups of **P5A^{Et}** pseudo[2]rotaxanes with the gold(I)-cyaphide complex, (IDipp)Au(CP), could be used as a capping technique to offer a general route to inorganic [2]rotaxanes.

3.2 Synthesis of pillar[5]arene-based inorganic [2]rotaxanes

3.2.1 Synthesis of a first-generation inorganic [2]rotaxane

First, we wanted to investigate the binding capabilities of **P5A^{Et}** with a simple axle containing azide end-groups. 1,8-diazidooctane was chosen as a simple analogue of the diisocyanide guests reported by Bunchuay, in anticipation that the electron-deficient alkyl linker would make them amenable to pseudo[2]rotoaxane formation. 1,8-diazidooctane was prepared *via* the conventional route of a double S_N2 reaction of the dibromo precursor with NaN_3 in DMSO, and **P5A^{Et}** was synthesised according to a previously reported procedure.[3] ^{1}H NMR binding titrations were performed by the successive addition of aliquots of 1,8-diazidooctane to a C_6D_6 solution of **P5A^{Et}** and monitoring the changes to the chemical shifts of the ^{1}H NMR resonances (**Figure 3.1**). Significant downfield shifts were observed for all resonances corresponding to **P5A^{Et}**. Fitting of one of these (H_1) to a 1:1 binding isotherm model using *Bindfit*[5] allowed quantification of the binding affinity ($K = 1.22 \times 10^2$ M^{-1}).

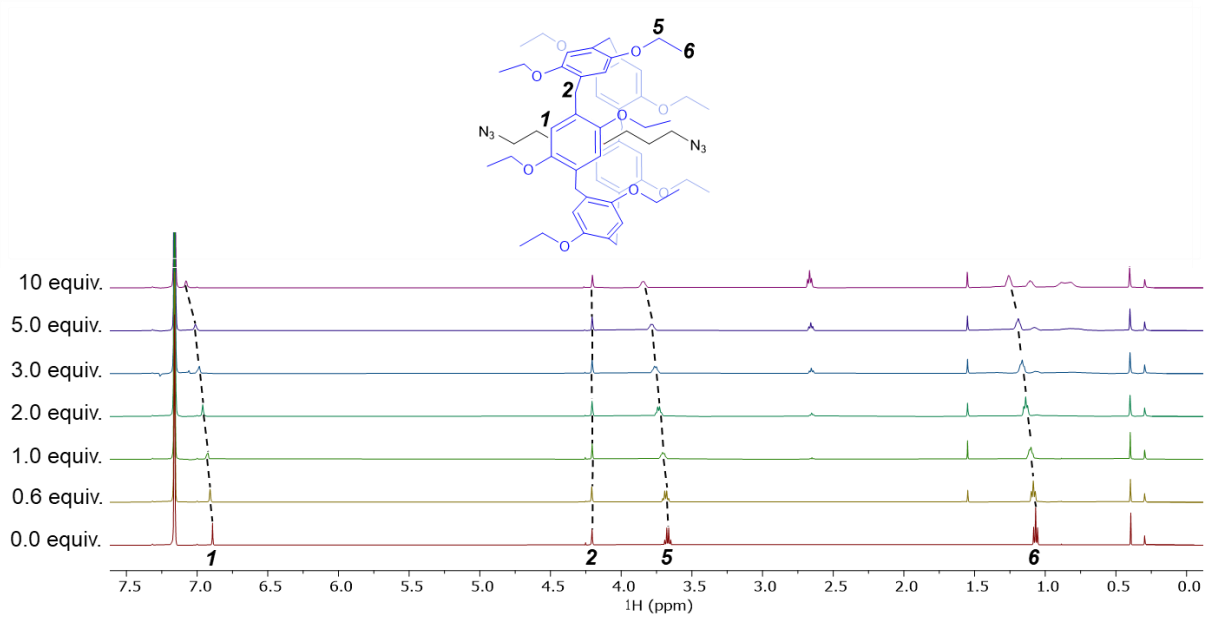

Figure 3.1. Stacked ^{1}H NMR spectra (C_6D_6) of **P5A^{Et}** with successive addition of 1,8-diazidooctane.

We then wanted to investigate whether the cyaphide-azide 1,3-dipolar cycloaddition reaction could be used to install bulky triazaphosphole stoppers to each end of the pseudo[2]rotaxane to afford the corresponding [2]rotaxane. Due to the weak binding affinity, five equivalents of **P5A^{Et}** were used in order to shift the binding equilibrium and favour the formation of the pseudo[2]rotaxane (**Scheme 3.6A**). Then, two equivalents of (IDipp)Au(CP) were added, resulting in its quantitative consumption after 3 hours at room temperature, and the concomitant emergence of two new peaks in the ^{31}P{^{1}H} NMR spectra. The peaks at 198.6 ppm and 199.9 ppm were present in a ratio of approximately 10:1 by their relative integrals, and in the region typical of gold(I)-triazaphospholes (Sections 2.2.1 and 2.2.2). They were therefore assigned to the [2]rotaxane **8a** and the corresponding non-interlocked axle **8b**. The axle **8b** could be independently synthesised in the absence of **P5A^{Et}**, by the reaction of 1,8-diazidooctane with two equivalents of (IDipp)Au(CP), which confirmed this assignment (**Scheme 3.6B**).

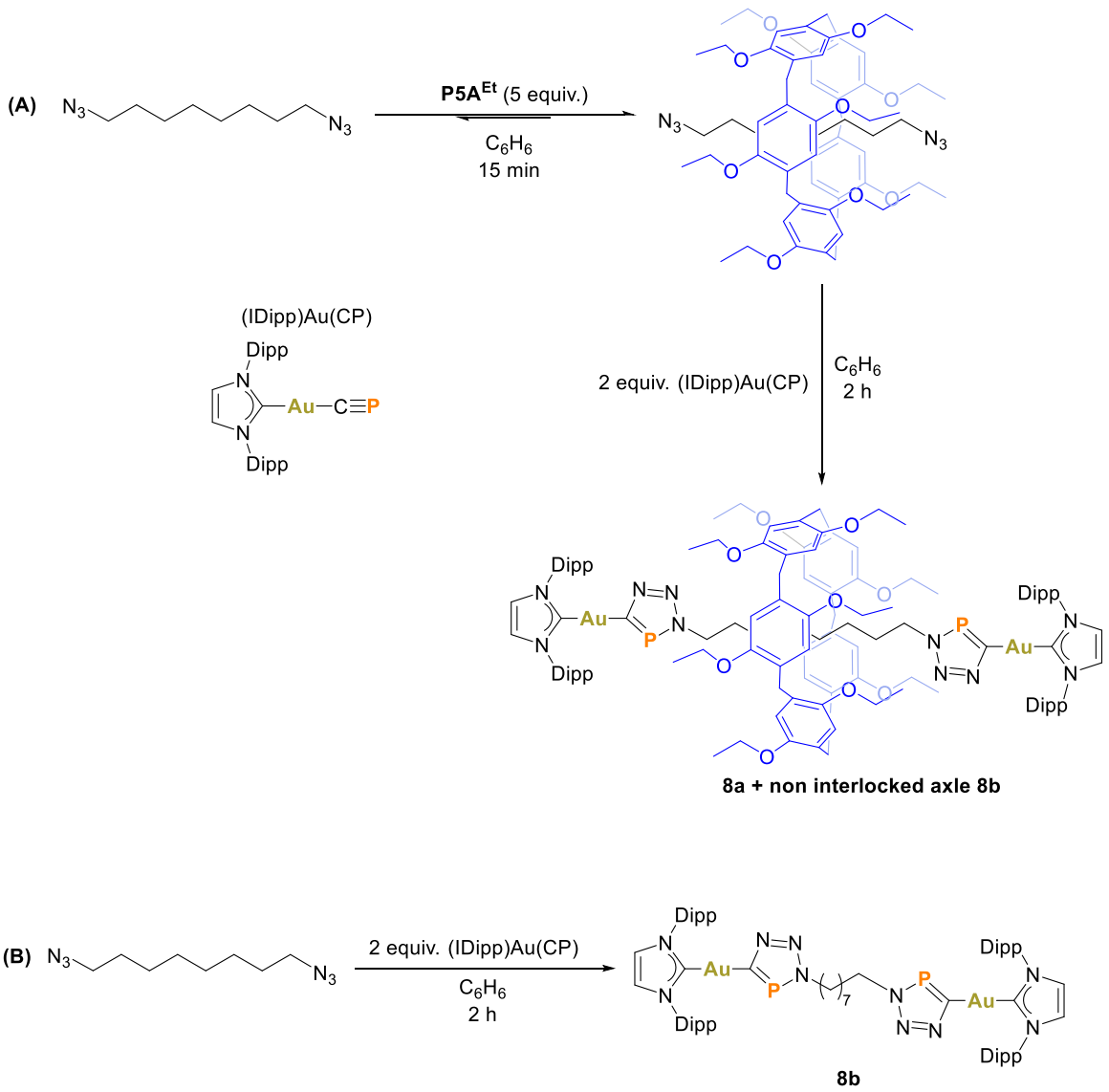

Scheme 3.6. (A) Synthesis of [2]rotaxane **8a** and **(B)** the independent synthesis of non-interlocked axle **8b**.

Crystals suitable for SC-XRD were obtained from the reaction mixture upon standing at room temperature, which confirmed the presence of the [2]rotaxane **8a** (**Figure 3.2**). The solid-state structure reveals two short C–H···π contacts (2.82 Å and 2.87 Å) between aliphatic hydrogen atoms on the axle and the benzene rings of the **P5A^{Et}** macrocycle, which is shorter than the sum of their van der Waals' radii (3.05 Å).[6] These types of non-covalent interactions are known to be stronger than dispersion forces,[7] and therefore drive the equilibrium towards the

pseudo[2]rotaxane, allowing the isolation of **8a** following the capping reaction. The distances between each benzene plane and the opposing methylene linker on the **P5A^{Et}** macrocycle range from 8.865–9.259 Å, giving an average cavity size of 9.046 Å. The size of each stopper can be taken by the distance between the *para*-carbon atoms on the Dipp substituents at 10.03(4) Å and 9.91(4) Å, both exceeding the cavity size and therefore providing sufficient steric bulk to act as stoppers in **8a**. The C2–Au1–C1 and C6–Au2–C5 angles distort slightly from linearity at 171.0(8)° and 175.7(8)°, respectively, presumably due to the steric encumbrance of the **P5A^{Et}** macrocycle. The remaining bond metrics about the gold atoms and the triazaphosphole heterocycle are similar to the 1,3-dipolar cycloaddition products reported in the previous chapter (Section 2.2.1). The Au1–C1 and Au2–C5 bond lengths are approximately the same at 2.03(2) Å and 2.00(2) Å, respectively, and The Au1–C2 and Au2–C6 bond lengths are also similar at 1.98(2) Å and 2.06(2) Å, respectively. The C1–P1 and C5–P2 bond lengths are 1.67(2) Å and 1.78(2) Å, respectively, and the C1–P1–N3 and C5–P2–N8 angles are 91(1)° and 85(1)°, respectively.

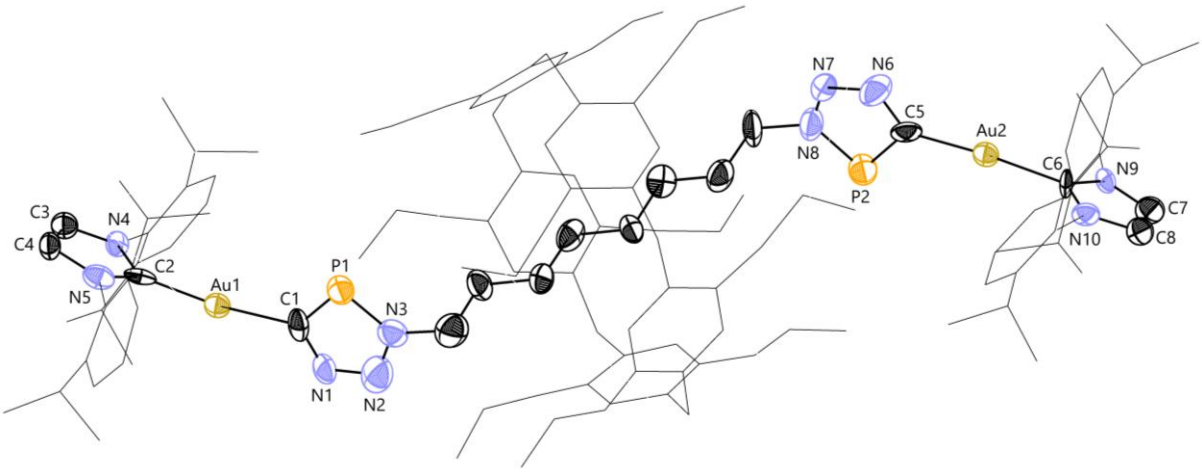

Figure 3.2. SC-XRD structure of the [2]rotaxane **8a**. Anisotropic displacement ellipsoids depicted at 30% probability. Hydrogen atoms, disorder components, and co-crystallised solvent molecules are omitted for clarity. Dipp substituents and **P5A^{Et}** are depicted as wireframes for clarity.

Crystallisation could not be used to purify **8a**. The $^{31}P\{^{1}H\}$ NMR spectrum of isolated crystals indicated the presence of small amounts of **8b**. As highlighted in Chapter 2 (Section 2.2.4), the stability of metal-triazaphospholes was found to be much greater than the parent cyaphide complexes, enabling them to be handled in air for short periods (approx. $t_{1/2}$ = 4 days). An aliquot of the reaction mixture was opened to air, and **8a** showed no signs of decomposition. Gratifyingly, **8a** could be purified by column chromatography (silica gel, EtOAc/hexane 3:7 v/v) in moderate yields (38%). The enhanced air and moisture tolerance of **8a** is presumably a result of kinetic stabilisation of the reactive triazaphosphole units by the **P5A^{Et}** macrocycle as it shuttles along the length of the axle. Indeed, samples of **8a** can be stored on the bench and show no signs of decomposition over the period of months, whereas the non-interlocked axle **8b** shows evidence of decomposition after a few days, similar to the other cycloaddition products (Chapter 2).

The ^{1}H NMR spectrum of **8a** contains all the resonances for the two components of the [2]rotaxane, although there are some differences which provide evidence of its interlocked nature (*vide infra*). The $^{13}C\{^{1}H\}$ NMR spectrum reveals doublet resonances for the triazaphosphole and IDipp carbene atoms at 206.74 ppm ($^{1}J_{C–P}$ = 82.7 Hz) and 196.17 ppm ($^{3}J_{C–P}$ = 10.4 Hz), respectively, which are very similar to the other gold(I)-triazaphosphole complexes (Section 2.2.1).

Comparing the ^{1}H NMR spectra of **P5A^{Et}**, **8a**, and **8b** provides further evidence for the formation of a [2]rotaxane (**Figure 3.3**). In the ^{1}H NMR spectrum of **8a**, three resonances corresponding to the methylene groups of the aliphatic axle chain (H_a, H_b, and H_c) undergo significant upfield shifts relative to that of the non-interlocked axle, **8b** [$\Delta\delta$ = −1.82 ppm (H_a); −1.18 ppm (H_b); and −0.38 ppm (H_c)]. These protons reside within the cavity of the **P5A^{Et}** macrocycle, resulting in shielding from the external magnetic field of the NMR spectrometer. By contrast, the methylene environment closest to the triazaphosphole

subunit (i.e. H_d) experiences a small downfield shift in **8a** relative to **8b** ($\Delta\delta = 0.10$ ppm), which suggests that the bulkiness of the Dipp substituted stoppers repels **P5A^{Et}**, preventing it moving along the full length of the axle.

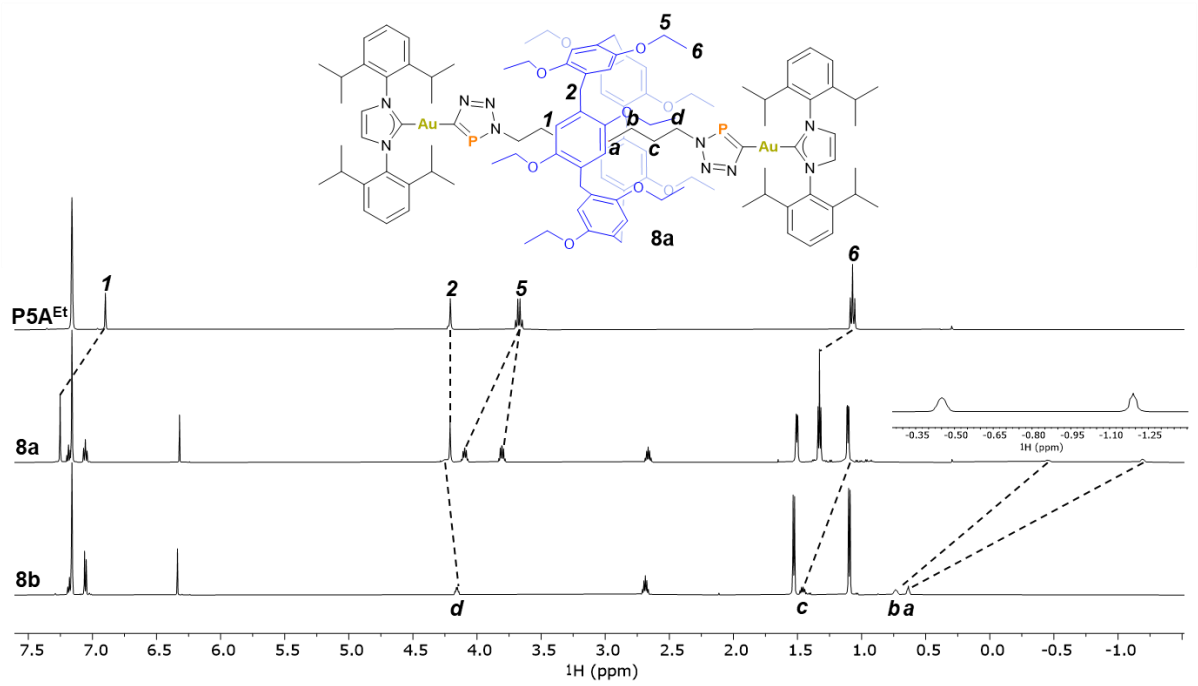

Figure 3.3. Stacked ^{1}H NMR spectra (C_6D_6) of: **P5A^{Et}**, [2]rotaxane **8a**, and axle **8b**.

Further evidence of the interlocked nature of **8a** is gleaned from changes in the ^{1}H NMR resonances of the **P5A^{Et}** subunit with respect to its non-threaded counterpart. The most significant change corresponds to the methylene proton signals of the ethoxy groups (H_5), which become diastereotopic and split into two multiplets. In **P5A^{Et}**, oxygen-through-annulus rotation allows rapid exchange of the two planar chiral conformers, resulting in the methylene protons being equivalent ($H_{5a} = H_{5b}$) (**Figure 3.4**).[8,9] However, the presence of the axle in the [2]rotaxane **8a** prevents this interconversion, rendering the methylene ethoxy protons inequivalent ($H_{5a} \neq H_{5b}$). As a result, each proton is pointing to the interior or exterior of the macrocycle cavity. This is further supported by the lack of splitting of the terminal methyl proton resonance of the ethoxy groups (H_6), which indicates the splitting of neighbouring methylene protons (H_5) is not due to different ethoxy environments. Downfield shifts are

observed for the ^{1}H NMR resonances of the aromatic (H_1) and ethoxy protons (H_5 and H_6), which are attributed to the C–H···π and C–H···N interactions, respectively.

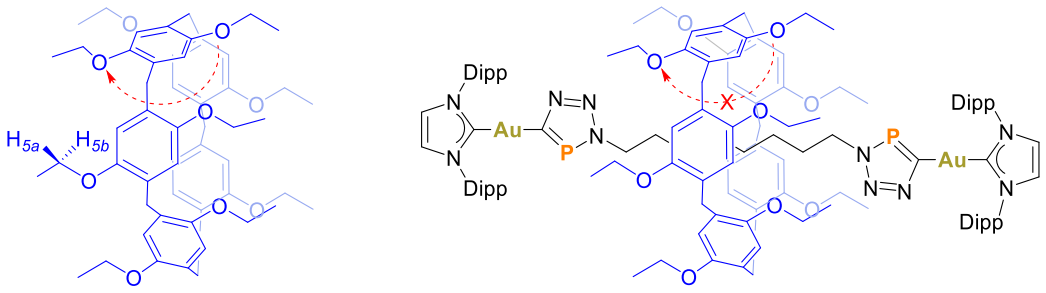

Figure 3.4. Oxygen-through-annulus rotation of **P5A^{Et}** (red dotted arrow) is blocked by the presence of the axle in [2]rotaxane **8a**.

High-resolution electrospray ionisation mass spectrometry (HR-ESI-MS) confirms the formation of **8a**, with peaks corresponding to the [**8a**+2H]$^{2+}$ species (*m*/*z* = 1173.0557; theoretical 1173.0573). The HR-ESI-MS of **8b** contains peaks for the [**8b**+H]$^+$ species (*m*/*z* = 1453.6072; theoretical 1453.6032). Alongside the SC-XRD structure and the diagnostic ^{1}H NMR perturbations relative to the non-interlocked axle **8b**, this HR-ESI-MS data provides unequivocal evidence for the formation of the [2]rotaxane **8a**.

3.2.2 Synthesis of a second-generation [2]rotaxane

To improve the binding affinity for pseudo[2]rotaxane formation and avoid the use of a large excess of **P5A^{Et}**, a new axle, **9**, was prepared based upon the work by Ogoshi.[4] The CuAAC reaction of 1,4-diazidobutane with two equivalents of 4-bromo-1-butyne, followed by a double S_N2 reaction with NaN_3, yielded the bis-azide thread **9** in 35% yield over two steps (**Scheme 3.7**).

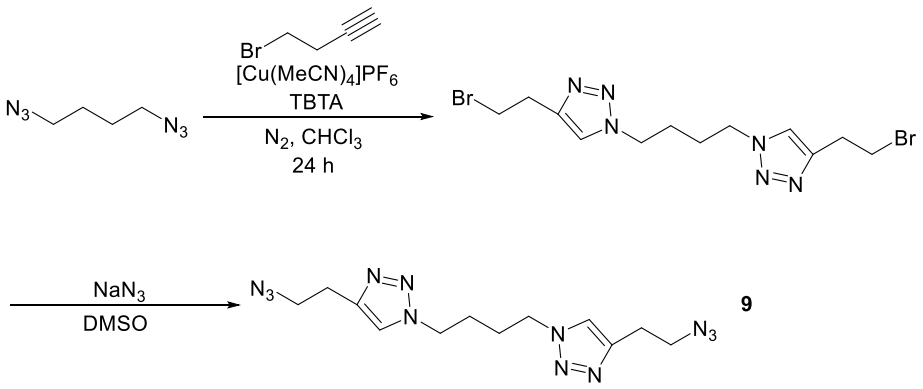

Scheme 3.7. Synthesis of triazole thread **9**.

^{1}H NMR binding titrations in C_6D_6 were carried out to determine the binding affinity for **P5A^{Et}** to thread **9** (**Figure 3.5**). A significant downfield shift for the aromatic ^{1}H NMR resonance (H*1*) of the **P5A^{Et}** was observed, even after the addition of the first aliquot, typical of strong binding.

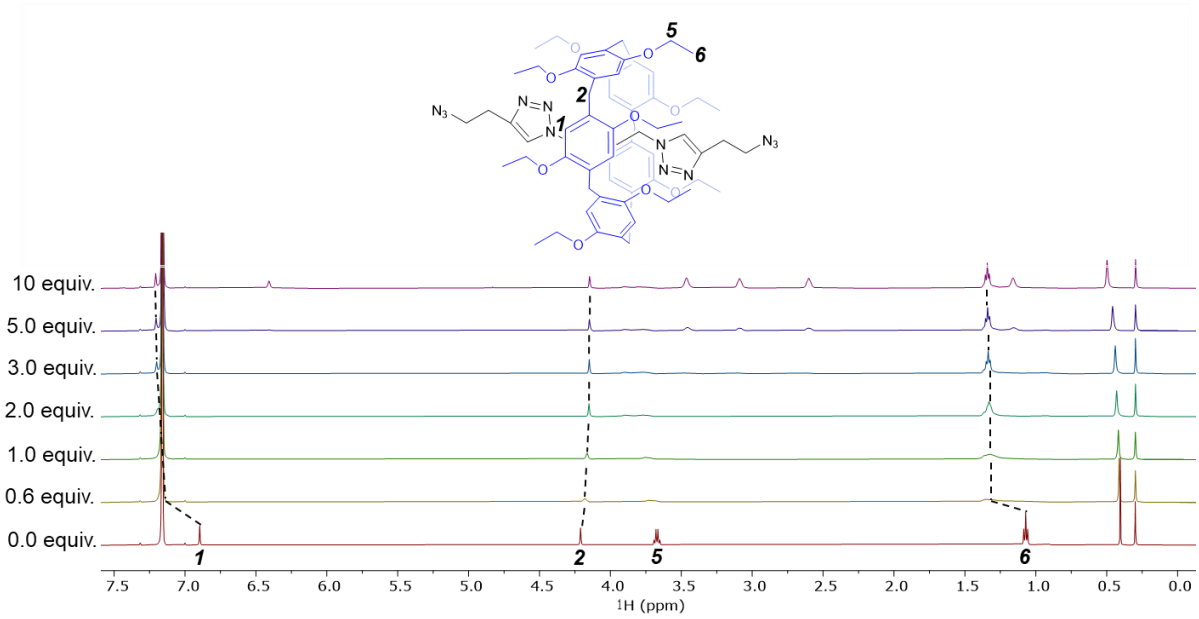

Figure 3.5. Stacked ^{1}H NMR spectra (C_6D_6) of **P5A^{Et}** with successive addition of bis-azide **9**.

The titration data was analysed in *Bindfit*[5] to produce a binding affinity (1.3×10^4 M^{-1}) that was significantly higher than 1,8-diazidooctane, and similar to N-terminated triazole-containing threads used by Ogoshi.[4] This is attributed to additional strong hydrogen bonds formed between the C–H bonds of the triazoles on **9** and the oxygen atoms of the **P5A^{Et}**

ethoxy groups. These findings suggest that a stoichiometric mixture of the **9** and **P5A^{Et}** should produce significant quantities of the corresponding pseudo[2]rotaxane.

Equimolar quantities of **9** and **P5A^{Et}** were stirred in C_6D_6 for a short period, followed by the addition of two equivalents of (IDipp)Au(CP) (**Scheme 3.8A**).

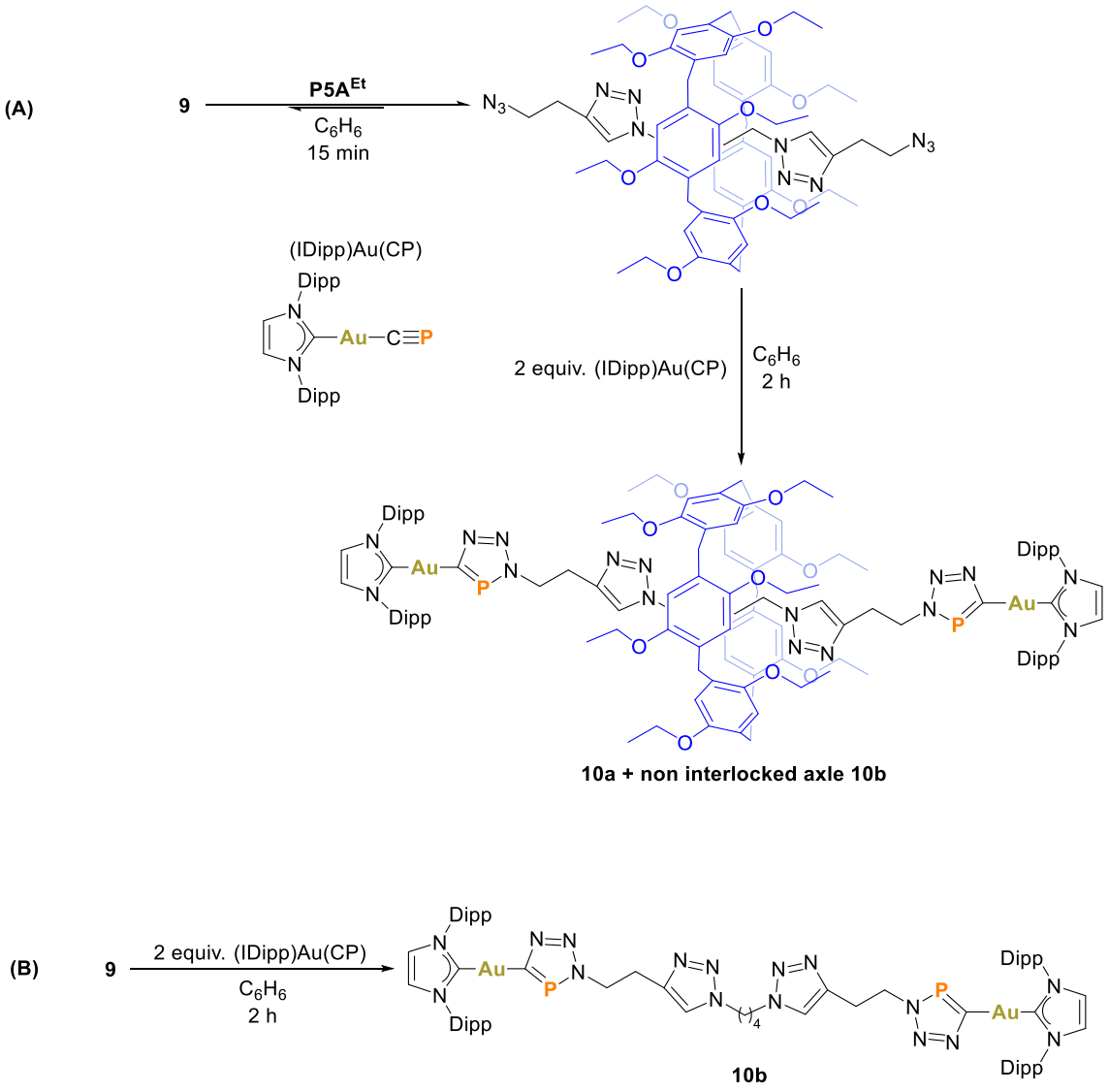

Scheme 3.8. (A) Synthesis of [2]rotaxane **10a** and (B) the independent synthesis of non-interlocked axle **10b**.

This resulted in the immediate emergence of two new peaks in the $^{31}P\{^{1}H\}$ NMR spectra at 201.3 ppm and 201.9 ppm (in approx. 10:1 ratio) for the [2]rotaxane **10a** and the

non-interlocked axle **10b**, respectively. Again, this was confirmed by the independent synthesis of **10b** in the absence of **P5A^{Et}** (**Scheme 3.8B**). Pure **10a** could be obtained in excellent yields (65%) by column chromatography (silica gel, EtOAc/hexane 1:1 v/v). The increase in yield in comparison to **8a** is significant, especially considering the stoichiometric nature of the reaction.

Crystals suitable for SC-XRD were obtained by slow diffusion of hexane into a saturated toluene solution of **10a**, confirming its identity as the [2]rotaxane (**Figure 3.6**). The compound crystallises as thin plates which have a tendency to stack on top of one another, making the selection of single crystals challenging. The data obtained is therefore not of sufficient quality for the discussion of bond metrics, but does provide evidence for the formation of a mechanically interlocked [2]rotaxane.

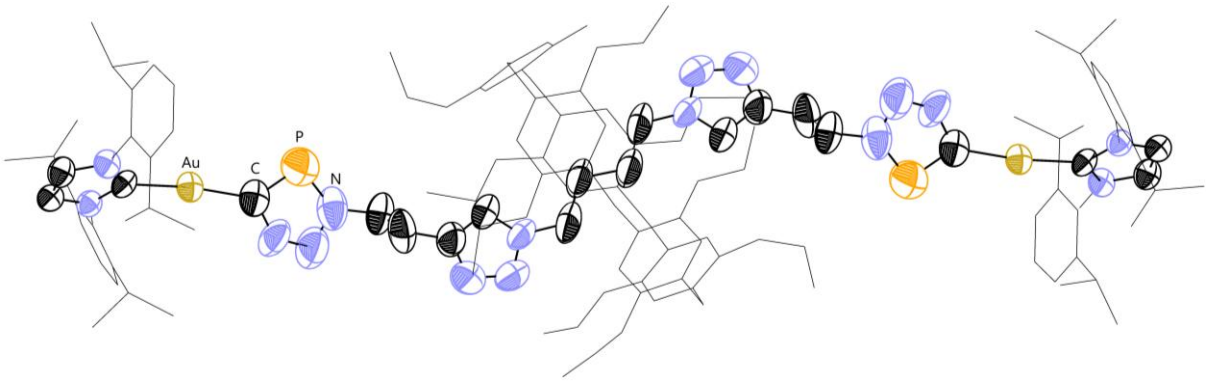

Figure 3.6. SC-XRD structure of the [2]rotaxane **10a**. Anisotropic displacement ellipsoids depicted at 30% probability. Hydrogen atoms, disorder components, and co-crystallised solvent molecules omitted for clarity. Dipp substituents and **P5A^{Et}** are depicted as wireframes for clarity.

Further evidence for the formation of a [2]rotaxane was gathered through comparison of the ^{1}H NMR spectra of **P5A^{Et}**, **10a**, and **10b** (**Figure 3.7**). The proton resonances corresponding to the methylene groups of the *N*,*N*-substituted linker (H_a and H_b) undergo significant upfield shifts in the ^{1}H NMR spectrum of **10a** relative to that of **10b** [$\Delta\delta$ = −1.83 ppm (H_a) and −1.26 ppm (H_b)]. In contrast, the methylene resonances on *C*,*N*-substituted linker in **10a** undergo a slight downfield shift relative to those in **10b**

[$\Delta\delta$ = 0.21 ppm (H_e) and 0.39 ppm (H_f)]. This is due to shielding of the *N*,*N*-substituted methylene protons by the **P5A^{Et}** macrocycle, suggesting that this is where it predominantly resides in solution on the NMR timescale. The triazole proton resonance (H_c) undergoes a significant downfield shift ($\Delta\delta$ = −2.67 ppm), which is attributed to a dominant deshielding effect due to hydrogen bonds formed with the oxygens of the ethoxy groups on the **P5A^{Et}** subunit, which itself is responsible for the improved binding affinity. The **P5A^{Et}** proton resonances in **10a** undergo similar changes as were observed for **8a**, most notably, the diastereotopic splitting of the methylene ethoxy resonances (H_5).

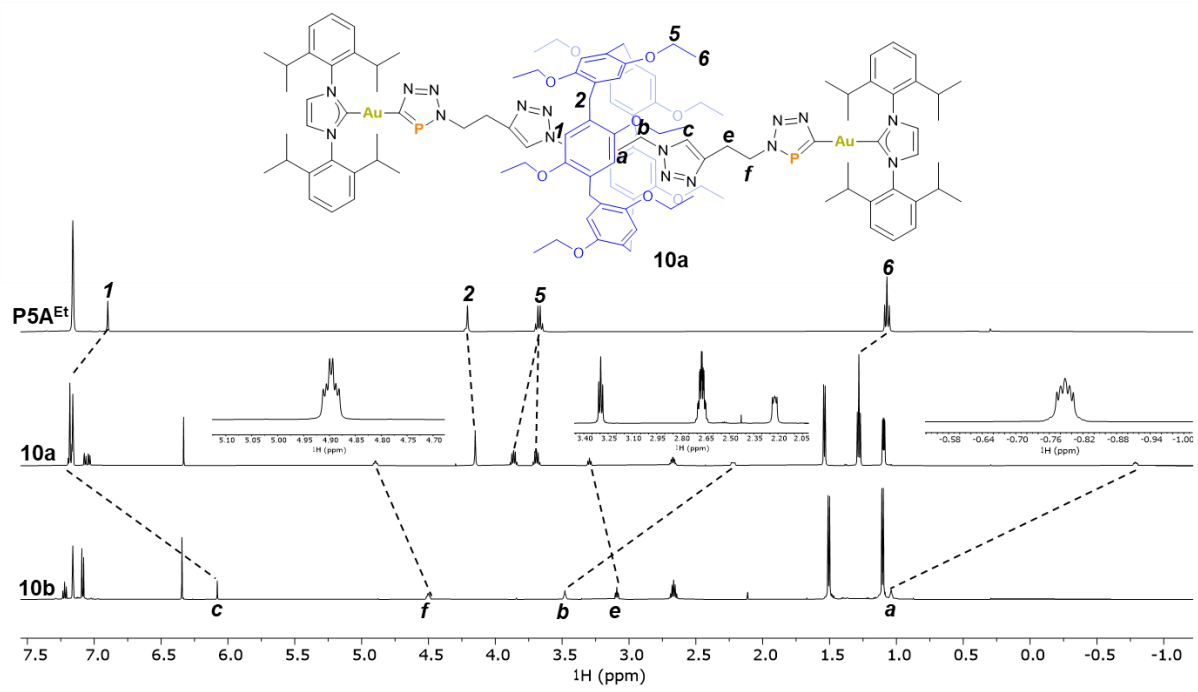

Figure 3.7. Stacked ^{1}H NMR spectra (C_6D_6) of **P5A^{Et}**, [2]rotaxane **10a**, and axle **10b**.

Similar to **8a**, the $^{13}C\{^1H\}$ NMR spectrum of **10a** contains doublets for the triazaphosphole and IDipp carbene atoms at 206.36 ppm ($^1J_{C-P}$ = 83.1 Hz) and 195.95 ppm ($^3J_{C-P}$ = 11.0 Hz), respectively. The HR-ESI-MS of **10a** and **10b** contains peaks for the [**10a**+2H]$^{2+}$ species (m/z = 1240.0733; theoretical 1240.0743) and the [**10b**+H]$^+$ species (m/z = 1587.6413; theoretical 1587.6388), respectively.

3.3 Conclusions

The cyaphide-azide 1,3-dipolar cycloaddition reaction was found to be an effective capping method for the synthesis of new organometallic [2]rotaxanes featuring bulky (IDipp)Au(CPN_3) stoppers. It emulates the advantages of the CuAAC reaction (Section 1.1.1), and is compatible with typical templating techniques for **P5A^{Et}** based rotaxanes. The stabilising effect of the mechanical bond imposed by the **P5A^{Et}** macrocycle renders the [2]rotaxanes air- and moisture-stable, allowing them to be purified by chromatographic means. They were isolated in excellent yields and characterised fully by NMR, SC-XRD, and HR-ESI-MS, providing comprehensive evidence of the formation of the MIMs.

The work in this chapter has been published in *Angewandte Chemie:*

A. Mapp, J. T. Wilmore, P. D. Beer, and J. M. Goicoechea, *Angew. Chem. Int. Ed.* **2023**, *62*, e202309211

Dr. Jamie T. Wilmore contributed to the ^{1}H NMR binding titration experiments in section 3.2.1 and 3.2.2.

3.4 Experimental

3.4.1 Synthesis of [2]rotaxane 8a

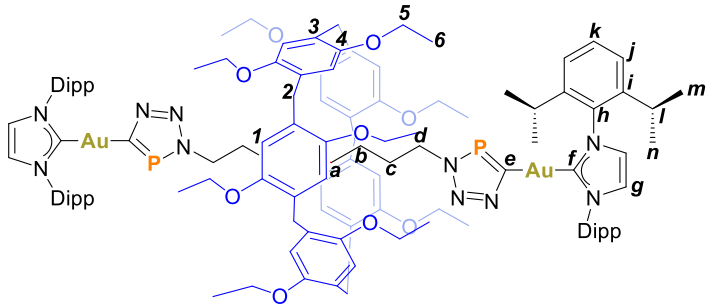

P5A^{Et} (103 mg, 0.115 mmol, 5.0 equiv.) was dissolved in a solution of 1,8-diazidooctane (4.5 mg, 22.9 μmol, 1.0 equiv.) in benzene (2 mL). (IDipp)Au(CP) (30.3 mg, 48.2 μmol, 2.10 equiv.) was added to the solution, and the reaction mixture was stirred for 16 h at room temperature. This resulted in the formation of a precipitate, which was isolated by filtration and dried *in vacuo*. The crude product was purified on a silica gel column using EtOAc/hexane (3:7 v/v) to afford product **8a** as a white residue. Yield: 20.5 mg, 8.71 μmol, 38%.

^{1}H NMR (600 MHz, C_6D_6): δ (ppm) 7.26 (s, 10H; H_1), 7.19 (m, 4H; H_k), 7.06 (pseudo-triplet, $^{3}J_{H–H}$ = 7.8 Hz, 8H; H_j), 6.31 (s, 4H; H_g), 4.26 (br, 4H; H_d), 4.22 (s, 10H; H_2), 4.10 (m, 10H; H_5), 3.81 (m, 10H; H_5), 2.67 (sept, $^{3}J_{H–H}$ = 6.9 Hz, 8H; H_l), 1.51 (d, $^{3}J_{H–H}$ = 6.9 Hz, 12H; $H_{m/n}$)*, 1.50 (d, $^{3}J_{H–H}$ = 6.9 Hz, 12H; $H_{m/n}$)*, 1.33 (t, $^{3}J_{H–H}$ = 6.9 Hz, 30H; H_6), 1.11 (d, $^{3}J_{H–H}$ = 6.9 Hz, 12H; $H_{m/n}$)*, 1.10 (d, $^{3}J_{H–H}$ = 6.9 Hz, 12H; $H_{m/n}$)*, 1.08 (q, $^{3}J_{H–H}$ = 7.7 Hz, 4H; H_c), –0.44 (br, 4H; H_b), –1.19 (br, 4H; H_a).

*H_m and H_n are split into inequivalent resonances due to restricted rotation about the C_h–N bond imparted by the **P5A^{Et}** macrocycle.

$^{13}C\{^1H\}$ NMR (151 MHz, C_6D_6): δ (ppm) 206.7 (d, $^1J_{C–P}$ = 82.7 Hz; C_e), 196.2 (d, $^3J_{C–P}$ = 10.4 Hz; C_f), 150.3 (C_4), 145.9 (C_i), 134.8 (C_h), 130.7 (C_k), 128.8 (C_3), 124.29 (C_j), 124.27 (C_j), 122.8 (C_g), 114.5 (C_1), 63.7 (C_5), 52.4 (d, $^2J_{C–P}$ = 9.6 Hz; C_d), 34.6 (C_c), 29.9 (C_2), 29.1 (C_l), 28.5 (C_a), 26.6 (C_b), 24.9 ($C_{m/n}$)*, 23.98 ($C_{m/n}$)*, 23.96 ($C_{m/n}$)*, 15.8 (C_6).

*C_m, C_n, and C_j are split into inequivalent resonances due to restricted rotation about the C_h–N bond imparted by the **P5A^{Et}** macrocycle.

$^{31}P\{^1H\}$ NMR (243 MHz, C_6D_6): δ (ppm) 198.6 (s).

HR-ESI-MS (+ve ion mode): m/z calcd. for $C_{119}H_{158}Au_2N_{10}O_{10}P_2$+2H$^+$: 1173.0573 $[M+2H]^{2+}$; found 1173.0557.

3.4.2 Synthesis of axle 8b

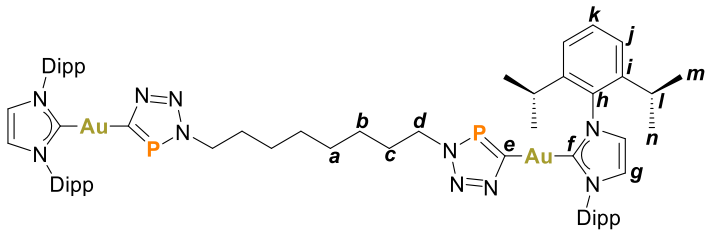

(IDipp)Au(CP) (29.6 mg, 47.1 μmol, 2.1 equiv.) was added to a solution of 1,8-diazidooctane (4.40 mg, 22.4 μmol, 1.0 equiv.) in benzene (0.5 mL) and stirred 16 h at room temperature. The solution was concentrated and layered with hexane (3 mL). The resulting crystals were isolated by filtration, washed with hexane (3 × 1 mL) and pentane (3 × 1 mL), then dried *in vacuo*. Yield: 23.1 mg, 15.9 μmol, 71%.

^1H NMR (400 MHz, C_6D_6): δ (ppm) 7.19 (m, 4H; H_k), 7.06 (d, $^3J_{H–H}$ = 7.8 Hz, 8H; H_j), 6.34 (s, 4H; H_g), 4.16 (m, 4H; H_d), 2.69 (sept, $^3J_{H–H}$ = 6.9 Hz, 8H; H_l), 1.53 (d, $^3J_{H–H}$ = 6.9 Hz,

24H, $H_{n/m}$), 1.46 (q, $^3J_{H–H}$ = 7.7 Hz, 4H; H_c), 1.10 (d, $^3J_{H–H}$ = 6.9 Hz, 24H; $H_{n/m}$), 0.74 (m, 4H; H_b), 0.63 (m, 4H; H_a).

$^{13}C\{^1H\}$ NMR (151 MHz, C_6D_6): δ (ppm) 207.2 (d, $^1J_{C–P}$ = 82.8 Hz; C_e), 196.4 (d, $^3J_{C–P}$ = 10.9 Hz; C_f), 145.9 (C_i), 134.8 (C_h), 130.7 (C_k), 124.3 (C_j), 122.7 (C_g), 51.4 (d, $^2J_{C–P}$ = 9.6 Hz; C_d), 32.8 (d, $^3J_{C–P}$ = 2.7 Hz; C_c), 29.2 (C_l),* 29.0 (C_a),* 26.7 (C_b), 24.9 ($C_{n/m}$), 24.0 (Dipp $C_{n/m}$).

*Assigned based on relative intensities.

$^{31}P\{^1H\}$ NMR (162 MHz, C_6D_6): δ (ppm) 199.9 (s).

HR-ESI-MS (+ve ion mode): *m*/*z* calcd. for $C_{64}H_{88}Au_2N_{10}P_2+H^+$: 1453.6072 $[M+H]^+$; found 1453.6032.

3.4.3 Synthesis of the dibromo-precursor to azide 9

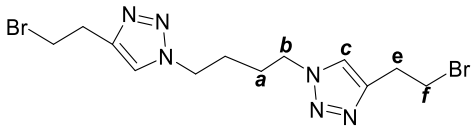

TBTA (56 mg, 0.11 mmol, 0.04 equiv.) was added to a solution of 1,4-diazidobutane (400 mg, 2.85 mmol, 1.0 equiv.) and 4-bromobutyne (797 mg, 6.00 mmol, 2.1 equiv.) in chloroform (10 mL) and stirred for 1 h at room temperature. $[Cu(MeCN)_4]PF_6$ (40.0 mg, 0.105 mmol) was added, and the reaction mixture was stirred for 24 h at room temperature. The reaction mixture was poured onto hexane, and the precipitate was collected. This was used without further purification. Yield: 720 mg, 1.77 mmol, 62%.

^1H NMR (600 MHz, $CDCl_3$): δ (ppm) 7.49 (s, br, 2H; H_c), 4.38 (s, br, 4H; H_b), 3.66 (s, br, 4H; H_f), 3.30 (s, br, 4H; H_e), 1.94 (s, br, 4H; H_a).

3.4.4 Synthesis of azide 9

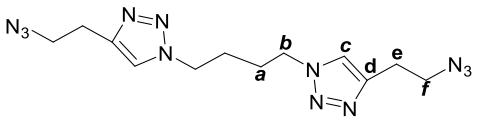

NaN_3 (458 mg, 7.05 mmol, 4.0 equiv.) and trace NaI (approx. 5 mg) were added to a solution of the dibromo-precursor (715 mg, 1.76 mmol, 1.0 equiv.) in DMSO (20 mL) and stirred overnight at room temperature. The solution was diluted with H_2O (100 mL), and the product was extracted with DCM (3 × 60 mL). The organic extracts were combined and washed with brine (3 × 60 mL), then dried over Na_2SO_4. The solvent was removed *in vacuo*, and the crude product was purified on a silica gel column using MeOH/DCM (1:9 v/v) to afford product **1b** as a white powder. Yield: 324 mg, 0.981 mmol, 56%.

^{1}H NMR (600 MHz, $CDCl_3$): δ (ppm) 7.37 (s, 2H; H_c), 4.36 (m, 4H; H_b), 3.62 (t, $^3J_{H–H}$ = 6.7 Hz, 4H; H_f), 3.00 (t, $^3J_{H–H}$ = 6.7 Hz, 4H; H_e), 1.93 (m, 4H; H_a).

^{13}C{^{1}H} NMR (151 MHz, $CDCl_3$): δ (ppm) 144.6 (C_d), 121.9 (C_c), 50.8 (C_f), 49.4 (C_b), 27.3 (C_a), 25.9 (C_e).

3.4.5 Synthesis of [2]rotaxane 10a

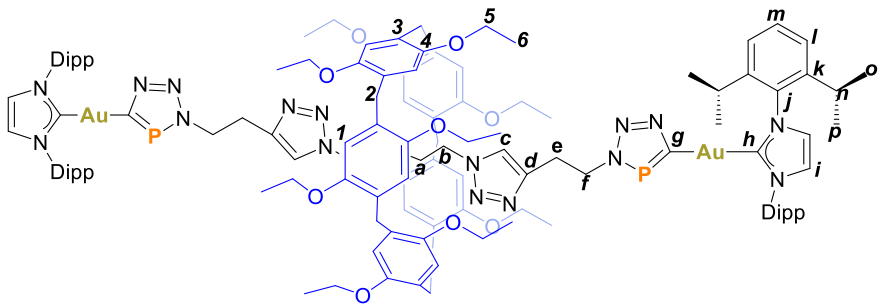

P5A^{Et} (40.6 mg, 45.1 µmol, 1.0 equiv.) was dissolved in a solution of **9** (14.9 mg, 45.1 µmol, 1.0 equiv.) in benzene (2 mL). Au(IDipp)(CP) (59.5 mg, 94.7 µmol, 2.10 equiv.) was added to the solution, and the reaction mixture was stirred overnight at room temperature. The solvent was removed *in vacuo*, and the crude product was purified on a silica gel column using

EtOAc/hexane (1:1 v/v) to afford product **3b** as a white powder. Yield: 72.9 mg, 29.3 μmol, 65%.

^{1}H NMR (600 MHz, C_6D_6): δ (ppm) 7.18 (m; H_{1}, H_c, H_m),* 7.08 (d, $^{3}J_{H–H}$ = 7.8 Hz, 2H; H_l),* 7.07 (d, $^{3}J_{H–H}$ = 7.8 Hz, 2H; H_l),* 7.04 (d, $^{3}J_{H–H}$ = 7.8 Hz, 2H; H_l),* 7.03 (d, $^{3}J_{H–H}$ = 7.8 Hz, 2H; H_l),* 6.33 (s, 4H; H_i), 4.90 (dt, $^{3}J_{H–H}$ = 7.3 Hz, $^{3}J_{H–P}$ = 3.6 Hz, 4H; H_f), 4.15 (s, 10H; H_2), 3.86 (m, 10H; H_5), 3.69 (m, 10H; H_5), 3.30 (t, $^{3}J_{H–H}$ = 7.3 Hz, 4H; H_e), 2.67 (sept, $^{3}J_{H–H}$ = 6.9 Hz, 4H; H_n), 2.67 (sept, $^{3}J_{H–H}$ = 6.9 Hz, 4H; H_n), 2.22 (m, 4H; H_b), 1.54 (d, $^{3}J_{H–H}$ = 6.9 Hz, 24H; $H_{o/p}$), 1.28 (t, $^{3}J_{H–H}$ = 6.9 Hz, 30H; H_6) 1.10 (d, $^{3}J_{H–H}$ = 6.9 Hz, 12H; $H_{o/p}$), 1.09 (d, $^{3}J_{H–H}$ = 6.9 Hz, 12H; $H_{o/p}$), –0.79 (m, 4H; H_a).

*H_1, H_c, and H_m are overlapping, preventing integration and multiplet analysis.

*H_l, H_n, H_o, and H_p are each split into inequivalent resonances due to restricted rotation about the C_j–N bond imparted by the **P5A^{Et}** macrocycle.

^{13}C{^{1}H} NMR (151 MHz, C_6D_6): δ (ppm) = 207.4 (d, $^{1}J_{C–P}$ = 83.1 Hz; C_g), 196.0 (d, $^{3}J_{C–P}$ = 11.0 Hz; C_h), 150.3 (C_4), 145.8 (C_k), 143.2 (C_d), 134.7 (C_j), 130.8 (C_m), 129.2 (C_3), 124.30 (C_l), 124.27 (C_l), 122.8 (C_i), 120.9 (C_c), 115.0 (C_1), 64.1 (C_5), 51.0 (d, $^{2}J_{C–P}$ = 10.1 Hz; C_f), 48.6 (C_b), 29.9 (C_2), 29.8 (C_e), 29.1 (C_n) 25.1 (C_a), 24.9 ($C_{o/p}$), 24.0 ($C_{o/p}$), 15.6 (C_6).

^{31}P NMR (243 MHz, C_6D_6): δ (ppm) 201.3 (s).

HR-ESI-MS (+ve ion mode): *m/z* calcd. for $C_{123}H_{160}Au_2N_{16}O_{10}P_2$+2H^{+}: 1240.0733 [*M*+2H]$^{2+}$; found 1240.0743.

3.4.6 Synthesis of axle 10b

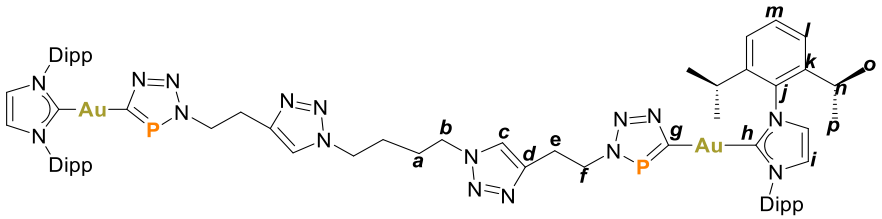

(IDipp)Au(CP) (19.2 mg, 30.5 μmol, 2.1 equiv.) was added to a solution of **9** (4.8 mg, 14.5 μmol, 1.0 equiv.) in benzene (0.5 mL) and stirred overnight at room temperature. The solution was concentrated and stored at –35 ºC for 7 days to yield yellow crystals. The supernatant was removed, and the crystals were washed with pentane (3 × 1 mL), then dried under vacuum. Yield: 17.9 mg, 11.3 μmol, 78%.

^{1}H NMR (600 MHz, C_6D_6): δ (ppm) 7.22 (t, $^{3}J_{H–H}$ = 7.8 Hz, 4H; H_m), 7.09 (d, $^{3}J_{H–H}$ = 7.8 Hz, 8H; H_l), 6.34 (s, 4H; H_i), 6.08 (s, 2H; H_c), 4.51 (dt, $^{3}J_{H–H}$ = 6.4 Hz, $^{3}J_{H–P}$ = 3.8 Hz, 4H; H_f), 3.48 (m, 4H; H_b), 3.09 (t, $^{3}J_{H–H}$ = 6.4 Hz, 4H; H_e), 2.67 (sept, $^{3}J_{H–H}$ = 6.9 Hz, 8H; H_n), 1.51 (d, $^{3}J_{H–H}$ = 6.9 Hz, 24H; $H_{o/p}$), 1.10 (d, $^{3}J_{H–H}$ = 6.9 Hz, 24H; $H_{o/p}$), 1.04 (m, 4H; H_a).

^{13}C{^{1}H} NMR (151 MHz, C_6D_6): δ (ppm) 207.49 (d, $^{1}J_{C–P}$ = 83.3 Hz; C_g), 195.80 (d, $^{3}J_{C–P}$ = 10.9 Hz; C_h), 145.81 (C_k), 144.05 (C_d), 134.68 (C_j), 130.87 (C_m), 124.36 (C_l), 122.83 (C_i), 121.96 (C_c) 50.95 (d, $^{3}J_{C–P}$ = 9.4 Hz; C_f), 48.34 (C_b), 29.41 (C_e), 29.15 (C_n), 26.49 (C_a), 24.90 ($C_{o/p}$), 23.96 ($C_{o/p}$).

^{31}P NMR (243 MHz, C_6D_6): δ (ppm) 201.9 (s).

HR-ESI-MS (+ve ion mode): *m*/*z* calcd. for $C_{68}H_{90}Au_2N_{16}P_2+H^+$: 1587.6413 $[M+H]^+$; found 1587.6388.

3.5 References

1. T. Ogoshi, S. Kanai, S. Fujinami, T. Yamagishi and Y. Nakamoto, *J. Am. Chem. Soc.* **2008**, *130*, 5022–5023.
2. T. Ogoshi, T. Yamagishi and Y. Nakamoto, *Chem. Rev.* **2016**, *116*, 7937–8002.
3. K. Khamphaijun, P. Namnouad, A. Docker, A. Ruengsuk, J. Tantirungrotechai, R. Díaz-Torres, D. J. Harding and T. Bunchuay, *Chem. Commun.* **2022**, *58*, 7253–7256.
4. T. Ogoshi, R. Iizuka, D. Kotera and T. Yamagishi, *Org. Lett.* **2015**, *17*, 350–353.
5. D. Brynn Hibbert and P. Thordarson, *Chem. Commun.* **2016**, *52*, 12792–12805.
6. H. Suezawa, T. Yoshida, M. Hirota, H. Takahashi, Y. Umezawa, K. Honda, S. Tsuboyama and M. Nishio, *J. Chem. Soc. Perkin Trans. 2* **2001**, 2053–2058.
7. S. Tsuzuki, K. Honda, T. Uchimaru, M. Mikami and K. Tanabe, *J. Am. Chem. Soc.* **2000**, *122*, 3746–3753.
8. T. Ogoshi, K. Kitajima, T. Aoki, S. Fujinami, T. Yamagishi and Y. Nakamoto, *J. Org. Chem.* **2010**, *75*, 3268–3273.
9. T. Ogoshi, K. Masaki, R. Shiga, K. Kitajima and T. Yamagishi, *Org. Lett.* **2011**, *13*, 1264–1266.

Chapter 4

Synthesis of Dinuclear Gold(I) Bis-cyaphide Compounds

Abstract

The synthesis of dinuclear gold(I) bis-cyaphide complexes was targeted through the use of bis-*N*-heterocyclic carbene (bis-NHC) ligands. Bis-cyaphide complexes of *Janus*-type (facially opposed) bis-NHCs rapidly decompose under an inert atmosphere. Although not isolable, bis-cyaphide complexes of alkyl-bridged bis-NHCs demonstrated improved stability, and could be trapped with an azide to yield cycloaddition products as adducts of the cyaphide transfer by-product, (^{Dipp}NacNac)MgCl.

4.1 Synthesis of [*n*]catenanes

As described in Section 1.1, another common type of MIM are [*n*]catenanes, consisting of *n* macrocycles that are mechanically interlocked like rings in a chain. They are typically prepared *via* a clipping strategy, where a macrocyclization reaction of the threaded axle of a pseudorotaxane covalently captures the product (see Figure 1.2 in Section 1.1.1). The synthesis of [*n*]catenanes is significantly more challenging than [*n*]rotaxanes, as it necessitates the formation of a large macrocycle, which is entropically disfavoured.[1] Another challenge arises from the requirement of acyclic precursors containing two reactive functional groups. These can undergo unwanted oligomerization reactions (that are entropically favoured over macrocycle formation), diminishing the yield of [*n*]catenane formation.

The templating strategies discussed in Section 1.1.1 have been used to preorganise the molecular components and overcome the entropic barriers of [*n*]catenane synthesis. High

dilution conditions are also used to minimise the frequency of intermolecular collisions (which favour oligomerization) and instead favour the intramolecular macrocyclization reaction required to form the [*n*]catenane. For example, Beer has used Na^+ cation templation under high dilution conditions to thread bis-azides through the cavity of a macrocycle, followed by simultaneous CuAAC reactions with a bis-iodoalkyne reagent to ring-close and form the [2]catenane (**Scheme 4.1**).[2] The CuAAC is a favoured covalent bond forming reaction for the reasons outlined in Section 1.1.1.

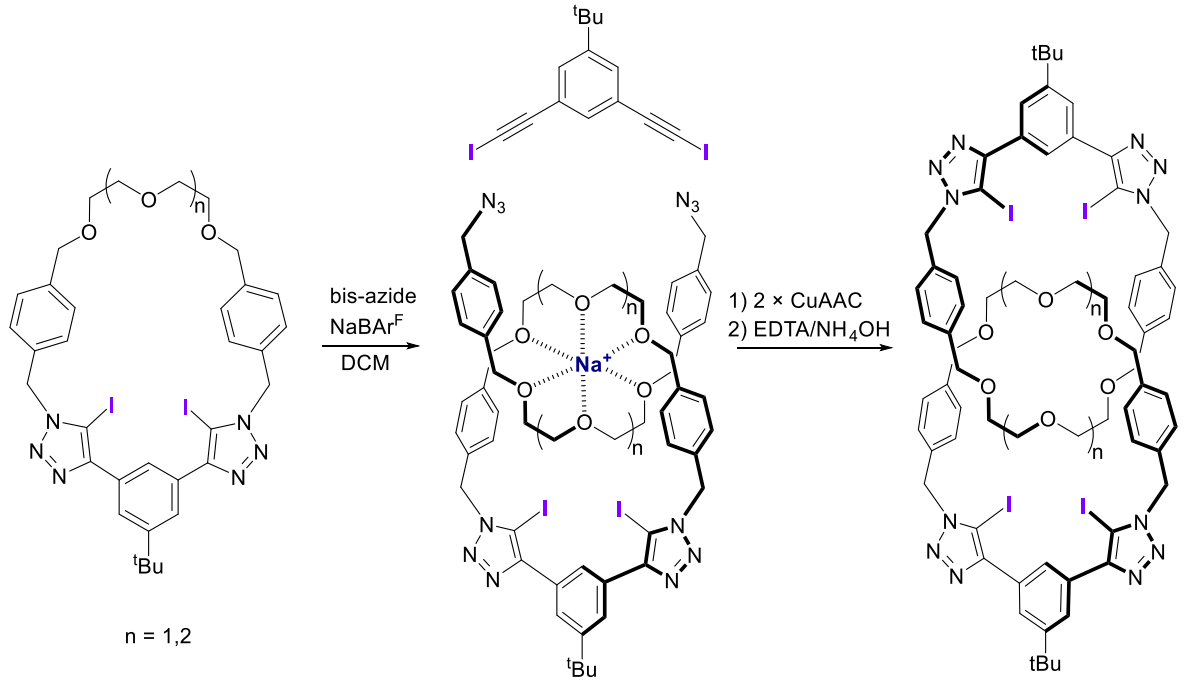

Scheme 4.1. Beer's cation-templated synthesis of heteroditopic [2]catenanes *via* CuAAC macrocyclisation reactions.[2]

Leigh has overcome the entropic challenges of [*n*]catenane formation by demonstrating the AMT synthesis of [2]catenanes using the CuAAC reaction (**Scheme 4.2**).[3] In this method, the reactive functionalities at each end of an acyclic precursor are brought together within the cavity of the macrocycle to undergo covalent bond formation in a macrocyclization reaction.

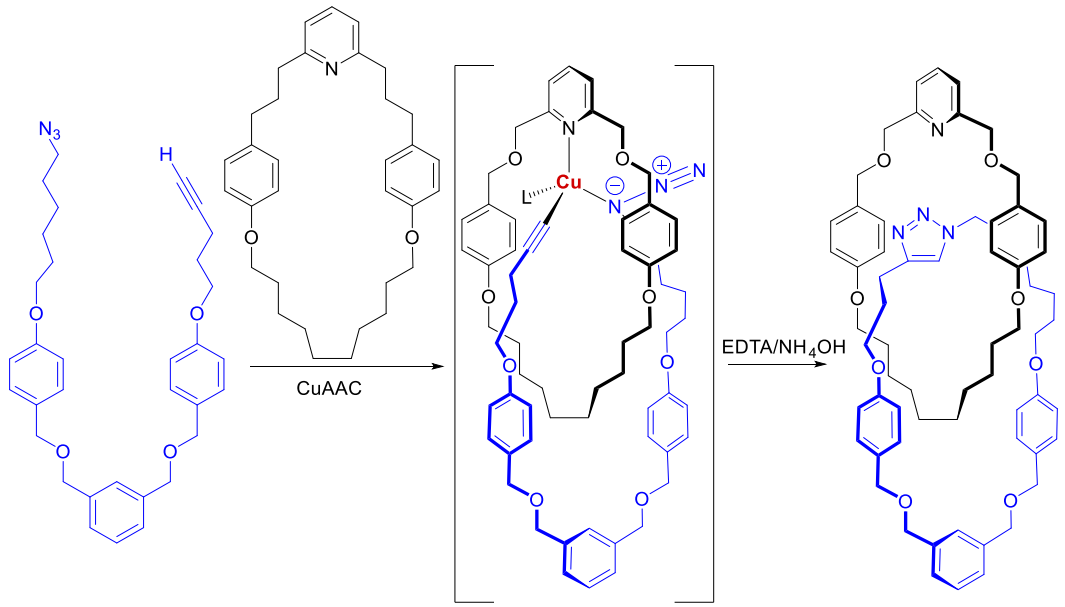

Scheme 4.2. Leigh's CuAAC-AMT synthesis of a [2]catenane via a macrocyclisation reaction.[3]

After successfully preparing [2]rotaxanes by the cyaphide-azide 1,3-dipolar cycloaddition reaction, we wanted to expand the scope of this reaction for the preparation of other types of inorganic MIMs. In order to prepare a [*n*]catenane by the cyaphide-azide 1,3-dipolar cycloaddition reaction, a reagent containing two reactive groups is required, such that it can undergo a macrocyclization reaction. This could be either a bis-cyaphide compound, or an acyclic compound containing a cyaphide and an azide group. We chose to avoid pursuing the latter, as it would likely prove difficult to install both functional groups onto the same chemical precursor due to the rapid kinetics of cyaphide azide 1,3-dipolar cycloaddition reaction.

4.2 Bis-phosphaalkynes and bis-cyaphide complexes

Despite the transient spectroscopic observation of P≡C–C≡P,[4] bis-phosphaalkynes remained elusive for over 20 years following the isolation of the first isolable phosphaalkyne, ^{t}Bu−C≡P.[5] This was until the remarkable synthesis of the air- and moisture-stable bis-phosphaalkynes by C. Jones, which owe their stability to the linear disposition and spatial separation of the phosphaalkyne moieties, which circumvents intramolecular coupling reactions (**Figure 4.1**).[6,7]

Despite their enormous potential as building blocks for organophosphorus polymers, coordination polymers, and phosphorus-containing macrocycles, no other bis-phosphaalkynes have been reported to date. Moreover, the 1,3-dipolar cycloaddition reactivity of bis-phosphaalkynes with azides remain unreported.

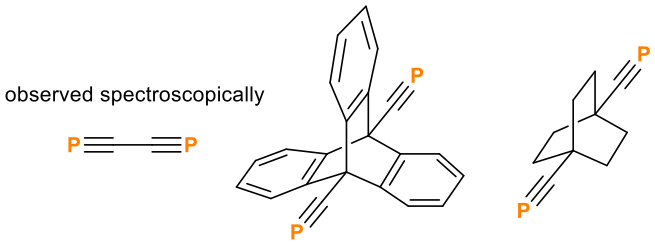

Figure 4.1. Examples of bis-phosphaalkynes.[4,6,7]

Since the development of the magnesium-cyaphide transfer reagent,[8] the number of examples of metal-cyaphide complexes has more than doubled, and their cycloaddition chemistry with azides has gained increased attention (Chapter 2).[9,10] The preparation of complexes containing multiple cyaphide moieties is an even more formidable challenge due to the high reactivity of the cyaphide ligand in oligomerization and coupling reactions.[11] Crossley and co-workers reported the first example of a metal complex containing two cyaphide ligands through base-induced desilylation of $Me_3SiC{\equiv}P$ ligands, stabilised by through-conjugation mediated by a dinuclear ruthenium(II) core (**Figure 4.2, left**).[12] The same group then went on to report the first example of a complex with two cyaphide ligands at a single metal centre, *trans*-$Ru(dppe)_2(CP)_2$ (dppe = 1,2-bis-(diphenylphosphino)ethane), using a similar step-wise variant of the previous strategy (**Figure 4.2, middle**).[13] Shortly after, our group reported the use of the air- and moisture-tolerant iron bis-cyaphide complex, *trans*-$Fe(depe)_2(CP)_2$ (depe = 1,2-bis-(diethylphosphino)ethane), to prepare conjugated multimetallic mixed valence compounds through end-on bridging cyaphide ligands (**Figure 4.2, right**).[14] In all of these examples, the cyaphide moieties are stabilised by through conjugation *via* the metal centre, affording complexes that appear to lack reactivity beyond further coordination at the cyaphide

ligand. Indeed, no reactivity was observed upon the addition of excess $^{t}BuN_3$ to a solution of *trans*-Fe(depe)$_2$(CP)$_2$.

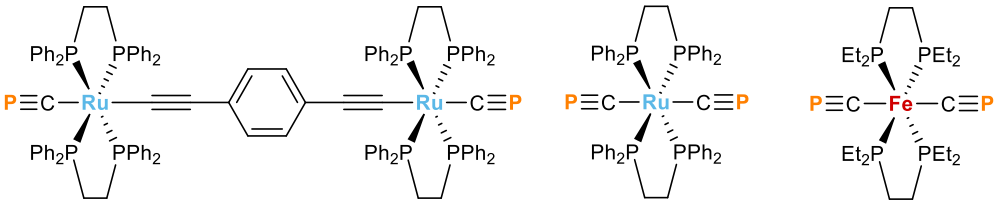

Figure 4.2. Examples of bis-cyaphide metal complexes.[12–14]

4.3 Dinuclear gold(I) bis-cyaphide complexes

4.3.1 *Janus*-bis-NHC complexes

To prepare a [*n*]catenane by the cyaphide-azide 1,3-dipolar cycloaddition reaction, a stable bis-cyaphide complex that retains cycloaddition reactivity is required. The mononuclear complex (IDipp)Au(CP) is an attractive building block due to its linear coordination and has been used for the preparation of [2]rotaxanes (Chapter 3). It is also remarkably stable despite the lack of steric protection around the cyaphide ligand, due to a high degree of covalency in the Au–CP bond. The strongly σ-donating NHC ligand coupled with the late 5d gold(I) metal forms strong covalent bonds with carbon due to relativistic contraction of the 6s orbital.[15] Indeed, in contrast to other metal (Ni or Sc) cyaphide complexes, oligomerization of the cyaphide ligand in the (IDipp)Au(CP) complex requires chemical reduction by Sm(Cp*)$_2$(OEt$_2$) (**Scheme 4.3**).[11]

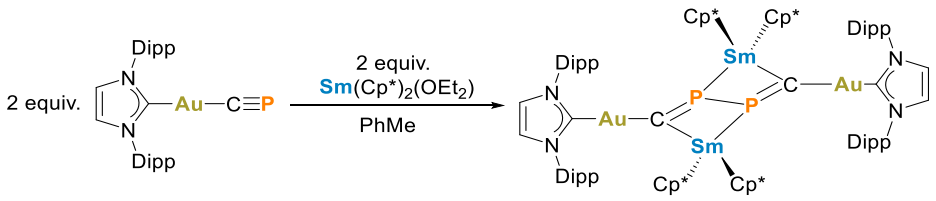

Scheme 4.3. Oligomerization of (IDipp)Au(CP) by chemical reduction.[11]

We therefore chose to target dinuclear gold(I) bis-cyaphide complexes, where a bis-NHC ligand links two gold(I) centres that are each bound to a cyaphide ligand. It is also desirable to spatially separate the cyaphide units and coordinate them in a *trans* manner in order to circumvent intramolecular coupling reactions. Bis-NHC ligands have been widely used for the preparation of metallosupramolecular architectures and organometallic polymers.[16] In particular, *Janus*-bis-NHCs, capable of coordinating two transition metals in a facially opposed manner, have been used extensively by Peris to construct metallocages (**Figure 4.3**).[17,18] A twisted metallocage was prepared through the use of the bent fused *Janus*-bis-NHC ligand (**Figure 4.3, bottom**).[17] Similarly, a metallocage capable of encapsulating polycyclic aromatic hydrocarbons was prepared by using the planar pyrene-fused *Janus*-bis-NHC ligand (**Figure 4.3, bottom**), demonstrating the versatility of these ligands as building blocks for metallosupramolecular architectures of different geometries.[18] Inspired by the work of Peris, we aimed to utilise this class of *Janus*-bis-NHC ligands to target dinuclear gold(I) bis-cyaphide complexes.

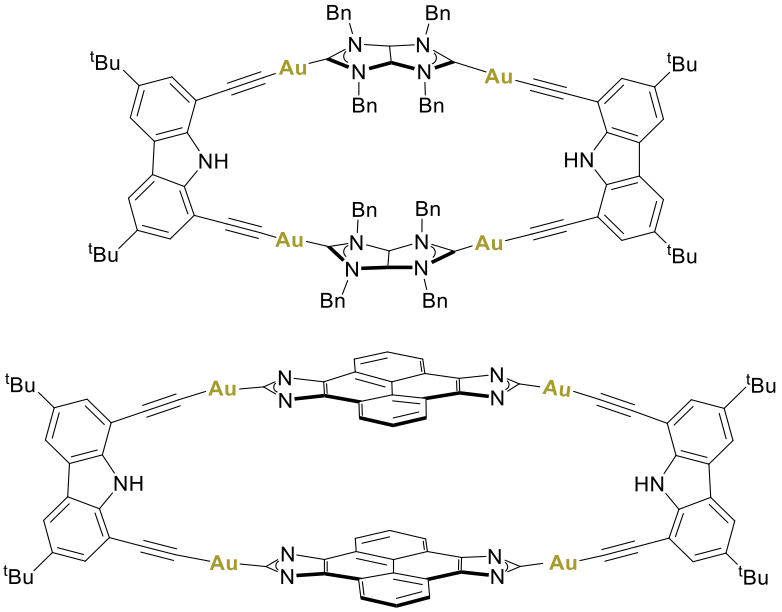

Figure 4.3. Metallocages prepared by Peris using Janus-bis-NHCs.[17,18]

We first used the bent fused *Janus*-bis-NHC dinuclear gold(I) chloride complex as a precursor. Due to the poor solubility of the gold(I) chloride precursor in aromatic solvents, cyaphide transfer was attempted in DCM (with a drop of dioxane to solubilise $[Mg(CP)]_2$) (**Scheme 4.4**). This resulted in the emergence of a new peak at 89.3 ppm in the $^{31}P\{^{1}H\}$ NMR spectrum (**Figure 4.4**).

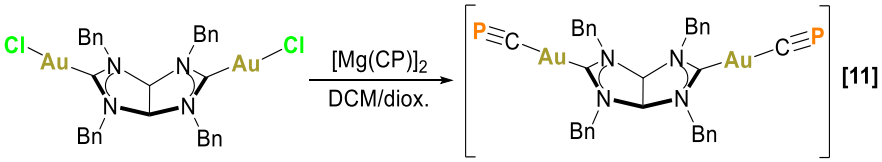

Scheme 4.4. Attempted synthesis of a bent fused *Janus*-NHC dinuclear gold(I) bis-cyaphide complex, **[11]**. Square brackets are used to show that this complex is unstable and could not be isolated.

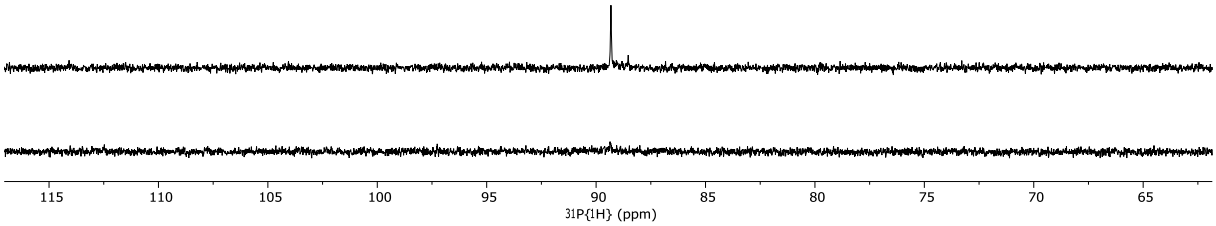

Figure 4.4. $^{31}P\{^{1}H\}$ NMR spectrum of the reaction mixture of Scheme 4.4 immediately after (top) and 3 hours later (bottom).

This chemical shift is in a similar region to the $^{31}P\{^{1}H\}$ NMR resonance of the previously reported (IDipp)Au(CP) complex (84.1 ppm in C_6D_6) and therefore was tentatively assigned as the bis-cyaphide complex **[11]**. Unfortunately, after a few hours at room temperature, the $^{31}P\{^{1}H\}$ NMR resonance disappeared and the solution became dark brown, likely due to oligomerization of the cyaphide, and so **[11]** was deemed too unstable to isolate. Due to the mild conditions and relatively fast reaction times of the cyaphide-azide cycloaddition reaction, kinetically unstable cyaphide complexes such as (^{Dipp}NacNac)Ge(CP) have been trapped through *in-situ* reactions with azides to yield the corresponding germanium(II) triazaphosphole

complex (**section 2.2.4**). Attempts to trap the product through an *in-situ* 1,3-dipolar cycloaddition reaction with ^{t}Bu–N$_3$ were unsuccessful and led to an intractable mixture of products, with multiple peaks in the region of the ^{31}P{^{1}H} NMR spectrum expected for the cycloaddition product (~196 ppm). This was evident even when conducted at low temperature, presumably due to the rapid decomposition of **[11]**.

We then turned our attention to a benzene-fused *Janus*-bis-NHC complex, similar to the pyrene-fused version used by Peris, in the hope that a conjugated ligand would improve the stability of the resulting dinuclear gold(I) bis-cyaphide complex. Complex **12** was prepared from the previously reported benzo-bis(imidazolium) salt,[19] using the strong-base route as previously used by Peris (**Scheme 4.5**).[20] The ^{1}H NMR spectrum of **12** displayed two peaks for the aromatic and ^{t}Bu environments, the relative integrals of which were as expected. The ^{13}C{^{1}H} NMR spectrum displayed a characteristic signal at 181.7 ppm for the carbene carbon nuclei.

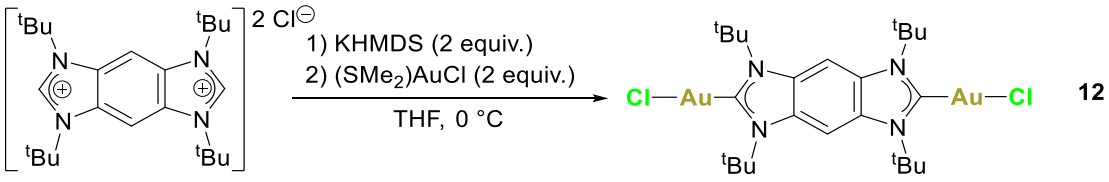

Scheme 4.5. Synthesis of the phenyl-fused *Janus*-bis-NHC dinuclear gold(I) chloride complex **12**.

Upon the addition of an equivalent of [Mg(CP)]$_2$ to complex **12** in DCM/dioxane, a new resonance at 92.1 ppm emerged in the ^{31}P{^{1}H} NMR spectrum, which was tentatively assigned to the dinuclear gold(I) bis-cyaphide complex **[13]**. Unfortunately, as with **[11]**, the peak disappeared after a few hours at room temperature (**Scheme 4.6 and Figure 4.5**). Attempts to trap **[13]** with ^{t}BuN$_3$ were similarly unsuccessful.

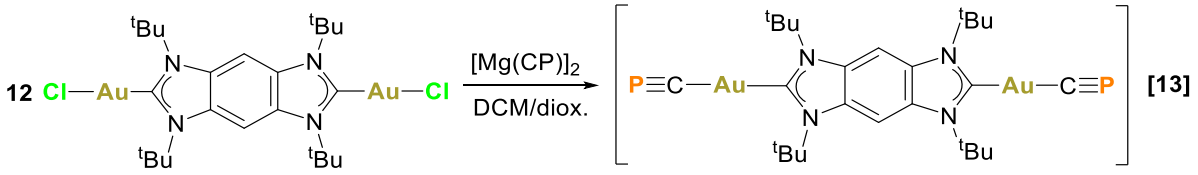

Scheme 4.6. Attempted synthesis of a planar phenyl-fused *Janus*-bis-NHC dinuclear gold(I) bis-cyaphide complex **[13]**.

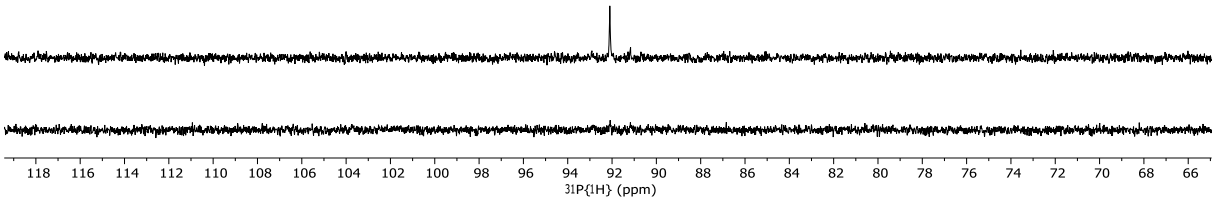

Figure 4.5. $^{31}P\{^{1}H\}$ NMR spectrum of the reaction mixture of Scheme 4.5 immediately after (top) and 3 hours after (bottom).

It should be noted here that there is little scope to increase the steric bulk at the nitrogen substituents for these carbenes, which could, in principle, help stabilise the targeted gold(I) bis-cyaphide complexes. The short length of these ligands results in the nitrogen substituents being in close proximity (approx. 5.9 Å),[19] meaning that such Janus-type carbenes are incompatible with bulky nitrogen groups.[21]

The fate of the cyaphide moiety in the attempted syntheses of **[11]** and **[13]** could not be determined, as the decomposition is rapid and no products in the reaction mixture could be isolated or characterised. Oxidative cyaphide oligomerisation is a plausible decomposition pathway due to relatively weak Au–CP bonds, as a result of weaker back bonding from the gold(I) to the cyaphide moiety due to the shared ligand system. This is evidenced by the slightly downfield shifted $^{31}P\{^{1}H\}$ NMR resonances relative to (IDipp)Au(CP), which suggests lower electron density at the phosphorus atoms. It is however unclear whether the cyaphide remains bound to the gold(I), and the exact nature of the decomposition pathway remains unclear.

4.3.2 Alkyl-bridged bis-NHC complexes

We reasoned that separating the two gold(I) cyaphide moieties by a longer bridging unit could increase the lifetime of such complexes by minimising the electronic conjugation between the two gold(I) centres. We selected a ligand from Nolan's report on alkyl-bridged bis-NHC dinuclear gold chloride complexes prepared *via* the weak-base route.[22] Again, due to the poor solubility of the gold chloride precursor in aromatic solvents, cyaphide transfer was carried out in DCM (with a drop of dioxane to solubilise $[Mg(CP)]_2$) (**Scheme 4.7**), and a new peak was observed at 85.7 ppm in the $^{31}P\{^{1}H\}$ NMR spectrum. This species was tentatively assigned as the dinuclear gold(I) bis-cyaphide complex **[14]** and had an extended lifetime when compared to **[11]** and **[13]**, with the resonance disappearing after approx. three days (**Figure 4.6**).

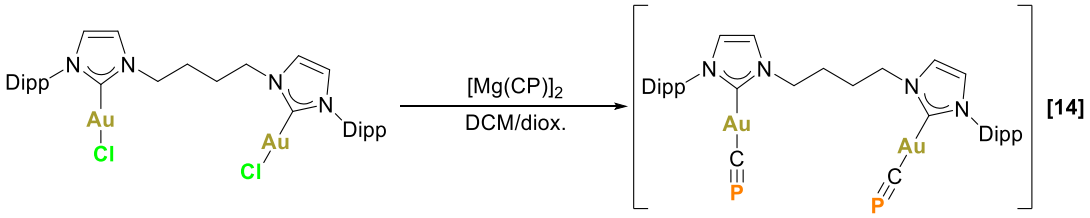

Scheme 4.7. Attempted synthesis of an alkyl-bridged bis-NHC dinuclear gold (I) bis-cyaphide complex **[14]**.

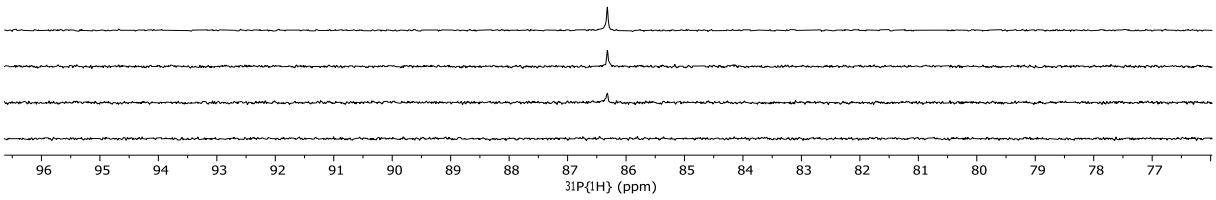

Figure 4.6. $^{31}P\{^{1}H\}$ NMR spectrum of the reaction mixture of Scheme 4.6 immediately after (top), and subsequent days after (top to bottom).

The $^{31}P\{^{1}H\}$ NMR resonance of **[14]** is shifted upfield in comparison to **[11]** and **[13]**, and is more comparable to (IDipp)Au(CP), as a result of increased electron density at the phosphorus. Unfortunately, **[14]** could not be isolated as the compound rapidly decomposed when subject

to vacuum. Clean ^{1}H and ^{13}C{^{1}H} NMR spectra of **[14]** were obtained by precipitation with Et_2O, followed by decanting the supernatant, washing the solids further with Et_2O, then quickly redissolving the solids in CD_2Cl_2. The cyaphide and carbene carbon resonances could be identified in the ^{13}C{^{1}H} NMR spectrum as doublets at 245.9 ppm ($^{1}J_{C–P}$ = 8.2 Hz) and 187.3 ppm ($^{3}J_{C–P}$ = 5.9 Hz), respectively. These are in a similar region to the (IDipp)Au(CP) complex (247.7 ppm, $^{1}J_{C–P}$ = 6.1 Hz and 193.0 ppm, $^{3}J_{C–P}$ = 5.0 Hz).

To confirm the identity of the dinuclear bis-cyaphide complex **[14]**, an *in-situ* generated solution of **[14]** was reacted with two equivalents of ^{t}Bu–N_3 (**Scheme 4.8**). This resulted in a single peak in the ^{31}P{^{1}H} NMR spectrum at 193.5 ppm, which is in the expected region for a cycloaddition product. This product was indefinitely stable in solution and could be isolated cleanly by crystallisation. The ^{1}H NMR spectrum revealed a diagnostic resonance at 5.03 ppm for the ^{Dipp}NacNac γ-H proton with a relative integral of two. Upon further inspection of the ^{1}H and ^{13}C{^{1}H} NMR spectra, the presence of two equivalents of the cyaphide transfer by-product, (^{Dipp}NacNac)MgCl, was evident. The triazaphosphole carbon was identified as a doublet at 210.8 ($^{1}J_{C–P}$ = 83 Hz) in the ^{13}C{^{1}H} NMR spectrum. The carbene carbon is shifted slightly upfield to 190.1 ppm in comparison to **[14]**, due to the stronger σ-donation of the triazaphospholide ligand, similar to what was observed for **1a–c** (Section 2.2.1).

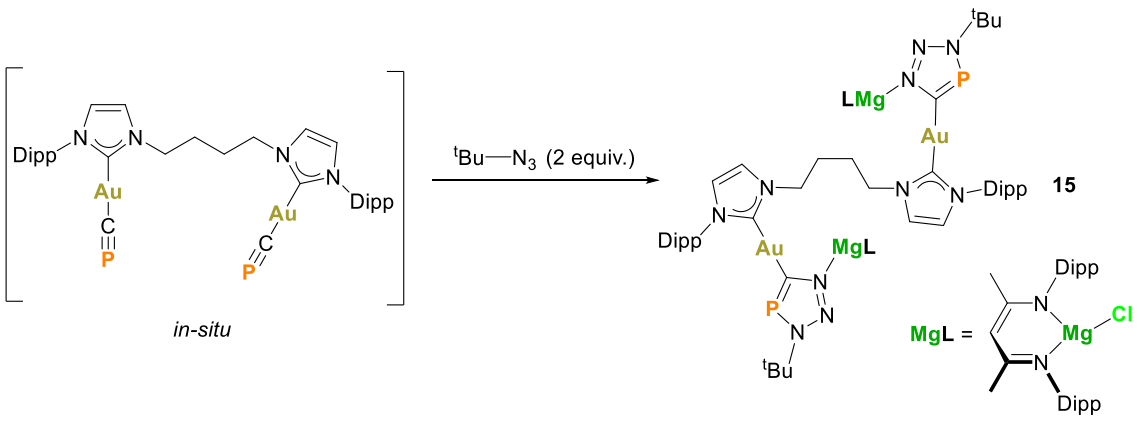

Scheme 4.8. *In situ* trapping of **[14]** with ^{t}Bu–N$_3$ to yield the corresponding dinuclear gold(I) triazaphosphole complex **15**.

The identity of **15** was confirmed by SC-XRD as the cycloaddition product of the reaction of each cyaphide ligand with ^{t}Bu–N$_3$, with (^{Dipp}NacNac)MgCl (**MgL**) coordinated to the most Lewis basic nitrogen (N1 and N1′) of each triazaphosphole (**Figure 4.7**). The solid-state structure of **15** reveals a bent-anti conformation, with a Au1–C2–C2′–Au1′ dihedral angle of 180.0(3)°, to minimise steric clash between the triazaphosphole–(^{Dipp}NacNac)MgCl units. The (^{Dipp}NacNac)MgCl units are also facing inwards, to minimise void space for effective crystal packing. The angle between the planes of the triazaphosphole and ^{Dipp}NacNac ligand is almost perpendicular at 89.92°, such that the bulky Dipp substituents sit above and below the triazaphosphole plane. The bond metrics in the NHC–Au–triazaphosphole unit are similar to the mononuclear gold-triazaphosphole complex **1a** (Section 2.2.1), with the exception of the C2–Au1–C1 and C2′–Au1–C1′ angles that are bent slightly to 176.6(3)° to accommodate the additional steric bulk of the (^{Dipp}NacNac)MgCl unit (179.5(3)° in **1a**). The Mg1–N1 and Mg1′–N1′ bond lengths are 2.125(6) Å.

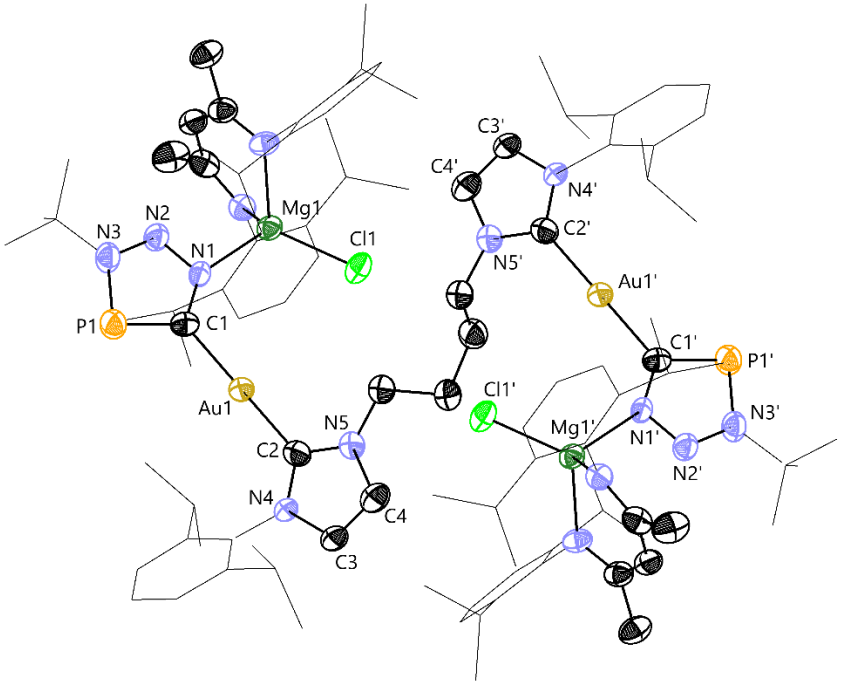

Figure 4.7. SC-XRD structure of the bis-NHC dinuclear gold(I) triazaphosphole complex **15**. Anisotropic displacement ellipsoids depicted at 50% probability. Hydrogen atoms, disorder components, and co-crystallised solvent molecules are omitted for clarity. Dipp substituents are depicted as wireframes for clarity.

HR-ESI-MS of **15** results in loss of the (^{Dipp}NacNac)MgCl adducts, and a peak corresponding to the protonated cycloaddition species [(**15**−2**MgL**)+H]$^+$ is present (*m*/*z* = 1189.4195; theoretical 1189.4197). The trapping of **[14]** with ^{t}Bu–N_3 to yield **15**, which can be isolated and fully characterised by NMR, SC-XRD, and HR-ESI-MS, provides indisputable evidence of the presence of a dinuclear gold(I) bis-cyaphide species **[14]**.

It should be noted that in this case, it is difficult to remove the by-product of cyaphide transfer, (^{Dipp}NacNac)MgCl, before the addition of the azide, due to its solubility in DCM. For the *in-situ* cyaphide-azide 1,3-dipolar cycloaddition reaction of (^{Dipp}NacNac)Ge(CP) (see Section 2.2.4), it was removed straightforwardly by filtration due to its insolubility in toluene.

4.4 Conclusions

Dinuclear gold(I) bis-cyaphide complexes using facially opposed *Janus*-bis-NHCs rapidly decompose and therefore cannot be isolated. Introducing an alkyl bridge to the bis-NHC ligand enhances the stability of the dinuclear gold(I) bis-cyaphide complexes to a lifetime of a few days, allowing characterisation by NMR spectroscopy. This species can be trapped *in situ* through the cycloaddition reaction with an azide, yielding the bis-triazaphosphole product as an adduct of the cyaphide transfer by-product, (^{Dipp}NacNac)MgCl. This compound was characterised by NMR, SC-XRD, and HR-ESI-MS, giving indisputable evidence of the transient existence of a dinuclear gold(I) bis-cyaphide complex.

4.5 Experimental

4.5.1 Synthesis of 12

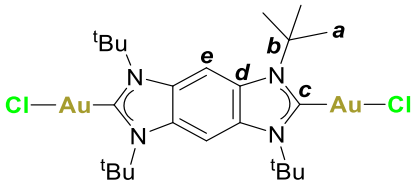

This complex was prepared using a method analogous to Peris.[20] Potassium bis(trimethylsilyl)amide (KHMDS) (74 mg, 0.373 mmol, 2.2 equiv.) was dissolved in toluene (0.5 mL) and added dropwise to a suspension of the benzo-bis(imidazolium) salt (77 mg, 0.169 mmol) in THF (10 mL) at 0 °C. After stirring at this temperature for 10 minutes, the solution was added dropwise to a stirred suspension of (SMe_2)AuCl (100 mg, 0.34 mmol, 2 equiv.) in THF (5 mL). The solution was stirred in the dark for 2 h. Under air, a spatula of activated charcoal was added, and the mixture was stirred for 30 minutes. The suspension was then filtered through Celite, and the charcoal was washed with DCM (2 × 10 mL). The filtrate was collected, and the solvent was removed *in vacuo*. The residue was dissolved in a minimum amount of DCM and precipitated with pentane to afford **12** as a pale-yellow solid. Yield: 25 mg, 0.0296 mmol, 18% yield.

^{1}H NMR (600 MHz, C_6D_6): δ(ppm) 8.39 (s, 2H; H_e), 2.23 (s, 36H; H_a).

^{13}C{^{1}H} NMR (151 MHz, C_6D_6): δ(ppm) 181.7 (C_c), 130.6 (H_d), 101.9 (H_e), 62.3 (C_b), 33.0 (C_a).

4.5.2 Attempted synthesis of [11] and [13]

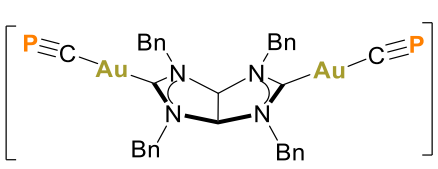

[11]

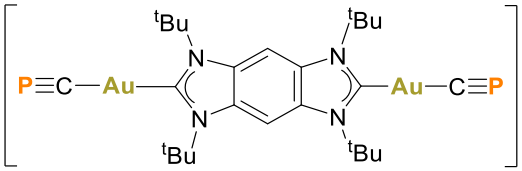

[13]

$[Mg(CP)]_2$ (approx. 15 mg scale, 1 equiv.) was dissolved in CD_2Cl_2 (0.5 mL) with one drop of dioxane. The *Janus*-bis-NHC dinuclear gold(I) chloride complex (1 equiv.) was added as a solid. The solution immediately went dark brown, and the $^{31}P\{^1H\}$ NMR spectra displayed no signal after 3 h.

[11] - $^{31}P\{^1H\}$ NMR (162 MHz, CD_2Cl_2): δ (ppm) = 89.3 (s).

[13] - $^{31}P\{^1H\}$ NMR (162 MHz, CD_2Cl_2): δ (ppm) = 92.1 (s).

4.5.3 Synthesis of compound [14] *in situ*

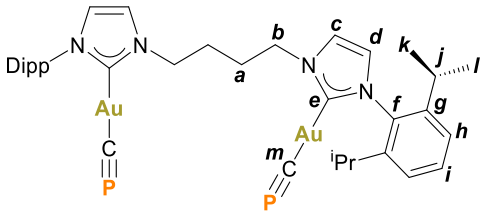

$[Mg(CP)]_2$ (15 mg, 0.015 mmol) was dissolved in DCM (0.5 mL) with one drop of dioxane. To this solution, the alkyl-bridged bis-NHC dinuclear gold(I) chloride complex (15 mg, 0.015 mmol) was added. $^{31}P\{^1H\}$ NMR spectroscopy revealed the presence of a single new phosphorus-containing compound. However, over the period of a few days, the reaction mixture darkened, and an insoluble precipitate was formed. This was indicative of decomposition, and the $^{31}P\{^1H\}$ NMR spectrum of the reaction mixture contained no signal. Despite efforts, attempts to isolate pure **14** were unsuccessful. Clean NMR spectra could be obtained by immediately precipitating **14** from the reaction mixture through the addition of

Et_2O (0.5 mL), removed the supernatant, washing with Et_2O (0.5 mL), followed by extraction with CD_2Cl_2.

^{1}H NMR (400 MHz, CD_2Cl_2): δ (ppm) 7.53 (t, $^3J_{H–H}$ = 7.8 Hz, 2H; H_i), 7.41 (d, $^3J_{H–H}$ = 1.9 Hz, 2H; $H_{c/d}$), 7.31 (d, $^3J_{H–H}$ = 7.8 Hz, 4H; H_h), 6.98 (d, $^3J_{H–H}$ = 1.9 Hz, 2H; $H_{c/d}$), 4.41 (t, $^3J_{H–H}$ = 6.7 Hz, 4H; H_b), 2.35 (sept, $^3J_{H–H}$ = 6.9 Hz, 4H; H_j), 2.07 (t, $^3J_{H–H}$ = 6.7 Hz, 4H; H_a), 1.28 (d, $^3J_{H–H}$ = 6.9 Hz, 12H; $H_{k/l}$), 1.12 (d, $^3J_{H–H}$ = 6.9 Hz, 12H; $H_{k/l}$).

^{13}C NMR (151 MHz, C_6D_6): δ (ppm) 246.3 (d, $^1J_{C–P}$ = 8.5 Hz; C_m), 187.3 (d, $^3J_{C–P}$ = 5.9 Hz; C_e), 146.3 (C_g), 134.7 (C_f), 130.9 (C_i), 124.6 ($C_{c/d}$), 124.5 (C_h), 121.4 ($C_{c/d}$), 50.5 (C_b), 28.8 (C_j), 28.2 (C_a), 24.6 ($C_{k/l}$), 24.4 ($C_{k/l}$).

^{31}P{^{1}H} NMR (162 MHz, C_6D_6): δ (ppm) = 86.3 (s).

4.5.4 Synthesis of 15

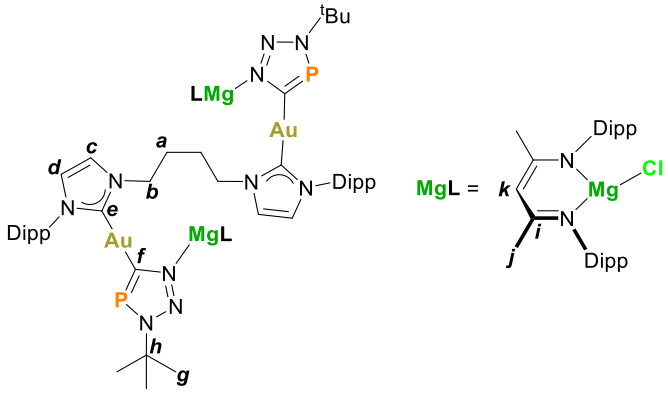

$[Mg(CP)]_2$ (50 mg, 0.052 mmol) was dissolved in DCM (1 mL) with four drops of dioxane. To this solution, the alkyl-bridged bis-NHC dinuclear gold(I) chloride complex (50 mg, 0.052 mmol) was added. After stirring for 10 minutes, *tert*-butyl azide was added to the solution. After stirring at room temperature for 16 h, the reaction mixture was filtered and layered with hexane. Storage at −35 ºC for 3 days yielded yellow crystals of **15** that were isolated by filtration, washed with pentane (2 × 1 mL), and dried under vacuum. Yield: 32 mg, 0.016 mmol, 30%.

^{1}H NMR (600 MHz, C_6D_6): δ (ppm) = 7.25 (t, $^{3}J_{H–H}$ = 7.8 Hz, 2H; Dipp Ar-H), 7.18 (4H; Dipp Ar-H), 7.11–7.08 (8H; Dipp Ar-H), 7.03 (4H; Dipp Ar-H), 6.89 (d, $^{3}J_{H–H}$ = 1.8 Hz, 2H; $H_{c/d}$), 6.34 (d, $^{3}J_{H–H}$ = 1.8 Hz, 2H; $H_{c/d}$), 5.03 (s, 2H; H_k), 3.93 (pseudo-triplet, 4H; H_b), 3.81 (sept, $^{3}J_{H–H}$ = 6.9 Hz, 4H; Dipp ^{i}Pr CH), 2.71 (sept, $^{3}J_{H–H}$ = 6.9 Hz, 4H; Dipp ^{i}Pr CH), 2.60 (sept, $^{3}J_{H–H}$ = 6.9 Hz, 4H; Dipp ^{i}Pr CH), 1.86 (pseudo-triplet, 4H; H_a), 1.72 (s, 12H; H_j), 1.61 (d, $^{3}J_{H–H}$ = 6.9 Hz, 12H; Dipp Me), 1.52 (s, 18H; H_g), 1.34 (d, $^{3}J_{H–H}$ = 6.9 Hz, 12H; Dipp Me), 1.22 (d, $^{3}J_{H–H}$ = 6.9 Hz, 12H; Dipp Me), 1.05 (d, $^{3}J_{H–H}$ = 6.9 Hz, 12H; Dipp Me), 1.04 (d, $^{3}J_{H–H}$ = 6.9 Hz, 12H; Dipp Me), 0.54 (d, $^{3}J_{H–H}$ = 6.9 Hz, 12H; Dipp Me).

^{13}C{^{1}H} NMR (151 MHz, C_6D_6): δ (ppm) = 210.8 (d, $^{1}J_{C–P}$ = 83 Hz; C_f), 190.1 (d, $^{3}J_{C–P}$ = 7.3 Hz; C_e), 168.10 (C_i), 146.6 (Dipp Ar-C), 146.2 (Dipp Ar-C), 143.3 (Dipp Ar-C), 143.1 (Dipp Ar-C), 135.8 (Dipp Ar-C), 130.0 (Dipp Ar-C), 124.8 (Dipp Ar-C), 123.9 (Dipp Ar-C), 123.7 (Dipp Ar-C), 123.4 (Dipp Ar-C), 122.5 ($C_{c/d}$), 122.3 ($C_{c/d}$), 95.3 (C_k), 61.9 (d, $^{2}J_{C–P}$ = 2.7 Hz; C_h), 50.6 (C_b), 31.4 (d, $^{3}J_{C–P}$ = 4.1 Hz; C_g), 28.8 (Dipp ^{i}Pr CH), 28.6 (Dipp ^{i}Pr CH), 27.9 (C_a), 27.9 (Dipp ^{i}Pr CH), 26.8 (Dipp Me), 25.0 (Dipp Me), 24.9 (Dipp Me), 24.7 (Dipp Me), 24.3 (Dipp Me), 24.3 (Dipp Me), 24.2 (C_j).

The Dipp resonances could not be distinguished between the IDipp and ^{Dipp}NacNac and are therefore assigned generally.

^{31}P{^{1}H} NMR (243 MHz, C_6D_6): δ (ppm) = 193.5 (s).

HR-ESI-MS (+ve ion mode): m/z calcd. for $C_{44}H_{64}Au_2N_{10}P_2+H^+$: 1189.4195 $[(M-2MgL)+H]^+$; found 1189.4197.

4.6 References

1. Q. Chen and K. Zhu, *Chem. Soc. Rev.* **2024**, *53*, 5677–5703.
2. H. M. Tay, Y. C. Tse, A. Docker, C. Gateley, A. L. Thompson, H. Kuhn, Z. Zhang and P. D. Beer, *Angew. Chem. Int. Ed.* **2023**, *62*, e202214785.
3. S. M. Goldup, D. A. Leigh, T. Long, P. R. McGonigal, M. D. Symes and J. Wu, *J. Am. Chem. Soc.* **2009**, *131*, 15924–15929.
4. M. Brönstrup, J. Gottfriedsen, I. Kretzschmar, S. J. Blanksby, H. Schwarz and H. Schumann, *Phys. Chem. Chem. Phys.* **2000**, *2*, 2245–2250.
5. G. Becker, G. Gresser and W. Uhl, *Z. Naturforsch. B.* **1981**, *36*, 16–19.
6. M. Brym and C. Jones, *Dalton Trans.* **2003**, 3665.
7. F. Brodkorb, M. Brym, C. Jones and C. Schulten, *J. Organomet. Chem.* **2006**, *691*, 1025–1029.
8. D. W. N. Wilson, S. J. Urwin, E. S. Yang and J. M. Goicoechea, *J. Am. Chem. Soc.* **2021**, *143*, 10367–10373.
9. E. S. Yang, A. Mapp, A. Taylor, P. D. Beer and J. M. Goicoechea, *Chem. Eur. J.* **2023**, *29*, e202301648.
10. D. González-Pinardo, J. M. Goicoechea and I. Fernández, *Chem. Eur. J.* **2024**, *30*, e202303977.
11. E. S. Yang, D. W. N. Wilson and J. M. Goicoechea, *Angew. Chem. Int. Ed.* **2023**, *62*, e202218047.
12. M. C. Leech and I. R. Crossley, *Dalton Trans.* **2018**, *47*, 4428–4432.
13. M. C. Levis, M. L. Helm, J. F. C. Turner and I. R. Crossley, *Chem. Eur. J.* **2024**, *30*, e202303370.
14. E. S. Yang, Á. García-Romero, C. Hu, J. Fletcher, C. M. Thomas and J. M. Goicoechea, *J. Am. Chem. Soc.* **2024**, *146*, 42, 29207–29213.

15. N. Kaltsoyannis, *J. Chem. Soc., Dalton Trans.* **1997**, 1–12.

16. M. Poyatos and E. Peris, *Dalton Trans.* **2021**, *50*, 12748–12763.

17. A. Gutiérrez-Blanco, S. Ibáñez, F. E. Hahn, M. Poyatos and E. Peris, *Organometallics* **2019**, *38*, 4565–4569.

18. S. Ibáñez and E. Peris, *Angew. Chem. Int. Ed.* **2020**, *59*, 6860–6865.

19. A. J. Boydston, D. M. Khramov and C. W. Bielawski, *Tetrahedron Lett.* **2006**, *47*, 5123–5125.

20. S. Gonell, M. Poyatos and E. Peris, *Angew Chem Int Ed* **2013**, *52*, 7009–7013.

21. D. M. Khramov, A. J. Boydston and C. W. Bielawski, *Org. Lett.* **2006**, *8*, 1831–1834.

22. T. A. C. A. Bayrakdar, F. Nahra, J. V. Davis, M. M. Gamage, B. Captain, M. Temprado, M. Marazzi, M. Saab, K. V. Hecke, D. Ormerod, C. D. Hoff and S. P. Nolan, *Organometallics* **2020**, *39*, 2907–2916.

Chapter 5

Synthesis and Reactivity of a Dinuclear Gold(I) Bis-cyaphide [2]Rotaxane

Abstract

A bis-imidazolium [2]rotaxane can be used to coordinate two gold(I) halide moieties, which can undergo cyaphide transfer. The resulting dinuclear gold(I) bis-cyaphide [2]rotaxane is indefinitely stable under an inert atmosphere in contrast to the related non-interlocked species discussed in Chapter 4. The bis-cyaphide [2]rotaxane can undergo straightforward post-synthetic modification *via* the cyaphide-azide 1 ,3-dipolar cycloaddition reaction, which has been used to generate a new efficient gold(I)-BODIPY photosensitizer for singlet oxygen generation. The conversion of the bis-cyaphide [2]rotaxane into a [2]catenane through its reaction with bis-azides proved challenging due to the rapid nature of the reaction, resulting in the formation of a multitude of cycloaddition products.

5.1 Enhancing stability with the mechanical bond

As discussed in the previous chapter, the synthesis of dinuclear gold(I) bis-cyaphide complexes is a significant challenge due to their rapid decomposition at room temperature. It has been well documented that the mechanical bond in MIMs can be used to alter the reactivity of the subcomponents.[1] In particular, it can be used to impart kinetic stability on otherwise reactive moieties by providing steric hindrance. For example, the [2]rotaxane prepared by Goldup (discussed in Section 1.1.2) contains an electron-rich alkyl phosphine and requires no special handling, whereas the corresponding non-interlocked species is oxidised to the phosphine oxide upon standing in air (**Figure 5.1**).[2] This prompted us to explore whether the mechanical

bond in a [2]rotaxane could be used to kinetically stabilise a dinuclear gold(I) bis-cyaphide species.

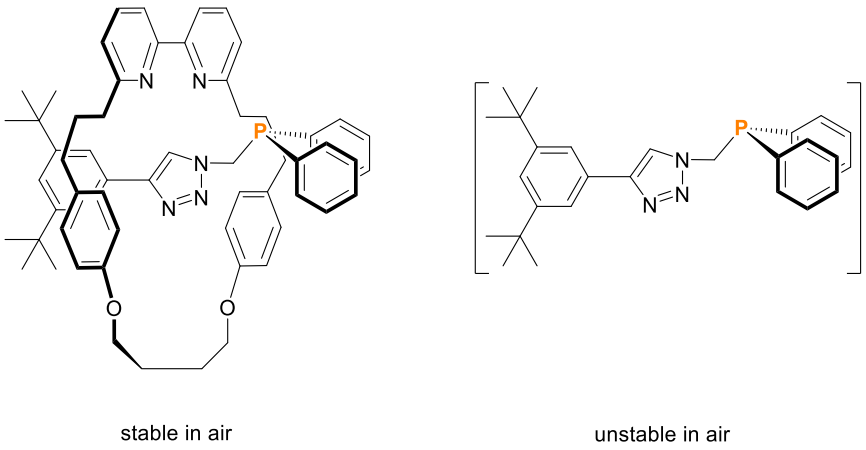

Figure 5.1. Kinetic stability comparison of the phosphine [2]rotaxane vs the non-interlocked phosphine axle.

5.2 Synthesis of a dinuclear gold(I) bis-cyaphide [2]rotaxane

5.2.1 Metal coordination at a bisimidazolium [2]rotaxane

Champness previously reported the synthesis of **P5A^{Me}**-based bis-imidazolium [2]rotaxanes *via* the S_N2 reaction of a threaded bis-imidazole axle with bulky 2-(iodomethyl)-1,3,5-trimethyl benzene stoppers (**Scheme 5.1**).[3] The resulting [2]rotaxanes are stable despite the presence of the nucleophilic iodide counterion.

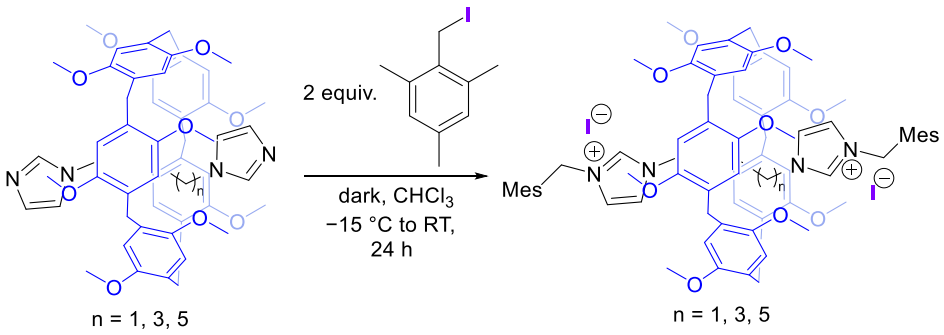

Scheme 5.1. Synthesis of bis-imidazolium [2]rotaxanes by Champness.[3]

^{1}H NMR experiments revealed that the **P5A^{Me}** macrocycle shuttles along the entire length of the axles in the bis-imidazolium [2]rotaxanes. Shuttling of the **P5A^{Me}** macrocycle along the axle was restricted to the alkyl linker following the formation of NHC–metal complexes upon deprotonation of the imidazolium units and coordination of silver(I) (**Scheme 5.2, top**). The dinuclear silver(I) [2]rotaxanes underwent transmetallation reactions to install bulkier PdI_2(pyridine) units (**Scheme 5.2, bottom**), which restricted the shuttling of the **P5A^{Me}** macrocycles along the axle even further.

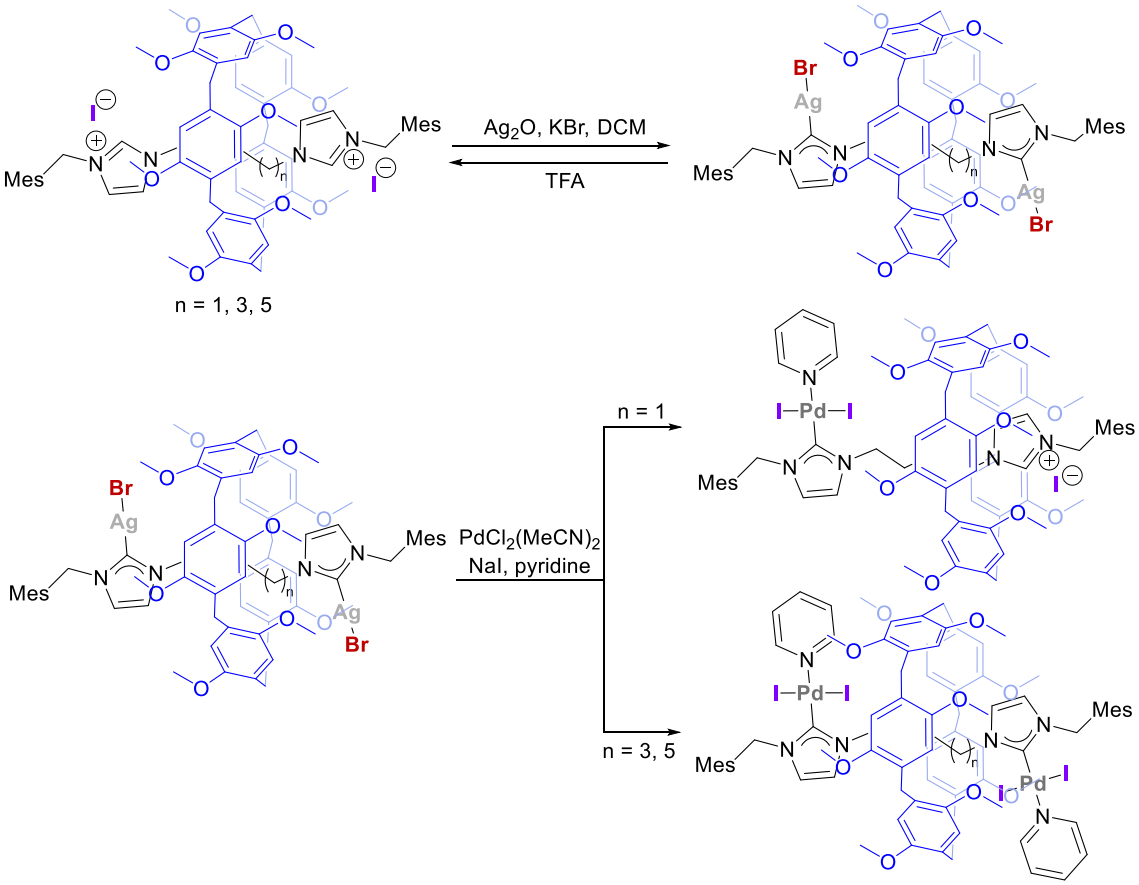

Scheme 5.2. Synthesis of a dinuclear silver(I) [2]rotaxane (top) and subsequent transmetallation to the palladium(II) [2]rotaxanes (bottom) by Champness.[3]

For the [2]rotaxane containing the shortest alkyl linker (n = 1), the **P5A^{Me}** prevents transmetallation at both NHC–Ag(I) moieties. Instead, transmetallation occurred only at one of the NHC units, allowing for the installation of just one PdI_2(pyridine) unit. The other NHC

unit reverted to the imidazolium salt under the reaction conditions. The **P5A^{Me}** component of the rotaxane was found to reside at the imidazolium terminal.

The formation of the aforementioned bis-NHC [2]rotaxanes and their ability to undergo subsequent metal coordination offers a potential avenue to explore for the formation of a dinuclear gold(I) bis-cyaphide [2]rotaxane. This prompted us to explore whether gold(I) coordination could be achieved at the same bis-imidazolium [2]rotaxane.

5.2.2 Coordination of gold(I) halides at a bis-imidazolium [2]rotaxane

The first synthetic target was a dinuclear gold(I) halide [2]rotaxane, capable of undergoing cyaphide transfer. The bis-imidazolium [2]rotaxane with the shortest C_4-alkyl linker (n = 1) was prepared according to the reported literature procedure.[3] The preparation of NHC–gold(I) compounds can be achieved through transmetallation from the silver(I) complex; however, in our hands, the preparation of the corresponding dinuclear silver(I) [2]rotaxane was unsuccessful. We then turned our attention to the strong base route, where deprotonation of the imidazolium units can be achieved by the addition of two equivalents of KHMDS, followed by the addition of two equivalents of (SMe_2)AuCl at −78 °C in THF. After stirring overnight, the ^{1}H NMR spectrum of the reaction revealed loss of the imidazolium proton resonance (8.60 ppm), indicating successful formation of NHC–Au bonds. TLC analysis of the crude mixture revealed the presence of two species, which could be separated by column chromatography. The ^{1}H NMR spectra of the two species were almost identical, differing only slightly in the imidazolium backbone region, and so were assigned as the dinuclear gold(I) iodide and gold(I) chloride [2]rotaxanes.

Halide scrambling has been previously reported for the synthesis of NHC gold(I) complexes, as a result of the strongly nucleophilic iodide being able to displace the lighter halides in (NHC)AuX (X = Cl, Br).[4] This can be circumvented by the addition of a large excess of

inorganic salt to push the equilibrium in favour of forming a single NHC gold(I) halide complex. The use of excess KCl (5 equiv.) to exclusively prepare the dinuclear gold(I) chloride [2]rotaxane was unsuccessful, as the crude NMR still revealed the presence of the gold(I) iodide species. In the presence of excess KI (5 equiv.), however, the dinuclear gold(I) iodide [2]rotaxane **16** was formed as the only gold(I) halide product, alongside some other impurities (**Scheme 5.3**). The crude reaction mixture was dark purple, presumably as a result of the formation of iodine and colloidal gold(0) due to redox side reactions. These undesired side-products can be removed by washing with sodium thiosulfate and filtration through silica, respectively. After work-up, **16** was isolated in moderate yields of 36%.

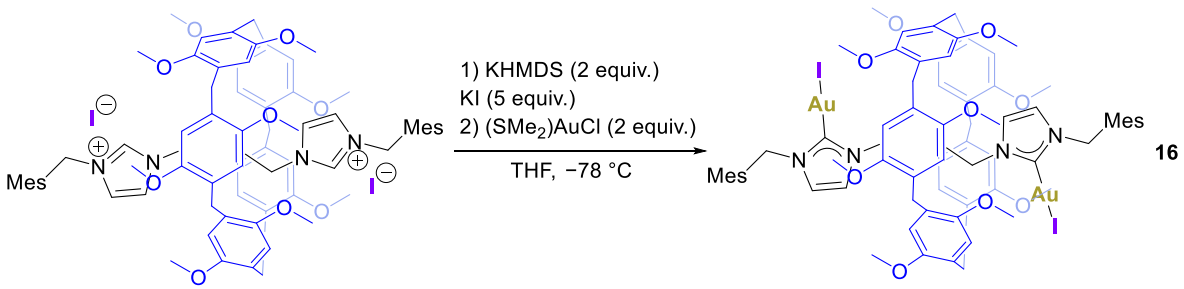

Scheme 5.3. Synthesis of a dinuclear gold(I) iodide [2]rotaxane **16**.

The ^{1}H and ^{13}C{^{1}H} NMR spectra of **16** are very similar to those previously reported for the dinuclear silver(I)–bromide [2]rotaxane.[3] The lack of symmetry of the NHC unit results in two distinct resonances for the imidazole protons, which appear as doublets in the ^{1}H NMR spectrum at 6.42 ppm and 5.89 ppm as a result of mutual coupling ($^{3}J_{H–H}$ = 1.9 Hz). Similar to the bis-imidazolium [2]rotaxane starting material, the methylene protons between the NHC units and Mes stoppers exhibit an AB quartet splitting pattern, as they are diastereotopic and undergo mutual coupling ($^{2}J_{H–H}$ = 14.4 Hz). This is induced by the chirality of the **P5A^{Me}** macrocycle. The ^{13}C{^{1}H} NMR spectrum revealed a resonance at 179.7 ppm, corresponding to the carbene carbon. At this point, it should be noted that the **16** is formed as the minor product when no KI is present (approx. 10% by integration of the imidazolium proton peaks).

Crystals suitable for SC-XRD were obtained by slow diffusion of hexane into a saturated chloroform solution, which confirmed the formation of the dinuclear gold(I) iodide [2]rotaxane species **16** (**Figure 5.2**).

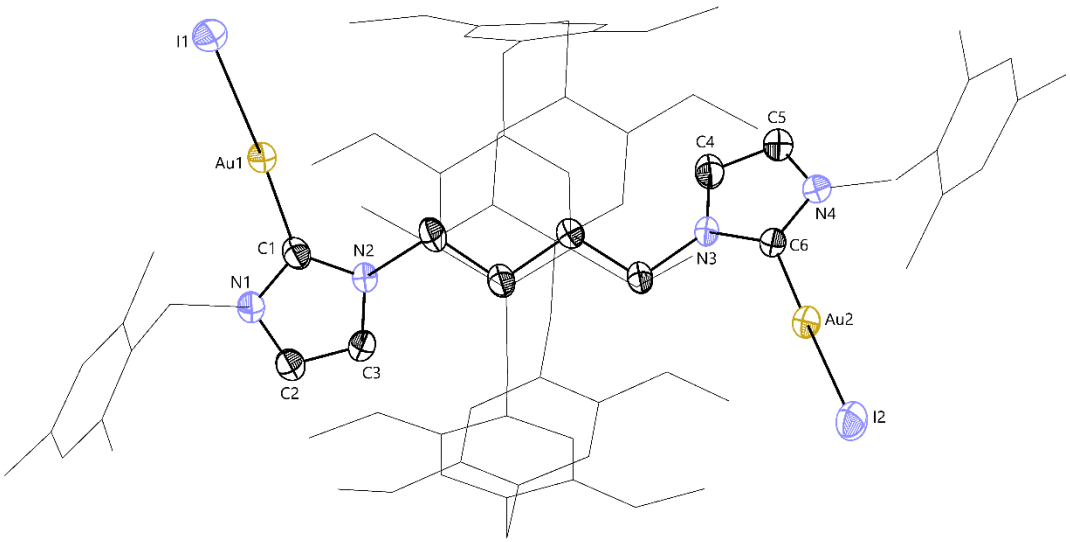

Figure 5.2. SC-XRD structure of the dinuclear gold(I) chloride [2]rotaxane **16**. Anisotropic displacement ellipsoids depicted at 50% probability. Hydrogen atoms, disorder components, and co-crystallised solvent molecules are omitted for clarity. Mes substituents and **P5A^{Me}** are depicted as wireframes for clarity.

The distances between the benzene planes and opposing methylene linkers on the **P5A^{Me}** macrocycle range from 8.922–9.269 Å, with an average cavity size of 9.071 Å, similar to [2]rotaxane **8a** discussed in Chapter 3 (9.046 Å). The C1–Au1 and C6–Au2 bond lengths are similar at 2.017(5) Å and 2.002(5) Å, respectively, as are the Au1–I1 and Au2–I2 bond lengths at 2.5651(5) Å and 2.5551(6) Å, respectively. The C1–Au1–I1 and C6–Au2–I2 bond angles are 178.5(2)° and 175.6(2)°, bent slightly from linearity in order to accommodate the **P5A^{Me}** macrocycle.

The HR-ESI-MS of solutions of **16** contained peaks for a [**16**+H]$^+$ adduct (*m*/*z* = 1853.3929; theoretical 1853.3994).

We also attempted to synthesise the corresponding dinuclear gold(I) iodide complexes of the non-interlocked axle (**Scheme 5.4**). Unfortunately, these were unsuccessful, despite attempting a variety of methods (e.g. strong-base route, transmetallation, or weak-base route) due to the poor solubility of the non-interlocked bis-imdiazolium salt. This highlights another significant advantage of using the **P5A^{Me}** [2]rotaxanes, in that the solubility is drastically improved, enabling further functionalisation.

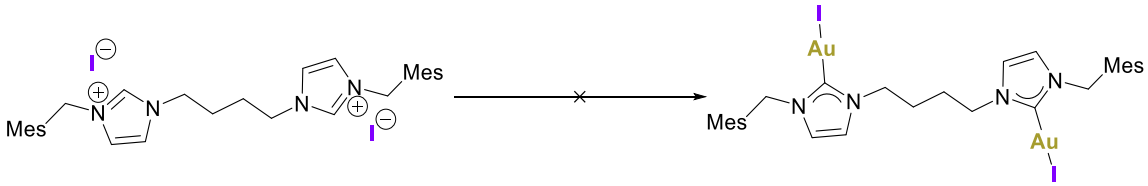

Scheme 5.4. Unsuccessful synthesis of the dinuclear gold(I) iodide complex of the non-interlocked axle.

We then turned our attention to targeting the pure dinuclear gold(I) chloride [2]rotaxane as an alternative starting material to avoid iodide salts in the hope for a cleaner reaction and improved yields. As we aim to use the dinuclear gold(I) halide [2]rotaxane as a precursor, it was important to maximise yields in every step. Anion exchange of the imidazolium iodide [2]rotaxane was achieved by stirring a chloroform/methanol (9:1 v/v) solution with Amberlite^{TM} IRA-402(Cl^-) ion exchange resin for 3 days. The resin was separated by filtration and washed thoroughly with DCM, after which the solvent was removed *in vacuo*, affording the imidazolium chloride [2]rotaxane **17** in near quantitative yield of 97% (**Scheme 5.5**).

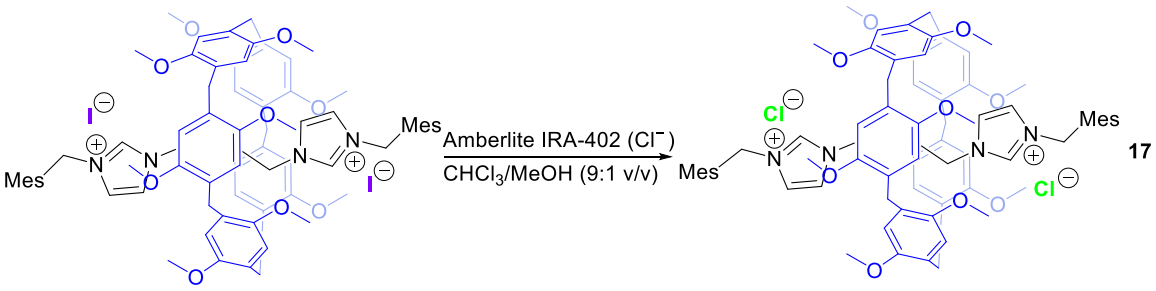

Scheme 5.5. Synthesis of the chloride salt of the bis-imidazolium rotaxane **17**.

Whilst the major features of the ^{1}H NMR spectrum of **17** appear identical to the iodide analogue, significant downfield shifts were observed for the imidazolium proton environments (H_e and H_d in **Figure 5.3**). This is due to the poorer shielding effect of the smaller chloride anion and suggests significant hydrogen bond association between the chloride anions and imidazolium protons in $CDCl_3$.

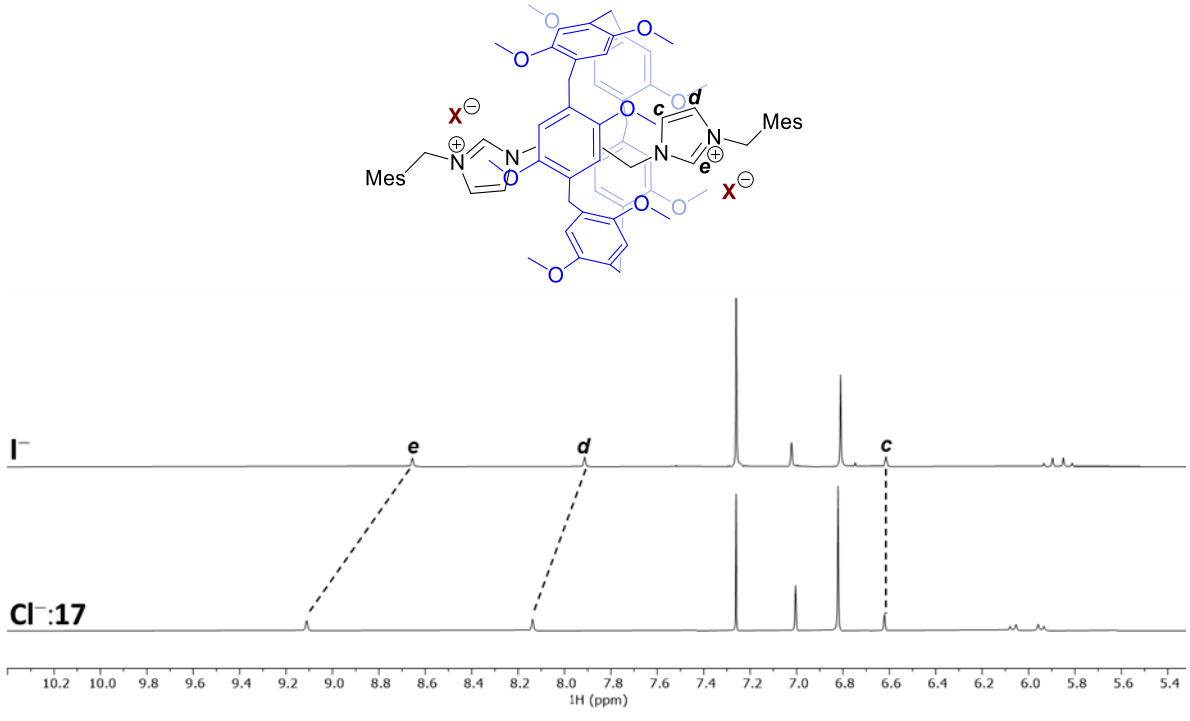

Figure 5.3. Stacked ^{1}H NMR spectra of the imidazolium [2]rotaxane iodide and chloride salts.

Using the strong-base route as mentioned previously, the dinuclear gold(I) chloride [2]rotaxane **18** was isolated as a single product following work up in much improved yields of 77% (**Scheme 5.6**).

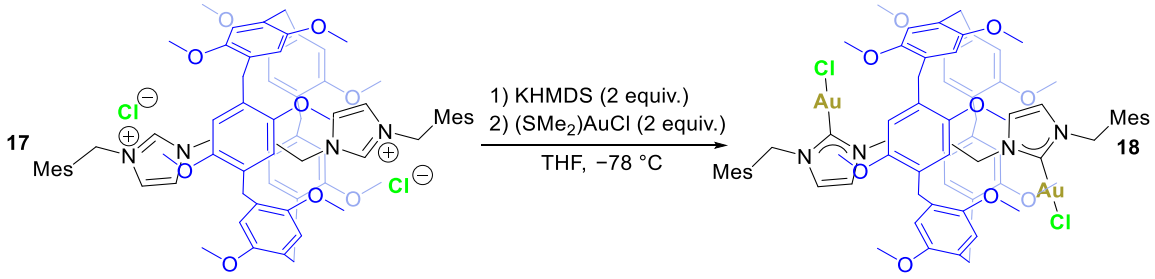

Scheme 5.6. Synthesis of the dinuclear gold(I) chloride [2]rotaxane **18**.

In this case, using the chloride imidazolium salt **17** as a starting material circumvents any unwanted halide scrambling, as only chloride is present in both the imidazolium [2]rotaxane and $(SMe_2)AuCl$. It also avoids the use of KI or KCl, which are difficult to remove and have a detrimental effect on the cyaphide transfer reaction (Section 5.2.3)

The ^{1}H and $^{13}C\{^{1}H\}$ NMR spectra of **18** show very subtle differences in comparison to **16**. The imidazole ^{1}H NMR resonances were observed as doublets at 6.40 ppm and 6.02 ppm, a result of mutual coupling ($^{3}J_{H-H} = 1.9$ Hz). The carbene carbon $^{13}C\{^{1}H\}$ NMR resonance is a singlet at 170.0 ppm, shifted slightly upfield in comparison to **16** (179.9 ppm), as a result of increased shielding at the carbene carbon due to the reduced *trans*-influence of the chloride ligand.[5] SC-XRD confirmed the identity of **18** as the dinuclear gold(I) chloride [2]rotaxane (**Figure 5.4**).

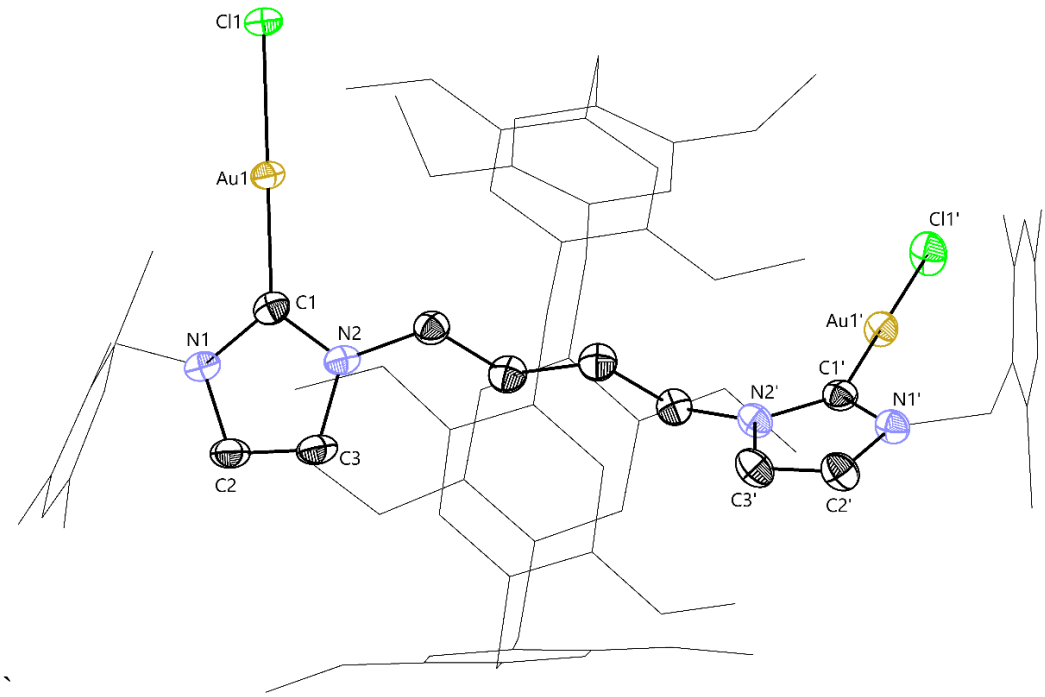

Figure 5.4. SC-XRD structure of the dinuclear gold(I) chloride [2]rotaxane **18**. Anisotropic displacement ellipsoids depicted at 50% probability. Hydrogen atoms, disorder components, and co-crystallised solvent molecules are omitted for clarity. Mes substituents and **P5A^{Me}** are depicted as wireframes for clarity.

18 displays similar bond metrics to **16**, with slightly shorter C1–Au1 and C1′–Au1′ bond lengths of 1.982(2) Å, consistent with stronger bonds, a result of the reduced *trans*-influence of the chloride. The Au1–Cl1 and Au1′–Cl1′ bond lengths are 2.2852(7) Å and the C1–Au1–Cl1 and C1′–Au1′–Cl1′ bond angles approach linearity at 179.68(7)° due to the smaller size of the chlorine atom.

The HR-ESI-MS contained a mass envelope corresponding to [**18**−2Cl$^-$]$^{2+}$ (*m*/*z* = 799.2867; theoretical 799.2910).

5.2.3 Synthesis of a dinuclear gold(I) bis-cyaphide [2]rotaxane

Immediately after the isolation of **16**, we attempted cyaphide transfer with the [Mg(CP)]$_2$ reagent (**Scheme 5.7**). Following the addition of one equivalent of [Mg(CP)]$_2$ to a DCM/diox.

solution of **16**, a single peak was observed in the $^{31}P\{^{1}H\}$ spectrum at 83.1 ppm, the expected region of a gold(I) cyaphide species.

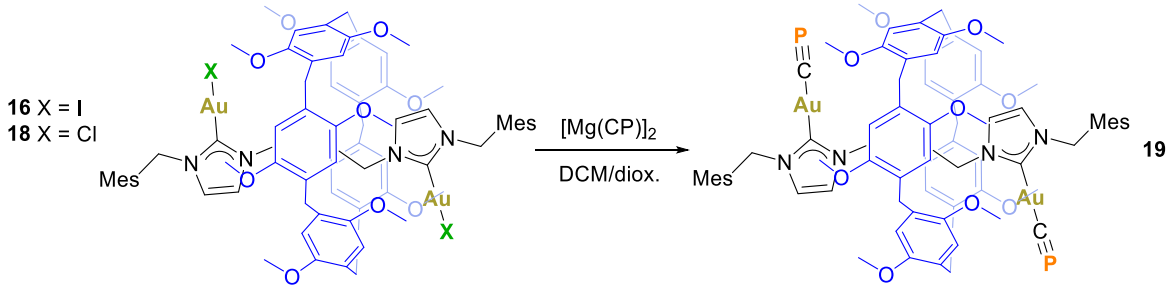

Scheme 5.7. Synthesis of a dinuclear gold(I) bis-cyaphide [2]rotaxane **19**.

Upon standing, crystals suitable for SC-XRD were obtained, which confirmed the formation of a dinuclear gold(I) bis-cyaphide [2]rotaxane **19** following ligand-exchange at each gold(I) centre (**Figure 5.5**).

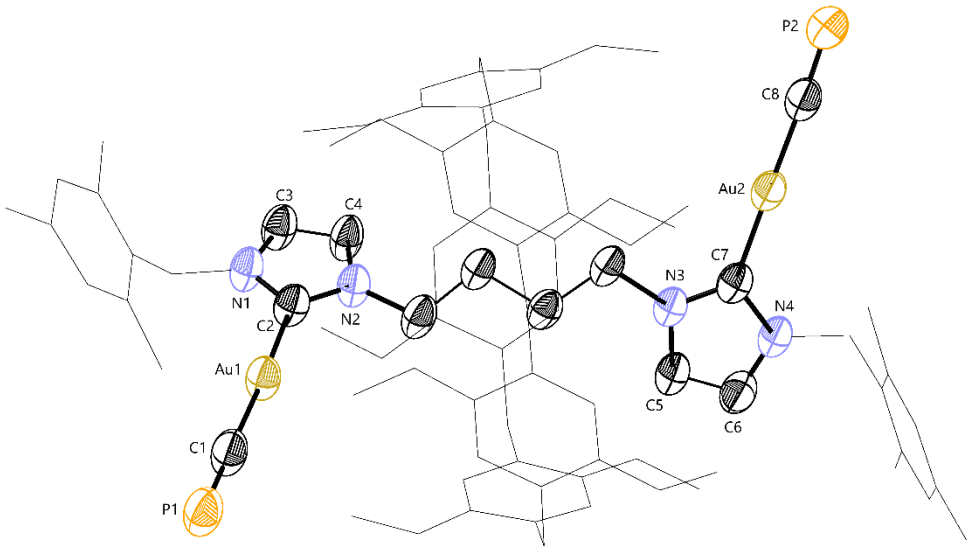

Figure 5.5. SC-XRD structure of the dinuclear gold(I) bis-cyaphide [2]rotaxane **19**. Anisotropic displacement ellipsoids depicted at 50% probability. Hydrogen atoms, disorder components, and co-crystallised solvent molecules are omitted for clarity. Mes substituents and **P5A^{Me}** are depicted as wireframes for clarity.

The NHC–Au–C≡P unit in **19** possesses similar bond metrics to the (IDipp)Au(CP) complex. The C2–Au1 and C7–Au2 bond lengths are 2.013(5) Å and 2.028(6) Å, respectively, and the Au1–C1 and Au2–C8 bond lengths are 1.991(5) Å and 1.994(8) Å, respectively. The C1–P1 and C8–P2 bond lengths are 1.530(6) Å and 1.517(8) Å, respectively. The corresponding bond lengths in (IDipp)Au(CP) are 2.034(6) Å, 1.972(6) Å, and 1.552(6) Å, respectively. This is indicates strong Au–CP bonds, consistent with a high degree of covalency as in the (IDipp)Au(CP) complex. There is a minor difference in that the C7–Au2–C8 and Au2–C8–P2 bond angles distort slightly from linearity to 174.9(2)° and 176.5(5)°, respectively, to accommodate the **P5A^{Me}** macrocycle.

The HR-ESI-MS of solutions of **19** contained peaks for a [**19**+Na]$^+$ adduct (*m*/*z* = 1707.5157; theoretical 1707.5199).

Despite many attempts to purify **19** through washing and recrystallisations, there were always other peaks present in the imidazolium region of the ^{1}H NMR spectrum. It should be noted that purification by column chromatography was not possible due to the air and moisture sensitivity of **19**. Although we could not identify the exact nature of these impurities, they were attributed to the presence of small amounts of nucleophilic iodide in the reaction mixture, which can undergo unwanted side reactions. The crude yield of **19** from cyaphide transfer at **16** was ca. 38%.

To target pure **19**, [2]rotaxane **18** was used instead as a starting material to avoid the presence of iodide. Inspection of the crude ^{1}H NMR spectrum following the addition of one equivalent of [Mg(CP)]$_2$ suggested the cyaphide transfer proceeded cleanly. Recrystallisation by layering a concentrated toluene solution of **19** with hexane, and storing at −30 °C allowed removal of the cyaphide transfer byproduct {(^{Dipp}NacNac)MgCl}$_2$ and isolation of **19** in excellent yields (91%) (**Scheme 5.7**). In order to use **19** as a starting point for the formation of a [2]catenane,

it needs to be made on a reasonable scale due to the typical poor yields of catenation reactions. Through optimisation of reaction conditions, **19** could be obtained on approx. 100 mg scale.

The ^{1}H NMR spectrum contained two doublets arising from the imidazolium protons at 6.40 ppm and 6.13 ppm with mutual coupling ($^{3}J_{H–H}$ = 1.9 Hz). Unusually, the typical diastereotopic splitting of the methylene protons between the NHC units and Mes stoppers was not observed. This had been attributed to steric hindrance in the previously reported metalated [2]rotaxanes, preventing the **P5A^{Me}** macrocycle from being sufficiently close for the transfer of chiral information.[3] The rationale of this anomaly is currently unclear, as the ^{1}H NMR of [2]rotaxanes with larger gold(I) moieties displays diastereotopic splitting (*vide infra*). The ^{13}C{^{1}H} NMR spectrum of **19** exhibits resonances for the cyaphide and carbene carbons at 250.8 ppm and 185.6 ppm, although these were broadened and C–P coupling could not be resolved. These are similar to the same resonances in the (IDipp)Au(CP) complex and the similar but non-interlocked complex **[14]** (see Section 4.3.2).

The similar spectroscopic profile of **19** with the (IDipp)Au(CP) complex and **[14]**, coupled with the SC-XRD data, suggests that the gold(I) centres are capable of forming strong covalent bonds with the cyaphide units. However, **19** is stable indefinitely under an inert atmosphere, whereas the similar non-interlocked complex **[14]** decomposes in a few days (Section 4.3.2). This highlights the importance of the **P5A^{Me}** macrocycle in stabilising the dinuclear gold(I) bis-cyaphide complex. The **P5A^{Me}** macrocycle offers significant steric stabilisation, which prevents the intermolecular close contact of the cyaphide moieties in molecules of **19**. The stabilisation may also be attributed to the prevention of intramolecular coupling reactions, as the two cyaphide moieties cannot come into contact due to the presence of the **P5A^{Me}** macrocycle. It is worth mentioning again that the **P5A^{Me}** also provides an advantage in improving the solubility in many common solvents (THF, toluene, benzene, DCM, Et_2O).

5.3 Functionalisation of a bis-cyaphide [2]rotaxane

The unique topology of the mechanical bond offers distinct advantages to MIMs, such as enhanced stability and solubility. There is also the potential to explore more sophisticated systems, such as molecular machines, where the molecular motion between the components can be controlled by a stimulus. As discussed in Chapter 1, the synthesis of MIMs in appreciable yields is challenging, limiting the scope of the molecular components to specific types capable of templation. It is therefore appealing to generate the mechanical bond in an earlier step from simple components, before using the resulting MIM as an interlocked building block towards functional materials, thereby transferring the inherent benefits of the mechanical bond.[6]

5.3.1 1,3-Dipolar cycloaddition reactions with simple azides

Having isolated **19**, which possesses two gold-cyaphide moieties, there is an opportunity to functionalise it through the 1,3-dipolar cycloaddition reaction with azides. We therefore investigated whether the cyaphide groups of **19** can undergo 1,3-dipolar cycloaddition chemistry with azides, despite the potential steric hindrance imparted by the **P5A^{Me}** macrocycle. We chose two simple azides, a simple small aliphatic azide (^{t}Bu–N$_3$) and a larger aromatic azide (Dipp–N$_3$). Gratifyingly, the addition of two equivalents of ^{t}Bu–N$_3$ or Dipp–N$_3$ to **19** resulted in the formation of the dinuclear gold(I) bis-triazaphosphole [2]rotaxanes [R = ^{t}Bu (**20a**), R = Dipp (**20b**); **Scheme 5.8**].

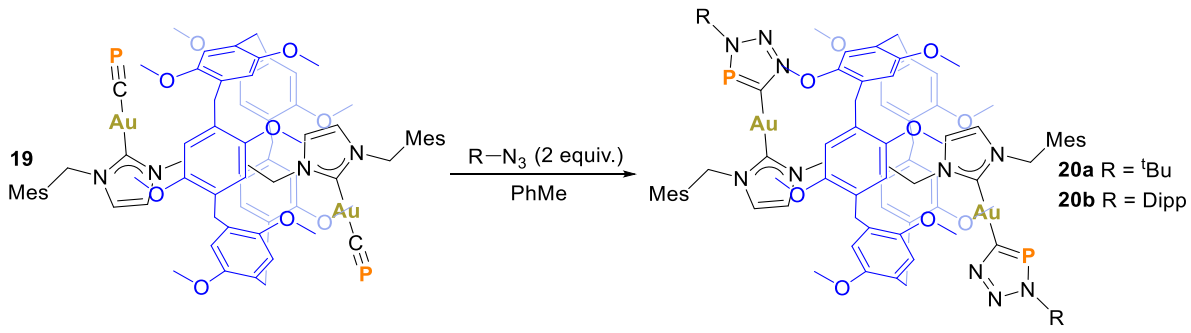

Scheme 5.8. Synthesis of the dinuclear gold(I) bis-triazaphosphole [2]rotaxanes **20a** and **20b**.

This was evidenced by the appearance of a single peak in their $^{31}P\{^{1}H\}$ NMR spectra, suggesting the reaction successfully occurs at both gold(I) centres. These peaks correspond to the newly formed triazaphosphole phosphorus atoms with chemical shifts at 192.7 ppm (**20a**) and 211.7 ppm (**20b**), similar to the cycloaddition products of the azides with (IDipp)Au(CP) (191.2 ppm and 209.3 ppm for **1a** and **1c**, respectively).

Unfortunately, we were unable to isolate crystals suitable for SC-XRD as removal of the solvent under vacuum resulted in oils in both cases. However, following washing with diethyl ether, the cycloaddition products **20a** and **20b** were obtained cleanly and fully characterised by NMR spectroscopy and HR-ESI-MS.

The triazaphosphole carbon atoms could be identified as doublets in their $^{13}C\{^{1}H\}$ NMR spectra at 209.4 ppm (**20a**: $^{1}J_{C–P}$ = 83.9 Hz) and 212.0 ppm (**20b**: $^{1}J_{C–P}$ = 84.2 Hz). Similarly, doublet resonances for the carbene carbon atoms were present at 185.6 ppm (**20a**: $^{3}J_{C–P}$ = 11.5 Hz) and 190.5 ppm (**20b**: $^{3}J_{C–P}$ = 10.6 Hz). Their ^{1}H NMR spectra were consistent with a fully symmetric structure as a result of cycloaddition reaction at both cyaphide moieties. For **20a**, the ^{1}H NMR spectrum features a singlet at 1.70 ppm with a relative integral consistent with two ^{t}Bu groups (18H). The ^{1}H NMR spectrum of **20b** also reveals 1,3-dipolar cycloaddition reactivity at each gold(I) cyaphide. The Dipp ^{i}Pr proton resonances are split into two septets at 2.66 ppm and 2.63 ppm, corresponding to two environments of the isopropyl

methine protons. This is presumably a consequence of restricted rotation about the C–N bond due to the presence of the **P5A^{Me}** macrocycle, resulting in chemically inequivalent environments.

The HR-ESI-MS confirmed the presence of **20a** (*m*/*z* = 1883.6901; theoretical 1883.6973) and **20b** (*m*/*z* = 2091.8154; theoretical 2091.8225) as the $[M+H]^+$ species.

The successful formation of **20a** and **20b** confirms that **19** is capable of undergoing cyaphide-azide 1,3-dipolar cycloaddition reactivity at both gold(I) cyaphide moieties, with both aliphatic and aromatic azides. Even with the bulkier Dipp–N_3, the reaction proceeds rapidly and straightforwardly, proving that the **P5A^{Me}** macrocycle does not sterically inhibit this type of reactivity.

5.3.2 Synthesis of a singlet oxygen photosensitizer

The generation of highly reactive singlet oxygen ($^1O_2$) through photosensitization has found a wide range of applications in photodynamic therapy, photocatalysis, and the destruction of environmental contaminants.[7] In these processes, the generation of $^1O_2$ is mediated by energy transfer from the relaxation of long-lived triplet excited states, which themselves are generated by intersystem crossing (ISC), following photoexcitation of the photosensitizer (**Scheme 5.9**).

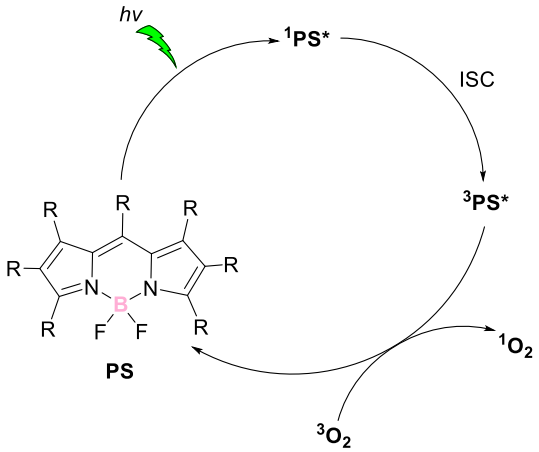

Scheme 5.9. General mechanism of $^1O_2$ generation by a BODIPY photosensitizer (PS).

Photosensitizers based on boron-dipyrromethene (BODIPY) dyes are becoming increasingly popular due to their high extinction coefficients, resistance to photobleaching, and synthetic modularity.[8] It is important to note that the unmodified BODIPY (tetramethyl-BODIPY) is photoinactive for $^1O_2$ generation, and modifications are required to produce efficient photosensitizers.[8] A well-known strategy is the introduction of heavy atoms, often achieved through halogenation or metal coordination to the BODIPY core. The introduction of gold(I) to generate highly efficient photosensitizers is becoming increasingly popular.[9] The heavy atoms enhance spin-orbit coupling (SOC), which in turn improves the efficiency of ISC and therefore increases the population of the excited triplet state, resulting in increased $^1O_2$ generation.

More recently, there has been increased activity in the synthesis of gold(I)-BODIPY photosensitizers, examples of which are provided below (**Figure 5.6**).[10,11] Due to the limited number of isolated species, the photophysical properties of gold(I) complexes remain poorly understood. Generally, close proximity of the gold(I) centre to the BODIPY fragment results in higher $^1O_2$ generation. However, this is not always the case, for example, in a complex in which the gold(I) centre is attached directly to the BODIPY backbone *via* a phosphine (**Figure 5.6, bottom left**), the $^1O_2$ quantum yield ($\Phi_{s.o}$) was found to be exceptionally low. The authors attributed this to a deactivation pathway *via* photoinduced electron transfer from the BODIPY excited state to the gold(I), followed by a non-radiative recombination of the charges.[11]

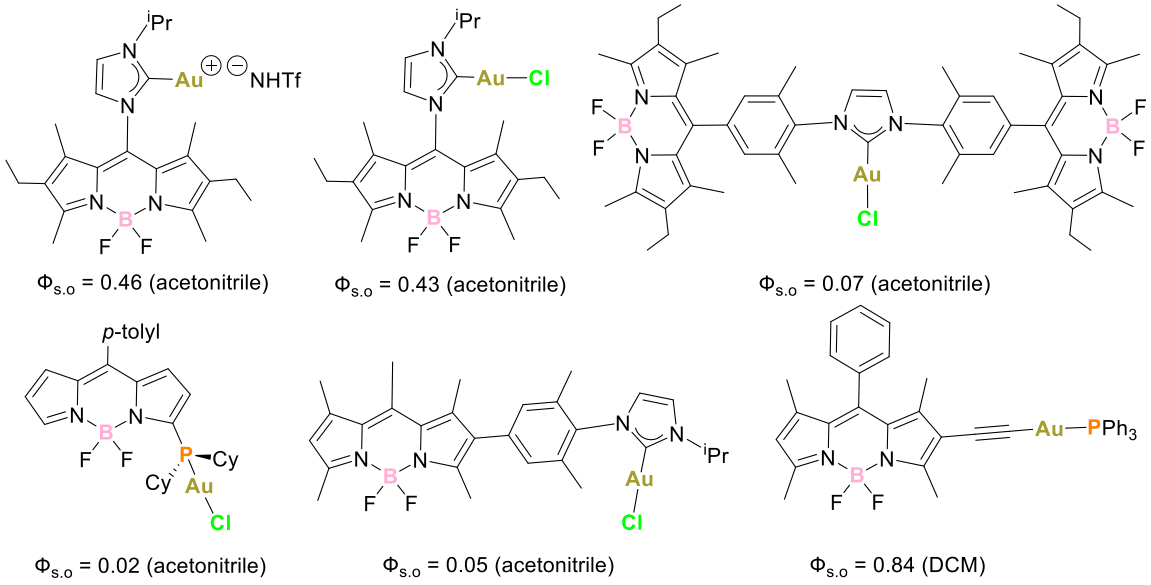

Figure 5.6. Literature examples of gold(I)-BODIPY photosensitizers their $^1O_2$ quantum yields ($\Phi_{s.o}$).

The Beer group have recently demonstrated that $^1O_2$ generation by aza-BODIPY compounds can be modulated through anion binding at halogen-bonding recognition sites (**Figure 5.7**).[12] The presence of chloride decreased the $\Phi_{s.o}$ by 37%, attributed to an increased rate of non-radiative decay processes. These processes compete with ISC, decreasing the population of the triplet excited state, necessary for $^1O_2$ generation.

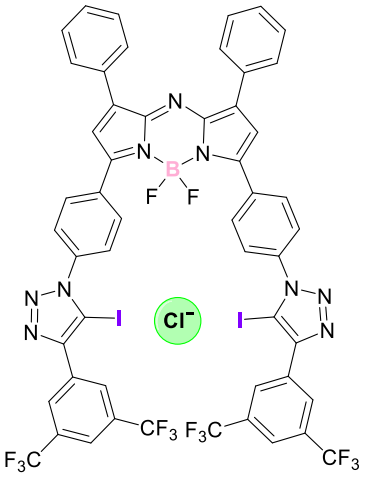

Figure 5.7. A halogen bonding aza-BODIPY photosensitizer.

The isolation of **19** presented an opportunity to install BODIPY units and synthesise a new gold(I)-BODIPY [2]rotaxane photosensitizer. We anticipated that the introduction of heavy gold(I) atoms would improve $^1O_2$ generation and were also interested in the potential of modulating it through anion binding. The benefits of the mechanical bond in **19** have already been inferred, in that the stability and solubility over non-interlocked analogues are drastically improved. Furthermore, the gold(I) cyaphide moieties open up the [2]rotaxane **19** to post-synthetic functionalisation through the efficient cyaphide-azide 1,3-dipolar cycloaddition reaction. It should also be noted that although the synthesis of **19** requires multiple steps, it can be prepared in high yields on a reasonable scale (approx. 100 mg).

Reaction of **19** with two equivalents of the iodo-triazole-BODIPY-azide[13] yielded the corresponding cycloaddition product, [2]rotaxane **21** as a bright red solid in very good yields of 80% (**Scheme 5.10**).

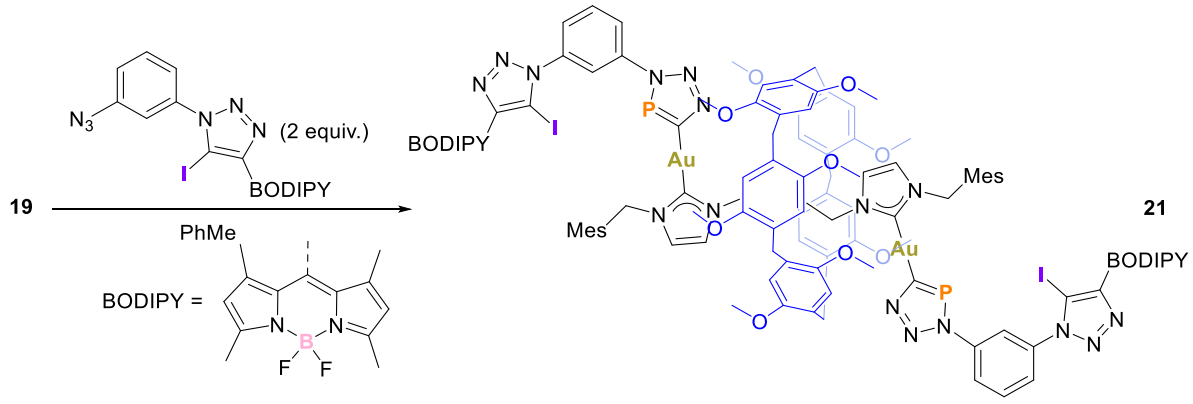

Scheme 5.10. Synthesis of a dinuclear gold(I)-BODIPY [2]rotaxane **21**.

The $^{31}P\{^1H\}$ NMR spectrum of **21** reveals a single resonance at 199.6 ppm. The ^1H and $^{13}C\{^1H\}$ NMR spectra are consistent with a fully symmetric structure, confirming functionalisation had successfully occurred at both gold(I) cyaphide units. The $^{13}C\{^1H\}$ NMR spectrum contained doublet peaks at 213.2 ($^1J_{C–P}$ = 85.4 Hz) and 189.6 ($^3J_{C–P}$ = 10.5 Hz) corresponding to the triazaphosphole carbon and carbene carbon atoms, respectively. The

$^{11}B\{^{1}H\}$ NMR spectrum contains a characteristic triplet at 1.35 ppm ($^{1}J_{B–F}$ = 32.6 Hz), while the $^{19}F\{^{1}H\}$ NMR spectrum revealed multiplets corresponding to the BODIPY groups. The HR-ESI-MS revealed peaks for a [**21**+H]$^{+}$ species (*m*/*z* = 2803.6926; theoretical 2803.7057). **21** displayed optical properties typical of BODIPY compounds (**Table 5.1**).

Table 5.1. Photophysical properties of **22** in DCM.

Compound	**[2]Rotaxane 21**
$\lambda_{max,abs}$ (nm)	516
ε (10^4 M^{-1} cm^{-1})	13.1
$\lambda_{max,em}$ (nm)	528
Stokes shift (nm)	12

We were interested in exploring the photosensitizing capability of **21** for generating $^{1}O_2$, and whether the presence of the heavy gold(I) atom enhances this phenomenon. As a comparison, we chose the previously reported BODIPY compound **A** (**Figure 5.8**),[13] where the gold-triazaphosphole [2]rotaxane unit is replaced by a phenyl-iodotriazole.

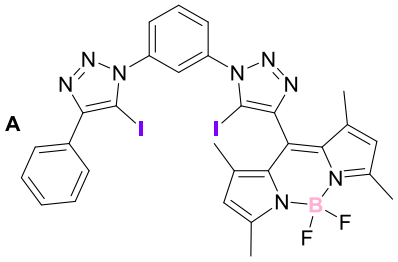

Figure 5.8. Compound **A**.

In a typical experiment, a DCM solution of the photosensitizers **21** or **A** in the presence of 1,3-diphenylisobenzofuran (DPBF), a $^{1}O_2$ quencher, is continuously irradiated close to the

absorption maxima of the photosensitizer (530 nm) for 10 minutes. The rate at which the DPBF absorbance maxima at 410 nm decreases is proportional to the $\Phi_{s.o}$.

Both **21** and **A** are capable of generating $^1O_2$, as shown by the decrease in the DPBF absorbance before and after 10 minutes of irradiation (**Figure 5.9**). It is quite clear that for **21**, the effect is much more significant. It should be noted that despite **21** containing an additional BODIPY to **A**, this was accounted for by altering the concentrations to ensure the concentration of BODIPY in the experiment was identical, as seen by the absorbance maxima at 516 nm. No changes in the BODIPY absorbance were observed during the experiment, demonstrating the photostability of **21** and **A**.

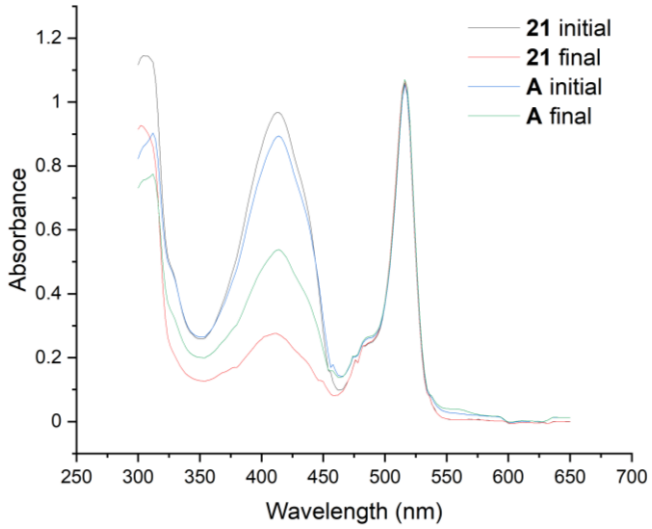

Figure 5.9. Absorbance spectrum of DCM solutions of **21** (5 μM) or **A** (16 μM) with DPBF (45 μM) before and after irradiation at 530 nm for 10 minutes.

The $\Phi_{s.o}$ for **21** and **A** can be compared by plotting the decrease in DPBF absorbance as a function of time (**Figure 5.10**). It can be clearly observed that replacing a phenyl-iodotriazole with a gold(I) triazaphosphole increases the $\Phi_{s.o}$ by 92%, consistent with a faster rate of decrease in DPBF concentration. It should also be noted that although the gold(I) centre is not in close proximity to the BODIPY core, its influence on $^1O_2$ generation is significant.

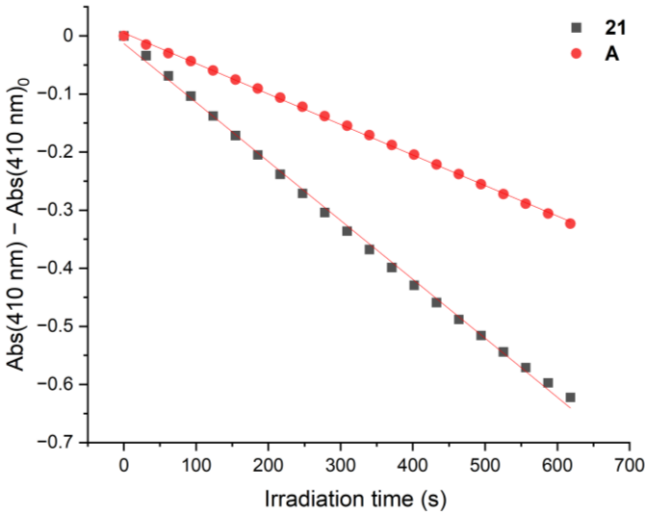

Figure 5.10. Kinetics plot of the decrease in DPBF absorbance against irradiation time for **21** and **A**.

Although **21** contains a triazaphosphole instead of the typical iodotriazole for halogen bonding, we were interested in the possibility of anion bonding within the cavity. This was probed by measuring the fluorescence emission spectrum following the gradual addition of aliquots of tetrabutylammonium chloride (TBACl) to a 1μM DCM solution of **21** (**Figure 5.11**). This induces a moderate fluorescence turn-on response, which was subsequently fitted to a 1:1 host–guest stoichiometric binding isotherm model to give an anion binding constant of K_a = 397 M^{-1}. This relatively modest binding constant is as expected due to the presence of only one iodotriazole and suggests the opposing triazaphosphole is not capable of anion binding. It also infers that the 1:2 binding constant is very weak and insignificant (K_a < 10 M^{-1}).

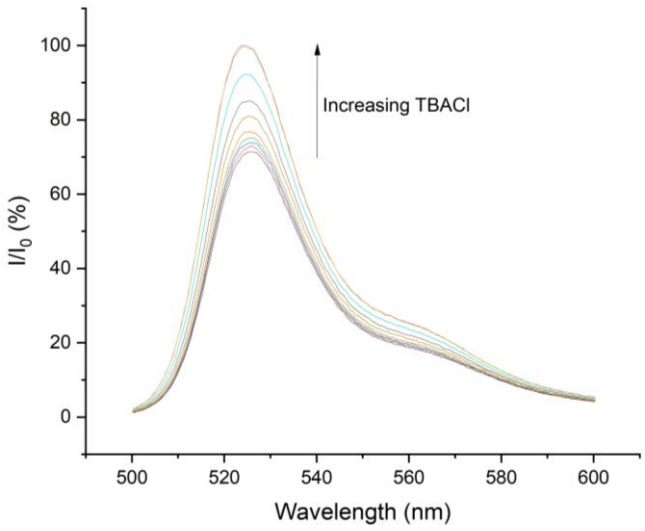

Figure 5.11. Normalised fluorescence emission response of **21** (1 μM) upon increasing additions of Cl^- (up to 5.7 mM) in DCM at 298 K.

By conducting a $^1O_2$ kinetics experiment analogous to those above in the presence of TBACl (2 mM), it can be seen that the $\Phi_{s.o}$ is not significantly influenced by the presence of chloride (**Figure 5.12**). This confirms that the chloride binding by a single iodotriazole is not strong enough to modulate $^1O_2$ generation.

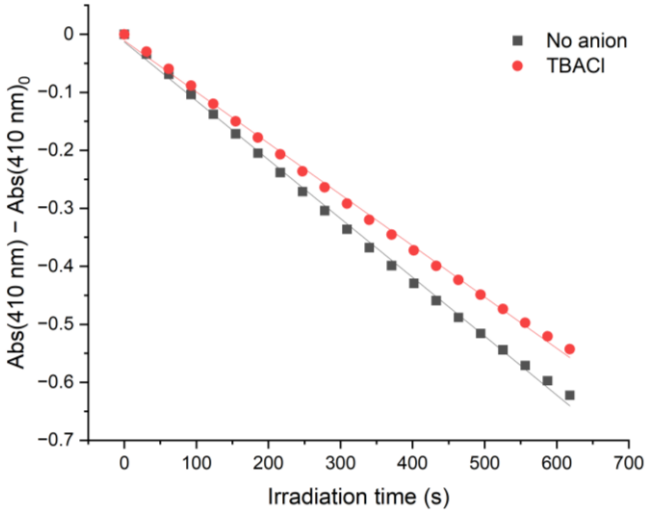

Figure 5.12. Kinetics plot of the decrease in DPBF absorbance against irradiation time for **21** in the presence and absence of TBACl.

5.3.3 Towards [*n*]catenanes: the 1,3-dipolar cycloaddition reactions with a bis-azide

Following the results obtained in Chapters 2 and 3, a principal aim of this project was to prepare a [*n*]catenane *via* the cyaphide-azide 1,3-dipolar cycloaddition reaction. Up until this point, it had proved to be difficult due to the instability of the targeted bis-cyaphide species. With **19** in hand, we have isolated a stable bis-cyaphide species that retains its 1,3-dipolar cycloaddition reactivity with azides. This gave us the opportunity to expand this reactivity to bis-azides, in order to transform [2]rotaxane **19** into an [*n*]catenane. The reaction between **19** and a long chain azide in a 1:1 stoichiometry would generate a [2]catenane, whilst increasing the stoichiometry (*n*:*n*) could generate higher order [*n*+1]catenanes.

Initially, it was anticipated that the easiest target would be a [2]catenane. This would require a long chain bis-azide with sufficient degrees of freedom that it can react at both cyaphide moieties by surpassing the steric bulk of the **P5A^{Me}** macrocycle. With this in mind, we chose a pyridyl-functionalised bis-azide we already had in hand.[14] As discussed in Section 4.1, templating strategies and high-dilution conditions have been used to pre-organise the molecular components and minimise the local concentrations of molecules to favour the final intramolecular macrocyclization reaction to form the [*n*]catenane. During initial attempts of [2]catenane synthesis, high dilution conditions were employed (5 mM), requiring dropwise addition of reagents, and sodium tetrakis[3,5-bis(trifluoromethyl)phenyl]borate (NaBAr^F) as a templating agent.[15–18] Despite many iterations on different conditions, there was no evidence for the formation of a [2]catenane. The resulting $^{31}P\{^1H\}$ NMR spectra contained many peaks in the triazaphosphole region, and TLC analysis also revealed the presence of multiple species.

We attributed this lack of success to the rapid nature of the cyaphide-azide 1,3-dipolar cycloaddition reaction. This favours oligomerization reactions before the second azide group is in the correct orientation for macrocyclization to occur and yield the [2]catenane. In order to control this reactivity, the catenation reaction was also attempted *via* the slow syringe-pump

dropwise addition (3 mL/h) of the bis-azide (3 mM) to a DCM solution of **19** (0.5 mM) at −15 °C (**Scheme 5.11**). In this case, $NaBAr^F$ was omitted for simplicity.

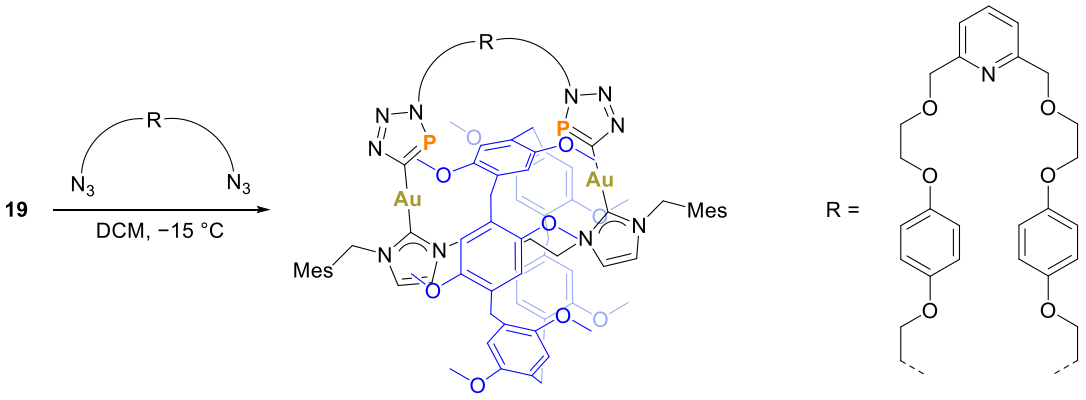

Scheme 5.11. Attempted catenation reaction of **19** with a long chain bis azide.

The $^{31}P\{^1H\}$ NMR spectrum of the crude reaction mixture was much cleaner, displaying a sharp peak at 207.1 ppm as and a multitude of peaks at approximately 206.6 ppm (**Figure 5.13**).

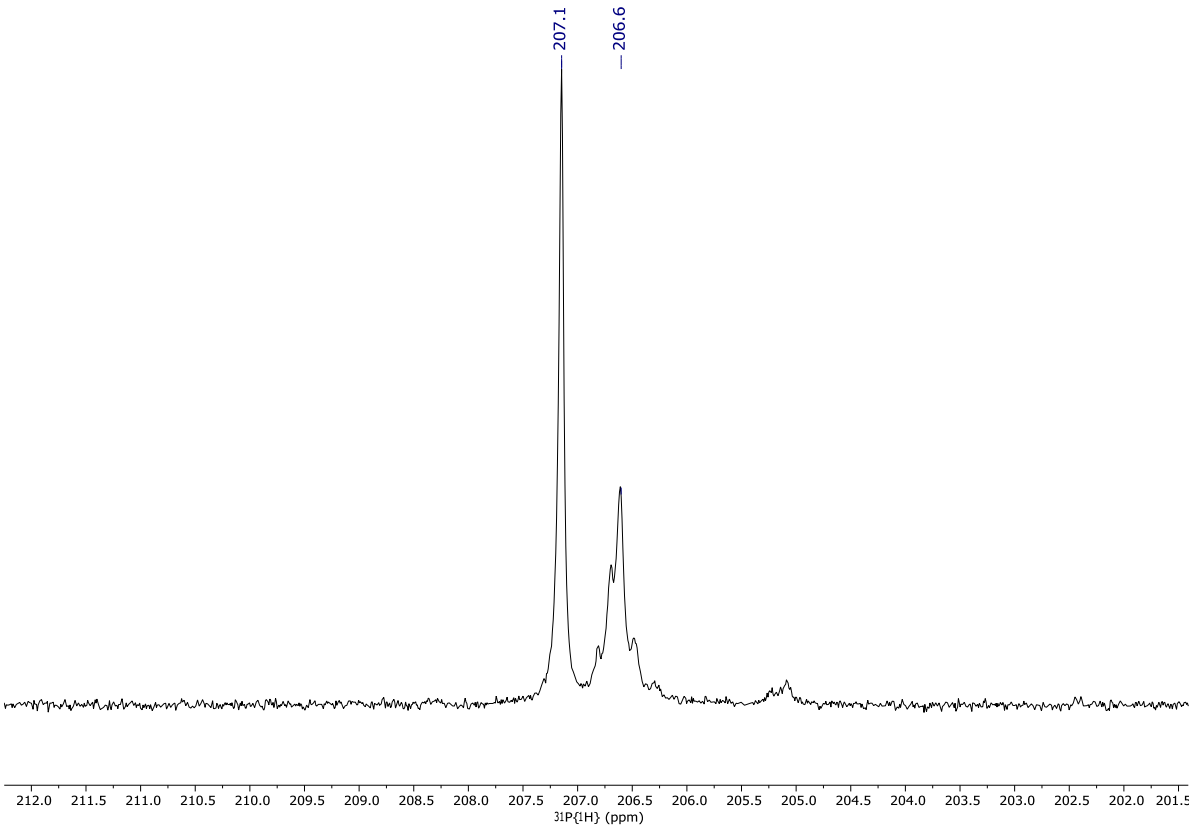

Figure 5.13. $^{31}P\{^1H\}$ NMR spectrum of the crude reaction mixture represented in Scheme 5.11.

These are in the region expected for the triazaphospholes, most likely [*n*]catenanes and short chain oligomers. TLC analysis revealed multiple species were still present in the reaction mixture. The HR-ESI-MS of the reaction mixture (**Figure 5.14**) revealed that [2]catenane had successfully formed with a peak corresponding to the $[M+H]^+$ species (*m*/*z* = 2234.7663; theoretical 2234.7716).

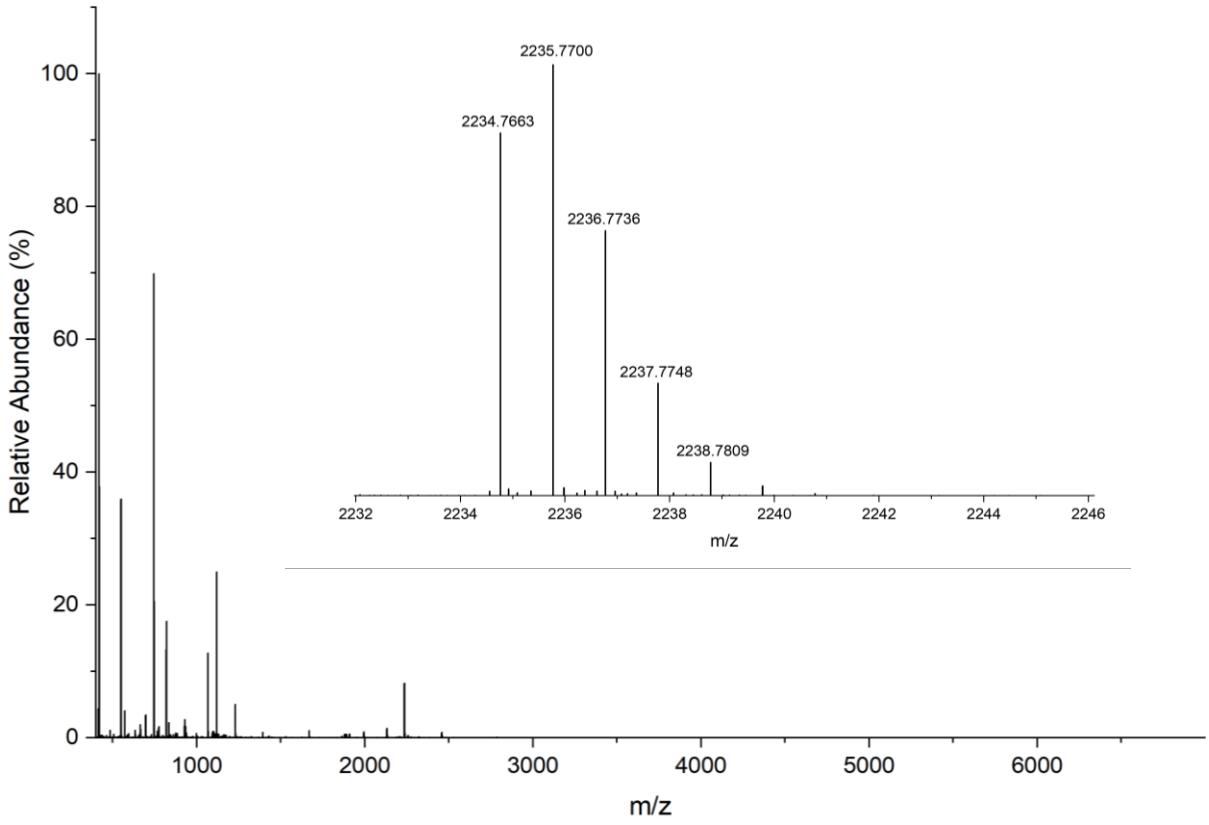

Figure 5.14. HR-ESI-MS of the reaction mixture of Scheme 5.11.

So far, the presence of a peak in the HR-ESI-MS is the best evidence we have for the successful formation of the [2]catenane. Attempts were made to obtain SC-XRD quality crystals of the [2]catenane, but these have ultimately been unsuccessful thus far. It is likely the [2]catenane is formed in poor yields due to the rapid nature of the cyaphide-azide 1,3-dipolar cycloaddition reaction, and instead the formation of oligomers is favoured. At this point, it should be noted that the cycloaddition products of **19** (**20a**, **20b**, and the catenation products) are unstable to chromatographic methods, preventing their facile purification.

5.4 Conclusions

A bis-imidazolium [2]rotaxane can be used to coordinate two gold(I) halide moieties through the formation of metal–carbene bonds. Whilst both are capable of undergoing cyaphide transfer to yield a dinuclear gold(I) bis-cyaphide [2]rotaxane, the gold(I) chloride variant yields the bis-cyaphide product in higher yields and purity. The resulting bis-cyaphide [2]rotaxane is stable indefinitely under an inert atmosphere in contrast to the similar non-interlocked products discussed in Chapter 4. The mechanical bond provides effective stabilisation to the bis-cyaphide species, presumably by increasing steric protection and preventing intramolecular decomposition pathways. It also improves solubility in many common solvents, allowing further functionalisation.

The gold(I)-cyaphide moieties in the [2]rotaxane remain reactive in the cyaphide-azide 1,3-dipolar cycloaddition reaction, allowing further post-synthetic functionalisation. This method can be used to install BODIPY dyes, producing an effective gold(I)-BODIPY photosensitizer for $^{1}O_2$ generation.

The conversion of the bis-cyaphide [2]rotaxane into a [2]catenane by its reaction with a bis-azide remains challenging due to the rapid nature of the cycloaddition reaction, leading to a multitude of products. High dilution, slow addition of reagents, and low temperature conditions can be used to produce the [2]catenane, as evidenced by HR-ESI-MS studies. Isolation of the [2]catenane by chromatographic purification is difficult due to its air sensitivity, as well as the small scale and low yields of the reaction.

The work in section 5.3.2 was completed in collaboration with Dr. Andrew Taylor.

5.5 Experimental

5.5.1 Synthesis of 16

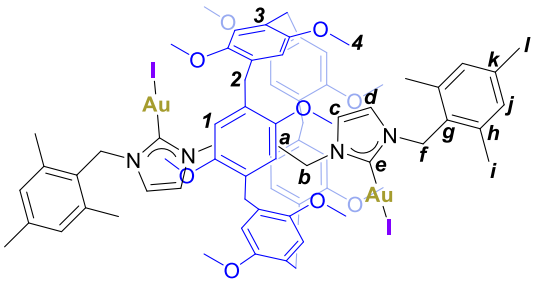

KHMDS (119 mg, 0.595 mmol, 2.2 equiv.) was dissolved in toluene (1 mL) and added dropwise to a suspension of the bis-imidazolium iodide [2]rotaxane (396 mg, 0.270 mmol) and KI (224 mg, 1.35 mmol, 5 equiv.) in THF (10 mL) at −78 °C. After stirring at this temperature for 1 h, the solution was added dropwise to a stirred suspension of $(SMe_2)AuCl$ (175 mg, 0.595 mmol, 2.2 equiv.) in THF (5 mL) at −78 °C. The solution was stirred in the dark for 24 h, and then the solvent was removed *in vacuo*. The residue was dissolved in DCM

(25 mL) and stirred aqueous $Na_2S_2O_8$ (10wt%, 50 mL) for 1 h. The product was extracted with DCM (3 × 10 mL) and washed with water (2 × 20 mL), then dried over $MgSO_4$. The crude product was purified on a silica gel column using DCM to afford **16** as a white powder. Yield: 180 mg, 0.097 mmol, 36% yield.

^{1}H NMR (600 MHz, $CDCl_3$): δ (ppm) = 6.99 (s, 4H; H_j), 6.88 (s, 10H; H_1), 6.42 (d, $^3J_{H–H}$ = 1.9 Hz, 2H; H_d), 5.89 (d, $^3J_{H–H}$ = 1.9 Hz, 2H; H_c), 5.54 (d, $^2J_{H–H}$ = 14.4 Hz, 2H; H_f), 5.48 (d, $^2J_{H–H}$ = 14.4 Hz, 2H; H_f), 3.74 (s, 10H; H_2), 3.56 (s, 30H; H_5), 2.41 (br, 2H; H_b), 2.38 (s, 12H; H_i), 2.36 (s, 6H; H_l), 2.28 (br, 2H; H_b), −1.39 (br, 4H; H_a).

^{13}C{^{1}H} NMR (151 MHz, $CDCl_3$): δ (ppm) = 179.7 (C_e), 151.2 (C_4), 139.3 (C_k), 137.9 (C_g), 129.9 (C_j), 129.6 (C_3), 127.9 (C_h), 121.0 (C_c), 117.0 (C_d), 115.7 (C_1), 57.8 (C_5), 49.1 (C_f), 49.0 (C_b), 29.3 (C_2), 22.6 (C_a), 21.3 (C_l), 20.2 (C_i).

HR-ESI-MS (+ve ion mode): m/z calcd. for $C_{75}H_{88}Au_2I_2N_4O_{10}+H^+$: 1853.3994 $[M+H]^+$; found 1853.3929.

5.5.2 Synthesis of 17

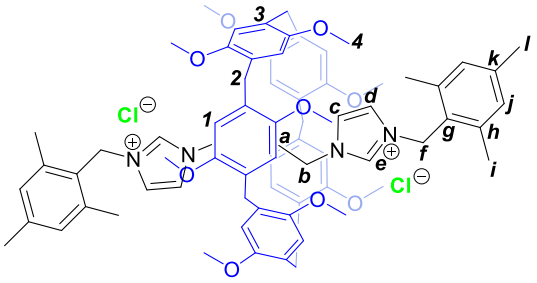

The bis-imidazolium iodide [2]rotaxane (380 mg, 0.256 mmol) and Amberlite^{TM} IRA-402($Cl^–$) ion exchange resin (3.5 g) were added to $CHCl_3$:MeOH (9:1, 30 mL) and stirred vigorously for 72 h. The resin was removed by filtration and washed with DCM (2 × 10 mL). The filtrate was collected and the solvent removed in vacuo to yield **17** as a pale-yellow solid. Yield: 323 mg, 0.252 mmol, 97%.

^{1}H NMR (600 MHz, CD_2Cl_2): δ (ppm) = 9.11 (2H; H_e), 8.14 (2H; H_d), 7.00 (4H; H_j), 6.82 (10H; H_1), 6.62 (2H; H_c), 6.07 (d, $^{2}J_{H–H}$ = 15.3 Hz, 2H; H_f), 5.95 (d, $^{2}J_{H–H}$ = 15.3 Hz, 2H; H_f), 3.70 (10H; H_2), 3.67 (30H; H_5), 2.42 (12H; H_i), 2.35 (6H; H_l), 1.78 (t, $^{3}J_{H–H}$ = 8.24 Hz, 4H; H_b), −1.11 (4H, m; H_a).

^{13}C{^{1}H} NMR (151 MHz, C_6D_6): δ (ppm) = 151.2 (C_4), 140.0 (C_k), 138.3 (C_h), 134.7 (C_e), 130.4 (C_3), 130.1 (C_j), 126.5 (C_g), 123.5 (C_d), 120.3 (C_c), 116.0 (C_1), 58.3 (C_5), 48.7 (C_f), 47.2 (C_b), 29.3 (C_2), 23.7 (C_a), 21.3 (C_l), 20.2 (C_i).

HR-ESI-MS (+ve ion mode): *m*/*z* calcd. for $C_{75}H_{90}N_4O_{10}^{2+}$: 603.3323 $[M]^{2+}$; found 603.3295.

5.5.3 Synthesis of 18

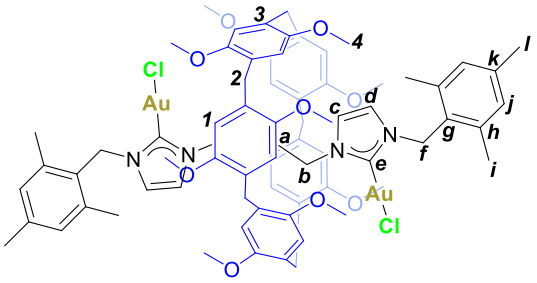

KHMDS (82 mg, 0.412 mmol, 2.2 equiv.) was dissolved in toluene (1 mL) and added dropwise to a suspension of **17** (240 mg, 0.187 mmol) in THF (10 mL) at −78 °C. After stirring at this temperature for 1 h, the solution was added dropwise to a stirred suspension of $(SMe_2)AuCl$ (121 mg, 0.412 mmol, 2.2 equiv.) in THF (5 mL) at −78 °C. The solution was stirred in the dark for 24 h, and then the solvent was removed *in vacuo*. The crude product was purified on a silica gel column using DCM:hex (9:1) to remove an impurity, then DCM:MeOH (9:1) to afford **18** as a white powder. Yield: 237 mg, 0.142 mmol, 76% yield.

^{1}H NMR (600 MHz, $CDCl_3$): δ (ppm) = 7.00 (4H; H_j), 6.90 (10H; H_1), 6.40 (d, $^{3}J_{H–H}$ = 1.9 Hz, 2H; H_d), 6.02 (d, $^{3}J_{H–H}$ = 1.9 Hz, 2H; H_c), 5.50 (d, $^{2}J_{H–H}$ = 14.4 Hz, 2H; H_f), 5.43 (d, $^{2}J_{H–H}$ = 14.4 Hz, 2H; H_f), 3.74 (10H; H_2), 3.57 (30H; H_5), 2.37 (12H; H_i), 2.36 (6H; H_l), 2.32 (4H, m; H_b), −1.40 (4H, m; H_a).

^{13}C{^{1}H} NMR (151 MHz, $CDCl_3$): δ (ppm) = 170.0 (C_e), 151.2 (H_4), 139.3 (C_k), 137.9 (C_h), 129.9 (C_j), 129.6 (H_3), 127.8 (C_g), 121.1 (C_c), 117.0 (C_d), 115.7 (C_1), 57.4 (C_5), 49.6 (C_f), 49.3 (C_b), 29.3 (C_2), 22.4 (C_a), 21.3 (C_l), 20.1 (C_i).

HR-ESI-MS (−ve ion mode): m/z calcd. for $C_{75}H_{88}Au_2N_4O_{10}$−2$Cl^-$: 799.2910 $[M−2Cl]^{2-}$; found 799.2867.

5.5.4 Synthesis of 19

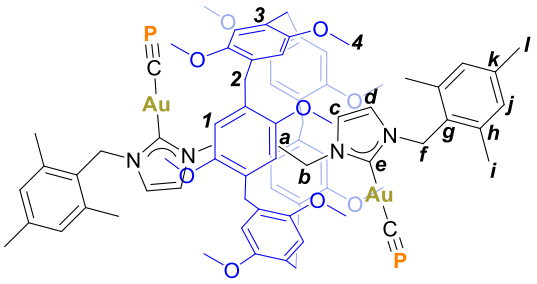

$[Mg(CP)]_2$ (64 mg, 0.066 mmol, 1.1 equiv.) was dissolved in toluene (3 mL) with 6 drops of dioxane. To this solution, **18** (100 mg, 0.060 mmol) was added, and the reaction mixture was stirred for 16 h. The solvent was removed *in vacuo*, and the solids were washed with hexane (3 × 2 mL), then extracted with toluene (5 mL). The toluene solution was concentrated under vacuum to 1 mL and layered with hexane. Storage at −35 ºC for 3 days yielded orange crystals

of **19** that were isolated by filtration, washed with hexane (2 × 1 mL) and pentane (2 × 1 mL), then dried under vacuum. Yield: 92 mg, 0.055 mmol, 91%.

^{1}H NMR (600 MHz, C_6D_6): δ (ppm) = 7.15 (10H; H_1), 6.71 (s, 4H; H_j), 6.40 (d, $^{3}J_{H–H}$ = 1.9 Hz, 2H; H_d), 6.13 (d, $^{3}J_{H–H}$ = 1.9 Hz, 2H; H_c), 5.15 (s, 4H; H_f), 4.04 (10H; H_2), 3.59 (30H; H_5), 2.71 (m, 2H; H_b), 2.55 (m, 2H; H_b), 2.11 (6H; H_l), 2.10 (12H; H_i), −1.11 (4H, m; H_a).

^{13}C{^{1}H} NMR (151 MHz, C_6D_6): δ (ppm) = 250.8 (Br; C_m), 185.6 (C_e), 151.7 (H_4), 138.9 (C_k), 138.0 (C_h), 129.9 (H_3), 129.8 (C_j), 128.8 (C_g), 121.8 (H_c), 117.2 (H_d), 115.9 (H_1), 57.5 (H_5), 49.5 (H_b), 49.0 (H_f), 29.7 (H_2), 23.1 (H_a), 21.1 (C_l), 19.9 (C_i).

HR-ESI-MS (+ve ion mode): *m/z* calcd. for $C_{77}H_{88}Au_2N_4O_{10}P_2$+$Na^+$: 1707.5199 $[M+Na]^+$; found 1707.5157.

5.5.5 Synthesis of 20a

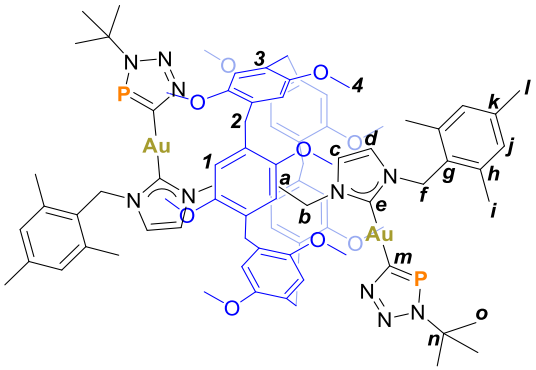

^{t}Bu–N_3 (3.00 mg, 0.0304 mmol, 2.05 equiv.) was added to a solution of **19** (25 mg, 0.0148 mmol) in toluene (1 mL), and the reaction mixture was stirred for 3 h. The solvent was removed *in vacuo*, and the residue was washed with Et_2O (2 × 1 mL). The residue was dried under vacuum to yield **20a** as a yellow oil. Yield: 23 mg, 0.0122 mmol, 83%.

^{1}H NMR (600 MHz, C_6D_6): δ (ppm) = 7.21 (10H; H_1), 6.73 (s, 4H; H_j), 6.52 (d, $^{3}J_{H–H}$ = 1.9 Hz, 2H; H_d), 6.12 (d, $^{3}J_{H–H}$ = 1.9 Hz, 2H; H_c), 5.48 (d, $^{2}J_{H–H}$ = 14.5 Hz, 2H; H_f), 5.40 (d, $^{2}J_{H–H}$ = 14.5 Hz, 2H; H_f), 4.07 (10H; H_2), 3.56 (30H; H_5), 2.80 (m, 4H; H_b), 2.24 (12H; H_i), 2.13 (6H; H_l), 1.70 (18H; H_o), −0.95 (4H, m; H_a).

^{13}C{^{1}H} NMR (151 MHz, C_6D_6): δ (ppm) = 209.4 (d, $^{1}J_{C–P}$ = 83.9 Hz; C_m), 185.6 (d, $^{3}J_{C–P}$ = 11.5 Hz; C_e), 151.6 (H_4), 138.7 (C_k), 138.1 (C_h), 129.8 (C_3), 129.7 (C_j), 128.4 (C_g), 121.8 (C_c), 117.2 (C_d), 115.8 (C_1), 60.4 (d, $^{2}J_{C–P}$ = 5.0 Hz, C_n), 57.1 (C_5), 49.5 (C_b), 49.0 (C_f), 32.4 (d, $^{4}J_{C–P}$ = 4.8 Hz, C_o), 29.8 (C_2), 23.7 (C_a), 21.1 (C_l), 20.1 (C_i).

HR-ESI-MS (+ve ion mode): *m*/*z* calcd. for $C_{85}H_{106}Au_2N_{10}O_{10}P_2+H^+$: 1883.6973 $[M+H]^+$; found 1883.6901.

5.5.6 Synthesis of 20b

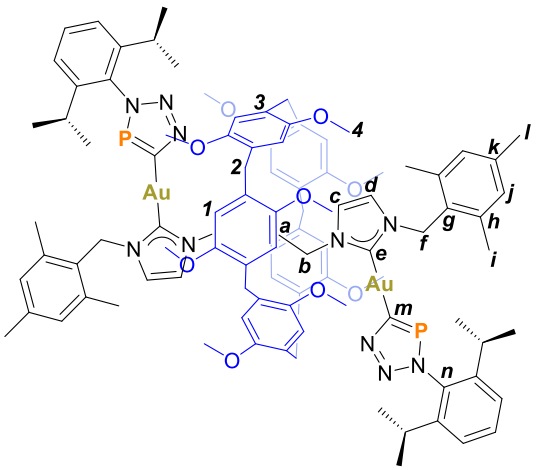

Dipp–N_3 (5.44 mg, 0.0268 mmol, 2.05 equiv.) was added to a solution of **19** (22 mg, 0.0131 mmol) in toluene (1 mL) and the reaction mixture was stirred for 3 h. The

solvent was removed *in vacuo*, and the residue was washed with Et_2O (2 × 1 mL), then dried under vacuum. Yield: 21 mg, 0.0101 mmol, 77%.

^{1}H NMR (600 MHz, C_6D_6): δ (ppm) = 7.28 (3H; Dipp Ar-H), 7.23 (10H; H_1), 7.18 (3H; Dipp Ar-H), 6.72 (s, 4H; H_j), 6.52 (d, $^3J_{H–H}$ = 1.9 Hz, 2H; H_d), 6.16 (d, $^3J_{H–H}$ = 1.9 Hz, 2H; H_c), 5.48 (d, $^2J_{H–H}$ = 14.5 Hz, 2H; H_f), 5.44 (d, $^2J_{H–H}$ = 14.5 Hz, 2H; H_f), 4.09 (10H; H_2), 3.59 (30H; H_5), 2.96 (m, 2H; H_b), 2.78 (m, 2H; H_b), 2.66 (sept, $^3J_{H–H}$ = 6.90 Hz, 2H; Dipp ^{i}Pr CH), 2.63 (sept, $^3J_{H–H}$ = 6.90 Hz, 2H; Dipp ^{i}Pr CH), 2.20 (12H; H_i), 2.11 (6H; H_l), 1.13 (m, 24H; Dipp Me), −0.93 (4H, m; H_a).

^{13}C NMR (151 MHz, C_6D_6): δ (ppm) = 212.0 (d, $^1J_{C–P}$ = 84.2 Hz; C_m), 190.5 (d, $^3J_{C–P}$ = 10.6 Hz; C_e), 151.7 (H_4), 146.5 (Dipp Ar-C), 138.8 (C_k), 138.3 (d, $^2J_{C–P}$ = 6.1 Hz; C_n), 138.1 (C_h), 129.8 (C_3), 129.8 (C_j), 129.4 (C_g), 129.2 (Dipp Ar-C), 123.7 (Dipp Ar-C), 121.8 (C_c), 117.2 (C_d), 115.9 (C_1), 57.2 (C_5), 49.6 (C_b), 49.1 (C_f), 29.8 (C_2), 28.8 (C_p), 24.5 (C_q), 23.5 (C_a), 21.1 (C_l), 20.1 (C_i).

The Dipp resonances could not be confidently assigned and are therefore assigned generally.

HR-ESI-MS (+ve ion mode): m/z calcd. for $C_{101}H_{122}Au_2N_{10}O_{10}P_2+H^+$: 2091.8225 $[M+H]^+$; found 2091.8154.

5.5.7 Synthesis of 21

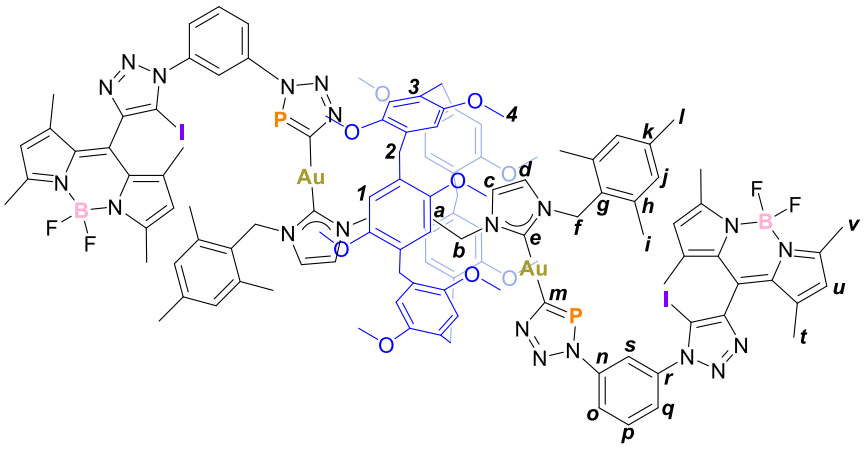

BODIPY-azide (17 mg, 0.0303 mmol, 2.05 equiv.) was added to a solution of **19** (25 mg, 0.0148 mmol) in toluene (2 mL) and the reaction mixture was stirred for 3 h. The solvent was removed *in vacuo*, and the residue was washed with Et_2O (2 × 2 mL). The solids were isolated by filtration and dried under vacuum to yield **21** as a bright red solid. Yield: 33 mg, 0.0118 mmol, 80%.

^{1}H NMR (600 MHz, C_6D_6): δ (ppm) = 8.54 (t, $^3J_{H–H}$ = 1.8 Hz, 2H; H_s), 7.95 (d, $^3J_{H–H}$ = 8.3 Hz, 2H; H_o) 7.26 (s, 10H; H_1), 7.21 (d, $^3J_{H–H}$ = 8.3 Hz, 2H; H_q), 6.94 (t, $^3J_{H–H}$ = 8.1 Hz, 2H; H_p), 6.75 (s, 4H; H_j), 6.56 (d, $^3J_{H–H}$ = 1.5 Hz, 2H; H_d), 6.23 (d, $^3J_{H–H}$ = 1.5 Hz, 2H; H_c), 5.53 (s, 4H; H_u), 5.48 (d, $^2J_{H–H}$ = 14.6 Hz, 2H; H_f), 5.43 (d, $^2J_{H–H}$ = 14.6 Hz, 2H; H_f), 4.11 (10H; H_2), 3.56 (30H; H_5), 2.80 (m, 4H; H_b), 2.54 (s, 12H; H_t), 2.24 (s, 12H; H_i), 2.13 (s, 6H; H_l), 1.48 (s, 12H; H_v), −0.92 (m, 4H; H_a).

^{13}C NMR (151 MHz, C_6D_6): δ (ppm) = 213.2 (d, $^1J_{C–P}$ = 85.4 Hz; C_m), 189.6 (d, $^3J_{C–P}$ = 10.5 Hz; C_e), 157.6 (BODIPY-C), 151.7 (H_4), 147.3, 143.7 (d, $^2J_{C–P}$ = 7.3 Hz; C_n), 142.4 (BODIPY-C), 139.0 (C_k), 138.0 (C_h), 138.0 (Ar-C), 132.8 (BODIPY-C), 130.6 (C_p), 129.9 (C_j), 129.8 (C_3), 129.1 (C_g), 124.0 (C_q), 123.5 (d, $^3J_{C–P}$ = 7.3 Hz; C_o), 122.0 (C_u), 121.9 (C_c), 119.1 (d, $^3J_{C–P}$ = 4.5 Hz; C_s), 117.5 (C_d), 115.9 (C_1), 82.9, 57.2 (C_5), 49.6 (C_b), 49.1 (C_f), 29.8 (C_2), 23.8 (C_a), 21.1 (C_l), 20.1 (C_i), 14.9 (C_t), 13.9 (C_v).

^{31}P{^{1}H} NMR (243 MHz, C_6D_6): δ(ppm) 199.6 (s).

^{19}F{^{1}H} NMR (565 MHz, C_6D_6): δ(ppm) −144.37–−145.79 (m).

^{11}B{^{1}H} NMR (128 MHz, C_6D_6): δ(ppm) 1.35 (t, $^1J_{B–F}$ = 32.6 Hz).

HR-ESI-MS (+ve ion mode): *m*/*z* calcd. for $C_{119}H_{126}Au_2B_2F_4I_2N_{20}O_{10}P_2+H^+$: 2803.7057 $[M+H]^+$; found 2803.6926.

5.5.8 Attempted synthesis of a [2]catenane

19 (50 mg, 0.0297 mmol) was dissolved in DCM (60 mL) and cooled to −15 °C. Pyridyl-bis-azide (16 mg, 0.0297 mmol) was dissolved in DCM (9.7 mL) and drawn up into a syringe. The bis-azide solution was added dropwise to the solution of **19** with vigorous stirring using a syringe at a rate of 3 mL/h. The reaction mixture was stirred overnight and concentrated *in vacuo* to 1 mL to give the crude $^{31}P\{^{1}H\}$ NMR spectrum. A sample of this was taken to obtain the HR-ESI-MS.

HR-ESI-MS (+ve ion mode): *m*/*z* calcd. for $C_{104}H_{118}Au_2N_{11}O_{16}P_2+H^+$: 2234.7716 $[M+H]^+$; found 2234.7663.

5.6 References

1. E. A. Neal and S. M. Goldup, *Chem Commun* **2014**, *50*, 5128–5142.
2. M. Galli, J. E. M. Lewis and S. M. Goldup, *Angew. Chem. Int. Ed.* **2015**, *54*, 13545–13549.
3. P. Langer, L. Yang, C. R. Pfeiffer, W. Lewis and N. R. Champness, *Dalton Trans.* **2019**, *48*, 58–64.
4. S. K. Goetzfried, P. Kapitza, C. M. Gallati, A. Nindl, M. Cziferszky, M. Hermann, K. Wurst, B. Kircher and R. Gust, *Dalton Trans.* **2022**, *51*, 1395–1406.
5. S. Dery, C. Ehinger, J. Roudin, Y. Kakiuchi, D. Gioffrè and C. Copéret, *J. Am. Chem. Soc.* **2025**, *147*, 18054–18063.
6. P. Waelès, M. Gauthier and F. Coutrot, *Angew. Chem. Int. Ed.* **2021**, *60*, 16778–16799.

7. I. Pibiri, S. Buscemi, A. Palumbo Piccionello and A. Pace, *ChemPhotoChem* **2018**, *2*, 535–547.

8. E. Bassan, A. Gualandi, P. G. Cozzi and P. Ceroni, *Chem. Sci.* **2021**, *12*, 6607–6628.

9. A. Pinto and L. Rodríguez, *Dalton Trans.* **2024**, *53*, 13716–13725.

10. M. Üçüncü, E. Karakuş, E. Kurulgan Demirci, M. Sayar, S. Dartar and M. Emrullahoğlu, *Org. Lett.* **2017**, *19*, 2522–2525.

11. S. Popov and H. Plenio, *Eur. J. Inorg. Chem.* **2022**, *2022*, e202200335.

12. A. J. Taylor and P. D. Beer, *Chem. Commun.* **2024**, *60*, 7983–7986.

13. A. J. Taylor, R. Hein, S. C. Patrick, J. J. Davis and P. D. Beer, *Angew. Chem. Int. Ed.* **2024**, *63*, e202315959.

14. A. Brown, T. Lang, K. M. Mullen and P. D. Beer, *Org. Biomol. Chem.* **2017**, *15*, 4587–4594.

15. S. Tung, C. Lai, Y. Liu, S. Peng and S. Chiu, *Angew. Chem. Int. Ed.* **2013**, *52*, 13269–13272.

16. A. Inthasot, S.-T. Tung and S.-H. Chiu, *Acc. Chem. Res.* **2018**, *51*, 1324–1337.

17. H. M. Tay, T. C. Tse, A. Docker, C. Gateley, A. L. Thompson, H. Kuhn, Z. Zhang and P. D. Beer, *Angew. Chem. Int. Ed.* **2023**, *62*, e202214785.

18. H. M. Tay, A. Docker, C. Hua and P. D. Beer, *Chem. Sci.* **2024**, *15*, 13074–13081.

Chapter 6

Conclusions and Future Work

6.1 Conclusions

The cyaphide-azide 1,3-dipolar cycloaddition reaction emulates many of the advantages of its organic variant, the copper-catalysed azide-alkyne click (CuAAC) reaction, which is popular in the synthesis of mechanically interlocked molecules. It proceeds rapidly and regioselectively at room temperature and is broadly applicable to a range of metal-cyaphide complexes and azides. In contrast to the CuAAC reaction, it proceeds spontaneously in the absence of a catalyst.

The reactivity of the resulting metal-triazaphospholes is dominated by the strong nucleophilicity of the nitrogen atom adjacent to the triazaphosphole carbon, demonstrated by Lewis acid coordination and methylation reactions. The metal–triazaphosphole bond can be cleaved by oxidation with iodine, yielding novel iodotriazaphospholes, providing insight into their potential halogen bonding capabilities.

The reaction can be used to prepare pillar[5]arene-based [2]rotaxanes efficiently *via* a capping approach through the installation of bulky organometallic metal-triazaphosphole stoppers. Notably, the mechanical bond in the [2]rotaxanes sterically shields and stabilises the triazaphospholes such that they can be handled indefinitely in air and purified by column chromatography.

The synthesis of bis-cyaphide species capable of undergoing 1,3-dipolar cycloaddition reactivity with azides is a significant challenge, limiting the potential of using this reaction for the synthesis of [*n*]catenanes. Dinuclear gold(I) bis-cyaphide compounds based upon Janus

bis-NHCs decompose rapidly under an inert atmosphere, presumably due to oxidative cyaphide oligomerisation. Increasing the distance between the two metal-cyaphide units by introducing an alkyl bridge increases their lifetime under an inert atmosphere to a few days, although they still cannot be isolated. This species can be trapped *in situ* by a cycloaddition reaction with two equivalents of a simple mono-azide, yielding the corresponding dinuclear gold(I) bis-triazaphosphole species as an adduct of the cyaphide transfer by-product, (^{Dipp}NacNac)MgCl.

The mechanical bond in a [2]rotaxane can be used to stabilise dinuclear gold(I) bis-cyaphide compounds, which are otherwise unstable under an inert atmosphere. The coordination of two gold(I) chloride units at each terminal of a bis-imidazolium [2]rotaxane can be achieved by the formation of gold(I)–carbene bonds. This species is capable of undergoing efficient cyaphide transfer to yield the corresponding dinuclear gold(I) bis-cyaphide [2]rotaxane. Unlike the non-interlocked analogues, this species is stable indefinitely under an inert atmosphere. This is attributed to the presence of the mechanical bond, which offers steric stabilisation and prevents intramolecular coupling reactions between the two cyaphide units.

The presence of the pillar[5]arene macrocycle in the dinuclear gold(I) bis-cyaphide [2]rotaxane enhances its stability and solubility compared to non-interlocked analogues, allowing further post-synthetic modifications. It is ameanable to further functionalisation *via* cyaphide-azide 1,3-dipolar cycloaddition reaction, which was used to install fluorescent BODIPY moieties to yield a highly efficient singlet oxygen photosensitizer. The heavy gold(I) atoms increase the efficiency of intersystem crossing through spin-orbit coupling, increasing the population of the triplet excited state necessary for singlet oxygen generation.

The use of the cyaphide-azide 1,3-dipolar cycloaddition reaction for the synthesis of [*n*]catenanes from the dinuclear gold(I) bis-cyaphide [2]rotaxane is challenging. Even under

high dilution and low temperature conditions, the reaction proceeds rapidly to form an intractable mixture of products. Although the [2]catenane can be identified in the high-resolution mass spectrum, its purification is not trivial due to low yields and air sensitivity of the product.

6.2 Future Work

The scope of using the cyaphide-azide 1,3-dipolar cycloaddition reaction for the synthesis of mechanically interlocked molecules is thus far limited to relatively simple [2]rotaxanes. This is largely due to the lack of availability of stable bis-cyaphide complexes that retain cycloaddition reactivity. Although this has been achieved in a dinuclear gold(I) bis-cyaphide [2]rotaxane, it would be desirable to target a simpler stabilised bis-cyaphide compound. It is worth investigating other bis-NHC ligand systems, for example, bis-CAAC ligands, to increase the σ-donor strength and stabilise the Au–CP bond. There may also be scope to increase steric bulk at the ligand system in an effort to kinetically stabilise the bis-cyaphide species. Using rigid linkers between the NHC units to inhibit intramolecular coupling reactions, whilst spatially separating the cyaphide units, could also be an interesting avenue to explore.

The rapid nature of the cyaphide-azide 1,3-dipolar cycloaddition reaction makes it difficult to use the dinuclear gold(I) bis-cyaphide [2]rotaxane in a macrocyclization reaction with a long-chain azide to prepare a [2]catenane, largely resulting in oligomerization products. Using a more rigid bis-azide containing for example, a biphenyl spacer group, with fewer degrees of freedom, could be used to target a [*n*]catenane under optimised high dilution and low temperature conditions. A variety of templating strategies could also be investigated in order to pre-organise a suitably designed bis-azide into the correct orientation to undergo a macrocyclization reaction. Smaller spacer-linked bis-azides could also be used to form higher-order [*n*]catenanes, although this may not be possible due to steric clash between the bulky [2]rotaxanes.

The bis-cyaphide [2]rotaxane discussed in Chapter 5 is an interesting proof of concept as an organometallic rotaxane synthon, and has demonstrated the advantage of incorporating gold(I) [2]rotaxanes into photosensitizers. It would be interesting to investigate whether singlet oxygen generation can be modulated by the presence of anions, by incorporating additional and/or more potent halogen bonding anion recognition groups appended to the pillar[5]arene macrocycle structural framework. The full potential of the interlocked nature of the [2]rotaxane has not been exploited, and more sophisticated derivatives of this framework, such as that below (**Figure 6.1**), could be used as a molecular machine.

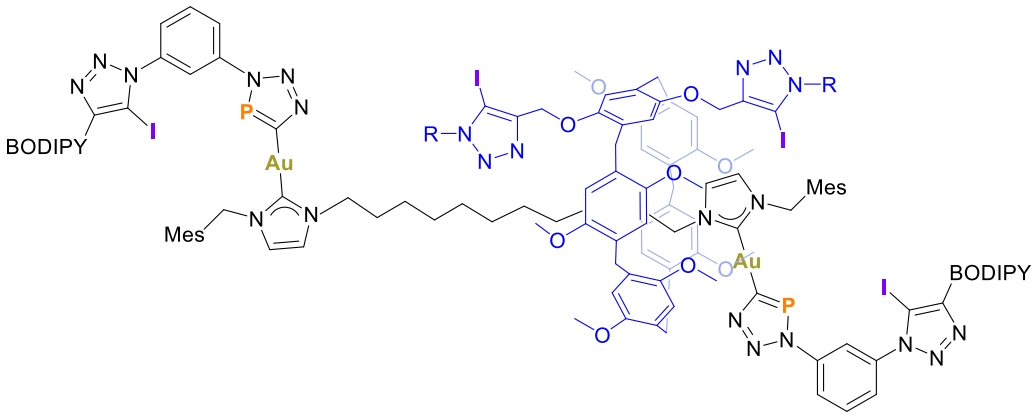

Figure 6.1. Future work target of a [2]rotaxane containing a pillar[5]arene functionalised with halogen bonding groups for anion recognition.

For example, the molecular motion of the two components would be expected to be controlled by anion binding, where in the presence of an anion, the halogen bonding appended pillar[5]arene macrocycle component shuttles towards the terminal axle BODIPY stopper halogen bonding recognition site of the [2]rotaxane to facilitate cooperative anion recognition. This could be monitored *via* the fluorescent BODIPY motifs and potentially modulate singlet oxygen production.

Chapter 7

Experimental Details

7.1 General experimental methods

7.1.1 Synthetic methods

Unless specified otherwise, all reactions and product manipulations were performed using standard Schlenk-line techniques under an atmosphere of argon, or in a dinitrogen-filled glovebox (MBraun UNIlab) maintained at <0.1 ppm H_2O and <0.1 ppm O_2. All anhydrous solvents were stored under an atmosphere of nitrogen or argon in gas-tight ampoules over activated 3 Å molecular sieves.

Hexane (Sigma Aldrich HPLC grade), pentane (Sigma Aldrich HPLC grade), benzene (Rathburn HPLC grade), dichloromethane (Sigma Aldrich HPLC grade), acetonitrile (Sigma Aldrich HPLC grade), diethyl ether (Sigma Aldrich HPLC grade), and toluene (Sigma Aldrich HPLC grade) were purified using an MBraun SPS-800 solvent system. THF (Sigma Aldrich HPLC grade) was distilled over sodium/benzophenone. C_6D_6 (Sigma Aldrich, 99.5%) and CD_2Cl_2 (Sigma Aldrich, 99.5%) were degassed and dried over CaH_2.

Tert-butyl azide,[1] 2,6-diisopropylphenyl azide,[2] 1,3-diazidobenzene,[3] (IDipp)AuCl,[4] (^{Dipp}NacNac)GeCl,[5] (^{Dipp}NacNac)Mg(CP)(diox.),[6] $[Mg(CP)]_2$,[7] $B(C_6F_5)_3$,[8] perethylated pillar[5]arene (**P5A^{Et}**),[9] bent *Janus*-bis-NHC gold(I) chloride,[10] benzo-bis(imidazolium) salt,[11] alkyl-bridged bis-NHC gold(I) chloride,[12] bis(imidazolium) rotaxane,[13] the BODIPY-azide,[14] compound **A**[14], and the pyridyl-functionalised bis-azide[15] were all prepared according to the referenced literature procedures.

Adamantyl azide (Sigma Aldrich, 97%), $[Me_3O][BF_4]$ (Fluorochem)**,** iodine (Sigma Aldrich, 99.8%), 1,8-diaminooctane (Alfa Aesar, 98%), 1,4-dibromobutane (Alfa Aesar, 98%), Potassium bis(trimethylsilyl)amide (KHMDS) (Sigma Aldrich, 95%), $(SMe_2)AuCl$ (Sigma Aldrich), potassium iodide (Alfa Aesar, 99%), and Amberlite^{TM} IRA-402(Cl^-) (ThermoScientific) were purchased and used as received. Benzyl azide (Alfa Aesar, 94%) was distilled and dried over 3 Å molecular sieves.

1,8-diazidooctane and 1,4-diazidobutane were synthesized in quantitative yield from the dibromo precursors – 1,8-dibromooctane (Alfa Aesar, 98%) and 1,4-dibromobutane (Alfa Aesar, 98%) – using NaN_3 in DMSO.

TBACl was purchased from a commercial supplier and stored in a vacuum desiccator prior to use.

7.1.2 Characterisation techniques

NMR samples were prepared inside an inert atmosphere glovebox in NMR tubes fitted with a gas-tight valve. NMR spectra were acquired on either a Bruker AVIII 400 MHz NMR spectrometer (^{1}H 400 MHz, ^{11}B 128 MHz, ^{19}F 377 MHz, ^{31}P 162 MHz), a Bruker AVIII 500 spectrometer (^{1}H 500 MHz, ^{13}C 126 MHz) or a Bruker Avance NEO 600 MHz NMR spectrometer with a broadband helium cryoprobe (^{1}H 600 MHz, ^{31}P 243 MHz, ^{13}C 151 MHz, ^{19}F 565 MHz). ^{1}H and ^{13}C NMR spectra were referenced to their respective solvent resonance (^{1}H NMR C_6D_6: $\delta = 7.16$ ppm, CD_2Cl_2: $\delta = 5.32$ ppm; ^{13}C NMR C_6D_6: $\delta = 128.1$ ppm, CD_2Cl_2: $\delta = 53.8$ ppm). ^{11}B NMR spectra were externally referenced to $BF_3{\cdot}Et_2O$ in C_6D_6. ^{19}F NMR spectra were externally referenced to $CFCl_3$. ^{31}P NMR spectra were externally referenced to an 85% solution of H_3PO_4 in H_2O.

High resolution electrospray ionisation (HR-ESI) mass spectrometry were acquired on a Thermo Orbitrap Exactive MS with Waters Acquity Ultraperformance LC system, 90 % MeOH, 0.1 % formic acid buffer, loop injection/direct infusion.

Elemental analyses were carried out by the Elemental Analysis Services Team (London Metropolitan University, U.K.). Samples (approximately 5 mg) were submitted in flame-sealed glass tubes.

7.1.3 ^{1}H NMR binding titrations

^{1}H NMR titrations were recorded on a Bruker AVIII 500 MHz NMR spectrometer equipped with an 11.75 T magnet at 298 K. Titrations were carried out by measuring the changes in chemical shift of a selected ^{1}H NMR resonance following the successive addition of a 50 mM stock solution of 1,8-diazidooctane or **9** to a 1 mM solution of host. Seven data points were collected, increasing to 10 equivalents of bisazide, which corresponds to a 100 μL stock solution added. The sample was thoroughly mixed by inversion of the NMR tube prior to each spectrum being collected. All systems for which binding constants are quoted displayed fast NMR exchange at 298 K. The changes in chemical shift upon binding were fitted using *Bindfit*[16] to a 1:1 stoichiometric binding model. In both cases, calculated errors in the binding constant were <10%.

7.1.4 UV-vis and Fluorescence measurments

UV-vis and fluorescence measurements were carried out on a Duetta (Horiba) using quartz cuvettes with a path length of 10 mm. Fluorescence spectra were acquired with a wavelength of excitation of 485 nm for receptor **21**, 5 nm excitation and emission slits, and were recorded in at least triplicate repeat measurements to ensure signal stability. Chloride anion titration studies were carried out by titrating a 1 μM solution of the receptor with aliquots of 20mM TBACl in the same receptor solution to ensure a constant receptor concentration. Photo-irradiation of samples for singlet oxygen experiments was accomplished using a Thorlabs

mounted LED (model M530L3), mounted in a custom set-up directly above the cuvette containing the liquid sample.

All data analysis and fitting were carried out with *OriginPro* 2023.[17]

7.2 Single crystal X-ray diffraction data

Single-crystal X-ray diffraction (SCXRD) data were collected using an Oxford Diffraction Supernova dual-source diffractometer equipped with a 135 mm Atlas CCD area detector. Crystals were selected under Paratone-N oil, mounted on micro-mount loops, and quench-cooled using an Oxford Cryosystems open flow N2 cooling device. Data were collected at 200 K or 150 K using mirror monochromated Cu Kα (λ = 1.54184 Å) radiation and processed using the CrysAlisPro package, including unit cell parameter refinement and inter-frame scaling (carried out using SCALE3 ABSPACK).[18] Equivalent reflections were merged and diffraction patterns processed with the CrysAlisPro suite. Structures were subsequently solved using direct methods and refined on F2 using the SHELXL package.[19–21]

Table 7.1. Selected X-ray data collection and refinement parameters for **1a**·C_6H_6, **1b**·tol, and **1c**·C_6H_6.

Compound	**1a**·C_6H_6	**1b**·tol	**1c**·C_6H_6
Formula	$C_{38}H_{51}AuN_5P$	$C_{45}H_{59}AuN_5P$	$C_{46}H_{59}AuN_5P$
CCDC	2263738	2263730	2263731
Fw [g mol^{-1}]	805.77	897.90	909.91
Crystal system	Orthorhombic	Monoclinic	Monoclinic
Space group	*Pnma*	*I2/a*	*P2$_1$/c*
a (Å)	16.2045(1)	20.7310(1)	12.5798(2)
b (Å)	10.6534(1)	16.1721(1)	16.7485(2)
c (Å)	23.8480(2)	26.0458(4)	22.2537(3)
α (°)	90	90	90
β (°)	90	102.7250(1)	106.371
γ (°)	90	90	90
V (Å^3)	4116.95(6)	8517.74(15)	4498.60(12)
Z	4	8	4
Radiation, λ (Å)	1.54184 (CuK$_\alpha$)	1.54184 (CuK$_\alpha$)	1.54184 (CuK$_\alpha$)
Temp (K)	200(2)	150(2)	150(2)
ρ_{calc} (g cm^{-3})	1.300	1.400	1.343
μ (mm^{-1})	7.296	7.113	6.742
Reflections collected	48427	100264	88948
Independent reflections	4547	8876	9366
Parameters	328	518	516
R(int)	0.0510	0.0394	0.0755
R1/wR2,[a] $I \geq 2\sigma I$ (%)	4.29 / 12.04	1.81 / 4.27	3.62 / 8.91
R1/wR2,[a] all data (%)	4.48 / 12.14	2.05 / 4.39	4.33 / 9.44
GOF	1.270	1.044	1.062

[a] $R1 = [\Sigma||F_o| - |Fc||]/\Sigma|Fo|$; $wR2 = \{[\Sigma w[(F_o)^2 - (Fc)^2]^2]/[\Sigma w(F_o^2)^2\}^{1/2}$; $w = [\sigma^2(F_o)^2 + (AP)^2 + BP]^{-1}$, where $P = [(F_o)^2 + 2(F_c)^2]/3$ and the A and B values are 0.0257 and 18.57 for **1a**·C_6H_6, 0.0193 and 9.81 for **1b**·tol, and 0.0399 and 9.14 for **1c**·C_6H_6.

Table 7.2. Selected X-ray data collection and refinement parameters for **2**, **3a**, and **3b**

Compound	**2**·tol	**3a**	**3b**·2tol
Formula	$C_{69}H_{84}Au_2N_{10}P_2$	$C_{68}H_{100}Mg_2N_{10}P_2$	$C_{81}H_{104}Mg_2N_{10}P_2$
CCDC	2263732	2263733	2263734
Fw [g mol^{-1}]	1509.33	1168.13	1328.30
Crystal system	Triclinic	Monoclinic	Triclinic
Space group	*P*–1	*C2/m*	*P*–1
a (Å)	14.1752(4)	18.1532(2)	13.0652(5)
b (Å)	21.0565(4)	19.1427(2)	13.1025(6)
c (Å)	24.3488(6)	12.4393(10)	14.2674(7)
α (°)	94.882(2)	90	114.624(4)
β (°)	90.052(2)	122.232(1)	113.693(4)
γ (°)	101.648(2)	90	95.063(4)
V (Å^3)	7090.9(3)	3656.53(7)	1934.86(17)
Z	4	2	1
Radiation, λ (Å)	1.54184 (CuK$_\alpha$)	1.54184 (CuK$_\alpha$)	1.54184 (CuK$_\alpha$)
Temp (K)	150(2)	150(2)	150(2)
ρ_{calc} (g cm^{-3})	1.328	1.061	1.140
μ (mm^{-1})	8.400	1.033	1.037
Reflections collected	72456	18582	18706
Independent reflections	24975	3960	7813
Parameters	1526	199	459
R(int)	0.0726	0.0202	0.0167
R1/wR2,[a] I ≥ 2σI (%)	6.52 / 17.69	3.46 / 10.15	6.11 / 16.10
R1/wR2,[a] all data (%)	8.49 / 19.33	3.71 / 10.47	6.33 / 16.21
GOF	1.106	1.051	1.126

[a] $R1 = [\Sigma||F_o| - |Fc||]/\Sigma|Fo|$; $wR2 = \{[\Sigma w[(F_o)^2 - (Fc)^2]^2]/[\Sigma w(F_o^2)^2]\}^{1/2}$; $w = [\sigma^2(F_o)^2 + (AP)^2 + BP]^{-1}$, where $P = [(F_o)^2 + 2(F_c)^2]/3$ and the A and B values are 0.0975 and 15.88 for **1d**·tol, 0.0610 and 1.85 for **2a**, and 0.0364 and 3.66 for **2b**·2tol.

Table 7.3. Selected X-ray data collection and refinement parameters for **4**, **5a**, and **5c**·2DCM

Compound	**4**	**5a**	**5c**·2DCM
Formula	$C_{34}H_{50}GeN_5P$	$C_{50}H_{45}AuBF_{15}N_5P$	$C_{61}H_{58}AuBCl_4F_{15}N_5P$
CCDC	2263735	2263736	2263737
Fw [g mol^{-1}]	632.35	1239.65	1513.65
Crystal system	Tetragonal	Orthorhombic	Monoclinic
Space group	*P*42/*n*	$P2_12_12_1$	$P2_1/n$
a (Å)	18.5981(1)	14.6085(2)	12.4556(2)
b (Å)	18.5981(1)	18.1164(2)	23.8012(3)
c (Å)	20.7899(1)	19.2324(3)	21.2193(2)
α (°)	90	90	90
β (°)	90	90	93.566(1)
γ (°)	90	90	90
V (Å^3)	7191.00(8)	5089.92(12)	6278.46(14)
Z	8	4	4
Radiation, λ (Å)	1.54184 (CuK$_\alpha$)	1.54184 (CuK$_\alpha$)	1.54184 (CuK$_\alpha$)
Temp (K)	150(2)	150(2)	150(2)
ρ_{calc} (g cm^{-3})	1.168	1.618	1.601
μ (mm^{-1})	1.783	6.576	6.979
Reflections collected	77157	28937	76418
Independent reflections	7522	9631	13093
Parameters	408	669	784
R(int)	0.0252	0.0262	0.0579
R1/wR2,[a] I ≥ 2σI (%)	3.01 / 8.21	2.30 / 5.69	3.54 / 8.19
R1/wR2,[a] all data (%)	3.46 / 8.69	2.46 / 5.84	4.74 / 8.85
GOF	1.038	1.051	1.076

[a] $R1 = [\Sigma||F_o| - |Fc||]/\Sigma|Fo|$; $wR2 = \{[\Sigma w[(F_o)^2 - (Fc)^2]^2]/[\Sigma w(F_o^2)^2]\}^{1/2}$; $w = [\sigma^2(F_o)^2 + (AP)^2 + BP]^{-1}$, where $P = [(F_o)^2 + 2(F_c)^2]/3$ and the A and B values are 0.0418 and 3.32 for **4**, 0.025 and 4.24 for **4a** and 0.0351 and 11.40 for **5c**·2DCM.

Table 7.4. Selected X-ray data collection and refinement parameters for **6**, **7a**, and **7b**

Compound	**6**	**7a**	**7b**
Formula	$C_{43}H_{60}AuBCl_4F_4N_5P$	$C_5H_9IN_3P$	$C_{11}H_{15}IN_3P$
CCDC	–	2263739	2263740
Fw [g mol^{-1}]	1103.50	269.02	347.13
Crystal system	Monoclinic	Tetragonal	Monoclinic
Space group	$P2_1/n$	$P4_32_12$	$P2_1/c$
a (Å)	12.40630(10)	8.9844(1)	13.2814(4)
b (Å)	25.1525(2)	8.9844(1)	6.9637(2)
c (Å)	16.04090(10)	22.4971(6)	13.6715(3)
α (°)	90	90	90
β (°)	92.1580(10)	90	96.888(2)
γ (°)	90	90	90
V (Å^3)	5002.00(6)	1815.95(6)	1255.32(6)
Z	4	8	4
Radiation, λ (Å)	Cu Kα (1.54184)	Cu Kα (1.54184)	Cu Kα (1.54184)
Temp (K)	150(2)	100(2)	150(2)
ρ_{calc} (g cm^{-3})	1.465	1.968	1.837
μ (mm^{-1})	8.200	28.879	21.062
Reflections collected	59899	20189	8550
Independent reflections	10403	1866	2600
Parameters	532	95	145
R(int)	0.0402	0.1251	0.0317
R1/wR2,[a] $I \geq 2\sigma I$ (%)	4.68 / 12.37	5.23 / 14.80	2.35 / 5.27
R1/wR2,[a] all data (%)	5.10 / 12.85	5.81 / 15.33	3.39 / 5.82
GOF	1.070	1.067	1.061

[a] $R1 = [\Sigma||F_o| - |Fc||]/\Sigma|Fo|$; $wR2 = \{[\Sigma w[(F_o)^2 - (Fc)^2]^2]/[\Sigma w(F_o^2)^2]\}^{1/2}$; $w = [\sigma^2(F_o)^2 + (AP)^2 + BP]^{-1}$, where $P = [(F_o)^2 + 2(F_c)^2]/3$ and the A and B values are 0.0893 and 1.67 for **6**, 0.0981 and 0.18 for **7a**, and 0.025 and 4.24 for **7b**.

Table 7.5. Selected X-ray data collection and refinement parameters for **8a**·3C_6H_6, 10**a**, and **15**·DCM

Compound	**8a**·3C_6H_6	**10a**	**15**·DCM
Formula	$C_{137}H_{176}Au_2N_{10}O_{10}P_2$	$C_{123}H_{164}Au_2N_{16}O_{10}P_2$	$C_{103}H_{148}Au_2Cl_4Mg_2N_{14}P_2$
CCDC	2271341	2271342	–
Fw [g mol^{-1}]	2578.74	2482.57	2228.64
Crystal system	Triclinic	Monoclinic	Orthorhombic
Space group	*P*1	$P2_1/n$	Pbca
a (Å)	12.5314(2)	12.3413(2)	18.7731(2)
b (Å)	14.0421(2)	43.5798(6)	19.6559(2)
c (Å)	19.8345(3)	12.7293(2)	30.0029(4)
α (°)	96.403(1)	90	90
β (°)	107.769(1)	95.536(2)	90
γ (°)	95.770(1)	90	90
V (Å^3)	3269.42(9)	6814.29(18)	11071.1(2)
Z	1	2	4
Radiation, λ (Å)	Cu Kα (1.54184)	Cu Kα (1.54184)	Cu Kα (1.54184)
Temp (K)	150(2)	150(2)	150(2)
ρ_{calc} (g cm^{-3})	1.310	1.210	1.337
μ (mm^{-1})	4.856	4.653	6.558
Reflections collected	79947	107442	117917
Independent reflections	25632	11989	9758
Parameters	1267	927	612
R(int)	0.0449	0.0937	0.0740
R1/wR2,[a] I ≥ 2σI (%)	3.93 / 9.61	11.30 / 25.73	5.76 / 12.26
R1/wR2,[a] all data (%)	4.91 / 10.43	12.42 / 26.07	7.70 / 13.07
GOF	1.057	1.134	1.144

[a] $R1 = [\Sigma||F_o| - |Fc||]/\Sigma|Fo|$; $wR2 = \{[\Sigma w[(F_o)^2 - (Fc)^2]^2]/[\Sigma w(F_o^2)^2]\}^{1/2}$; $w = [\sigma^2(F_o)^2 + (AP)^2 + BP]^{-1}$, where $P = [(F_o)^2 + 2(F_c)^2]/3$ and the A and B values are 0.0480 and 4.80 for **8a**·C_6H_6, 0.040 and 128.18 for **10a**, and 0.0191 and 103.76 for **15**·DCM.

Table 7.6. Selected X-ray data collection and refinement parameters for **16**, **18**·2DCM, **19**·$(tol)_2(hex)_{0.5}$

Compound	**16**	**18**·2DCM	**19**·$(tol)_2(hex)_{0.5}$
Formula	$C_{75}H_{88}Au_2I_2N_4O_{10}$	$C_{77}H_{92}Au_2Cl_6N_4O_{10}$	$C_{94}H_{111}Au_2N_4O_{10}P_2$
CCDC	–	–	–
Fw [g mol^{-1}]	1853.22	1840.17	1912.73
Crystal system	Monoclinic	Monoclinic	Monoclinic
Space group	$P2_1/c$	C2/c	$P2_1/c$
a (Å)	21.0037(1)	20.8870(2)	18.9367(1)
b (Å)	17.4936(1)	13.4703(1)	20.2475(1)
c (Å)	24.2602(1)	27.4902(2)	22.2358(1)
α (°)	90	90	90
β (°)	115.1540(10)	101.8870(10)	99.0310(10)
γ (°)	90	90	90
V ($Å^3$)	8068.61(9)	7568.62(11)	8419.98(8)
Z	4	4	4
Radiation, λ (Å)	Cu Kα (1.54184)	Cu Kα (1.54184)	Cu Kα (1.54184)
Temp (K)	150(2)	150(2)	100(2)
ρ_{calc} (g cm^{-3})	1.526	1.615	1.509
μ (mm^{-1})	13.174	9.616	7.307
Reflections collected	296160	80148	366594
Independent reflections	16642	7913	17360
Parameters	853	447	1009
R(int)	0.1004	0.0508	0.0442
R1/wR2,[a] $I \geq 2\sigma I$ (%)	4.82 / 13.01	2.16 / 5.34	5.51 / 15.76
R1/wR2,[a] all data (%)	5.00 / 13.14	2.61 / 5.60	5.95 / 16.19
GOF	1.083	1.024	1.078

[a] $R1 = [\Sigma||F_o| - |Fc||]/\Sigma|Fo|$; $wR2 = \{[\Sigma w[(F_o)^2 - (Fc)^2]^2]/[\Sigma w(F_o^2)^2\}^{1/2}$; $w = [\sigma^2(F_o)^2 + (AP)^2 + BP]^{-1}$, where $P = [(F_o)^2 + 2(F_c)^2]/3$ and the A and B values are 0.0668 and 37.00 for **16**, 0.0312 and 9.42 for **18**·2DCM, 0.105 and 11.40 for **19**·$(tol)_2(hex)_{0.5}$.

7.3 References

1. P. Margaretha, S. Solar and O. E. Polansky, *Angew. Chem. Int. Ed.* **1971**, 10, 412–413.
2. K. Barral, A. D. Moorhouse and J. E. Moses, *Org. Lett.* **2007**, 9, 1809–1811.
3. H. Gallardo, A. J. Bortoluzzi and D. M. P. De Oliveira Santos, *Liq. Cryst.* **2008**, 35, 719–725.
4. F. Nahra, N. V. Tzouras, A. Collado and S. P. Nolan, *Nat. Protoc.* **2021**, 16, 1476–1493.
5. Y. Ding, H. W. Roesky, M. Noltemeyer, H.-G. Schmidt and P. P. Power, *Organometallics* **2001**, 20, 1190–1194.
6. D. W. N. Wilson, S. J. Urwin, E. S. Yang and J. M. Goicoechea, *J. Am. Chem. Soc.* **2021**, 143, 10367–10373.
7. D. C. Wannipurage, E. S. Yang, A. D. Chivington, J. Fletcher, D. Ray, N. Yamamoto, M. Pink, J. M. Goicoechea and J. M. Smith, *J. Am. Chem. Soc.* **2024**, 146, 27173–27178.
8. M. Santi, D. M. C. Ould, J. Wenz, Y. Soltani, R. L. Melen and T. Wirth, *Angew. Chem. Int. Ed.* **2019**, 58, 7861–7865.
9. K. Khamphaijun, P. Namnouad, A. Docker, A. Ruengsuk, J. Tantirungrotechai, R. Díaz-Torres, D. J. Harding and T. Bunchuay, *Chem. Commun.* **2022**, 58, 7253–7256.
10. A. Gutiérrez-Blanco, S. Ibáñez, F. E. Hahn, M. Poyatos and E. Peris, *Organometallics* **2019**, 38, 4565–4569.
11. A. J. Boydston, D. M. Khramov and C. W. Bielawski, *Tetrahedron Lett.* **2006**, 47, 5123–5125.
12. T. A. C. A. Bayrakdar, F. Nahra, J. V. Davis, M. M. Gamage, B. Captain, M. Temprado, M. Marazzi, M. Saab, K. V. Hecke, D. Ormerod, C. D. Hoff and S. P. Nolan, *Organometallics* **2020**, 39, 2907–2916.
13. P. Langer, L. Yang, C. R. Pfeiffer, W. Lewis and N. R. Champness, *Dalton Trans.* **2019**, 48, 58–64.

14. A. J. Taylor, R. Hein, S. C. Patrick, J. J. Davis and P. D. Beer, *Angew. Chem. Int. Ed.* **2024**, 63, e202315959.

15. A. Brown, T. Lang, K. M. Mullen, and P. D. Beer, *Org. Biomol. Chem.* **2017**, *15*, 4587–4594.

16. D. Brynn Hibbert and P. Thordarson, *Chem. Commun.* **2016**, *52*, 12792–12805.

17. Origin Corporation, 2023.

18. CrysAlisPro, Agilent Technologies, Version 1.171.41.117a

19. G. M. Sheldrick, *SHELXL97, Programs for Crystal Structure Analysis (Release 97-2),* Tammanstrasse 4, D-3400 Göttingen, Germany, **1998**.

20. G. M. Sheldrick, Acta Crystallogr. A **1990**, *46*, 467–473.

21. G. M. Sheldrick, Acta Crystallogr A **2008**, *64*, 112–122.